Spring 3-25-2013

Rapid, Efficient and Versatile Strategies for Functionally Sophisticated Polymers and Nanoparticles: Degradable Polyphosphoesters and Anisotropic Distribution of Chemical Functionalities

Shiyi Zhang
Washington University in St. Louis

WASHINGTON UNIVERSITY IN ST. LOUIS

Department of Chemistry

Dissertation Examination Committee
Karen L. Wooley, Chair
John-Stephen A. Taylor, Co-Chair
Suzanne E. Lapi
Joshua A. Maurer
Shelly E. Sakiyama-Elbert
Jacob Schaefer

Rapid, Efficient and Versatile Strategies for Functionally Sophisticated Polymers and Nanoparticles: Degradable Polyphosphoesters and Anisotropic Distribution of Chemical Functionalities

By

Shiyi Zhang

A dissertation presented to the
Graduate School of Arts and Sciences
of Washington University in
partial fulfillment of the
requirements for the degree
of Doctor of Philosophy

May 2013

St. Louis, Missouri

TABLE OF CONTENTS

LIST OF FIGURES

Chapter 1

Chapter 2

the next step, the absorption peak of hybrid nanoclusters largely shifted to 536 nm because of a change of refractive index caused by SCKs that attached on the GNPs surfaces. Finally, the absorbance band blue shifted back to 529 nm after the GNPs were recovered by ligand exchange reactions. b, TEM image of initial alkyne-functionalized GNPs; average diameter is 46 ± 6 nm. c, TEM image of recovered alkyne-functionalized GNPs; average diameter is 46 ± 7 nm, after counting more than 100 particles. Scale bars: 200 nm. d, DLS results of initial alkyne-functionalized GNPs. e, DLS results of recovered alkyne-functionalized GNPs.

Chapter 6

LIST OF SCHEMES

LIST OF TABLES

Acknowledgements

This dissertation, which contains eight chapters, took me five years. My life has been reshaped in this five years more than any thus period of time in my past. I owe my greatest appreciation to all these people who have helped with the dissertation and many beautiful changes in my life.

First, with deepest sincerity, I would like to thank my advisor and mentor, Professor Karen L. Wooley, for your invaluable guidance and unreserved support over the past five years at both Washington University in St. Louis and Texas A&M University. Your passion for science is lightening me up that I will continue walking on this road. Your kindness to people is moving me that I will continue passing the favor forward. I may not be able to recall my dissertation title in a couple of years, but I know that I will always vividly remember Karen, your work style, your caring mind, and your enthusiasm. I believe in an old Chinese axiom, *once a mentor, forever a parenthood*.

Special recognition must also be given to professors who have served as my instructors and committee members. I wish to thank my research committee members, Prof. John-Stephen A. Taylor and Prof. Joshua A. Maurer for their inspirational suggestions towards the completion of this dissertation. I also appreciate Prof. Jacob Schaefer, Prof. Suzanne E. Lapi and Prof. Shelly E. Sakiyama-Elbert for providing valuable advices, inputs and discussions while serving on my defense committee.

Many brilliant scientists, with whom I have been working, made this dissertation possible. I would like to thank those people, in no particular order: Prof. Darrin J. Pochan and his former student Dr. Jiahua Zhu for more than three years of fruitful collaboration. Prof. Craig J. Hawker and Prof. Darrin J. Pochan for their generous support for my job hunting. Prof. John-Stephen A. Taylor and Miss. Yuefei Shen, Doctor-to-be, for their careful judgment and great patience which led to the finding of a new phenomenon. Prof. Suzanne E. Lapi and Dr. Tolulope A. Aweda for their helps and teaching me the radio-labeling techniques. Prof. Carolyn L. Cannon and her lab members Dr. Parth N. Shah and Mr. Justin Smolen for allowing me to learn *in vivo* techniques in their labs and performing experiments. Prof. James C. Sacchettini and Dr. Dwight Baker for the valuable advice and suggestion. Dr. Ang Li for the great roommateship and friendship. The interesting couple Dr. Nam S. Lee and Dr. Lily Yun Lin for the years' friendship and many

career suggestions. Dr. Zhou Li and Miss. Adriana Pavia for their supplies of gorgeous pictures. Dr. Jiong Zou for his inspirational discussions and ideas. Dr. Guorong Sun for discussions and constant beating me up that fostered better ideas and designs. Former Wooley group members at Washington University in St. Louis, Dr. Jeremy Bertels, Dr. Jennifer L. Sorrells, Dr. Ritu Shrestha, Dr. Philip M. Imbesi, Dr. Jun Ma, Dr. Rhiannon K. Iha, Dr. Ke Zhang, Dr. Solène Cauët and Dr. Christopher Fidge for their helps for starting my research and the tolerance of a junior troublemaker, who has become a senior troublemaker. Friends in Wooley team at Texas A&M University, Dr. Mahmoud El Sabahy, Dr. Jeffery Raymond, Dr. Celine Besset, Dr. Koichiro Mikami, Dr. Scott Zawko, Dr. Tiffany Gustafson, Dr. Marco Giles, Mr. Sangho Cho, Mr. Jingwei Fan, Miss. Simcha Felder, Mr. Jeniree Flores, Mr. Xun He, Mr. Gyu Seong Heo, Ms. Samantha Kristufek, Mr. Richen Li, Mr. Young Lim, Ms. Lauren Link, Mr. Alexander Lonnecker, Ms. Danielle Policarpio, Mr. Kevin Pollack, Dr. Sandani Samarajeewa, Ms. Kellie Seetho, Ms. Jennifer Summerhill, Mr. Hai Wang and Mr. Fuwu for the friendly working environment. I appreciate many faculty, staff members and colleagues from both Washington University in St. Louis and Texas A&M University Department of Chemistry for their help in many aspects.

Most importantly, I wish to thank my mother, my father and my wife, to whom this dissertation is dedicated, for their support and love. A huge thank you to my mother, Xiaorong Jian, for fostering my initial interest in Chemistry when I was in the middle school and for directing me to the major in Chemistry, the same major which she devoted her career into. To my father, Xiaochi Zhang, thank you for teaching me, by his words and deeds, to do what I need to do, to do what I'm good at and to do what I love. Luckily, after the five years' graduate school life, I found all three things in one, Chemistry. To my wife, Jie Luo, thank you for coming to my life, for allowing me to be myself just like my parents do, and especially for always standing by my side through our past journey – three years of long distance relationship due to my relocation from St. Louis to College Station.

(Individual funding acknowledgements are included in the respective chapters)

For my parents, Xiaochi Zhang and Xiaorong Jian

and my wife, Jie Luo

ABSTRACT OF THE DISSERTATION

Rapid, Efficient and Versatile Strategies for Functionally Sophisticated Polymers and Nanoparticles: Degradable Polyphosphoesters and Anisotropic Distribution of Chemical Functionalities

by

Shiyi Zhang

Doctor of Philosophy in Chemistry

Washington University in St. Louis, 2013

Professor Karen L. Wooley, Chairperson

The overall emphasis of this dissertation research included two kinds of asymmetrically-functionalized nanoparticles with anisotropic distributions of chemical functionalities, three degradable polymers synthesized by organocatalyzed ring-opening polymerizations, and two polyphosphoester-based nanoparticle systems for various biomedical applications.

Inspired by the many hierarchical assembly processes that afford complex materials in Nature, the construction of asymmetrically-functionalized nanoparticles with efficient surface chemistries and the directional organization of those building blocks into complex structures have attracted much attention. The first method generated a Janus-faced polymer nanoparticle that presented two orthogonally click-reactive surface chemistries, thiol and azido. This robust method involved reactive functional group transfer by templating against gold nanoparticle substrates. The second method produced nanoparticles with sandwich-like distribution of crown ether functionalities through a stepwise self-assembly process that utilized crown ether-ammonium supramolecular interactions to mediate inter-particle association and the local intra-particle phase separation of unlike hydrophobic polymers.

With the goal to improve the efficiency of the production of degradable polymers with tunable chemical and physical properties, a new type of reactive polyphosphoester was synthesized bearing alkynyl groups by an organocatalyzed ring-opening polymerization, the chemical availability of the alkyne groups was investigated by employing “click” type azide-alkyne Huisgen cycloaddition and thiol-yne radical-mediated reactions. Based on this alkyne-functionalized polyphosphoester polymer and its two available “click” type reactions, two degradable nanoparticle systems were developed. To develop the first system, the well defined poly(ethylene oxide)-*block*-polyphosphester diblock copolymer was transformed into a multifunctional Paclitaxel drug conjugate by densely attaching the polyphosphoester block with azide-functionalized Paclitaxel by azide-alkyne Huisgen cycloaddition. This Paclitaxel drug conjugate provides a powerful platform for combinational cancer therapy and bioimaging due to its ultra-high Paclitaxel loading (> 65 wt%), high water solubility (>6.2 mg/mL for PTX) and easy functionalization. Another polyphosphoester-based nanoparticle system has been developed by a programmable process for the rapid and facile preparation of a family of nanoparticles with different surface charges and functionalities. The non-ionic, anionic, cationic and zwitterionic nanoparticles with hydrodynamic diameters between 13 nm to 21 nm and great size uniformity could be rapidly prepared from small molecules in 6 h or 2 days. The anionic and zwitterionic nanoparticles were designed to load silver ions to treat pulmonary infections, while the cationic nanoparticles are being applied to regulate lung injuries by serving as a degradable iNOS inhibitor conjugates.

In addition, a direct synthesis of acid-labile polyphosphoramidate by organobase-catalyzed ring-opening polymerization and an improved two-step preparation of polyphosphoester ionomer by acid-assisted cleavage of phosphoramidate bonds on polyphosphoramidate were developed. Polyphosphoramidate and polyphosphoester ionomers may be applied to many applications, due to their unique chemical and physical properties.

Chapter 1

Introduction

Nanotechnology. The field of nanotechnology has become one of the most popular areas for current research and development in basically all scientific and technical disciplines, after Nobel Laureate Richard Feynman first described the concept of nanotechnology in a lecture, entitled *There's Plenty of Room at the Bottom*, at an American Physical Society meeting on December 29, 1959. Nanotechnology is defined as the technology where dimensions in the range 0.1-100 nm play a critical role.(1) Today, “nanoscience” has emerged as a multidisciplinary effort, wherein obtaining a fundamental understanding of the chemical, physical and biological properties of nanostructures provides the basis and explosive growth for other scientific and technological developments and promises to deliver functional materials for a variety of applications.(2)

There are two major approaches in terms of the design and construction of nanometer sized materials and devices: "bottom-up" approach and "top-down" approach.(3) In the "bottom-up" approach, materials and devices are designed and made from molecular level components which assemble themselves chemically or physically by principles of molecular recognition and hierarchical assembly processes.(4-13) In the "top-down" approach, objects are constructed from larger entities by slicing or successive cutting of a bulk material.(14-19) Both approaches play very important roles in nanotechnology, and sometimes merge together to fabricate more sophisticated nanomaterials with multi-functions.(20-25) Though the "bottom-up" approach is more often emphasized in nanotechnology due to the better chance it offers to obtain nanostructures with less defects, and more homogeneous chemical composition, it is not a new concept. All the living beings in nature grow by this "bottom-up" approach, by which the molecular self-assembly underlies the construction of biologic macromolecular assemblies in living organisms.(26-29) The cell offers countless examples of functional self-assembly that stimulate scientists to design non-living nanosystems with Nature-mimicking complexity and functionality.(30-34)

Self-assembly and Janus Nanoparticles. Natural nanobiosystems are primarily organic, mainly composed of polypeptides, polynucleic acids, or polysaccharides, each of which is based on the covalent linking of small molecules that program supramolecular (intramolecular and intermolecular) interactions to guide the self-assembly into nanoscopic functional entities.(35) To mimic the same general scheme for the construction of nanostructures, self-assembly of amphiphlic block copolymers is emerging as an elegant, 'bottom-up' method for fabricating nanostructured materials.(36-38) Nanoparticles constructed from synthetic, amphiphilic block copolymers provide the opportunity to control structure both within individual block copolymer nanoparticles as well as between multiple nanoparticles for hierarchical assembly.(39-44) Not only have particles been constructed with unique shapes, such as disks,(45, 46) branched rods,(47) and toroids,(48) but new nanostructures with compositional complexity, or complex nanoparticles, such as anisotropic particles(49) that include patchy,(50, 51) multicompartment,(52-54) and Janus particles,(55) also have been explored.

Janus nanoparticles, named after the double-faced Roman God, whose surfaces have two or more distinct chemical or physical properties.(56) Due to this special non-centrosymmetric surface feature, the preparation of Janus particles, especially nanometer-sized particles, remained challenging for a long time.(57) Inspired by the many selective, hierarchical assembly processes that afford complex materials in Nature, the directional organization of Janus particles into complex structures has attracted much attention. However, the routine ability to build hierarchical superstructures from designed nanoscale building units by controllable inter-nanoparticle association is not yet possible due to the challenges of the fabrication of asymmetrically functionalized nanometer-sized particles equipped with efficient surface chemistries. The fabrication of Janus nanoparticles without anisotropic distributions of efficient chemical functionalities were limitedly reported to be made in two strategies: templating against the flat surfaces and some specially-designed self-assembly.(56, 57)

In the Chapter 2 and 3, two strategies towards the asymmetrically functionalized nanoparticles with anisotropic distribution of azido and thiol or crown ether functionality will be discussed, as shown in **Figure 1-1**.

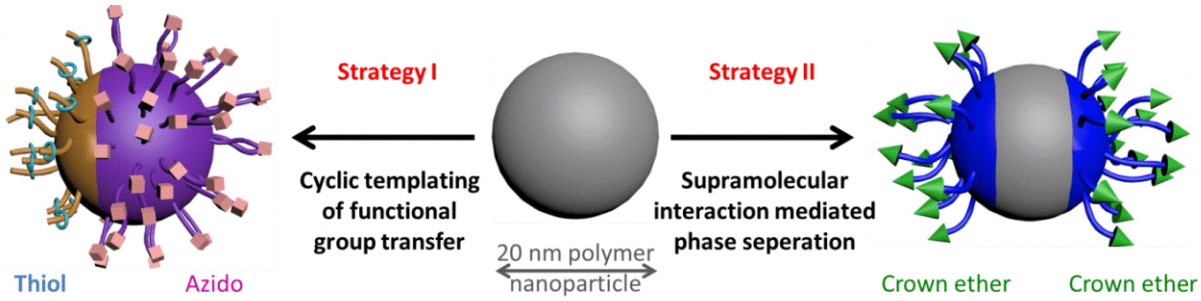

Figure 1-1. Schematic representation of strategies discussed in Chapter 2 and 3.

In the Chapter 2, a robust Janus-faced polymer nanoparticle framework that presents two orthogonally click-reactive surface chemistries, has been generated by a recyclable strategy that involves reactive functional group transfer by templating against gold nanoparticle substrates, as shown in **Figure 1-2**.(58) This anisotropic functionalization approach is compatible with a wide range of soft materials, providing Janus nanoparticles for the construction of dual-functionalized devices by accurately controlling chemical functionality at the nanoscopic level.

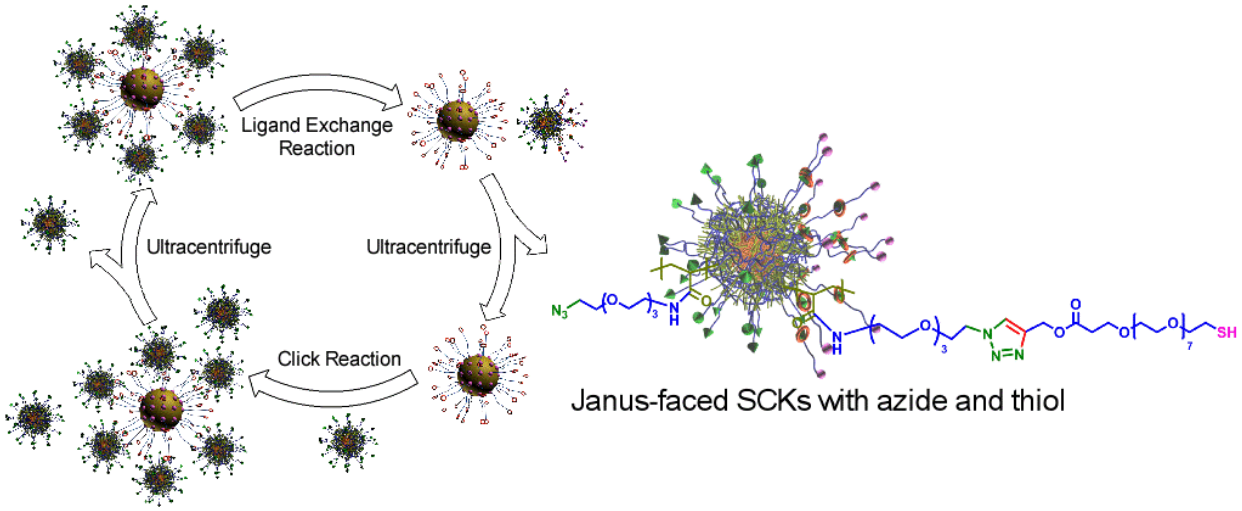

Figure 1-2. Schematic representation of the strategy discussed in Chapter 2.

In the Chapter 3, a hierarchical assembly strategy of utilizing pre-formed block copolymer nanoparticles as building units and regionally-seletive supramolecular interaction, crown ether-ammonium interaction, to assemble into higher-ordered, multicompartment superstructures including 1-D chains, 2-D rings and 3-D aggregates, has been developed, as shown in **Figure 1-3**.(59) This combination of selective chemical modification and kinetically-controlled assembly demonstrates the great potential of complex block copolymer nanoparticles for hierarchical material construction by inter-nanoparticle association.

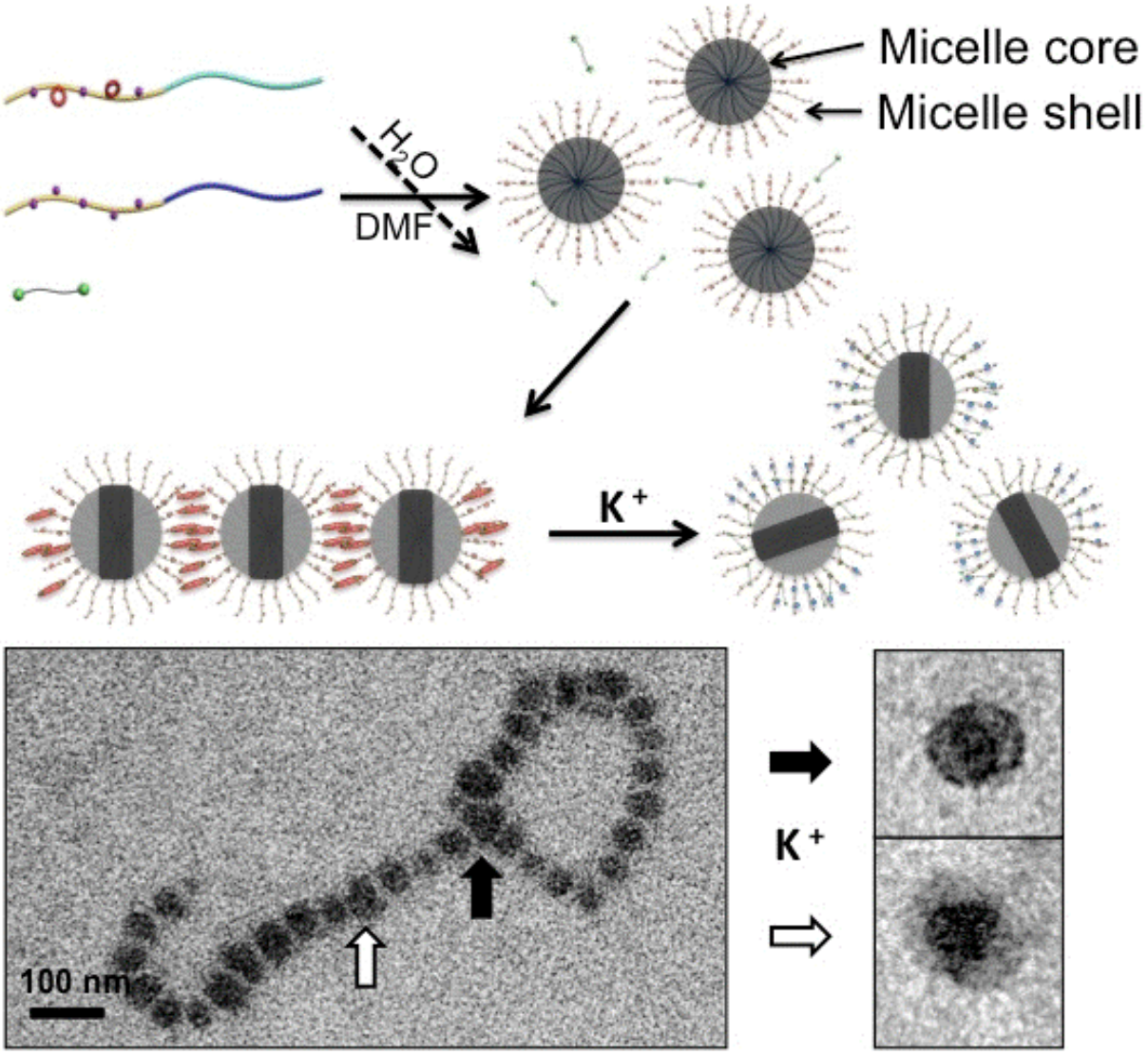

Figure 1-3. Schematic representation of the strategy discussed in Chapter 3.

Well-defined Polymers and Controlled Polymerizations. Among all kinds of synthetic molecules that can undergo self-assembly to form sophisticated nanostrutures,(60) well-defined block copolymers with predetermined properties have attracted significant attention in nanotechnological applications recently, due to the convenient tunability of size, shape, and periodicity afforded by changing their molecular parameters.(61-66) Developments of living or controlled polymerization techniques and post-polymerization functionalization methods have greatly enriched the library of well-defined block

copolymers which could be used, studied and applied for the fabrication of nanomaterials, both in bulk self-assembly and solution self-assembly.(67-73) A variety of polymers with different chemical compositions, narrow molecular weight distributions, controlled architectures and chain-ends functionalities have been synthesized by atom transfer radical polymerization (ATRP),(74, 75) reversible addition-fragmentation chain transfer (RAFT),(76, 77) nitroxide mediated living radical polymerization (NMP),(78, 79) ring-opening metathesis polymerization (ROMP),(80, 81) ring-opening polymerization of cyclic ester monomers (ROP),(67, 82, 83) and N-Carboxyanhydride Polymerization (NCA),(84, 85) and other modern controlled or living polymerization techniques, as shown in **Scheme 1-1**.

Scheme 1-1. (a) General ATRP reaction, X stands for halogen. (b) General RAFT reaction. (c) General NMP reaction. (d) General ROMP reaction, M stands for the ROMP catalyst. (e) General ROP reaction. (f) General NCA reaction.

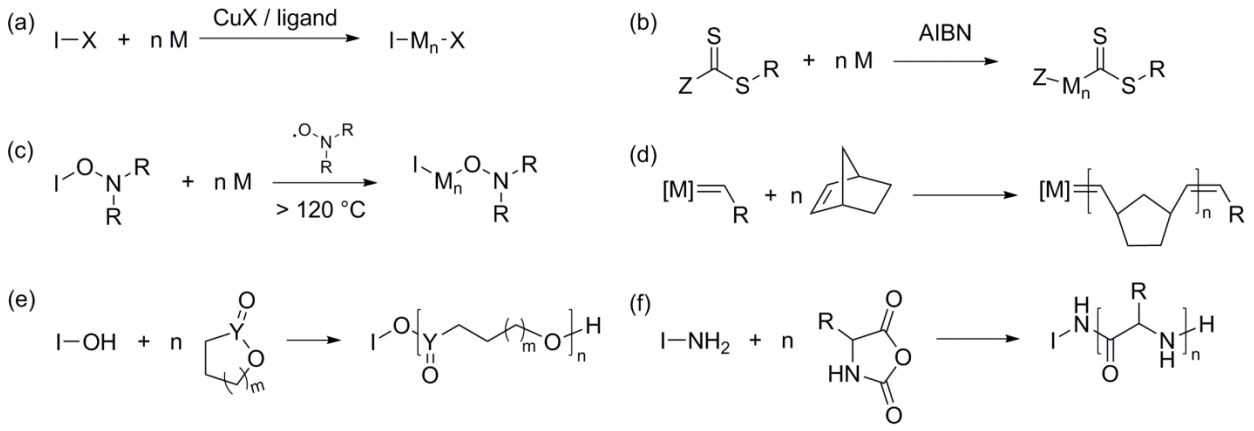

ROP and Polyphosphoesters. Among all kinds of polymerization techniques listed above, ROP of cyclic ester monomers is of particular interest due to the degradability (through enzymatic or hydrolytic degradation processes) and the biological applications of the product polymers.(86) Biodegradable synthetic polymers have been wildly applied for many biomedical applications, for instance in tissue engineering, regenerative medicine, gene therapy, and controlled drug delivery.(87) Organic catalysis in ROP has become a powerful alternative to more traditional metal-based catalysts, because of the

elimination of the usage of environmentally-sensitive metal compounds, to fulfill the requirements of biomedical applications.(88-90) Since the first report of the use of organic small compound 4-dimethylaminopyridine (DMAP) for the ROP of lactide in 2001,(91) the field of organo-catalyzed ROP has rapid grown to the current stage that it now provides a synthetic tool to prepare a large library of high molecular weight degradable polymers, including polyesters,(92-94) polycarbonates,(95-97) polyphosphoesters(98, 99) and others,(100, 101) with the control over the polymer molecular weights, molecular weight distributions, compositions and structures.

Besides polyesters and polycarbonates, polyphosphoesters are attractive for bio-related fields due to their biocompatibility, biodegradability (through hydrolysis that is either spontaneous or catalyzed by certain enzymes), and their structural similarity to nucleic and teichoic acids.(102) Compared with polycarbonates and polyphosphoesters, polyphosphoesters are more easily functionalizable and more water soluble. The functionalities and properties of polyphosphoesters are conveniently controlled by manipulation of pendant groups on the pentavalent phosphorus atom of cyclic phospholane monomer precursors. Early kinetics and thermodynamics studies of both cationic (103) and anionic (104) polymerizations of 2-methoxy-2-oxo-1,3,2-dioxaphosphorinane, the six-membered ring phosphate monomer, suggested that cyclic six-membered phosphate monomers only oligomerized (DP ≤ 10) because the polymerization process was reversible and accompanied by effective chain transfer to the monomer. Due to the more strained five-membered ring of cyclic phospholane monomers, the polymerization of those monomers yielded corresponding high-molecular-weight polymers with a very high monomer conversion. Five-membered ring cyclic phospholane monomers are usually prepared from the condensation of commercially available 2-chloro-2-oxo-1,3,2-dioxaphospholane (COP) and an alcohol. A variety of functional cyclic phospholane monomers have been reported, including methyl,(105) ethyl,(106) isopropyl,(107) PEGylated,(108, 109) hydroxyl-functionalized,(110, 111) protected hydroxyl-functionalized,(112) protected amino-functionalized,(113, 114) protected thiol-functionalized,(115) acrylate-functionalized,(116) methacrylate-functionalized,(117) alkyne-functionalized(118) and alkene-functionalized.(119, 120) The ROP of those functional monomers produced corresponding high

molecular weight functional polyphosphoesters. Due to the hydrogen bonding with water, polyphosphoesters with short side groups were usually water soluble. The hydrophobicity of the polyphosphoester system can be tuned by changing the alkyl side chains of the monomer or by copolymerizing monomers with different alkyl side chains, but the water solubility of alkyl-substituted polyphosphoesters has been typically observed to be temperature dependent.(105, 106)

Nanomedicine. Medical applications of nanotechnology for treatment, diagnosis, monitoring, and control of diseases has recently been defined to as "nanomedicine" by the National Institutes of Health.(121) Nanomedicine is believed to have great potential to turn molecular discoveries arising from genomics and proteomics into widespread benefit for patients who suffered from various diseases.(122-124) Drug delivery, utilizing nanoparticles to improve the bioavailability and pharmacokinetics of therapeutics, has become one of the major biomedical applications of nanomedicine that accounts for three-quarters of the research activity and market.(125) The main focuses of the development of nanoparticles for the drug delivery are to achieve controlled, localized, triggered or targeted drug delivery by tuning the fundamental properties, such as solubility, blood circulation time, toxicity, diffusivity and immunogenicity.(126, 127)

In the past two decades, there has been an explosive expansion of nanoparticles delivered therapeutics in the market and under clinical trials for the treatment of a broad range of diseases including metastatic breast cancer (Genexol-PM®), hepatitis B, hepatitis C (Pegasys®), hepatitis A (Epaxal®), viral infection (Abelcet®, AmBisome®), leukemia (Oncaspar®), influenza (Inflexal V®), viral infection (Abelcet®, AmBisome®), multiple sclerosis (Copaxone®) and many others.(128) All of these applications require sophisticated design of the nanoparticles with different properties to be able to pass different biological barriers such as skin, blood, mucus, extracellular matrix before eventually delivering large amount of payloads through the cellular and subcellular barriers.

The foci of Chapters 4-7 of this dissertation range from the synthesis of functional polyphosphoesters and related polymers by ring-opening polymerization, (Chapter 4 and Chapter 7), to the design of degradable nanoparticle system (Chapter 5) and the biomedical applications of developed nanoparticle systems (Chapter 6).

In Chapters 4-6, two degradable nanoparticle systems based on different functionalized diblock polyphosphoesters and their biomedical applications in treating different diseases, such as pulmonary infections, injuries and cancers, will be discussed, as shown in **Figure 1-4**. The two nanoparticle systems were both derived from an alkyne-functionalized polyphosphoester which was prepared from the organocatalyst-promoted ring-opening polymerization of a stable alkyne-functionalized phospholane monomer, as discussed in the Chapter 4. In the first system, as discussed in the Chapter 5, the easily functionalizable side-chain of polyphosphoester allowed us to prepare a family of polymeric nanoparticles with different surface charge types, non-ionic, anionic, cationic and zwitterionic, in a rapid and versatile manner. The anionic and zwitterionic nanoparticles were designed to load silver ions to treat pulmonary infections, while the cationic nanoparticles were applied to regulate lung injuries by a nanoparticle/siRNA delivery approach. The second system, as discussed in the Chapter 6, highly water soluble backbone of polyphosphoester endowed the first system with ultrahigh paclitaxel loading capacity (55 wt%) and high paclitaxel (PTX) water solubility (6.2 mg/mL PTX in water). The PTX drug conjugates were applied to treat lung cancers. This presentation will discuss the detailed design, synthesis, characterization and applications of those two nanoparticle systems, and will highlight the rapid, efficient and versatile chemistry involved in each stage of the production and utilization of these unique functional polymers and nanomaterials.

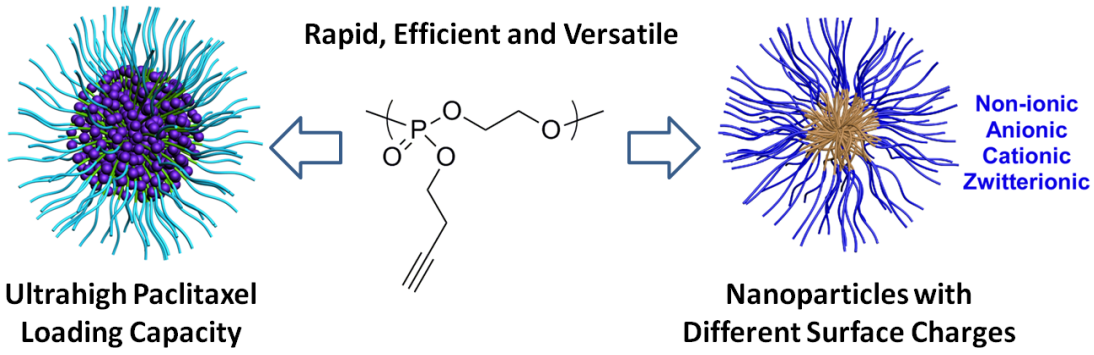

Figure 1-4. Schematic representation of strategies discussed in Chapter 4-6.

In the Chapter 5, azide-alkyne Huisgen cycloaddition and thiol-yne reactions, two classical "click" chemistries, were employed to functionalize biodegradable, clickable polyphosphoester homopolymers and their water-soluble copolymers, as showed in **Figure 1-5**.(116) A stable alkyne-functionalized phospholane monomer was synthesized, its organocatalyzed polymerization kinetics were evaluated, and the resulting (co)polymers were utilized to develop this facile method that provides the synthesis of clickable, water-soluble and degradable polyphosphoesters, which can be adapted for various applications. The polymer and chemistries explored here have been further expanded into many directions towards different biological applications.

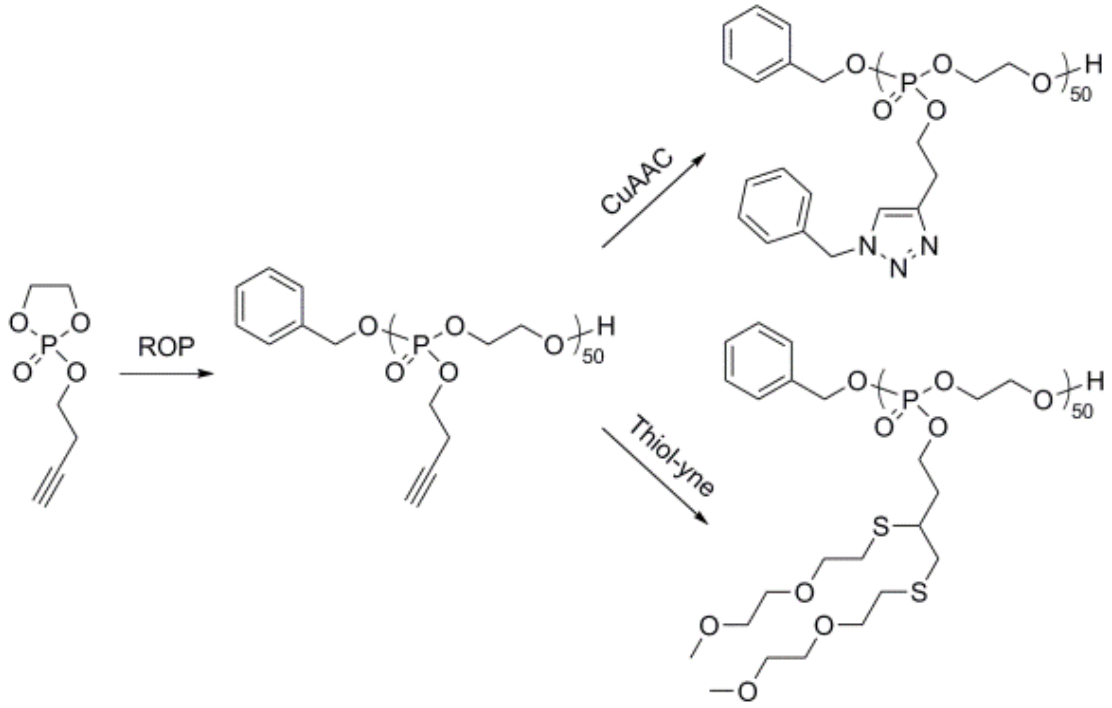

Figure 1-5. Schematic representation of the strategy discussed in Chapter 4.

In the Chapter 5, a retrosynthetic methodology has been used to develop a versatile platform for the rapid construction of a family of polymeric micelles with varying surface charges and functionalities based on biodegradable polyphosphoesters, as shown in Figure **1-6**.(129) Currently, this degradable nanoparticle family is being applied to various bio-applications. The applications of this degradable nanoparticles family are covered in this dissertation, but will be discussed in the defense talk and presented in the latter manuscripts.

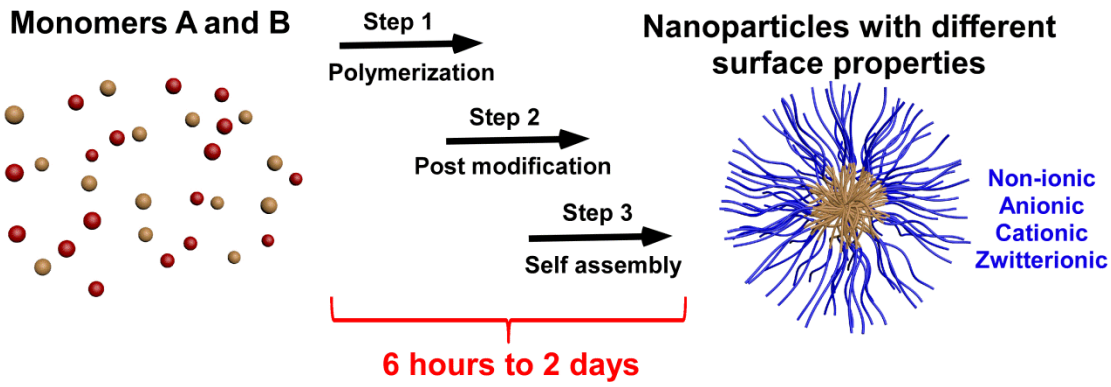

Figure 1-6. Schematic representation of the strategy discussed in Chapter 5.

In the Chapter 6, a new type of degradable, nanoscopic polymer assembly containing ultra-high levels of drug loading *via* covalent attachment within amphiphilic core-shell nanoparticle morphology has been generated as an effective and safe anti-cancer agent, as shown in **Figure 1-7**. The PEO-*b*-PPE-*g*-PTX formed well-defined micelles in aqueous solution, with a PTX loading capacity as high as 65 *wt*%, and a maximum PTX concentration of 6.2 mg/mL in water, which is 25000-fold higher than the aqueous solubility of free PTX.

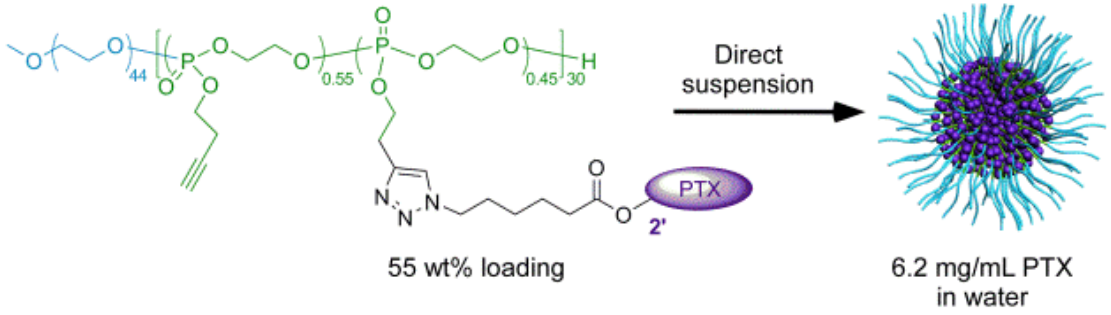

Figure 1-7. Schematic representation of the strategy discussed in Chapter 6.

In the Chapter 7, an acid-labile polyphosphoramidate was prepared by direct organo-base catalyzed ring-opening polymerization of cyclic phospholane amidate monomer. The cleavage of acid-labile phosphoramidate bond on polyphosphoramidate was evaluated at different acidic pH solutions, and the complete side chain cleavage produced another type of polymer, polyphosphoester ionomer, as shown in **Figure 1-8**. This methodology developed here has enriched the family of degradable polymers synthesized by organo-catalyzed ring-opening polymers and provided two novel polymer structures with numerous potential applications.

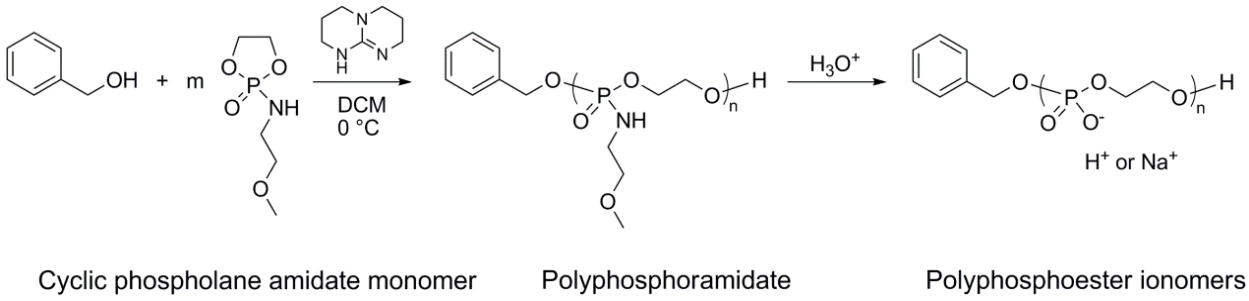

Figure 1-8. Schematic representation of the strategy discussed in Chapter 7.

The following chapters of this dissertation will discuss the detailed design, preparation, characterization and applications of those systems for the rapid, efficient and versatile preparation of functionally sophisticated polymers and nanoparticles.

Reference:

(1) Franks, A. *J Phys E Sci Instrum* **1987**, *20*, 1442.

(2) Nayak, S.; Lyon, L. A. *Angew Chem Int Edit* **2005**, *44*, 7686.

(3) Rabe, K. M. *Nat Nanotechnol* **2006**, *1*, 171.

(4) Shimomura, M.; Sawadaishi, T. *Curr Opin Colloid In* **2001**, *6*, 11.

(5) Sada, K.; Takeuchi, M.; Fujita, N.; Numata, M.; Shinkai, S. *Chem Soc Rev* **2007**, *36*, 415.

(6) Lu, W.; Lieber, C. M. *Nat Mater* **2007**, *6*, 841.

(7) Xu, H.; Srivastava, S.; Rotello, V. A. *Adv Polym Sci* **2007**, *207*, 179.

(8) LoPresti, C.; Lomas, H.; Massignani, M.; Smart, T.; Battaglia, G. *J Mater Chem* **2009**, *19*, 3576.

(9) Ariga, K.; Nakanishi, T.; Hill, J. P. *Curr Opin Colloid In* **2007**, *12*, 106.

(10) Senaratne, W.; Andruzzi, L.; Ober, C. K. *Biomacromolecules* **2005**, *6*, 2427.

(11) Nie, Z. H.; Kumacheva, E. *Nat Mater* **2008**, *7*, 277.

(12) Murugavel, R.; Walawalkar, M. G.; Dan, M.; Roesky, H. W.; Rao, C. N. R. *Accounts Chem Res* **2004**, *37*, 763.

(13) Ariga, K.; Ji, Q. M.; Hill, J. P.; Kawazoe, N.; Chen, G. P. *Expert Opin Biol Th* **2009**, *9*, 307.

(14) Heule, M.; Vuillemin, S.; Gauckler, L. J. *Adv Mater* **2003**, *15*, 1237.

(15) Salaita, K.; Wang, Y. H.; Mirkin, C. A. *Nat Nanotechnol* **2007**, *2*, 145.

(16) Randall, C. L.; Leong, T. G.; Bassik, N.; Gracias, D. H. *Adv Drug Deliver Rev* **2007**, *59*, 1547.

(17) Wang, X. R.; Dai, H. J. *Nat Chem* **2010**, *2*, 661.

(18) Wang, M. F.; Raghunathan, N.; Ziaie, B. *Langmuir* **2007**, *23*, 2300.

(19) Nakaji, K.; Li, H.; Kiba, T.; Igarashi, M.; Samukawa, S.; Murayama, A. *Nanoscale Res Lett* **2012**, *7*.

(20) Hawker, C. J.; Russell, T. P. *Mrs Bull* **2005**, *30*, 952.

(21) Cheng, J. Y.; Ross, C. A.; Smith, H. I.; Thomas, E. L. *Adv Mater* **2006**, *18*, 2505.

(22) Bang, J.; Jeong, U.; Ryu, D. Y.; Russell, T. P.; Hawker, C. J. *Adv Mater* **2009**, *21*, 4769.

(23) Segalman, R. A. *Science* **2008**, *321*, 919.

(24) Darling, S. B. *Prog Polym Sci* **2007**, *32*, 1152.

(25) Ambrosi, M.; Fratini, E. L.; Canton, P.; Dankesreiter, S.; Baglioni, P. *J Mater Chem* **2012**, *22*, 23497.

(26) Tu, R. S.; Tirrell, M. *Adv Drug Deliver Rev* **2004**, *56*, 1537.

(27) Kowalczyk, S. W.; Blosser, T. R.; Dekker, C. *Trends Biotechnol* **2011**, *29*, 607.

(28) Saito, A. *Sci Technol Adv Mat* **2011**, *12*.

(29) Whitesides, G. M.; Grzybowski, B. *Science* **2002**, *295*, 2418.

(30) Meyers, M. A.; Chen, P. Y.; Lin, A. Y. M.; Seki, Y. *Prog Mater Sci* **2008**, *53*, 1.

(31) Barron, A. E.; Zuckermann, R. N. *Curr Opin Chem Biol* **1999**, *3*, 681.

(32) Lee, K.; Wagermaier, W.; Masic, A.; Kommareddy, K. P.; Bennet, M.; Manjubala, I.; Lee, S. W.; Park, S. B.; Colfen, H.; Fratzl, P. *Nat Commun* **2012**, *3*.

(33) Lu, Y.; Dong, L.; Zhang, L. C.; Su, Y. D.; Yu, S. H. *Nano Today* **2012**, *7*, 297.

(34) Cui, Y.; Kim, S. N.; Naik, R. R.; Mcalpine, M. C. *Accounts Chem Res* **2012**, *45*, 696.

(35) Elsabahy, M.; Wooley, K. L. *J Polym Sci Pol Chem* **2012**, *50*, 1869.

(36) Elsabahy, M.; Wooley, K. L. *Chem Soc Rev* **2012**, *41*, 2545.

(37) Meyers, M. A.; Chen, P. Y.; Lopez, M. I.; Seki, Y.; Lin, A. Y. M. *J Mech Behav Biomed* **2011**, *4*, 626.

(38) Chen, P. Y.; McKittrick, J.; Meyers, M. A. *Prog Mater Sci* **2012**, *57*, 1492.

(39) Zhang, L. F.; Eisenberg, A. *Science* **1995**, *268*, 1728.

(40) Discher, B. M.; Won, Y. Y.; Ege, D. S.; Lee, J. C. M.; Bates, F. S.; Discher, D. E.; Hammer, D. A. *Science* **1999**, *284*, 1143.

(41) Jain, S.; Bates, F. S. *Science* **2003**, *300*, 460.

(42) Cui, H. G.; Chen, Z. Y.; Zhong, S.; Wooley, K. L.; Pochan, D. J. *Science* **2007**, *317*, 647.

(43) Wang, X. S.; Guerin, G.; Wang, H.; Wang, Y. S.; Manners, I.; Winnik, M. A. *Science* **2007**, *317*, 644.

(44) Groschel, A. H.; Schacher, F. H.; Schmalz, H.; Borisov, O. V.; Zhulina, E. B.; Walther, A.; Muller, A. H. E. *Nat Commun* **2012**, *3*.

(45) Edmonds, W. F.; Li, Z. B.; Hillmyer, M. A.; Lodge, T. P. *Macromolecules* **2006**, *39*, 4526.

(46) Yin, L. G.; Hillmyer, M. A. *Macromolecules* **2011**, *44*, 3021.

(47) Li, Z. B.; Chen, Z. Y.; Cui, H. G.; Hales, K.; Wooley, K. L.; Pochan, D. J. *Langmuir* **2007**, *23*, 4689.

(48) Pochan, D. J.; Chen, Z. Y.; Cui, H. G.; Hales, K.; Qi, K.; Wooley, K. L. *Science* **2004**, *306*, 94.

(49) Du, J.; O'Reilly, R. K. *Chem Soc Rev* **2011**, *40*, 2402.

(50) Du, J. Z.; Chen, Y. M. *Angew Chem Int Edit* **2004**, *43*, 5084.

(51) Christian, D. A.; Tian, A. W.; Ellenbroek, W. G.; Levental, I.; Rajagopal, K.; Janmey, P. A.; Liu, A. J.; Baumgart, T.; Discher, D. E. *Nat Mater* **2009**, *8*, 843.

(52) Li, Z. B.; Hillmyer, M. A.; Lodge, T. P. *Macromolecules* **2006**, *39*, 765.

(53) Dupont, J.; Liu, G. *Soft Matter* **2010**, *6*, 3654.

(54) Pochan, D. J.; Zhu, J. H.; Zhang, K.; Wooley, K. L.; Miesch, C.; Emrick, T. *Soft Matter* **2011**, *7*, 2500.

(55) Walther, A.; Muller, A. H. E. *Soft Matter* **2008**, *4*, 663.

(56) Li, F.; Josephson, D. P.; Stein, A. *Angew Chem Int Edit* **2011**, *50*, 360.

(57) Lattuada, M.; Hatton, T. A. *Nano Today* **2011**, *6*, 286.

(58) Zhang, S. Y.; Li, Z.; Samarajeewa, S.; Sun, G. R.; Yang, C.; Wooley, K. L. *J Am Chem Soc* **2011**, *133*, 11046.

(59) Zhu, J.; Zhang, S.; Zhang, F.; Wooley, K. L.; Pochan, D. J. *Advanced Functional Materials* **2013**, DOI: 10.1002/adfm.201202323.

(60) Whitesides, G. M.; Mathias, J. P.; Seto, C. T. *Science* **1991**, *254*, 1312.

(61) Xia, Y. N.; Whitesides, G. M. *Annu Rev Mater Sci* **1998**, *28*, 153.

(62) Riess, G. *Prog Polym Sci* **2003**, *28*, 1107.

(63) Park, C.; Yoon, J.; Thomas, E. L. *Polymer* **2003**, *44*, 7779.

(64) Stuparu, M. C.; Khan, A.; Hawker, C. J. *Polym Chem-Uk* **2012**, *3*, 3033.

(65) Li, S. L.; Xiao, T. X.; Lin, C.; Wang, L. Y. *Chem Soc Rev* **2012**, *41*, 5950.

(66) Paul, D. R.; Robeson, L. M. *Polymer* **2008**, *49*, 3187.

(67) Dechy-Cabaret, O.; Martin-Vaca, B.; Bourissou, D. *Chem Rev* **2004**, *104*, 6147.

(68) Patten, T. E.; Matyjaszewski, K. *Adv Mater* **1998**, *10*, 901.

(69) Hawker, C. J.; Wooley, K. L. *Science* **2005**, *309*, 1200.

(70) Kobayashi, S.; Uyama, H.; Kimura, S. *Chem Rev* **2001**, *101*, 3793.

(71) Asua, J. M. *Prog Polym Sci* **2002**, *27*, 1283.

(72) Gunay, K. A.; Theato, P.; Klok, H. A. *J Polym Sci Pol Chem* **2013**, *51*, 1.

(73) Coulembier, O.; Degee, P.; Hedrick, J. L.; Dubois, P. *Prog Polym Sci* **2006**, *31*, 723.

(74) Wang, J. S.; Matyjaszewski, K. *J Am Chem Soc* **1995**, *117*, 5614.

(75) Braunecker, W. A.; Matyjaszewski, K. *Prog Polym Sci* **2007**, *32*, 93.

(76) Chiefari, J.; Chong, Y. K.; Ercole, F.; Krstina, J.; Jeffery, J.; Le, T. P. T.; Mayadunne, R. T. A.; Meijs, G. F.; Moad, C. L.; Moad, G.; Rizzardo, E.; Thang, S. H. *Macromolecules* **1998**, *31*, 5559.

(77) Moad, G.; Rizzardo, E.; Thang, S. H. *Aust J Chem* **2005**, *58*, 379.

(78) Hawker, C. J.; Barclay, G. G.; Orellana, A.; Dao, J.; Devonport, W. *Macromolecules* **1996**, *29*, 5245.

(79) Hawker, C. J.; Bosman, A. W.; Harth, E. *Chem Rev* **2001**, *101*, 3661.

(80) Schrock, R. R. *Accounts Chem Res* **1990**, *23*, 158.

(81) Bielawski, C. W.; Grubbs, R. H. *Angew Chem Int Edit* **2000**, *39*, 2903.

(82) Albertsson, A. C.; Varma, I. K. *Biomacromolecules* **2003**, *4*, 1466.

(83) O'Keefe, B. J.; Hillmyer, M. A.; Tolman, W. B. *J Chem Soc Dalton* **2001**, 2215.

(84) Kukula, H.; Schlaad, H.; Antonietti, M.; Forster, S. *J Am Chem Soc* **2002**, *124*, 1658.

(85) Deming, T. J. *J Polym Sci Pol Chem* **2000**, *38*, 3011.

(86) Nair, L. S.; Laurencin, C. T. *Prog Polym Sci* **2007**, *32*, 762.

(87) Tian, H. Y.; Tang, Z. H.; Zhuang, X. L.; Chen, X. S.; Jing, X. B. *Prog Polym Sci* **2012**, *37*, 237.

(88) Kamber, N. E.; Jeong, W.; Waymouth, R. M.; Pratt, R. C.; Lohmeijer, B. G. G.; Hedrick, J. L. *Chem Rev* **2007**, *107*, 5813.

(89) Kiesewetter, M. K.; Shin, E. J.; Hedrick, J. L.; Waymouth, R. M. *Macromolecules* **2010**, *43*, 2093.

(90) Dove, A. P. *Acs Macro Lett* **2012**, *1*, 1409.

(91) Nederberg, F.; Connor, E. F.; Moller, M.; Glauser, T.; Hedrick, J. L. *Angew Chem Int Edit* **2001**, *40*, 2712.

(92) Coulembier, O.; Mespouille, L.; Hedrick, J. L.; Waymouth, R. M.; Dubois, P. *Macromolecules* **2006**, *39*, 4001.

(93) Pounder, R. J.; Fox, D. J.; Barker, I. A.; Bennison, M. J.; Dove, A. P. *Polym Chem-Uk* **2011**, *2*, 2204.

(94) Jeong, W.; Shin, E. J.; Culkin, D. A.; Hedrick, J. L.; Waymouth, R. M. *J Am Chem Soc* **2009**, *131*, 4884.

(95) Nederberg, F.; Lohmeijer, B. G. G.; Leibfarth, F.; Pratt, R. C.; Choi, J.; Dove, A. P.; Waymouth, R. M.; Hedrick, J. L. *Biomacromolecules* **2007**, *8*, 153.

(96) Tempelaar, S.; Mespouille, L.; Coulembier, O.; Dubois, P.; Dove, A. P. *Chem Soc Rev* **2013**, *42*, 1312.

(97) Sanders, D. P.; Fukushima, K.; Coady, D. J.; Nelson, A.; Fujiwara, M.; Yasumoto, M.; Hedrick, J. L. *J Am Chem Soc* **2010**, *132*, 14724.

(98) Iwasaki, Y.; Yamaguchi, E. *Macromolecules* **2010**, *43*, 2664.

(99) Clement, B.; Grignard, B.; Koole, L.; Jerome, C.; Lecomte, P. *Macromolecules* **2012**, *45*, 4476.

(100) Raynaud, J.; Absalon, C.; Gnanou, Y.; Taton, D. *J Am Chem Soc* **2009**, *131*, 3201.

(101) Lohmeijer, B. G. G.; Dubois, G.; Leibfarth, F.; Pratt, R. C.; Nederberg, F.; Nelson, A.; Waymouth, R. M.; Wade, C.; Hedrick, J. L. *Org Lett* **2006**, *8*, 4683.

(102) Wang, Y. C.; Yuan, Y. Y.; Du, J. Z.; Yang, X. Z.; Wang, J. *Macromol Biosci* **2009**, *9*, 1154.

(103) Lapienis, G.; Penczek, S. *Macromolecules* **1977**, *10*, 1301

(104) Lapienis, G.; Penczek, S. *J. of Polym. Sci.: Part A: Polym. Chem.* **1977**, *15*, 371

(105) Wang, Y. C.; Li, Y.; Yang, X. Z.; Yuan, Y. Y.; Yan, L. F.; Wang, J. *Macromolecules* **2009**, *42*, 3026.

(106) Iwasaki, Y.; Wachiralarpphaithoon, C.; Akiyoshi, K. *Macromolecules* **2007**, *40*, 8136.

(107) Iwasaki, Y.; Nakagawa, C.; Ohtomi, M.; Ishihara, K.; Akiyoshi, K. *Biomacromolecules* **2004**, *5*, 1110.

(108) Du, J. Z.; Chen, D. P.; Wang, Y. C.; Xiao, C. S.; Lu, Y. J.; Wang, J.; Zhang, G. Z. *Biomacromolecules* **2006**, *7*, 1898.

(109) Zhu, W. P.; Sun, S.; Xu, N.; Gou, P. F.; Shen, Z. Q. *J Appl Polym Sci* **2012**, *123*, 365.

(110) Liu, J. Y.; Huang, W.; Pang, Y.; Zhu, X. Y.; Zhou, Y. F.; Yan, D. Y. *Biomaterials* **2010**, *31*, 5643.

(111) Liu, J. Y.; Pang, Y.; Huang, W.; Zhu, Z. Y.; Zhu, X. Y.; Zhou, Y. F.; Yan, D. Y. *Biomacromolecules* **2011**, *12*, 2407.

(112) Song, W. J.; Du, J. Z.; Liu, N. J.; Dou, S.; Cheng, J.; Wang, J. *Macromolecules* **2008**, *41*, 6935.

(113) Sun, T. M.; Du, J. Z.; Yan, L. F.; Mao, H. Q.; Wang, J. *Biomaterials* **2008**, *29*, 4348.

(114) Sun, T. M.; Du, J. Z.; Yao, Y. D.; Mao, C. Q.; Dou, S.; Huang, S. Y.; Zhang, P. Z.; Leong, K. W.; Song, E. W.; Wang, J. *Acs Nano* **2011**, *5*, 1483.

(115) Wang, Y. C.; Li, Y.; Sun, T. M.; Xiong, M. H.; Wu, J. A.; Yang, Y. Y.; Wang, J. *Macromol Rapid Comm* **2010**, *31*, 1201.

(116) Shao, H.; Zhang, M.; He, J.; Ni, P. *Polymer* **2012**, *53*, 2854.

(117) Wachiralarpphaithoon, C.; Iwasaki, Y.; Akiyoshi, K. *Biomaterials* **2007**, *28*, 984.

(118) Zhang, S. Y.; Li, A.; Zou, J.; Lin, L. Y.; Wooley, K. L. *Acs Macro Lett* **2012**, *1*, 328.

(119) Clément, B.; Grignard, B.; Koole, L.; Jérôme, C.; Lecomte, P. *Macromolecules* **2012**, *45*, 4476.

(120) Du, J. Z.; Du, X. J.; Mao, C. Q.; Wang, J. *J Am Chem Soc* **2011**, *133*, 17560.

(121) Moghimi, S. M.; Hunter, A. C.; Murray, J. C. *Faseb J* **2005**, *19*, 311.

(122) Astruc, D.; Boisselier, E.; Ornelas, C. *Chem Rev* **2010**, *110*, 1857.

(123) Nasongkla, N.; Bey, E.; Ren, J. M.; Ai, H.; Khemtong, C.; Guthi, J. S.; Chin, S. F.; Sherry, A. D.; Boothman, D. A.; Gao, J. M. *Nano Lett* **2006**, *6*, 2427.

(124) Torchilin, V. P. *Adv Drug Deliver Rev* **2012**, *64*, 302.

(125) Wagner, V.; Dullaart, A.; Bock, A. K.; Zweck, A. *Nat Biotechnol* **2006**, *24*, 1211.

(126) Kataoka, K.; Harada, A.; Nagasaki, Y. *Adv Drug Deliver Rev* **2001**, *47*, 113.

(127) Langer, R. *Nature* **1998**, *392*, 5.

(128) Zhang, L.; Gu, F. X.; Chan, J. M.; Wang, A. Z.; Langer, R. S.; Farokhzad, O. C. *Clin Pharmacol Ther* **2008**, *83*, 761.

(129) Zhang, S. Y.; Zou, J.; Zhang, F. W.; Elsabahy, M.; Felder, S. E.; Zhu, J. H.; Pochan, D. J.; Wooley, K. L. *J Am Chem Soc* **2012**, *134*, 18467.

Chapter 2

Orthogonally dual-clickable Janus nanoparticles *via* a cyclic templating strategy

[Portions of this work have been published previously as Shiyi Zhang, Zhou Li, Sandani Samarajeewa, Guorong Sun, Chao Yang and Karen L. Wooley, *J. Am. Chem. Soc.* **2011**, *133*, 11046–11049]

Abstract

Synthetic asymmetrical systems, Janus particles and patchy particles, are capable of undergoing hierarchical assembly processes that mimic those of Nature, to serve as switchable devices, optical probes, phase-transfer catalysts and multi-functional drug carriers, each of which benefits from opposing surface patterns behaving differently. Production of nanometer-sized Janus particles that are equipped with efficient chemistries remains a challenge. A robust Janus-faced polymer nanoparticle framework that presents two orthogonally click-reactive surface chemistries, has been generated by a recyclable strategy that involves reactive functional group transfer by templating against gold nanoparticle substrates. This anisotropic functionalization approach is compatible with a wide range of soft materials, providing Janus nanoparticles for the construction of dual-functionalized devices by accurately controlling chemical functionality at the nanoscopic level.

Introduction

Inspired by the many selective, hierarchical assembly processes that afford complex materials in Nature, the directional organization of Janus particles into complex structures has attracted much attention.(1,2) Beyond fundamental studies, the differentiation of chemistries across the surface regions of Janus nanoparticles could lead to their development as components in the construction of switchable devices,(3) optical probes,(4) phase-transfer catalysts,(5) multi-functional drug carriers,(6) and other applications, each of which could benefit from the different surface functionalities being featured in an efficient and orthogonal way.(7) During the past decade, “click chemistry”(8) has provided a library of chemical

reactions for the preparation and functionalization of new soft materials, based on robust, efficient, and orthogonal chemistries.(9) At the current stage, limited approaches are available for the production of microscopic Janus particles carrying one kind of click chemistry for efficient chemical modification.(10,11) As we have a keen interest in highly complex nanomaterials, we have developed an economically-efficient, cyclic strategy to produce nanoscopic Janus particles that bear two kinds of clickable surface functional groups (thiol and azide), while also being comprised of an amphiphilic core-shell morphology, illustrated in **Fig. 2-1, A**. Therefore, the differentiations of chemistry proceed about the external surface of the nanoparticles and also concentrically within their internal region.

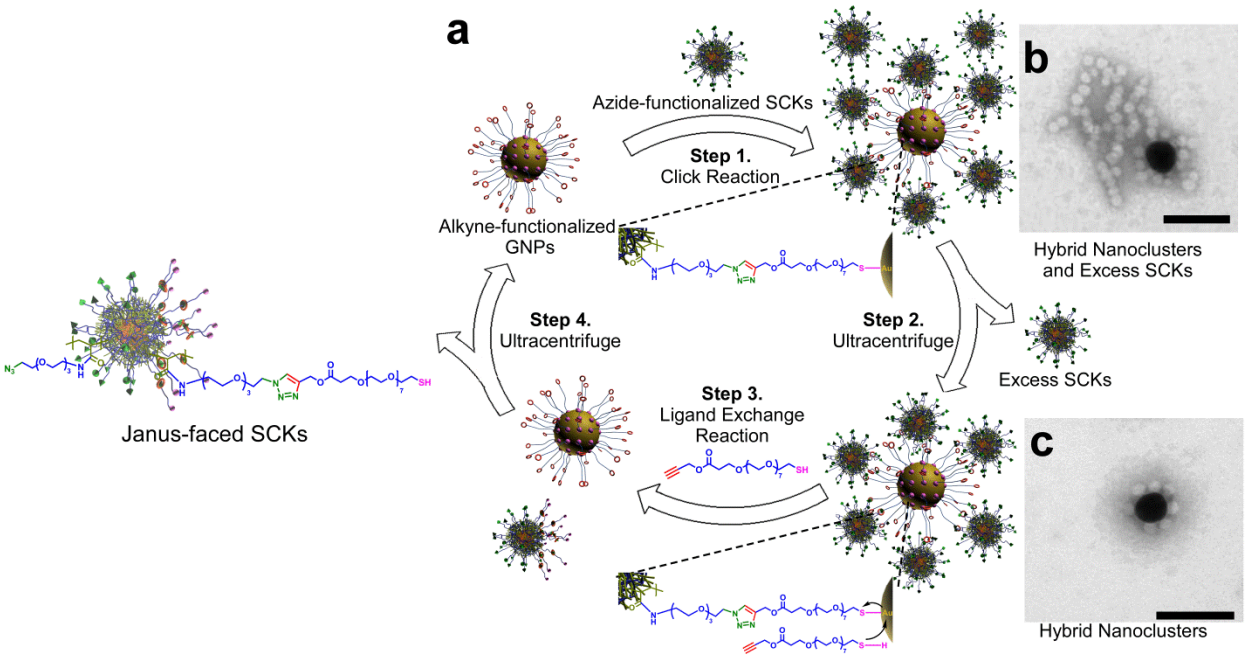

Figure 2-1. a, Schematic representation of the overall strategy. b, TEM image of hybrid nanoclusters, consisting of one GNP surrounded by several SCKs, and an excess of SCKs, after the first step click reaction. c, TEM image of isolated hybrid nanoclusters after removal of unbound SCKs by ultracentrifugation. Scale bars: 100 nm.

The cyclic nano-patterning process involved covalent attachment of pre-established amphiphilic core-shell polymer nanoparticles (shell crosslinked knedel-like (SCK) nanoparticles) onto inorganic

nanoparticle substrates, followed by their displacement by a manner that resulted in the chemical modification of the contact portion of the SCKs, with coincident regeneration of the template (**Figure 2-1 a**). In the first step of this cycle, the uniformly azide-functionalized polymer nanoparticles (D_n = 22 $\pm$ 3 nm) were attached onto alkyne-functionalized gold nanoparticles (GNPs) (D_n = 46 $\pm$ 6 nm) to form hybrid nanoclusters by aqueous click reactions (**Figure 2-1 b**). After separation (step 2, **Figure 2-1 c**), the SCKs were detached from the GNPs with the assistance of ligand exchange by breaking the Au-S bonds (step 3) and replacing the consumed alkynyl ligands. The resulting azide-functionalized SCKs contained a patch of thiol groups (with the possibility of residual azides also being present within this templated domain); meanwhile, the alkyne-functionalized GNPs were recovered and recycled as multi-use nano-templates (step 4). The anisotropic distribution of thiol groups on the SCK surfaces and the orthogonality of the two clickable functionalities were then demonstrated.

Results and Discussion

By our approach, preparation of the Janus nanoparticles within the desymmetrization cycle, in which thiol groups were introduced onto one surface of the azide-functionalized SCKs by covalent transfer of alkyne-oligo(ethylene oxide)-thiol units from the GNPs, required establishment of each of the GNP template and the functionalizable SCK. The alkyne-OEO-thiol-functionalized GNPs that serve as the clickable template were prepared (**Scheme. 2-1 a**) according to a previously reported well-established protocol.(12) We also prepared its counterpart (see experimental), the azide-functionalized SCKs (**Scheme. 2-1 b**) through self assembly of amphiphilic poly(acrylic acid)-*block*-polystyrene (PAA_{105}-*b*-PS_{135}) block copolymers in water, followed by azide functionalization and intra-micellar crosslinking. The post-micellization chemical modification technique using hydrophilic ethyleneoxy repeating units of 11-azido-3,6,9-trioxaundecan-1-amine was chosen to increase the flexibility and availability of azide functionalities on the surface of the micelles and SCKs. Azide-functionalized micelles were then crosslinked, to afford the robust SCKs, which are stable,(13) biocompatible,(14) and capable of being loaded with hydrophobic guest molecules for controlled release purposes.(15)

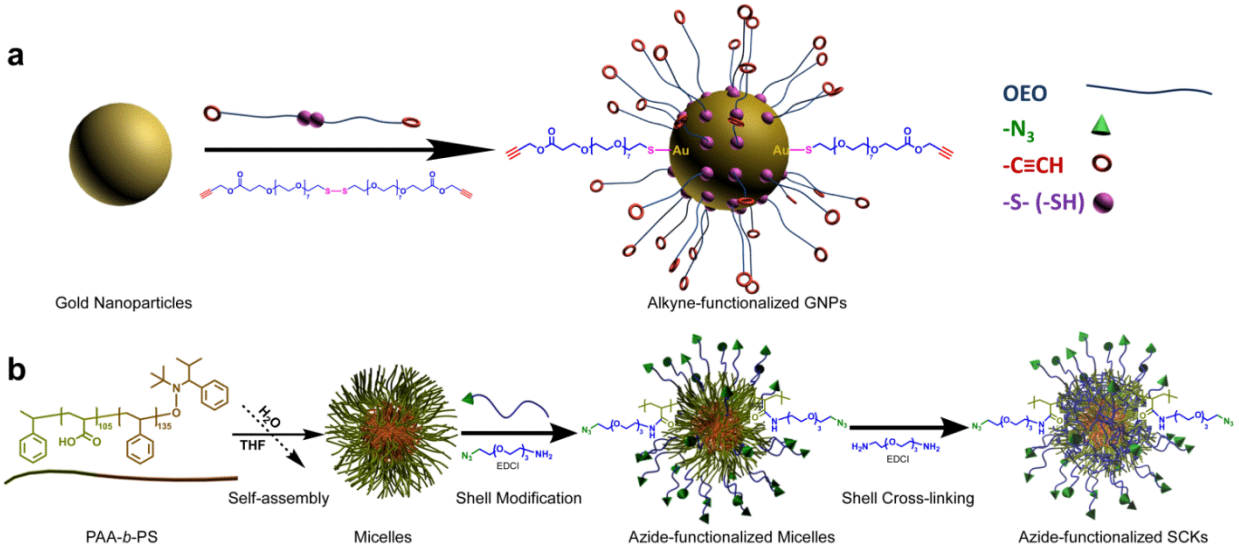

Scheme 2-1. a, Preparation of alkyne-functionalized gold nanoparticle templates. b, Preparation of azide-functionalized SCKs.

Although click chemistry has been widely used in bio- and nano-science technologies, there are few examples(16) in which two kinds of nanoparticles act as substrates. Click reactions carried out between azide-functionalized SCKs and alkyne-functionalized GNPs represent a new direction to engineer surface-functionalized nanostructures toward tailor-made complex architectures with hybrid composites in the field of nanotechnology. Due to the multi-functional nature of the two nanoparticle surfaces, crosslinked networks were generated initially by Cu-catalyzed azide/alkyne cycloaddition (CuAAC) reactions (**Figure 2-2**). For instance, visible precipitation was observed when a near 1:1 ratio of clickable nanoparticles was allowed to undergo reaction, whereas interparticle crosslinking was suppressed when the feed ratio of SCKs to GNPs was increased to *ca*. 500:1. As a result, those SCKs that were attached to GNPs had only one surface binding to the GNPs. The transmission electron microscopy (TEM) images clearly showed hybrid nanocluster satellite structures,(17) consisting of one GNP surrounded by several SCKs, together with populations of unbound SCKs (**Figure 2-1b**). It is noteworthy that the binding

capacity of SCKs onto GNPs allows for production of dual-clickable Janus SCKs at levels that far exceed the quantity of materials and cyclability than could be achieved on a planar two-dimensional substrate.[18] It is calculated that as many as 27 SCKs can be accommodated onto each GNP, according to the geometry and relative size of these two particles (**Figure 2-3**). The hybrid nanoclusters could be isolated from unbound SCKs by ultracentrifugation (**Figure 2-1 c** and **Figure 2-4**, **2-5**). The recovered SCKs were then collected and purified by dialysis for recycling.

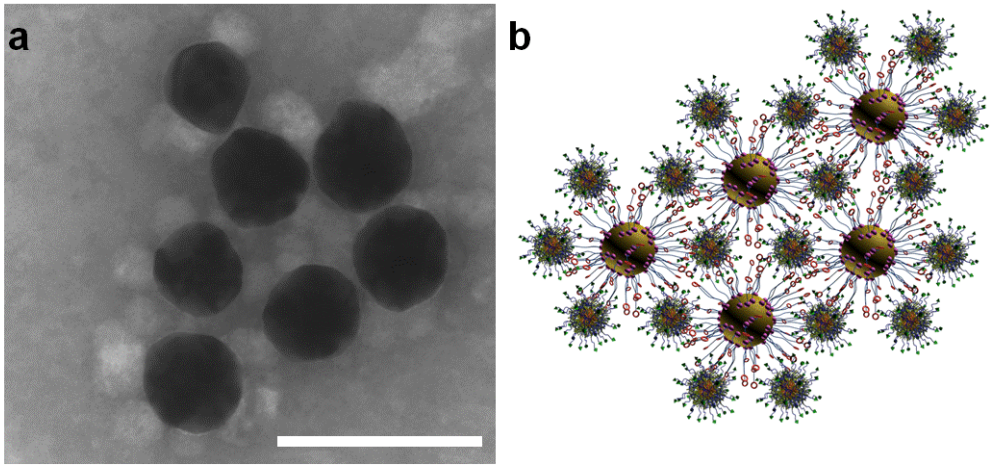

Figure 2-2. Hybrid crosslinked network. a, TEM image of hybrid crosslinked network made from azide-functionalized SCKs and alkyne-functionalized GNPs in near 1:1 ratio. Scale bar: 100 nm. b, Schematic representation of hybrid crosslinked network of GNPs and SCKs.

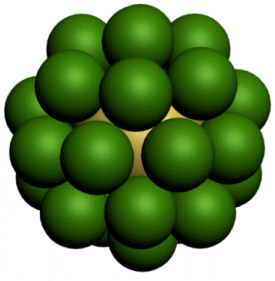

Figure 2-3. Schematic illustration of 27 SCKs (with a diameter of 28 nm) packing at the surface of one GNP (with a diameter of 53 nm) based on "hard sphere" surface contacts. Using the angle (40.4°)

between two adjacent circles of radius 28 on the surface of a circle radius 53, the maximum number of smaller spheres that can be packed on the surface of the larger sphere is 27. Sloane, N. J. A.; Hardin, R. H.; Smith, W. D., and others. Spherical Codes. http://www2.research.att.com/~njas/packings/ (accessed January 2011).

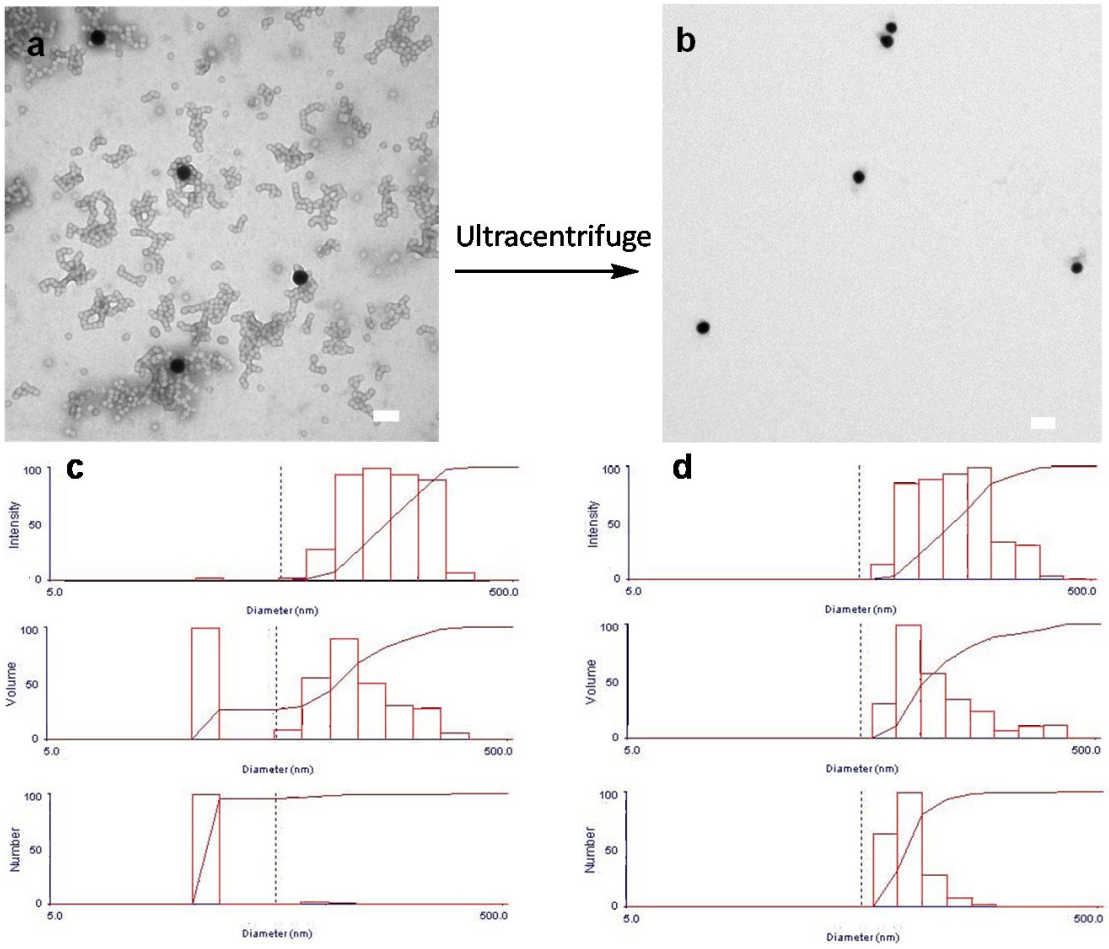

Figure 2-4. a, TEM image of hybrid nanoclusters, consisting of one GNP surrounded by several SCKs, and an excess of SCKs. b, TEM image of isolated hybrid nanoclusters after ultracentrifuge. Scale bars: 100 nm. c, DLS results of hybrid nanoclusters formed after click reaction. The number distribution plot shows that there is only a small portion of hybrid nanoclusters. d, DLS results of hybrid nanoclusters isolated by ultracentrifugation. The number distribution plot confirms successful removal of unbound SCKs.

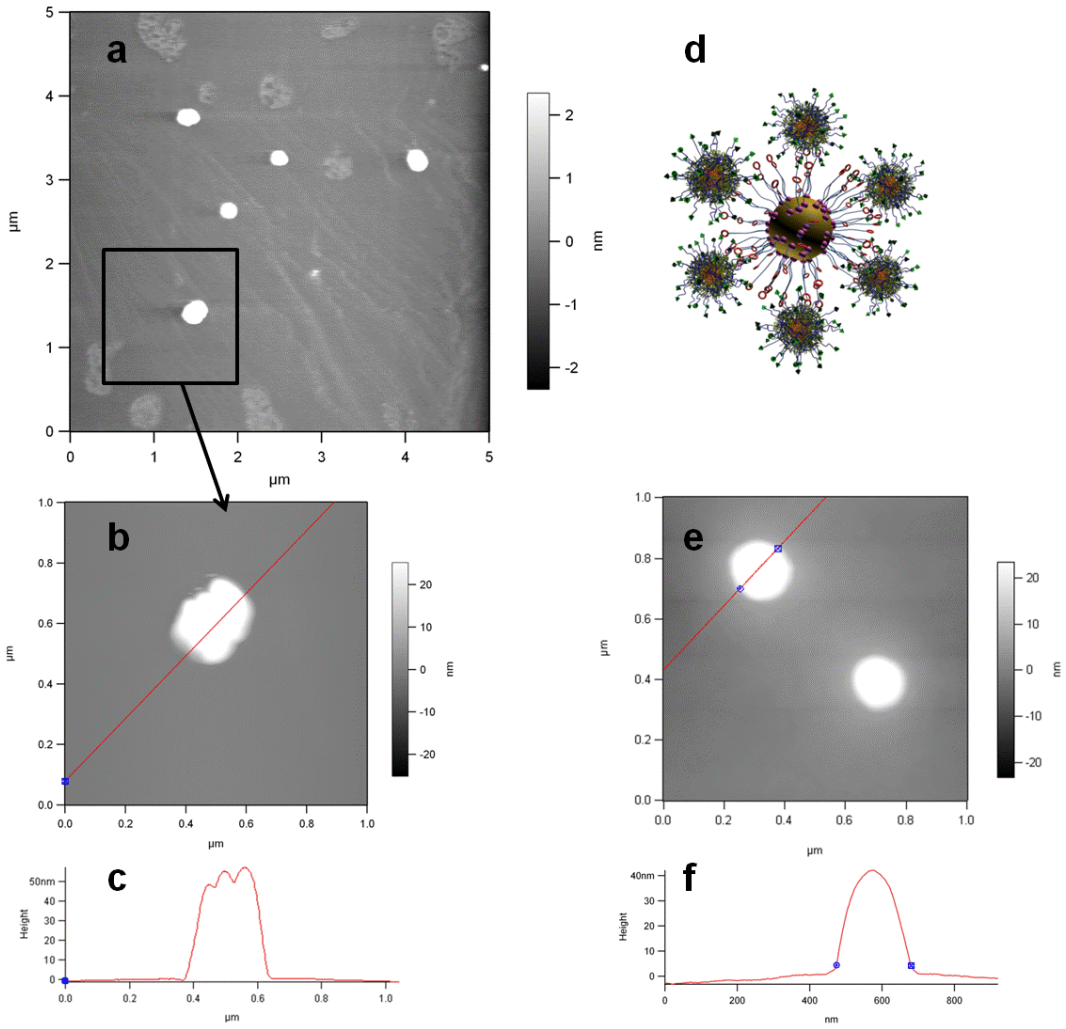

Figure 2-5. a, AFM height image of hybrid nanoclusters on AP-mica. b, Height image of an enlarged part of image a, showing a single hybrid nanocluster. c, Section analyses corresponding to the lines in image d. The height of the hybrid nanocluster is in agreement with the average height of a GNP plus two-fold the average height of an SCK. The wave-like shape of the pattern indicates that several SCKs are on the top of the GNP. d, Schematic representation of hybrid nanoclusters. e, Height image of two alkyne-functionalized GNPs. f Section analyses corresponding to the lines in image e.

The hybrid nanoclusters were then dismantled to provide the dual-clickable Janus SCKs and to regenerate the nano-template alkyne-functionalized GNPs. During the ligand-exchange reaction,(19) SCKs were detached from GNPs after excess alkyne-OEO-thiol was added. After Au-S bonds in the hybrid nanoclusters were broken, the detached SCKs contained a patch of thiol functionalities. Ultracentrifugation was applied to separate the Janus-faced SCKs (JSCKs) from the alkyne-functionalized GNPs by taking advantage of their different densities. Each step of the desymmetrization cycle was monitored by ultraviolet-visible spectroscopy (UV-vis) measurements of the gold surface plasmon resonance band in the solution, which reflects the surface functionality of GNPs. As observed from UV-vis, dynamic light scattering (DLS) and TEM (**Figure 2-6**), the recovered alkyne-functionalized GNPs were of comparable size, shape and surface functionality to the freshly-synthesized GNPs. The recovered alkyne-functionalized GNPs were, therefore, reused to desymmetrize another batch of SCKs. This cyclic approach (**Figure 2-1a**) greatly enhances the atom efficiency of the solid phase synthesis strategy, which is widely used to desymmetrize and regionally functionalize microparticles and nanoparticles,(20) and has a potential for large scale synthesis of Janus nanoparticles by using recyclable nanoscopic templates rather than singly-used templates. In our approach, as the nano-template can be recovered and reused in an economical cyclic manner, it can be applied to other soft matter particles with various sizes and compositions.

To confirm the anisotropic distribution of thiol groups on the resultant JSCKs, the thiol-functionalized regions of JSCKs were labeled with 2 nm citrate-stabilized GNPs. As revealed by TEM analyses (**Figure 2-7**), a relatively high population of JSCKs, 72% by counting more than 100 JSCKs, was attached to one or two 2 nm GNPs on one side, where thiol functionalities were expected. These TEM images strongly suggest the Janus nature of JSCKs and confirm the anisotropic distribution of thiol functionalities. Additionally, these JSCKs were found to undergo attachment of three or even more GNPs on one surface (**Figure 2-8**). Negative and positive control experiments were conducted based upon uniformly azide- or thiol-functionalized SCKs, respectively.(21) The negative control experiment demonstrated that citrate-

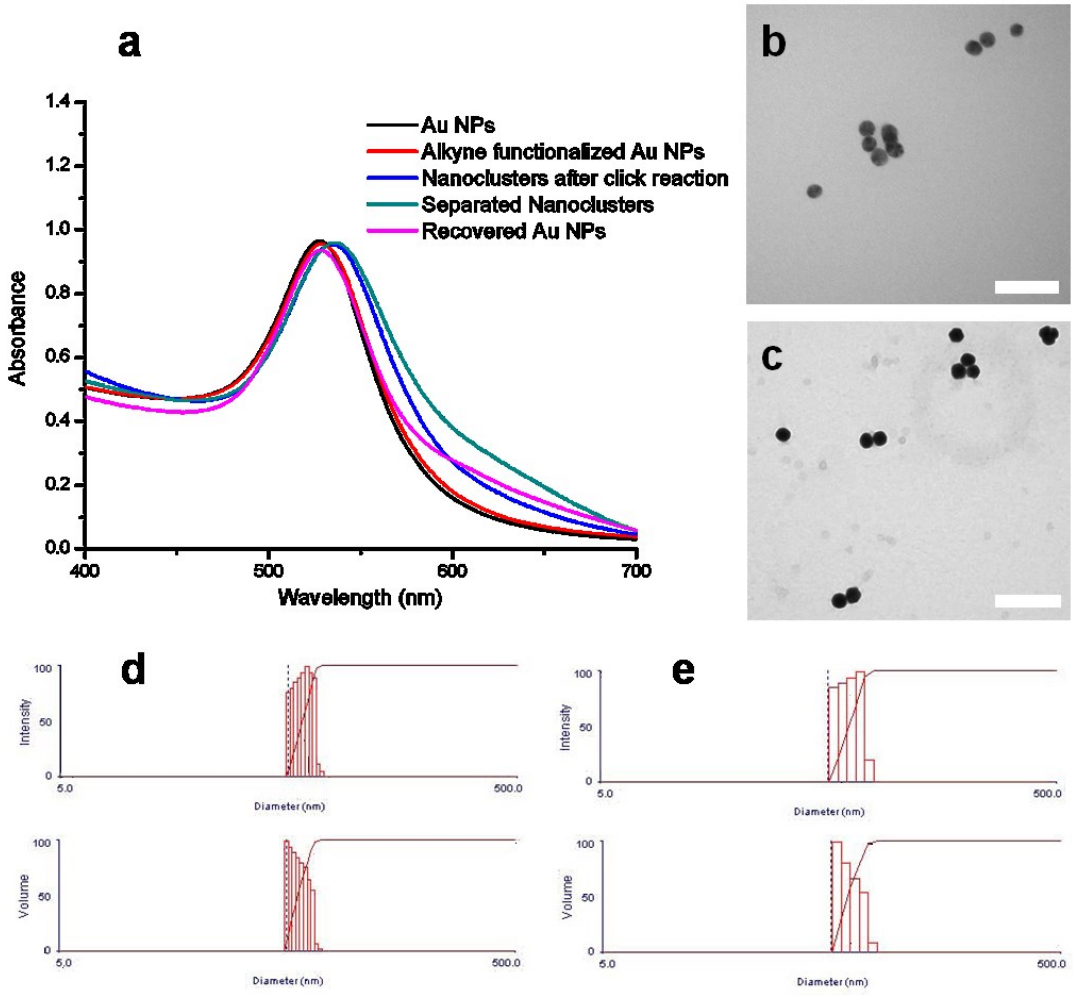

Figure 2-6. a, Monitoring the desymmetrization cycle by UV-vis of the gold surface plasmon resonance band in the solution, reflecting the surface functionality of the GNPs. At the beginning, 40 nm GNPs have a strong absorption at 527 nm, due to the characteristic surface plasmon resonance. After alkyne functionalization, the absorption peak slightly red shifted to 529 nm. In the next step, the absorption peak of hybrid nanoclusters largely shifted to 536 nm because of a change of refractive index caused by SCKs that attached on the GNPs surfaces. Finally, the absorbance band blue shifted back to 529 nm after the GNPs were recovered by ligand exchange reactions. b, TEM image of initial alkyne-functionalized GNPs; average diameter is 46 ± 6 nm. c, TEM image of recovered alkyne-functionalized GNPs; average diameter is 46 ± 7 nm, after counting more than 100 particles. Scale bars: 200 nm. d, DLS results of initial alkyne-functionalized GNPs. e, DLS results of recovered alkyne-functionalized GNPs.

stabilized GNPs did not interact favorably with azide- functionalized SCK nanoparticles (**Figure 2-9.** b and **e**). In the positive control experiment, thiol-functionalized SCKs had strong tendency to form aggregates and undergo precipitation, due to the formation of disulfide bonds between SCKs upon oxidation;(22) in contrast, JSCKs showed no precipitation as a result of only few thiol groups functionalized on one side of each nanoparticle. Meanwhile, the GNPs were attached onto multiple places of homogeneously thiol-functionalized SCKs, but didn't undergo close-packing to cover the entire surface (**Figure 2-9, c** and **f**). These phenomena can be attributed to steric effects and static repulsion among GNPs. Therefore, it is expected that there are more thiol groups on the JSCKs than it appears.

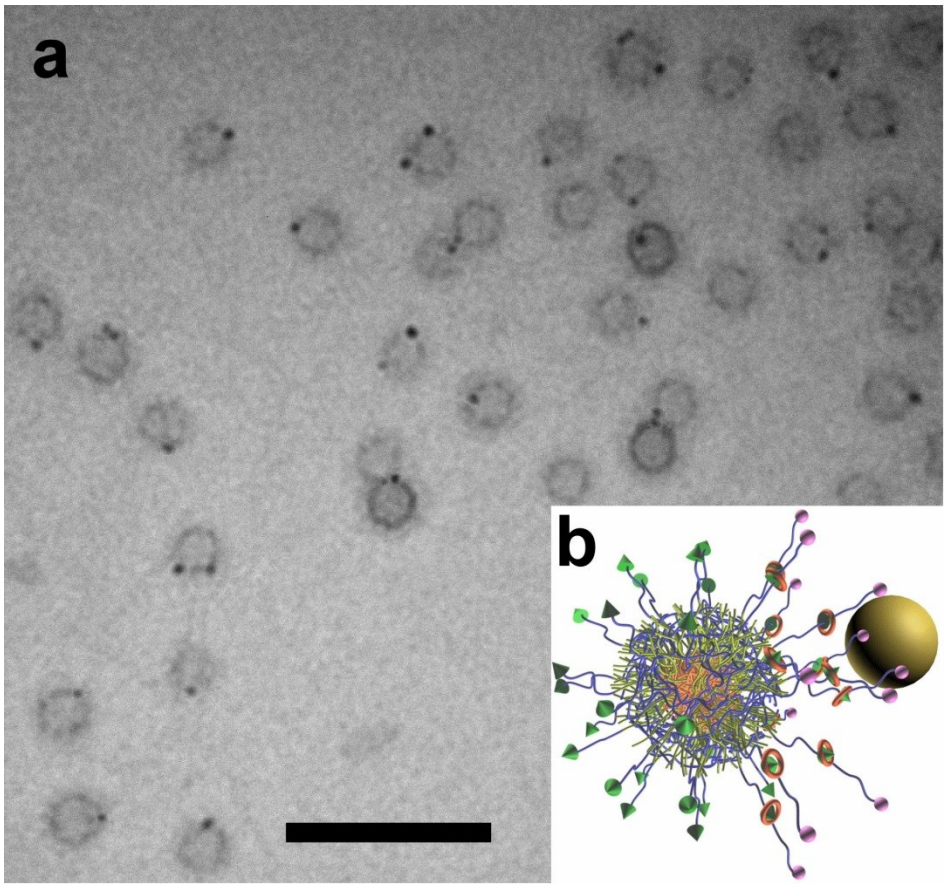

Figure 2-7. a, TEM image of JSCKs labeled with 2 nm GNPs. b, Schematic representation of JSCKs labeled with GNPs. Scale bar: 100 nm.

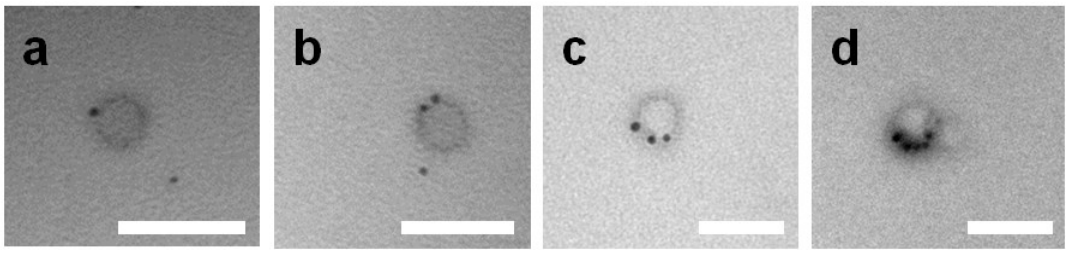

Figure 2-8. Selective TEM images of JSCKs labeled with 2 nm GNPs. Scale bars: 50 nm.

Figure 2-9. a, TEM image of JSCKs labeled with 2 nm GNPs. b, TEM image of azide-functionalized SCKs mixed with 2 nm GNPs as negative control. c, TEM image of thiol-functionalized SCKs labeled with 2 nm GNPs as positive control. d, Schematic representation of JSCKs labeled with GNPs. e, Schematic representation of negative control. f, Schematic representation of positive control. Scale bars: 100 nm.

Two types of click reactions were conducted, CuAAC and thiol-maleimide Michael addition, to demonstrate the presence and chemical availability of azide and thiol groups on the JSCKs. Alkyne-functionalized fluorescein was conjugated onto the residual azides of the JSCKs in the presence of $CuSO_4$/sodium ascorbate catalyst in water, followed by installation of thiol-reactive BODIPY 577/618 maleimide onto the thiol-functionalized patches on the JSCKs, by reaction in sodium carbonate buffered solution. After removal of the excess unreacted dyes, the presence of the two click-reactive dyes coupled onto JSCKs was studied by pH-dependent fluorescence experiments (**Figure 2-10**) and their amounts were quantified by UV-vis spectroscopy.(23) The ratio of fluorescein to BODIPY was calculated as 5:1, which indicated that *ca*. 17% of the azide groups on the SCKs were substituted by thiol groups, under the assumption of quantitative conversion and yield for the click reactions.(24) Such orthogonality and efficiency of click chemistry together with the Janus nature will allow for precise functionalization of polymer nanoparticles with targeted biological moieties, such as peptides, proteins, enzymes, and viral systems, to produce multifunctional synthetic polymer-biological chimeras for sophisticated applications.

This JSCK system is currently being extended to load with a pair of FRET dyes, which will provide additional information to further understand the distribution of azide and thiol groups.

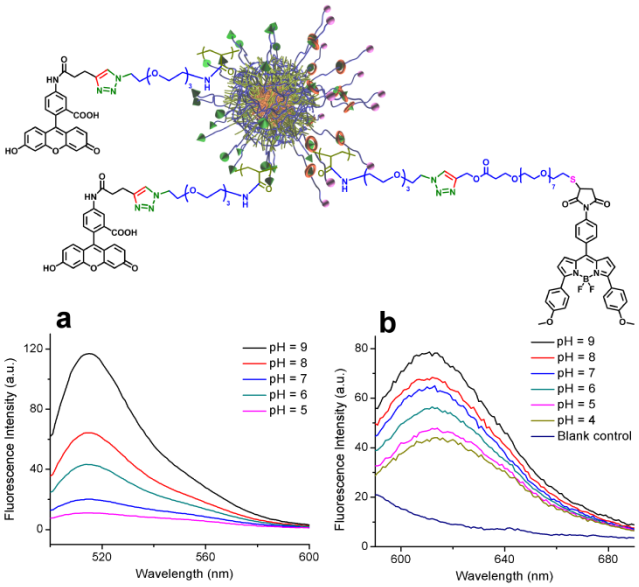

Figure 2-10. a, pH-dependent fluorescence spectrum (λ_{ex} = 488 nm) of JSCKs labeled with alkyne-functionalized fluorescein and thiol-reactive BODIPY 577/618 maleimide, showing the presence of fluorescein. b, pH-dependent fluorescence spectrum (λ_{ex} = 577 nm), showing the presence of BODIPY 577/618 maleimide. The chemical structures of each of the conjugated dyes are shown above the corresponding spectra.

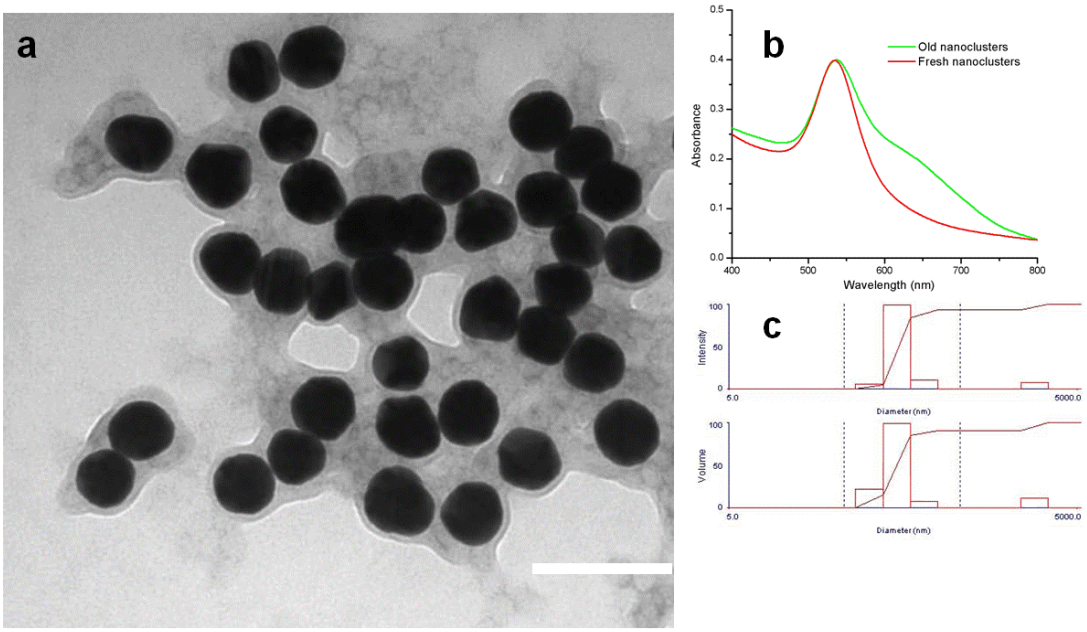

Figure 2-11. a, TEM image of hybrid nanoclusters five days after micelles were attached onto GNPs by CuAAC. Scale bar: 100 nm. b, UV-vis spectra of fresh hybrid nanoclusters and after five days. c, DLS of hybrid nanoclusters five days after CuAAC. Micron-sized species had been detected by DLS, which is in agreement with the TEM results.

In comparison to SCKs, the results of click reaction between azide-functionalized micelles and alkyne-functionalized GNPs were unsatisfactory. As illustrated by TEM imaging (**Figure 2-11 a**), five days after micelles were attached onto GNPs, the boundaries between different micelles became indistinct and eventually disappeared to form a polymer layer coated on the GNPs.(25) The polymer encapsulated GNP aggregates may be responsible for the red shift observed in UV-Vis spectra and micron-sized particle distribution as detected by DLS (**Figure 2-11, b** and **c**). Upon adsorption and attachment of the polymer micelles onto the GNPs, the changes in local concentration and surface forces serve as stimuli to trigger the disassembly and reorganization of block copolymers. Therefore, the micelles could be taken no further in the process toward Janus nanostructures. The robustness should be taken into consideration when engineering self-assembled nanostructures toward hierarchical architectures. Chemical cross-

linking is an efficient protocol to overcome this impediment and facilitate the “bottom-up” fabrication of self-assembled nanostructures.(26)

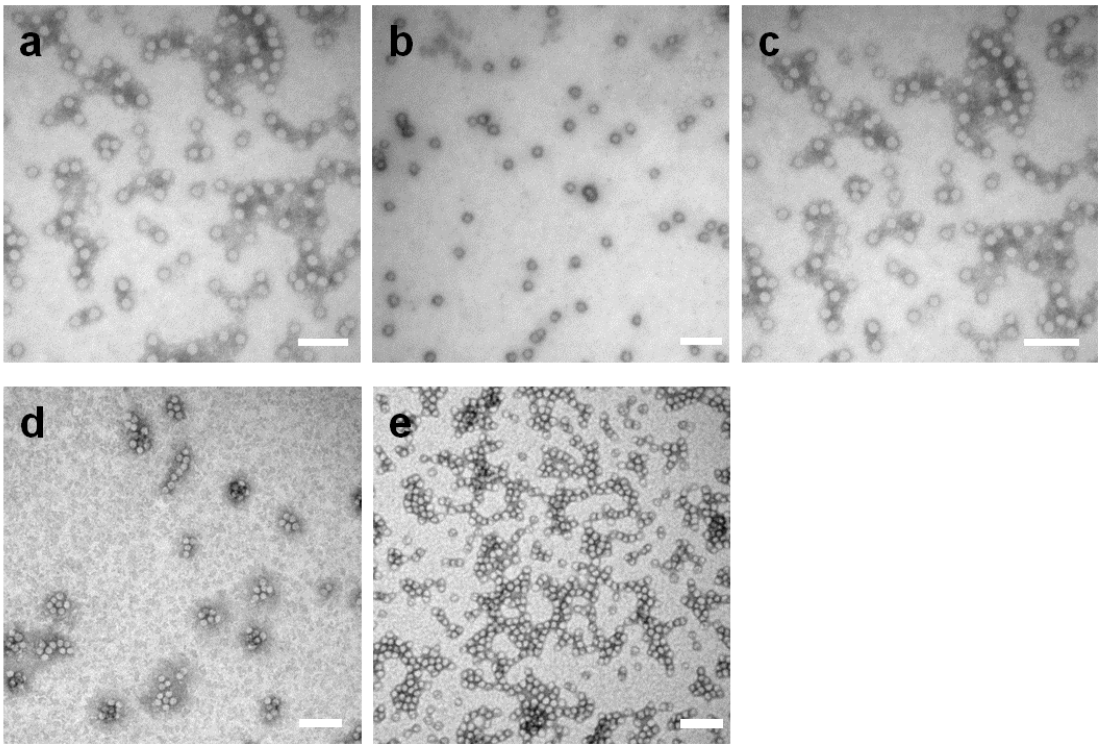

Figure 2-12. TEM images of all polymer nanoparticles. a, PAA_{105}-*b*-PS_{135} micelles. b, Azide-functionalized micelles. c, Azide-functionalized SCKs. d, Janus-faced thiol-functionalized SCKs. e, Recovered azide-functionalized SCKs. Scale bars: 100 nm.

Conclusion

In summary, we have demonstrated a novel, efficient and cyclic approach to construct orthogonal dual-clickable Janus nanoparticles, through a desymmetrization cycle based on complementarily reactive nanoscopic templates and covalent pattern transfer. The robustness of nanostructures is critical in this approach. This strategy can be further expanded as a general route to desymmetrize and dual-

functionalize a large family of soft matter nanoparticles for anisotropic modification toward complex devices.

Experimental

Materials. Poly(acrylic acid)-block-polystyrene (PAA_{105}-*b*-PS_{135}) copolymers were synthesized by acidolysis of P*t*BA_{105}-*b*-PS_{135} (PDI<1.16) precursors, which were prepared by sequential polymerization of *tert*-butyl acrylate and styrene *via* nitroxide mediated radical polymerization (NMP), followed by trifluoroacetic acid (TFA) deprotection, as reported in the literature.(23) Citrate stabilized 40 nm gold nanoparticles were purchased from Nanopartz Inc., and 2 nm gold nanoparticles stabilized in citrate solution were obtained from Strem Chemicals, Inc. Tetrahydrofuran (THF), copper sulfate pentahydrate, sodium ascorbate, propargyl alcohol, 11-azido-3,6,9-trioxaundecan-1-amine, 4-(dimethylamino)pyridine (DMAP), 2,2'-(ethylenedioxy)bis(ethylamine), N,N'-dicyclohexylcarbodiimide (DCC), 1-[3'-(dimethylamino)propyl]-3-ethylcarbodiimide methiodide (EDCI) and 4,7,10,13,16,19,22,25,32,35,38,41,44,47,50,53-hexadecaoxa-28,29-dithiahexapentacon-tanedioic acid were used as received from Sigma-Aldrich Company (St. Louis, MO).

Instrumentation. ^{1}H NMR and ^{13}C NMR spectra were recorded on Varian Inova 300 MHz or Varian Mercury 300 MHz spectrometers interfaced to a UNIX computer using VnmrJ software. Chemical shifts were referred to the solvent resonance signals.

Gel permeation chromatography was performed on a Waters Chromatography, Inc., 1515 isocratic HPLC pump equipped with an inline degasser, a model PD2020 dual-angle, light scattering detector (Precision Detectors, Inc.), a model 2414 differential refractometer (Waters, Inc.), and four PL_{gel} polystyrene-*co*-divinylbenzene gel columns (Polymer Laboratories, Inc.) connected in series: 5 μm Guard (50 × 7.5 mm), 5 μm Mixed C (300 × 7.5 mm), 5 μm 10^4 (300 × 7.5 mm), and 5 μm 500 Å (300 × 7.5 mm) using the Breeze (version 3.30, Waters, Inc.) software. The instrument was operated at 35 °C with THF as eluent (flow rate set to 1.0 mL/min). Polymer solutions were prepared at a known concentration (*ca*. 3 mg/mL)

and an injection volume of 200 µL was used. Data collection was performed with Precision Acquire 32 Acquisition program (Precision Detectors, Inc.) and analyses were carried out using Discovery32 software (Precision Detectors, Inc.) with a system calibration curve generated from plotting molecular weight as a function of retention time for a series of broad polydispersity poly(styrene) standards.

IR spectra were recorded on an IR Prestige 21 system (Shimadzu Corp., Japan) and analyzed using IRsolution v. 1.40 software.

Ultraviolet-visible spectroscopy (UV-vis) absorption measurements were made using a UV-2550 system (Shimadzu Corp., Japan) using PMMA cuvettes. Spectra were analyzed with UV-Probe v. 2.33 software.

Fluorescence spectra were obtained using a RF-5301 PC system (Shimadzu Corp., Japan) and analyzed with Panaroma Fluorescence v. 2.1 software.

Glass transition temperatures (T_g) were measured by differential scanning calorimetry on a Mettler-Toledo DSC822® (Mettler-Toledo, Inc., Columbus, OH), with a heating rate of 10 °C /min. Measurements were analyzed using Mettler-Toledo Star^e v. 7.01 software. The T_g was taken as the midpoint of the inflection tangent, upon the third heating scan. Thermogravimetric analysis was performed under N_2 atmosphere using a Mettler-Toledo model TGA/SDTA851^e, with a heating rate of 5 °C /min. Measurements were analyzed using Mettler-Toledo Star^e v. 7.01 software.

Dynamic light scattering measurements were conducted with a Brookhaven Instruments, Co. (Holtsville, NY) DLS system equipped with a model BI-200SM goniometer, BI-9000AT digital correlator, and a model EMI-9865 photomultiplier, and a model Innova 300 Ar ion laser operated at 514.5 nm (Coherent Inc., Santa Clara, CA). Measurements were made at 25 ± 1 °C. Prior to analysis, solutions were filtered through a 0.45 µm Millex®-GV PVDF membrane filter (Millipore Corp., Medford, MA) to remove dust particles. Scattered light was collected at a fixed angle of 90°. The digital correlator was operated with 522 ratio spaced channels, and initial delay of 5 µs, a final delay of 50 ms, and a duration of 8 minutes. A photomultiplier aperture of 400 µm was used, and the incident laser intensity was adjusted to obtain a photon counting of between, 200 and 300 kcps. The calculations of the particle size distributions and distribution averages were performed with the ISDA software package (Brookhaven Instruments

Company), which employed single-exponential fitting, Cumulants analysis, and CONTIN particle size distribution analysis routines. All determinations were average values from ten measurements.

Transmission electron microscopy (TEM) bright-field imaging was conducted on a Hitachi H-7500 microscope, operating at 100 kV. The TEM imaging at high magnification was carried out on a FEI Tecnai G2 F20 microscope, operating at 200 kV. The samples were prepared as following: 4 μL of the dilute solution (with a polymer concentration of *ca.* 0.2 ─ 0.5 mg/mL) were deposited onto a carbon-coated copper grid, which was pre-treated with absolute ethanol or oxygen plasma to increase the surface hydrophilicity. After 1 min, the excess of the solution was quickly wicked away by a piece of filter paper. The samples were then negatively stained with 4 μL of 1 wt% phosphotungstic acid (PTA) aqueous solution. After 30 seconds, the excess PTA solution was quickly wicked away by a piece of filter paper and the samples were left to dry under room temperature overnight.

Atomic force microscopy (AFM) imaging was performed using a MFP-3D system (Asylum Research, Santa Barbara, CA) in tapping mode using standard silicon tips (AC160TS, 160 μM, spring constant 42 N m^{-1}). Samples were prepared by direct deposition onto freshly cleaved mica or AP-mica substrates and allowed to stand for 30 s after which the excess solution was wicked off using a filter paper and air-dried.

Preparation of PAA_{105}-*b*-PS_{135} micelle. A round-bottom flask equipped with a stir bar was charged with PAA_{105}-*b*-PS_{135}, (M_n^{NMR} = 21000 g/mol; 0.60 g, 3.0 mmol of acrylic acid groups), THF (300 mL) was added and the solution was allowed to stir at room temperature for 2 hours to ensure the mixture was homogeneous. Nanopure water (300 mL) was added *via* a metering pump at the rate of 15 mL/h. After all the water had been added and further stirred for 12 hours, the micelle solution was transferred to presoaked dialysis membrane tubes (MWCO *ca*. 6-8 kDa), and dialyzed against nanopure water for 4 days, to remove all THF. The final concentration of micelle solution was 0.67 mg/mL. D_h (DLS, number) = 25 ± 7 nm; D_h (DLS, volume) = 31 ± 13 nm; D_h (DLS, intensity) = 55 ± 22 nm; D_{av} (TEM) = 21 ± 2 nm; D_{av} (AFM) = 84 ± 14 nm; H_{av} (AFM) = 5 ± 1 nm. Lyophilization of an aliquot of this solution gave a white solid for characterization. DSC: $(T_g)_{PAA}$ = 133 ℃, $(T_g)_{PS}$ = 101 ℃. TGA in N_2: 200–300 °C, 16% mass loss;

380–450 °C, 71% mass loss, 10% mass remaining above 450 °C. IR: 3550-2900, 1895, 1721, 1603, 1584, 1491, 1456, 1232, 1177, 1026, 912, 878, 758, 703 cm^{-1}.

Preparation of azide-functionalized [PAA_{84}-*co*-$PAA(N_3)_{21}$]-*b*-PS_{135} micelle. To a stirred solution of micelle (100 mL, 0.67 mg/mL, 0.34 mmol of acrylic acid) in a round-bottom flask was added a solution of 11-azido-3,6,9-trioxaundecan-1-amine (14.8 mg, 0.068 mmol) in nanopure water (1.5 mL). The solution was allowed to stir for two hours at room temperature. To this reaction mixture was added dropwise, *via* a metering pump at the rate of 6 mL/h, a solution of EDCI (22.1 mg, 0.075 mmol) dissolved in nanopure water (6 mL). The reaction mixture was allowed to stir overnight at room temperature and was then transferred to presoaked dialysis membrane tubes (MWCO *ca*. 6-8 kDa), and dialyzed against nanopure water for 4 days to remove small molecule contaminants. Final concentration of azide-functionalized micelle solution was 0.54 mg/mL. D_h (DLS, number) = 30 ± 8 nm; D_h (DLS, volume) = 35 ± 19 nm; D_h (DLS, intensity) = 49 ± 20 nm; D_{av} (TEM) = 22 ± 3 nm; D_{av} (AFM) = 92 ± 18 nm; H_{av} (AFM) = 6 ± 2 nm. Lyophilization of an aliquot of this solution gave a white solid for characterization. DSC: $(T_g)_{PAA}$ = 138 ℃, $(T_g)_{PS}$ = 105 ℃. TGA in N_2: 200–300 °C, 10% mass loss; 380–450 °C, 80% mass loss, 10% mass remaining above 450 °C. IR: 3500-3100, 3080, 3026, 2921, 2100, 1721, 1658, 1565, 1493, 1452, 1387, 1263, 1146, 761, 700, 621 cm^{-1}.

Preparation of azide-functionalized shell crosslinked (SCK) nanoparticle. To a stirred solution of azide-functionalized micelle (100 mL, 0.54 mg/mL, 0.18 mmol of acrylic acid, 0.04 mmol of azide groups) in a round-bottom flask equipped with a stir bar was added, dropwise over 10 minutes, a solution of 2,2'-(ethylenedioxy)bis(ethylamine) (5.2 mg, 0.034 mmol) in nanopure water (1.0 mL). The solution was allowed to stir for 3 h at room temperature. To this reaction mixture was added dropwise, *via* a metering pump at the rate of 2 mL/h, a solution of EDCI (12.1 mg, 0.041 mmol) dissolved in nanopure water (2 mL). The reaction mixture was allowed to stir overnight at room temperature and was then transferred to presoaked dialysis membrane tubes (MWCO *ca*. 6-8 kDa), and dialyzed against nanopure water for 4

days to remove small molecule contaminants. Final concentration of SCK solution was 0.46 mg/mL. D_h (DLS, number) = 28 ± 10 nm; D_h (DLS, volume) = 51 ± 17 nm; D_h (DLS, intensity) = 73 ± 29 nm; D_{av} (TEM) = 22 ± 3 nm; D_{av} (AFM) = 98 ± 17 nm; H_{av} (AFM) = 5 ± 2 nm. Lyophilization of an aliquot of this solution gave a white solid for characterization. DSC: $(T_g)_{PS}$ = 105 °C. TGA in N_2: 200–300 °C, 12% mass loss; 380–450 °C, 73% mass loss, 10% mass remaining above 450 °C. IR: 3400-3140, 3027, 2972, 2921, 2100, 1720, 1655, 1635, 1561, 1493, 1452, 1397, 1164, 1009, 808, 764, 692 cm^{-1}.

Synthesis of alkyne-OEO-disulfide. To a solution of 4,7,10,13,16,19,22,25,32,35,38,41,44,47,50,53-hexadecaoxa-28,29-dithiahexapentacontanedioic acid (azide-OEO-disulfide, 243 mg, 0.27 mmol) in 4 mL of dry CH_2Cl_2 at room temperature were added DMAP (17.7 mg, 0.15 mmol) and DCC (0.123 g, 0.60 mmol), and the reaction mixture was stirred for 10 minutes. After the addition of propargyl alcohol (60.0 mg, 0.50 mmol), the reaction mixture was further stirred 20 hours at room temperature. Then the reaction mixture was filtered with Celite and the filtrate was concentrated to *ca*. 0.3 mL. The crude product obtained was further purified by flash column chromatography (8-9% MeOH/CH_2Cl_2, v/v) to afford alkyne-OEO-disulfide as a light yellow solid (0.289 g, 98% yield). Alkyne-OEO-disulfide was stored under nitrogen atmosphere at -15 °C. ^{1}H NMR ($CDCl_3$, ppm): δ 4.65 (s, 4H, OC*H*$_2$C≡CH), 3.75-3.57 (m, 64H, OC*H*$_2$CH$_2$, C*H*$_2$CH$_2$C(O)O, and C*H*$_2$CH$_2$S), 2.84 (t, *J* = 6.9 Hz, 4H, CH$_2$C*H*$_2$C(O)O), 2.61 (t, *J* = 6.9 Hz, 4H, CH$_2$C*H*$_2$S), 2.48 (s, C≡C*H*). ^{13}C NMR ($CDCl_3$, ppm): δ 170.7, 77.1, 75.0, 70.6-70.3, 69.6, 66.3, 51.9, 38.4, 34.8.

Preparation of alkyne-functionalized gold nanoparticles (GNPs). To a stirred solution of 40 nm GNPs colloid solution (0.05 mg/mL, 70000 Au surface atoms per particle, particle concentration = 8.7 × 10^{10} per mL, surface Au concentration = 1.0 × 10^{-5} mmol/mL, 100 mL) at pH 9 in a round-bottom flask, a solution of alkyne-OEO-disulfide in ethanol (10 mg/mL, 0.8 mL, 16 times excess than needed) was added. After being stirred for 24 hours at room temperature, alkyne-functionalized GNPs solution was ultracentrifuged for 5 min (at 13 krpm, 20 °C), followed by decantation of supernatants and subsequent dispersal into

same volume of nanopure water. Ultracentrifugation and re-dispersal were repeated three times to remove all unreacted small molecules. Alkyne-functionalized GNPs solution was stored at – 4 °C. D_h (DLS, number) = 55 ± 5 nm; D_h (DLS, volume) = 56 ± 7 nm; D_h (DLS, intensity) = 57 ± 10 nm; D_{av} (TEM) = 46 ± 6 nm; D_{av} (AFM) = 230 ± 40 nm; H_{av} (AFM) = 45 ± 7 nm. UV-vis: (H_2O) λ_{max} = 529 nm ($\varepsilon = 7 \times 10^9$ $M^{-1}cm^{-1}$). 40 nm GNPs: D_h (DLS, intensity) = 49 ± 5 nm; D_h (DLS, volume) = 50 ± 5 nm; D_h (DLS, number) = 51 ± 7 nm; D_{av} (TEM) = 46 ± 4 nm.

Cu-catalyzed azide/alkyne cycloaddition (CuAAC) reaction between nanoparticles. To a stirred solution of alkyne-functionalized GNPs (30 mL) in a round-bottom flask, was added a solution of azide-functionalized micelles or SCKs (15 mL), a solution of sodium ascorbate (250 mM, 0.90 mL) and a solution of CuSO4•5H_2O (50 mM, 0.90mL). Once all reagents were added, one to five minutes sonication was applied to the reaction mixture to avoid aggregation at the beginning of the click reaction. After being stirred for 10 hours at room temperature, the reaction mixture was ultracentrifuged for 5 min (at 13 krpm, 20 °C), followed by decantation of supernatants and subsequent dispersal into same volume of nanopure water. Ultracentrifugation and re-dispersal were repeated three times to ensure complete separation. The supernatant solutions were combined, dialyzed against nanopure water for 4 days to remove small molecule contaminants, and ultracentrifuged for 10 minutes to precipitate remaining dense species, to yield a solution of recovered azide-functionalized micelles or SCKs. The precipitate was re-dispersed into 30 mL nanopure water to yield a solution of hybrid nanoclusters. The final concentration of hybrid nanoclusters in the solution was 8.7×10^{10} particles per mL, as estimated from the concentration of GNPs. The solution of hybrid nanoclusters was stored at – 4 °C. Hybrid nanoclusters containing GNPs and SCKs: D_h (DLS, number) = 81 ± 19 nm; D_h (DLS, volume) = 117 ± 38 nm; D_h (DLS, intensity) = 136 ± 36 nm; D_{av} (TEM, GNPs) = 45 ± 7 nm; D_{av} (TEM, SCKs) = 20 ± 2 nm; D_{av} (AFM) = 240 ± 40 nm; H_{av} (AFM) = 53 ± 7 nm. UV-vis: (H_2O) λ_{max} = 536 nm ($\varepsilon = 7 \times 10^9$ $M^{-1}cm^{-1}$). Recovered azide-functionalized SCKs: D_h (DLS, intensity) = 28 ± 7 nm; D_h (DLS, volume) = 33 ± 12 nm; D_h (DLS, number) = 48 ± 23 nm; D_{av} (TEM) = 22 ± 3 nm; D_{av} (AFM) = 91 ± 15 nm; H_{av} (AFM) = 5 ± 2 nm.

Formation of Janus-faced thiol-modified SCKs (JSCKs) by ligand exchange reaction. To a solution of hybrid nanoclusters containing GNPs and SCKs (30 mL), was added a solution of alkyne-OEO-disulfide in ethanol (8.0 mg/mL, 1.2 mL, 100 times excess than needed) and a solution of sodium ascorbate (250 mM, 0.60 mL).(19) The reaction mixture was stirred at room temperature for 3 days, with application of sonication intermittently for 30 minutes four times per day. Afterwards, the reaction mixture was ultracentrifuged for 5 min (at 13 krpm, 20 °C), followed by decantation of supernatants and subsequent dispersal into same volume of nanopure water. Ultracentrifugation and re-dispersal were repeated three times to ensure complete separation. The supernatant solutions were combined, dialyzed against nanopure water for 4 days to remove small molecule contaminants, and ultracentrifuged for 10 minutes to precipitate remaining dense species, to yield a solution of Janus-faced thiol-modified SCKs (JSCKs). The precipitate was re-dispersed into 30 mL nanopure water to yield a solution of recovered alkyne-functionalized GNPs. The recovered alkyne-functionalized GNPs solution was stored at – 4 °C. JSCKs: D_h (DLS, intensity) = 29 ± 15 nm; D_h (DLS, volume) = 34 ± 19 nm; D_h (DLS, number) = 46 ± 27 nm; D_{av} (TEM) = 23 ± 2 nm; D_{av} (AFM) = 89 ± 12 nm; H_{av} (AFM) = 4 ± 2 nm. Recovered alkyne-functionalized GNPs: D_h (DLS, intensity) = 62 ± 13 nm; D_h (DLS, volume) = 60 ± 15 nm; D_h (DLS, number) = 58 ± 10 nm; D_{av} (TEM) = 46 ± 7 nm. UV-vis: (H_2O) λ_{max} = 529 nm ($\varepsilon = 7 \times 10^9\ M^{-1}cm^{-1}$).

Fluorescein labeling by Cu-catalyzed azide/alkyne cycloaddition (CuAAC) reaction. To an aqueous solution of the JSCKs (10 mL) was added a solution of alkyne-functionalized fluorescein (2 mg/mL, 0.5 mL, large excess) in methanol, a solution of sodium ascorbate (50 mM, 0.5 mL) and solution of $CuSO4•5H_2O$ (50 mM, 0.50 mL). The reaction mixture was allowed to stir for 2 days and was then transferred to presoaked dialysis tubing (MWCO *ca*. 6000-8000 Da) and extensively dialyzed against nanopure water for 5 days to remove excess dye and copper catalyst. UV-vis: (H_2O) λ_{max} = 490.5 nm.

BODIPY 577/618 maleimide labeling by thiol-maleimide Michael addition. To an aqueous solution of the JSCKs (10 mL) or fluorescein labeled JSCKs (10 mL) was added a solution of thiol-reactive BODIPY

577/618 maleimide in a pH=10 sodium carbonate buffered solution (2 mg/mL, 1.5 mL, large excess). The reaction mixture was allowed to stir for 2 days under a nitrogen atmosphere in the presence of tris(2-carboxyethyl)phosphine and was then transferred to presoaked dialysis tubing (MWCO *ca*. 6000-8000 Da) and extensively dialyzed against nanopure water for 5 days to remove excess dye. UV-vis: (H_2O) λ_{max} = 599.5 nm.

Preparation of thiol-functionalized shell crosslinked (SCK) nanoparticles. To an aqueous solution of azide-functionalized SCKs (10 mL) was added a solution of alkyne-OEO-disulfide in ethanol (10 mg/mL, 2.0 mL, large excess), sodium ascorbate (250 mM, 0.040 mL) and solution of CuSO4•5H_2O (50 mM, 0.040 mL). The reaction mixture was allowed to stir for 2 days and was then transferred to presoaked dialysis tubing (MWCO *ca*. 6000-8000 Da) and dialyzed against nanopure water for 5 days to remove excess alkyne-OEO-thiol.

Studies of the association of 2 nm GNPs with JSCKs, thiol-functionalized SCKs and azide-functionalized SCKs. To an aqueous solution of the JSCKs (1 mL) was added a solution of citrate stabilized 2 nm GNPs (several drops). To an aqueous solution of the thiol-functionalized SCKs (1 mL) was added a solution of citrate stabilized 2 nm GNPs (several drops). To an aqueous solution of the azide-functionalized SCKs (1 mL) was added a solution of citrate stabilized 2 nm GNPs (several drops). Three reaction mixtures were allowed to stir for 2 days and were then transferred to presoaked dialysis tubings (MWCO *ca*. 6000-8000 Da) and dialyzed against nanopure water for 5 days to remove most unbound 2 nm GNPs.(27)

Acknowledgements

We gratefully acknowledge financial support from the National Heart Lung and Blood Institute of the National Institutes of Health as a Program of Excellence in Nanotechnology (HHSN268201000046C) and

the National Science Foundation under grant numbers DMR-0906815 and DMR-1032267. The Welch Foundation is gratefully acknowledged for support through the W. T. Doherty-Welch Chair in Chemistry, Grant No. A-0001. The transmission electron microscopy facilities at Washington University in St. Louis, Department of Otolaryngology, Research Center for Auditory and Visual Studies funded by NIH P30 DC004665 are gratefully acknowledged. We thank Jiahua Zhu and Ang Li for discussions and support.

Reference

(1) For reviews about soft Janus particles: (a) Wurm, F.; Kilbinger, A. F. M. *Angew. Chem. Int. Edit.* **2009**, *48*, 8412. (b) Du, J. Z.; O'Reilly, R. K. *Chem. Soc. Rev.* **2011**, *40*, 2402. (c) Walther, A.; Muller, A. H. E. *Soft Matter* **2008**, *4*, 663.

(2) (a) Glotzer, S. C. *Science* **2004**, *306*, 419. (b) Walther, A.; Drechsler, M.; Rosenfeldt, S.; Harnau, L.; Ballauff, M.; Abetz, V.; Muller, A. H. E. *J. Am. Chem. Soc.* **2009**, *131*, 4720. (c) Hermans, T. M.; Broeren, M. A. C.; Gomopoulos, N.; van der Schoot, P.; van Genderen, M. H. P.; Sommerdijk, N. A. J. M.; Fytas, G.; Meijer, E. W. *Nat. Nanotechnol.* **2009**, *4*, 721. (d) Roh, K.-H.; Martin, D. C.; Lahann, J. *Nat. Mater.* **2005**, *4*, 759. (e) Chen, Q.; Bae, S. C.; Granick, S. *Nature* **2011**, *469*, 381. (f) Percec, V.; Wilson, D. A.; Leowanawat, P.; Wilson, C. J.; Hughes, A. D.; Kaucher, M. S.; Hammer, D. A.; Levine, D. H.; Kim, A. J.; Bates, F. S.; Davis, K. P.; Lodge, T. P.; Klein, M. K.; DeVane, H.; Aqad, E.; Rosen, B. M.; Argintaru, A. O.; Sienkowska, M. J.; Rissanen, K.; Nummelin, S.; Ropponen, J. *Science* **2010**, *328*, 1009-1014.

(3) Berger, S.; Synytska, A.; Ionov, L.; Eichhorn, K. J.; Stamm, M. *Macromolecules* **2008**, *41*, 9669.

(4) Wu, L. Y.; Ross, B. M.; Hong, S.; Lee, L. P. *Small* **2010**, *6*, 503.

(5) Crossley, S.; Faria, J.; Shen, M.; Resasco, D. E. *Science* **2010**, *327*, 68.

(6) Suci, P. A.; Kang, S.; Young, M.; Douglas, T. *J. Am. Chem. Soc.* **2009**, *131*, 9164.

(7) Gillies, E. R.; Fréchet, J. M. J. *J. Am. Chem. Soc*. **2002**, *124*, 14137.

(8) Kolb, H. C.; Finn, M. G.; Sharpless, K. B. *Angew. Chem. Int. Edit.* **2001**, *40*, 2004.

(9) Iha, R. K.; Wooley, K. L.; Nystrom, A. M.; Burke, D. J.; Kade, M. J.; Hawker, C. J. *Chem. Rev.* **2009**, *109*, 5620.

(10) Chen, R. T.; Muir, B. W.; Such, G. K.; Postma, A.; McLean, K. M.; Caruso, F. *Chem. Commun.* **2010**, *46*, 5121.

(11) Zhang, J.; Wang, X. J.; Wu, D. X.; Liu, L.; Zhao, H. Y. *Chem. Mater.* **2009**, *21*, 4012.

(12) Elghanian, R.; Storhoff, J. J.; Mucic, R. C.; Letsinger, R. L.; Mirkin, C. A. *Science* **1997**, *277*, 1078.

(13) Thurmond, K. B.; Kowalewski, T.; Wooley, K. L. *J. Am. Chem. Soc.* **1996**, *118*, 7239.

(14) Sun, G.; Hagooly, A.; Xu, J.; Nystrom, A. M.; Li, Z. C.; Rossin, R.; Moore, D. A.; Wooley, K. L.; Welch, M. J. *Biomacromolecules* **2008**, *9*, 1997.

(15) Lin, L. Y.; Lee, N. S.; Zhu, J.; Nyström, A. M.; Pochan, D. J.; Dorshow, R. B.; Wooley, K. L. *J. Control. Release.* **2011**, *152*, 37.

(16) Dach, B. I.; Rengifo, H. R.; Turro, N. J.; Koberstein, J. T. *Macromolecules* **2010**, *43*, 6549.

(17) (a) Huo, F. W.; Lytton-Jean, A. K. R.; Mirkin, C. A. *Adv. Mater.* **2006**, *18*, 2304. Xu, X.; Rosi, N. L.; (b) Wang, Y.; Huo, F.; Mirkin, C. A. *J. Am. Chem. Soc.* **2006**, *128*, 9286.

(18) Lattuada, M., Hatton, T. A. *J. Am. Chem. Soc.* **2007**, *129*, 12878.

(19) Latham, A. H.; Williams, M. E. *Langmuir* **2006**, *22*, 4319.

(20) (a) Worden, J. G.; Shaffer, A. W.; Huo, Q. *Chem. Commun.* **2004**, 518. (b) Wang, B. B.; Li, B.; Zhao, B.; Li, C. Y. *J. Am. Chem. Soc.* **2008**, *130*, 11594. (c) Maye, M. M.; Nykypanchuk, Cuisinier, M.; van der Lelie, D.; Gang, O. *Nature Mater.* **2009**, *8*, 388. (d) Sardar, R.; Heap, T. B.; Shumaker-Parry, J. S. *J. Am. Chem. Soc.* **2007**, *129*, 5356.

(21) Takahara, Y. K.; Ikeda, S.; Ishino, S.; Tachi, K.; Ikeue, K.; Sakata, T.; Hasegawa, T.; Mori, H.; Matsumura, M.; Ohtani, B. *J. Am. Chem. Soc.* **2005**, *127*, 6271.

(22) Kakwere, H.; Perrier, S. *J. Am. Chem. Soc.* **2009**, *131*, 1889.

(23) O'Reilly, R. K.; Joralemon, M. J.; Wooley, K. L.; Hawker, C. J. *Chem. Mater.* **2005**, *17*, 5976.

(24) Hawker, C. J.; Wooley, K. L. *Science* **2005**, *309*, 1200.

(25) Wang, H.; Xu, J.; Wang, J. H.; Chen, T.; Wang, Y.; Tan, Y. W.; Su, H. B.; Chan, K. L.; Chen, H. Y. *Angew. Chem. Int. Edit.* **2010**, *49*, 8426.

(26) Pochan, D. J.; Chen, Z. Y.; Cui, H. G.; Hales, K.; Qi, K.; Wooley, K. L. *Science* **2004**, *306*, 94.

(27) He, T.; Adams, D. J.; Butler, M. F.; Cooper, A. I.; Rannard, S. P. *J. Am. Chem. Soc.* **2009**, *131*, 1495-1501.

Chapter 3

Hierarchical assembly of complex block copolymer nanoparticles into multicompartment superstructures through tunable inter-particle associations

[Portions of this work have been published previously as Jiahua Zhu[†], Shiyi Zhang[†], Fuwu Zhang, Karen L. Wooley, Darrin J. Pochan *Adv. Func. Mater.* **2013**, *ASAP*]

[†] These two authors contributed equally.

Abstract

A challenging aim in both materials physics and chemistry is the construction of complex and functional superstructures from designed nanoscale building units. Block copolymer nanoparticles with morphological variety and compositional complexity have been made with solution-based assembly. However, routine ability to build hierarchical superstructures by inter-nanoparticle association is not yet possible. We report here a hierarchical assembly strategy of organizing pre-formed spherical block copolymer nanoparticles into superstructures, including linear, circular, and close-packed arrays, via tunable inter-particle interactions. Solution-state mixtures were made of two amphiphilic diblock copolymers, poly(acrylic acid)-block-poly(methyl methacrylate) (PAA-b-PMMA) and poly(acrylic acid)-block-polybutadiene (PAA-b-PB) with additional crown ether functionalities grafted onto 40 mol% of the AA repeat units on the PAA-b-PMMA diblock copolymer. Through kinetic control of the solution assembly process in aqueous/*N*,*N*-dimethylformamide (DMF) mixtures (4:1 water:DMF), spherical nanoparticles with compositional complexity confined in both the core and shell were obtained. Benefiting from host-guest chemistry, inter-particle association was triggered and tuned by the addition of di-functional organoamines due to amine–crown ether complexation. The resultant multiparticle superstructures contained well-defined multicompartments within individual, constituent nanoparticles due to the local separation of unlike PB and PMMA hydrophobic blocks within the cores of the individual particles. Through competitive complexation with potassium ions, the superstructures were disassembled into individual multicomparment nanoparticles.

Introduction

Inspired by natural superstructure in biological systems, considerable efforts have been devoted to the understanding and manipulation of the hierarchical assembly behavior of diverse, non-natural, nanoscale units such as designed DNA nanotechnology(1) and colloidal crystal engineering.(2-4) Recent success in hierarchical assembly relies on two facets: complex particle construction and controllable particle-particle interactions. Nanoparticles constructed from synthetic, amphiphilic block copolymers provide the opportunity to control structure both within individual block copolymer nanoparticles as well as between multiple nanoparticles for hierarchical assembly.(5-10) We report here a strategy to construct spherical nanoparticles from the blending of two diblock copolymers, forced to reside in a common nanoparticle through kinetic control of solvent mixing. These blended, complex nanoparticles then can serve as hierarchical building units and assemble into desired superstructures including linear, circular, and close-packed arrays, by tuning the inter-particle associations.

The development of nanostructures derived from block copolymer assembly has been studied intensively in the last decade. By taking advantage of synthetic methodologies to afford varied block copolymer structures,(11-14) and extensive exploration of molecular solution assembly,(5-10, 15) block copolymer assemblies have exhibited prodigious morphological diversity at the nanoscale beyond traditional spheres, cylinders, and vesicles. Not only have particles been constructed with unique shapes, such as disks,(16,17) branched rods,(7,18) and toroids,(19) but new nanostructures with compositional complexity, or complex nanoparticles, such as anisotropic particles(20) that include patchy,(21,22) multicompartment,(14,23-25) and Janus particles,(26) also have been explored. Anisotropic particles created from block copolymer assemblies contain a non-centrosymmetric distribution of both compositions and properties within the core and/or on the surface of the particles. The compartments in the core are promising sites for multiple/selective loading, transport and release of a wide variety of compounds such as drugs/genes, dyes, inorganic nanoparticles, and catalysts.(8,25,27) The diversity of

chemistry displayed from a particle surface provides patches that can be used as specific sites for organic or inorganic grafts(28,29) or inter-particle associations.(20,31)

The importance of particle anisotropy has been realized recently in complex hierarchical structure assembly using larger length-scale colloidal systems(3,4,32,33) to produce novel structures beyond highly symmetric close-packed clusters assembled from hard spheres with short-range isotropic interactions.(34) Block copolymer nanoparticles with anisotropic cores, such as multicompartment micelles (MCMs), have been successfully fabricated from star terpolymer(14,35) or linear triblock copolymer(22,36) assembly. These types of particles can also be made with mixtures of different block copolymers and variation of the ratio of molecules in the assembly mixture. Moreover, without being covalently linked in the same molecular backbone, components in the mixture are responsive to various external stimuli such as solvent exchange,(37) changes in temperature, pH,(38) ionic strength,(22) and assembly kinetics.(25) Also, the components are dynamic enough to demix internally into compartments of diverse sizes and geometries depending on the type and amount of block copolymers in the original mixture. Complex particles from block copolymer mixtures introduce opportunities for novel superstructures that are distinguished from rigid colloidal systems. However, significant challenges exist in how to precisely control the block copolymer nanoparticle-nanoparticle interactions due to their nanoscale size and dynamic nature.

Since block copolymer nanoparticles are usually isolated in solution due to steric or electrostatic inter-micellar repulsions between the hydrophilic or charged corona in aqueous conditions, specific inter-particle associations cannot be achieved until desired physical or chemical attractions are introduced in the shells. For example, by mixing with a specific unfavorable solvent for shell-forming blocks, solvent-phobic, hierarchical association between micellar shells can occur, giving rise to patchy spherical(10) or striped cylindrical aggregates.(8,36) This approach relies on critical solvent condition manipulation and block composition design. Herein, we report a new, post-polymerization chemical modification method for

hierarchical inter-particle assembly of block copolymer nanoparticles. Crown ether functionalities were grafted onto shell-forming hydrophilic blocks as active sites capable of controlled inter-particle association and disassociation due to unique host-guest chemistry.(39)

In the present study, we selected a diblock copolymer pair of poly(acrylic acid)-*block*-poly(methyl methacrylate) (PAA-*b*-PMMA) and poly(acrylic acid)-*block*-polybutadiene (PAA-*b*-PB) with crown ether grafted to only the PAA-*b*-PMMA. Through kinetic control of the assembly process facilitated by solvent mixing, complex, spherical, micelle-like nanoparticles, with PMMA and PB mixed in the core and crown ether and PAA mixed in the shell, were assembled. As will be shown, tunable, subsequent inter-particle association was achieved by diammonium-crown ether inter-particle attractions after the addition of organic diamines.(39) Hierarchical formations, including one-dimensional micelle chains, two-dimensional micelle rings, and three-dimensional micelle aggregates, were obtained with easy manipulation of the extent of attraction by the amount of added diamines or blending ratio of the two diblock copolymers. The block copolymer nanoparticles that comprised the interparticle superstructures were dynamic internally to allow PMMA and PB to segregate into varying morphologies within the particle cores. By taking advantage of the reversible host-guest chemistry of crown ethers, disassembly of the hierarchical structures was then accomplished by the addition of potassium ion as a competitive guest. The ionic potassium competed with ammonium to associate with the crown ether in the shell of the nanoparticles, consequently cleaving the inter-particle diammonium-crown ether bonds and resulting in individual, multicompartment nanoparticles.

Results and Discussion

First, we prepared PAA_{90}-*b*-$PMMA_{100}$ and purchased PAA_{75}-*b*-PB_{104} diblock copolymers. The two diblock copolymers consisted of a PAA block with similar chain length and two different hydrophobic blocks, PMMA or PB. A post-polymerization chemical modification was applied to the PAA block of PAA_{90}-*b*-$PMMA_{100}$ only, with functionalization of approximately 40 percent of the AA units with 18-crown-6

functionalities, to obtain 18-crown-6-grafted PAA_{90}-*b*-$PMMA_{100}$ (P(crown$_{0.4}$-*g*-$AA_{0.6}$)$_{90}$-*b*-$PMMA_{100}$) (see experimental section for the detailed experiments and characterization data). The controlled solution-state assembly pathway for these amphiphilic diblock copolymers began with the dissolution of a desired amount of both of the diblock copolymers in *N,N*-dimethylformamide (DMF), a good solvent for all blocks. Subsequent fast addition of water had the combined effect of aggregating the hydrophobic PMMA and PB blocks into nanoparticle hydrophobic cores while concurrently swelling and solubilizing the hydrophilic blocks into the nanoparticle corona-like shell. Final spherical micelle-like particle formation was accomplished when water addition reached a volume ratio of 4:1, water:DMF in a rapid manner. Then, a certain amount of diamine, 2,2'-(ethylenedioxy)bis(ethylamine) (EDDA), was added into the particle solution. Amine groups in diamines are able to complex with both acid groups in acrylic acid side chains and the grafted crown ethers. It was found that diblock copolymer mixtures of PAA-*b*-PMMA and PAA–*b*-PB assembled into isolated spherical nanoparticles, confirmed by electron microscopy imaging with uranyl acetate negative staining (**Figure 3-1A**) or OsO_4 staining (**Figure 3-1B,** OsO_4 selectively stained PB by reacting with double bonds). No clear, segregated PB-rich domains were observed in the nanoparticle cores after OsO_4 staining, indicating PMMA and PB chains were initially well mixed in the nanoparticle cores. Interestingly, the exact same solution conditions and assembly pathway produced unique superstructures, such as the chain- and ring-like arrays of spherical particles as displayed in **Figure. 3-1C, 3D, and 3-7**, when the PAA-*b*-PMMA diblock with the 18-crown-6 modification was used in the diblock blend. Along a single chain of nanoparticles or nanoparticle ring formation, the sizes of individual particles varied slightly, similar to the nanoparticles from copolymer mixtures without the 18-crown-6 modification, **Figure 3-1B**. Of note, the chains and rings here produced from interparticle assembly are different from our earlier reported rods or toroids.(19) These earlier 1-D and ring-like assemblies were co-assembled from diamines and PAA-containing block copolymers in dilute solution, in which the diamines complexed with intra-micellar acrylic acid side chains to tune the hydrophilic-hydrophobic interfacial curvature and nanoparticle geometry into cylindrical hydrophobic core/hydrophilic corona micelle-like particles. In the earlier assemblies without crown ether modifications, no associations between individual particles were found, consistent with the observations here in **Figure 3-1A** and **3-1B**. Distinguished from all of our previous block copolymer assemblies,(8,19,25,39,41-43)(39) in the current

work the diamines were added into a pre-formed spherical nanoparticle solution of diblock copolymers (**Figure 3-6A**) at a controlled moment of choice to trigger the interparticle aggregation of particles.

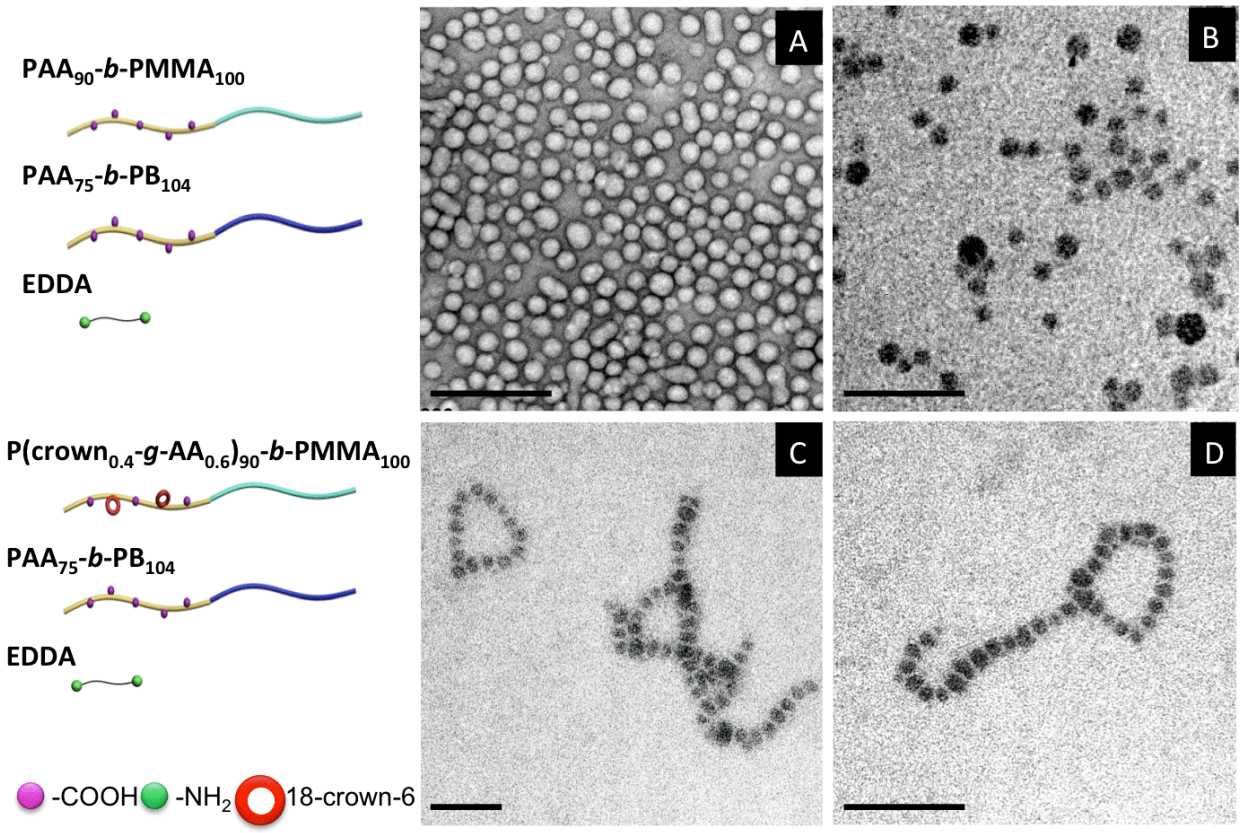

Figure 3-1. TEM images (A) and (B) of isolated particles assembled from PAA_{90}-*b*-$PMMA_{100}$ and PAA_{75}-*b*-PB_{104} diblock copolymer mixture in a 1:4 volume ratio of DMF and water mixture with added EDDA diamine (amine-to-PAA acid side chain molar ratio = 0.5:1.0), stained by uranyl acetate and osmium tetroxide, respectively; (C) and (D) show the nanoparticle chains and rings from $P(crown_{0.4}$-*g*-$AA_{0.6})_{90}$-*b*-$PMMA_{100}$ and PAA_{75}-*b*-PB_{104} mixture with added EDDA diamine (amine-to-PAA acid and crown ether side chain molar ratio = 0.5:1.0). Both block copolymer mixing molar ratios are 1:1.5. Samples were aged for 1 day and stained by OsO_4 before imaging. Scale bars = 200 nm.

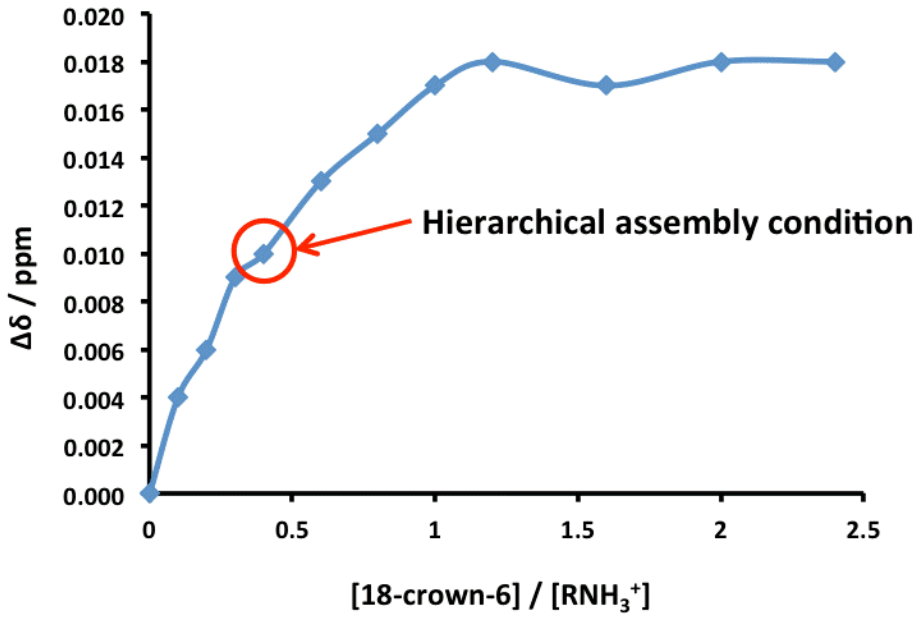

Figure 3-2. ^{1}H NMR titration curve for the solution of acetic acid and EDDA (acid : amine = 4 : 2.5) with the solution of 18-crown-6, in which the shift of $CH_2OCH_2\mathit{CH}_2NH_3^+$ peak (at ca. δ = 3.22 ppm) is monitored. The molar ratio of acid:18-crown-6:amine was 4:1:2.5 in the circled point, modeling the solution assembly condition employed for the polymer system.

In order to clarify the interactions driving the assembly, ^{1}H NMR studies were performed on small, model compounds under conditions that mimicked those used for block copolymer assembly. Acetic acid (modeling PAA) and diamine (EDDA) were mixed in D_2O at concentrations similar to the acid and base compositions present in the block copolymer assembly conditions. The signal at a chemical shift of 3.220 ppm refers to the amine-acid complex formation of $(CH_2OCH_2\mathit{CH}_2NH_3^+)_2$, in which the minority component amines were protonated by excess acid. This solution was then mixed with the D_2O solution of 18-crown-6 in a variety of ratios, and the chemical shifts of the $CH_2OCH_2\mathit{CH}_2NH_3^+$ peak (on the guest molecule EDDA) were monitored and plotted in **Figure 3-2**. The chemical shift kept changing until the ratio of crown ether to ammonium ion reached 1:1, where ammonium ions were all bound to crown ethers into 1:1 complexes. This observation demonstrated that the ammonium ion preferred to complex with crown ether over acetate due to the high stability of ammonium-crown ether complex structure. The

crown ether:RNH_3^+ ratio of ~0.4 in **Figure 3-2** matches the crown ether:amine ratio present in the block copolymer assembly condition in **Figure 3-1C** and **2-1D**. At this ratio, it is expected that all crown ethers were complexed with EDDA. Together with the TEM results, the NMR data suggest that the strong ammonium-crown ether binding enables inter-particle associations. The strength of inter-particle attraction is, thus, determined by the relative amount of crown ether functionalities as well as the added diamines.

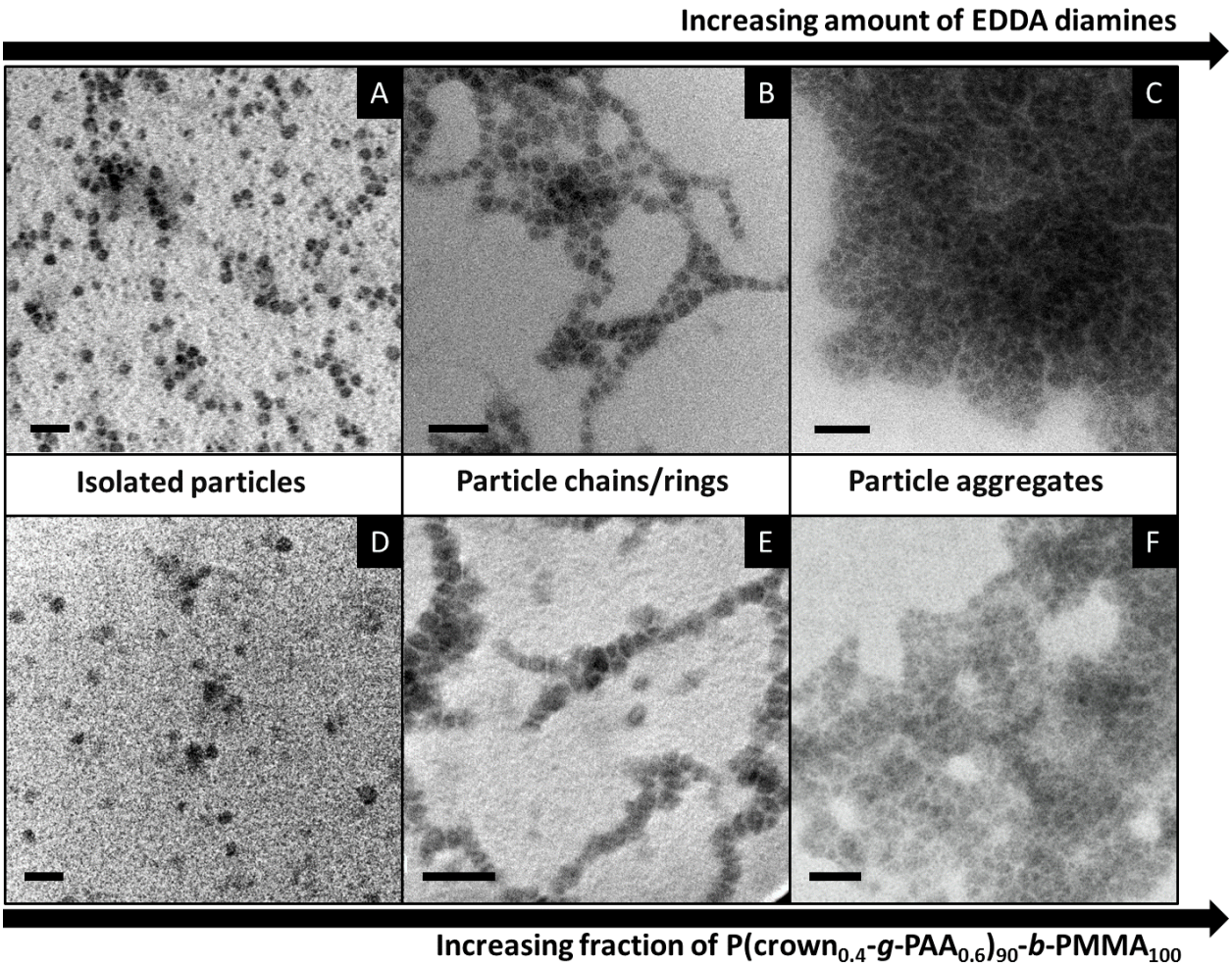

Figure 3-3. Morphological manipulation among isolated nanoparticles, particle chains/rings, and particle aggregates by differing the amounts of added diamine and diblock copolymer blending ratios. TEM images show the superstructures formed by P(crown$_{0.4}$-*g*-AA$_{0.6}$)$_{90}$-*b*-PMMA$_{100}$ and PAA$_{75}$-*b*-PB$_{104}$ mixed at a 1:1.5 molar ratio in a 1:4 volume ratio of DMF and water solution with EDDA at increasing amine to

(acid+crown ether) ratios from (A) 0, (B) 1:1, to (C) 2:1; At a fixed amine to (acid+crown ether) ratio of 0.5, varied superstructures were obtained from P(crown$_{0.4}$-*g*-AA$_{0.6}$)$_{90}$-*b*-PMMA$_{100}$ and PAA$_{75}$-*b*-PB$_{104}$ mixed at varied molar ratios from (D) 0, (E) 1:8, to (F) 5:1. Samples were aged for 1 day and stained by OsO_4 before imaging. Scale bars = 100 nm.

Geometrical variation in the hierarchical superstructures due to tunable inter-particle interactions could be accomplished by changing the amount of added EDDA or the mass blending ratios of diblock copolymers. In the absence of diamines, due to the electrostatic repulsion between the deprotonated PAA chains in the shell, isolated spherical nanoparticles were obtained in water/DMF solution (**Figure 3-3A**). When added EDDA reached a 0.5:1 molar ratio of amine-to PAA acid and crown ether side chain, short chains of spheres and rings of spheres were obtained as shown in **Figure 3-1C** and **3-1D**. Further addition of EDDA led to branched chains and chain networks (**Figure 3-3B**), and eventually to dense 3-D aggregates (**Figure 3-3C**). Similar structural transformations from isolated spheres (**Figure 3-3D**) to sphere chains (**Figure 3-3E**) and sphere aggregates (**Figure 3-3F**) were achieved by simply varying the blending ratios of the two diblock copolymers with a constant amount of EDDA. For example, by increasing the fraction of P(crown$_{0.4}$-*g*-AA$_{0.6}$)$_{90}$-*b*-PMMA$_{100}$ in the mixture, more crown ether groups in the particle shell improved the inter-particle attraction and less acrylic acids reduced the charge repulsion.

On the basis of evidence described above, we propose an assembly mechanism responsible for the hierarchical formations as illustrated in **Figure 3-4**. The solvent mixing process gives rise to complex nanoparticles with PMMA and PB blocks from different diblock copolymers mixed in the core and crown ether and acid side chains mixed in the shell. The nanoparticles are initially separated in solution because PAA is a weak acid and becomes slightly negatively charged in aqueous mixtures. When the diamine EDDA is added to the solution, EDDA complexes with the acid side chains ubiquitous in the shells of the nanoparticles. However, as shown in the NMR measurements summarized in **Figure 3-2,** after protonation due to interactions with PAA acid side chains, the protonated amines can then interact

strongly with crown ether functionalities also present in the shells of the nanoparticles. Only diamines that complex with crown ether groups from two neighboring particles can link the particles together as a nucleus from which further nanoparticles can connect to and grow into superstructures. As shown in **Figure 3-4**, the addition of a third particle can have three typical cases: linear packing, branched packing, and close packing, corresponding to position 1, 2, and 3. The final formations are determined by the relationship between charge repulsive forces due to deprotonated acid side chains in the shells of all nanoparticles and the attractions due to amine-crown ether inter-particle bindings that are position dependent; for instance, the repulsive force at position 3 is approximately twice that at position 1 or 2. The relative attractive forces are dependent on the fraction of crown either-containing PAA present in the shell and available amine present that can complex with the crown ether and link particles together. Samples with less crown either functionality or lower amount of amines will link in a linear fashion as highlighted in **Figure 3-4** at position 1 or 2 for linear and branched packing with minor shell contact. Case 2 can occur with a slightly higher amount of crown ether-diamine complexation in a particle adding to a linear chain, but, as seen in **Figure 3-1** and **3-2,** occurs much less in frequently than case 1 attachment. Finally, if there is more crown ether and diamine present, additional spheres will tend to interact as closely as possible with growing domains in order to maximize shell contact. Therefore, 3-D growth is preferred. As a result overall, one-dimensional chains of spheres, two-dimensional sphere rings, and three-dimensional sphere aggregates are three typical resultant formations correlated to the growth mechanisms of linear, branched and close packing, respectively.

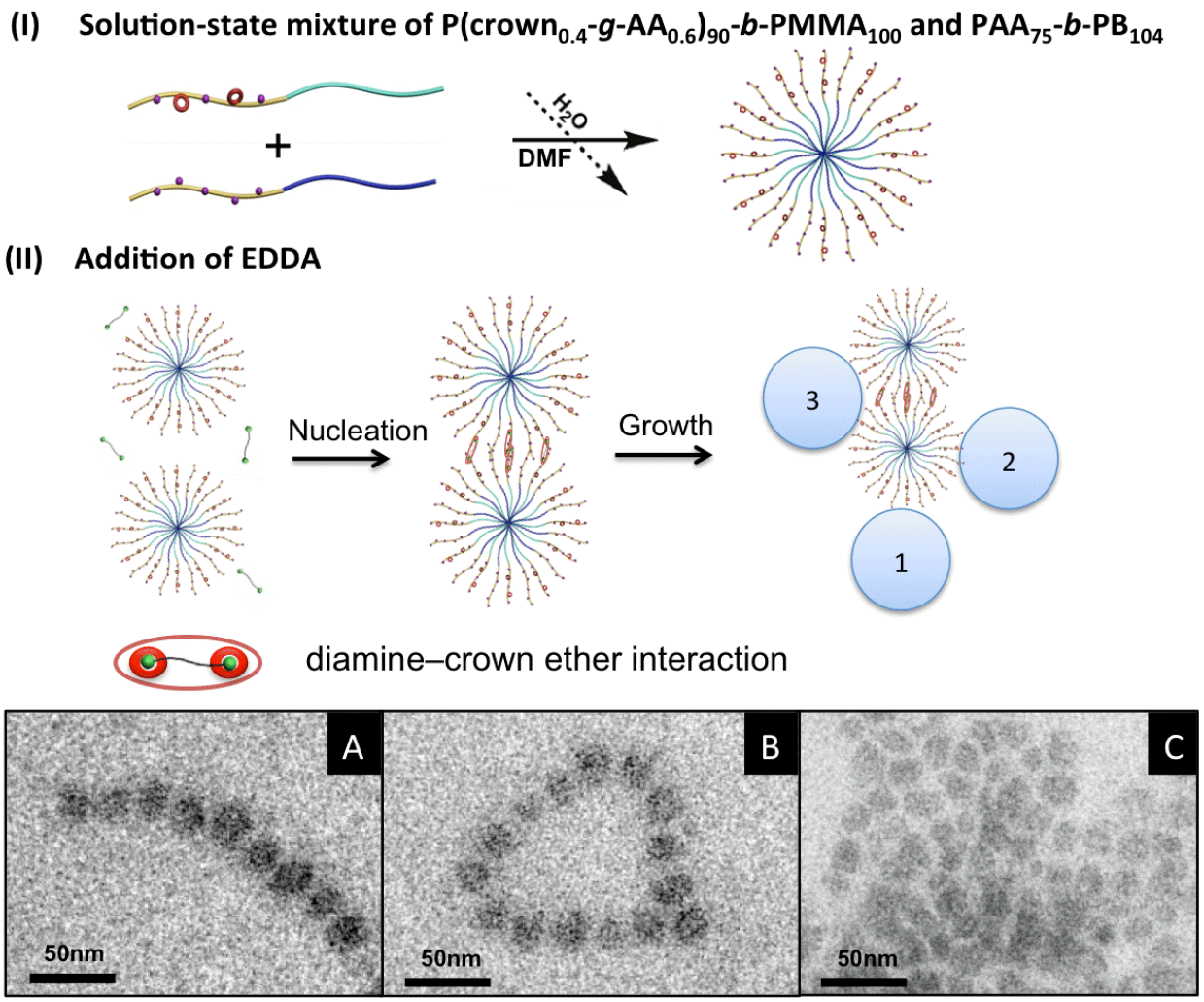

Figure 3-4. Hierarchical assembly process for superstructure formation consists of (I) nanoparticle assembly as building units, and (II) interparticle association. First, isolated nanoparticles were assembled from a diblock copolymer mixture of P(crown$_{0.4}$-*g*-AA$_{0.6}$)$_{90}$-*b*-PMMA$_{100}$ and PAA$_{75}$-*b*-PB$_{104}$ via fast water addition into DMF solution to a 4:1 volume ratio of water:DMF. Then, inter-micellar association is triggered by addition of diamine, EDDA. Through a proposed growth process, superstructures, such as (A) chains, (B) rings, and (C) 3-D aggregates were built with linear, branched, and close packing (corresponding to position 1, 2 and 3 in the illustration), respectively. TEM samples were stained by OsO_4.

Amphiphilic block copolymer assembles in solution are known as non-ergodic systems in which polymer chains are dynamic primarily within assemblies. The inability of the global system to equilibrate over relatively brief periods of time allows the production of kinetically-defined structural diversity and manipulation. In dilute solutions, mobility of polymer chains is typically limited for inter-micellar exchange due to the high molecular weight and the physical characteristics of the polymer segments,(46) yet available relatively fast for intra-micellar relaxation, inversion or segregation.(8) In case of isolated spherical micelles with PMMA and PB mixed core trapped within the same amine-PAA complexed shell, the initially well-mixed PMMA and PB blocks slowly phase-separated. As shown in **Figure 3-5B**, OsO_4 stained TEM image revealed dark semi-spherical PB-rich domains and light semi-spherical PMMA-rich domains in the particle cores. The volume ratio of the PB and PMMA subdomains well represented that of the original diblock copolymer mixtures. Directed by core phase separation, PAA blocks that are covalently linked to PB or PMMA blocks segregate in the shell as well. Therefore, in the case of inter-particle association in chains, the mobility and segregation of core blocks are strongly affected by supramolecular interactions in the shell. The chains of nanoparticles (**Figure 3-5D**) assembled from P(crown$_{0.4}$-*g*-AA$_{0.6}$)$_{90}$-*b*-PMMA$_{100}$ and PAA$_{75}$-*b*-PB$_{104}$ with EDDA eventually evolved into striped cylinders as shown in **Figure 3-5E**. The dark stripes perpendicular to the cylinder axis indicate layers of PB-rich domains that are selectively stained by OsO_4. The light stripes are composed of PMMA segments and EDDA-complexed P(crown$_{0.4}$-*g*-AA$_{0.6}$)$_{90}$ blocks.

The morphological evolution of the hierarchical structure is considered as an interparticle interaction-directed phenomenon as shown in **Figure 3-5F**. Once the micelles linked together into linear chains due to crown ether-containing PAA residing predominately in between connected particles, unmodified PAA chains moved away from the neighboring micelles to avoid energetically unfavorable electrostatic contacts. As a result, more stable, sandwich-like distribution of hydrophilic blocks was slowly reached where PAA segments packed in the middle perpendicular to the particle chain axis and P(crown$_{0.4}$-*g*-AA$_{0.6}$) segments aligned along the chain axis. This shell morphology directed unlike PB and PMMA blocks to progressively segregate into sandwich-like core subdomains, accordingly.

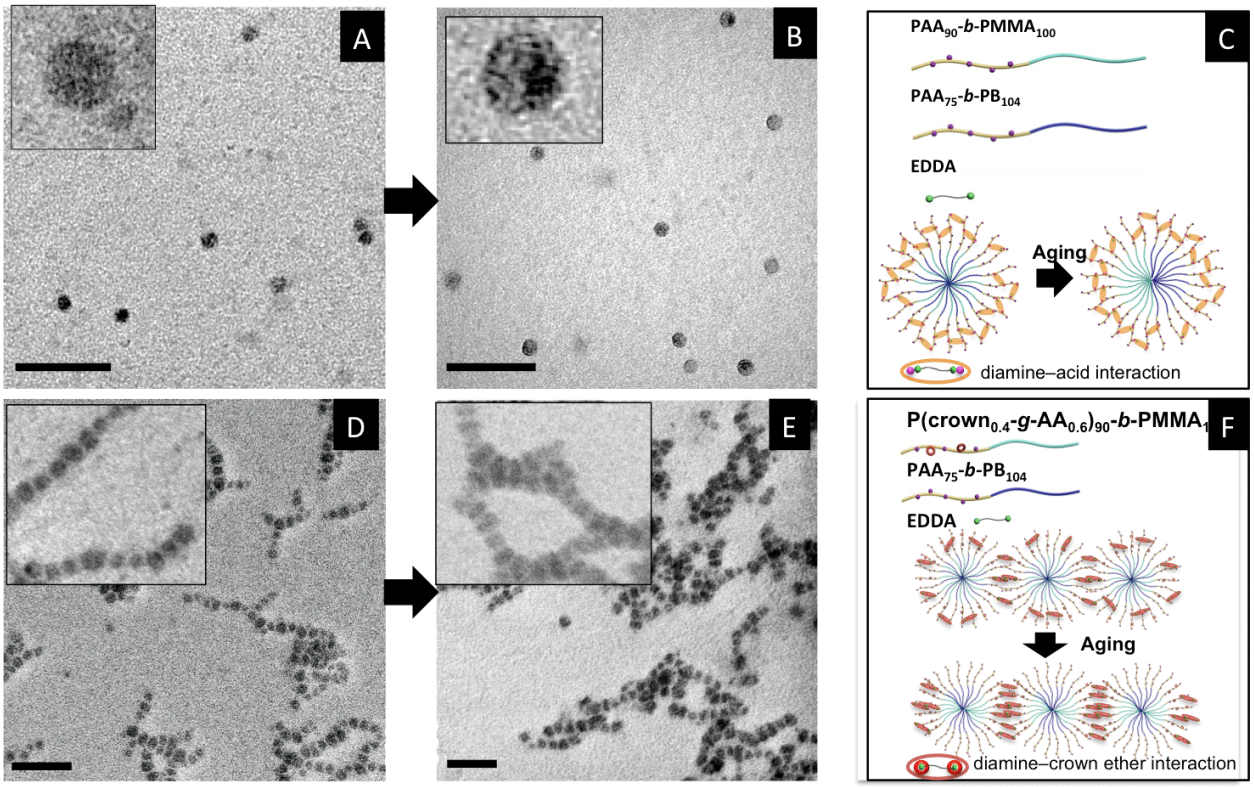

Figure 3-5. Morphological evolution of both isolated spherical nanoparticles and sphere chains. After 3 days aging, (B) multicompartment spherical nanoparticles were obtained from (A) mixed sphere of PAA_{90}-*b*-$PMMA_{100}$ and PAA_{75}-*b*-PB_{104} in a 1:4 volume ratio of DMF and water mixture with additional EDDA diamine (amine-to-PAA acid side chain molar ratio = 0.5:1.0). After 7 days aging of (D) sphere micelle chains from $P(crown_{0.4}$-*g*-$AA_{0.6})_{90}$-*b*-$PMMA_{100}$ and PAA_{75}-*b*-PB_{104} mixtures in a 1:4 volume ratio of DMF and water mixture with additional EDDA at an amine-to-PAA acid side chain molar ratio = 0.5:1.0, (E) striped cylinders were obtained. The proposed shell interaction-directed mechanism is illustrated in (F). All block copolymer mixing molar ratios (PMMA to PB volume ratios) were 1:1.5 (1:1). Samples were stained by OsO_4. Scale bars = 200 nm.

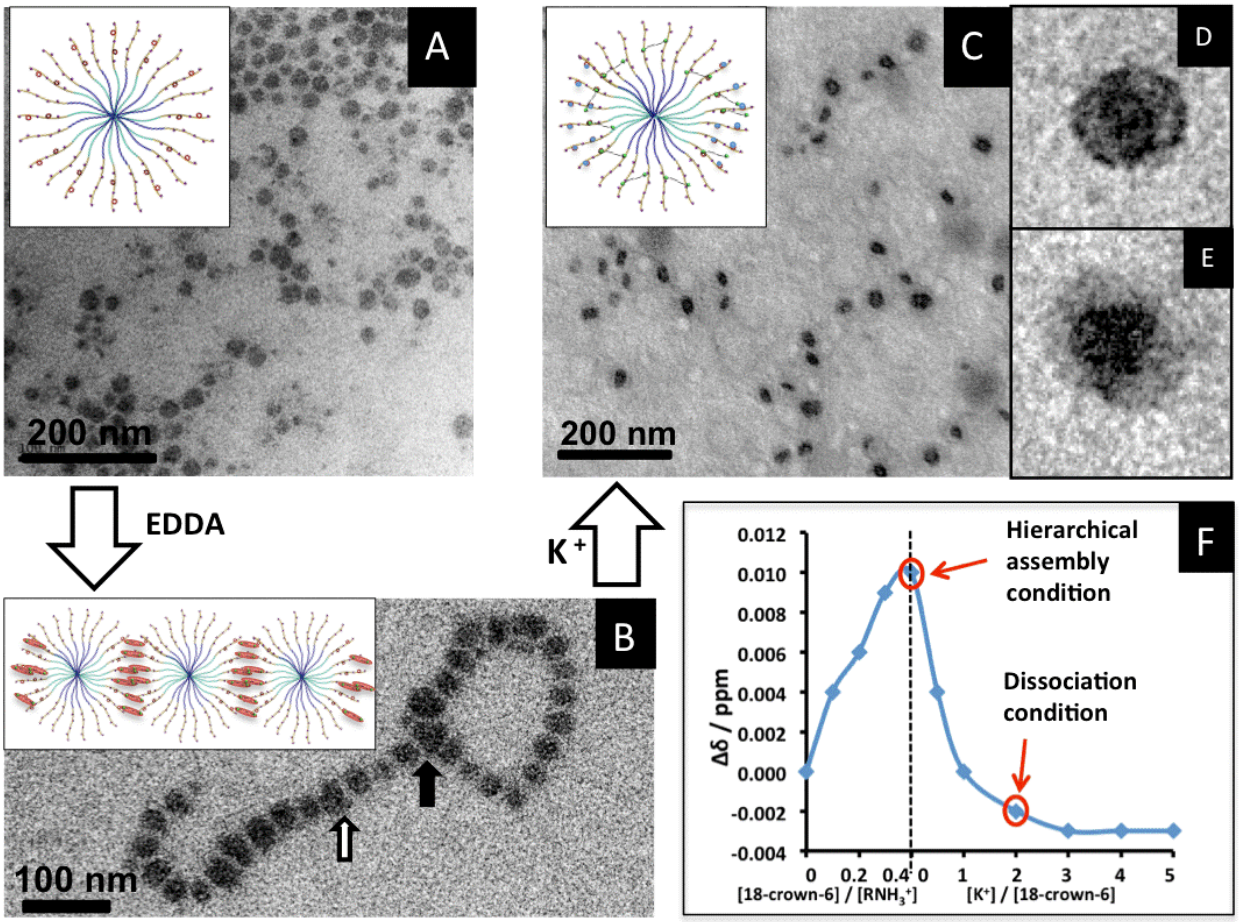

Figure 3-6. (A) Isolated spherical nanoparticles were obtained from P(crown$_{0.4}$-*g*-AA$_{0.6}$)$_{90}$-*b*-PMMA$_{100}$ and PAA$_{75}$-*b*-PB$_{104}$ at a mixing molar ratio (PMMA to PB volume ratio) of 1:1.5 (1:1) via fast water addition into DMF solution. Subsequent addition of EDDA gave rise to (B) nanoparticle chains and rings with multiple segregated core domains after 3 days aging. Through addition of excess K^+ (2:1 molar ratio of K^+ to crown ether), the hierarchical superstructures were cleaved into separated nanoparticles (C). Both sandwich (D) and concentric triangle (E) shaped multicompartment particles were obtained, which are correlated to the micelles that existed on the backbone (white arrow) and junction points (solid black arrow) of the micelle chains and rings (B), respectively. Samples were stained with OsO_4. (F) NMR shift of the $CH_2NH_3^+$ peak (at *ca.* δ = 3.22 ppm) of guest molecule EDDA on the addition of 18-crown-6 and followed by the addition of K^+. The molar ratio of acid:18-crown-6:amine:K^+ was 4:1:2.5:2 in the lower cycled point, modeling the addition of K^+ ion to trigger the dissociation.

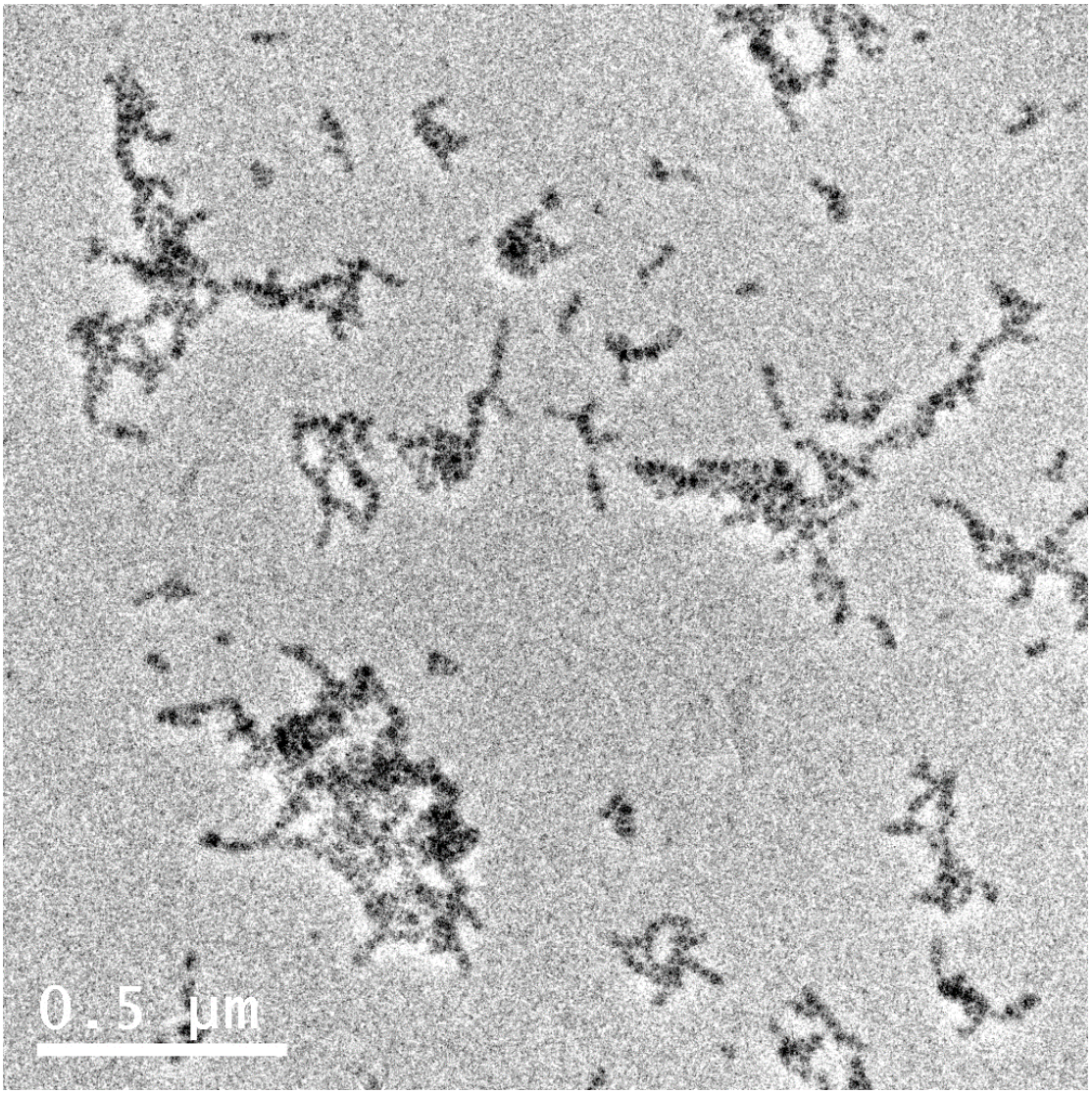

Figure 3-7. TEM image showing the nanoparticle chains and rings from P(crown$_{0.4}$-*g*-AA$_{0.6}$)$_{90}$-*b*-PMMA$_{100}$ and PAA$_{75}$-*b*-PB$_{104}$ mixture with added EDDA diamine (amine to PAA acid and crown ether side chain) molar ratio = 0.5:1.0). Block copolymer mixing molar ratios (PMMA to PB volume ratio) are 1:1.5 (1:1). Samples were aged for 1 day and stained by OsO_4 before imaging.

Disassembly of crown ether-ammonium linked superstructures was achieved by addition of competitive potassium ion (**Figure 3-6**).(39) Through addition of excess K^+ to break the linkage between the particle shells, the striped cylinders dissociated into separated nanoparticles (**Figure 3-6C**) that retained the

separated PB and PMMA compartments in the cores. Both sandwich (**Figure 3-6D**) and concentric triangle (**Figure 3-6E**) shaped multicompartment particles were obtained that correlated with the precursor particles that existed in the backbone (hollow black arrow) and junction points (solid black arrow) of the striped cylinder particle morphologies (**Figure 3-6B**), respectively. To verify the proposed mechanism for the dissociation of the nanoparticles with the addition of potassium ions, an additional ^{1}H NMR study on the model compounds was performed. As shown in **Figure 3-6F**, at the assembly condition for striped cylinders, EDDA was present in an excess relative to the crown ether and was completely protonated by the excess acid, allowing for complete complexation of the minority crown ether functionalities. Upon the addition of potassium ion, which binds to crown either 2 to 3 orders of magnitude more strongly than does the RNH_3^+,(47) the more weakly bound ammonium cation was released from the crown ether-ammonium complex. The addition of one equivalent of potassium ion was sufficient to complete this process to replace ammonium ion in the crown ether. The major advantage of using supramolecular chemistry for hierarchical assembly, apart from its relative ease, is the fact that the process is a reversible one, and the inter-particle associations can be broken at a controlled moment of choice. This method opens the possibility of controlled release due to a transition between wormlike and spherical particles,(48) as well as a "top-down" method(49) to fabricate novel, complex nanoparticles.

Conclusion

Here we reported a hierarchical assembly strategy of utilizing pre-formed block copolymer nanoparticles as building units to assemble into higher-ordered, multicompartment superstructures including 1-D chains, 2-D rings and 3-D aggregates. The complex block copolymer nanoparticles were pre-formed through a simple rapid solvent mixing process from a blend of two diblock copolymers sharing the same PAA hydrophilic block chemistry and having either PB or PMMA as the hydrophobic segment. Crown ether moieties were incorporated into the PAA block of the PAA-b-PMMA copolymer, through a post-polymerization modification, to provide tunable inter-particle interactions and hierarchical assembly processes with easy manipulation of added guest molecules (diamine or potassium ion) or the blending ratio of polymers. Interestingly, internal nanoparticle core morphological phase segregation of the PB and

PMMA was affected by associations between the shells of different nanoparticles, driven by supramolecular crown ether-ammonium interactions facilitated by small molecule diamine additives. The hierarchical assemblies could then be disassembled by addition of potassium ion into multicompartment nanoparticles, including sandwich-like and concentric triangle-shaped structures. This combination of selective chemical modification and kinetically-controlled assembly demonstrates the great potential of complex block copolymer nanoparticles for hierarchical material construction by inter-nanoparticle association.

Experimental

Materials

Poly(acrylic acid)$_{90}$-*b*-poly(methyl methacrylate)$_{100}$ (PAA$_{90}$-*b*-PMMA$_{100}$) diblock copolymers were synthesized by acidolysis of P*t*BA$_{90}$-*b*-PMMA$_{100}$ (PDI<1.20) precursors, which were prepared by sequential polymerization of methyl methacrylate and *tert*-butyl acrylate *via* atom transfer radical polymerization (ATRP).(50) IR: 3100-2900, 1750-1620, 1447, 1270-1080 cm^{-1}. ^{1}H NMR (DMF-d$_7$, ppm): δ 3.92-3.75 (s, -OC*H*$_3$), 2.76–1.26 (br,-C*H*C*H*$_2$- of the polymer backbone), 1.23-0.91 (s, C*H*$_3$). ^{13}C NMR (DMF-d7, ppm): δ 177.8, 176.4, 54.4-51.7, 44.6-41.5, 36.7-35.5. DSC: $(T_g)_{PMMA}$ = 119.5 °C, $(T_g)_{PAA}$ = 133.5 °C. TGA in N_2: 200–330 °C, 20% mass loss; 330–450 °C, 64% mass loss, 10% mass remaining above 450 °C.

Poly(18-crown-6-*g*-acrylic acid)$_{90}$-*b*-poly(methyl methacrylate)$_{100}$ (P(crown$_{0.4}$-*g*-AA$_{0.6}$)$_{90}$-*b*-PMMA$_{100}$) diblock copolymers were synthesized by amidation of PAA$_{90}$-*b*-PMMA$_{100}$ with commercially-available 2-aminomethyl-18-crown-6. EDCI, 1-HOBt and 2-aminomethyl-18-crown-6 were used (0.45 equivalent to acid unit) and the mixture was allowed to undergo reaction for 24 hours. After dialysis for three days to remove byproducts and unreacted compounds, the white powder-like product was obtained from lyophilization with a 85% yield. ^{1}H NMR confirmed that the conjugation efficiency was about 90%. IR: 3650-3020, 3020-2780, 1728, 1643, 1558, 1450, 1242, 1103, 964 cm^{-1}. ^{1}H NMR (DMF-d$_7$, ppm): δ 3.92-

2.98 (br,-OCH_2CH_2O- and -OCH_3), 2.76–1.26 (br,-CHCH_2- of the polymer backbone), 1.23-0.91 (s, CH_3). ^{13}C NMR (DMF-d7, ppm): δ 177.8, 176.4, 174.9, 72.0-67.4, 54.6-51.7, 44.6-41.3, 36.9-35.4. DSC: $(T_g)_{PMMA}$ = 120.8 ℃, $(T_g)_{crown\text{-}g\text{-}PAA}$ = 157.2 ℃. TGA in N_2: 310–410 °C, 47% mass loss; 410–500 °C, 12% mass loss, 35% mass remaining above 500 °C.

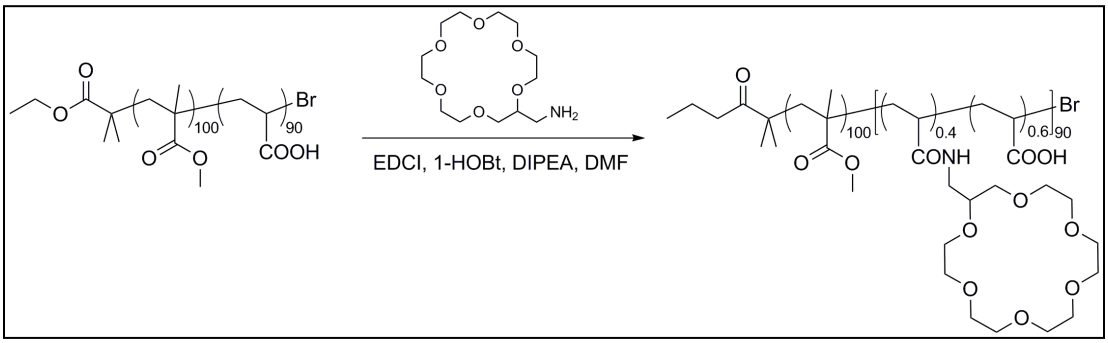

Scheme 2-1. Synthesis of poly(18-crown-6-*g*-acrylic acid)$_{90}$-*b*-poly(methyl methacrylate)$_{100}$

Poly(acrylic acid)$_{75}$-*b*-polybutadiene$_{104}$ (PAA$_{75}$-*b*-PB$_{104}$) diblock copolymers

PAA-*b*-PB diblock copolymer was purchased from Polymer Source, Inc. and used as received. PDI = 1.10.

2,2'-(Ethylenedioxy)bis(ethylamine) (EDDA) was purchased from Sigma-Aldrich Corporation.

Dimethylformamide (DMF) was purchased from Acros Organics.

2. Sample preparation and characterizations

Complex nanoparticle assembly

PAA$_{90}$-*b*-PMMA$_{100}$ or P(crown$_{0.4}$-*g*-AA$_{0.6}$)$_{90}$-*b*-PMMA$_{100}$ and PAA$_{75}$-*b*-PS$_{104}$ diblock copolymers at a certain blending ratio were first dissolved in DMF to produce a 0.1 weight percent solution of block copolymer. Fast water addition was accomplished by simply pipetting a certain amount of water into the polymer-DMF solution. After addition of a certain amount of diamine EDDA, sample solutions were sealed in vials at ambient condition before characterization. The time duration was recorded as aging time.

Transmission electron microscopy (TEM)

TEM imaging was performed on a Tecnai 12 microscope operating at an accelerating voltage of 120 kV. TEM samples were prepared by applying a drop of polymer solution (about 2–4 ul) onto a carbon-coated copper TEM grid and allowing the solvents to evaporate under ambient conditions. Images were collected on a Gatan CCD. A vapor staining method was applied to TEM samples. Dried TEM grids were placed on a 25x75x1 mm glass slide to sit in a sealed 100 mL glass bottle suspended above 1 mL 4 wt% osmium tetroxide aqueous solution (purchased from Electron Microscopy Sciences). OsO_4 vapor staining process lasted from 6 hours to 24 hours for different samples.

^{1}H nuclear magnetic resonance (^{1}H NMR)

^{1}H NMR spectra were recorded on an Inova 500 MHz spectrometer interfaced to a UNIX computer using VnmrJ software. Chemical shifts were referenced to the internal 3-trimethylsilylpropionate-d_6 (TSP). The chemical shift of TSP was reported to be pH dependent.(51) The chemical shifts of TSP were referenced to the internal acetone, and showed no change over the pH range of the entire experiment.

Solution A was 0.4630 g of EDDA and 0.6020 g of acetic acid dissolved in 20 mL of D_2O. The molar ratio of amine to acid was 2.5 : 4, which was the final ratio in the polymer self-assembly condition.

Solution B was 0.3320 g of 18-crown-6 dissolved in 10 mL of D_2O. In the same volume of respective solutions, the molar ratio of acetic acid to 18-crown-6 was 4:1, which was the ratio in the polymer self-assembly condition.

Solution C was 0.938 g of potassium chloride dissolved in 10 mL of D_2O. In the same volume of respective solutions, the molar ratio of KCl to 18-crown-6 was 1:1.

The chemical shift of $(CH_2OCH_2\mathit{CH}_2NH_3^+)_2$ was 3.220 ppm in solution A. The changes of this chemical shift were recorded as evidence of complexation and dissociation. Solution A and solution B were mixed

in the ratios of 1:0.25, 1:0.5, 1:0.75, 1:1, 1:1.5, 1:2; 1:2.5; 1:3, 1:4, 1:5, 1:6, among which the ratio of 1:1 mimicked the ratio of EDDA, PAA and crown ether present in the polymer self-assembly condition (**Figure 3-1**). Solution A, solution B and solution C were mixed in the ratios of 1:1:0.5, 1:1:1, 1:1:2, 1:1:3, 1:1:4, 1:1:5, among which the ratio of 1:1:2 mimicked the ratio of the addition of KCl to trigger the dissociation.

Acknowledgements

This material is based upon work supported by the National Science Foundation under grants DMR-0906815 (DJP and KLW) and DMR-1105304 (KLW) and the W. T. Doherty-Welch Chair in Chemistry, Grant No. A-0001 (KLW). Prof. George W. Gokel is acknowledged for insightful background contributions (S.Z.). We thank the Keck Electron Microscopy lab at University of Delaware, Prof. Chaoying Ni and Mr. Frank Kriss for microscopy assistance.

Reference

(1) Pinheiro, A. V.; Han, D.; Shih, W. M.; Yan, H. *Nat. Nano.* **2011**, 6, 763-772.

(2) Miszta, K.; de Graaf, J.; Bertoni, G.; Dorfs, D.; Brescia, R.; Marras, S.; Ceseracciu, L.; Cingolani, R.; van Roij, R.; Dijkstra, M.; Manna, L. *Nat. Mater.* **2011**, 10, 872-876.

(3) Chen, Q. ; Whitmer, J. K.; Jiang, S.; Bae, S. C.; Luijten, E.; Granick, S. *Science* **2011**, 331, 199-202.

(4) Chen, Q.; Bae, S. C.; Granick, S. *Nature* **2011**, 469, 381-384.

(5) Zhang, L.; Eisenberg, A. *Science* **1995**, 268, 1728-1731.

(6) Discher, B.M.; Won, Y.-Y.; Ege, D.S.; Lee, J. C.-M.; Bates, F.S.; Discher, D.E.; Hammer, D.A. *Science* **1999,** 284, 1143-1146.

(7) Jain, S.; Bates, F.S. *Science* **2003**, 300, 460-464.

(8) Cui, H.; Chen, Z.; Zhong, S.; Wooley, K. L.; Pochan, D.P. *Science* **2007**, 317, 647-650.

(9) Wang, X.; Guerin, G.; Wang, H.; Wang, Y.; Manners, I.; Winnik, M.A. *Science* **2007**, 317, 644-647.

(10) Gröschel, A. H.; Schacher, F. H.; Schmalz, H.; Borisov, O. V.; Zhulina, E. B.; Walther, A.; Müller, A. H. E. *Nat. Commun.* **2012**, 3, 710.

(11) Bielawski, C. W.; Grubbs, R. H. *Prog. Polym. Sci.* **2007**, 32, 1–29.

(12) Tsarevsky, N. V.; Matyjaszewski, K. *Chem. Rev.* **2007**. 107*,* 2270-2299.

(13) Hawker, C. J.; Wooley, K. L. *Science* **2005**, 309, 1200-1205.

(14) Li, Z. B.; Kesselman, E.; Talmon, Y.; Hillmyer, M. A.; Lodge, T. P. *Science* **2004**, 306, 98-101.

(15) Hayward, R.C.; Pochan, D.J. *Macromolecules* **2010**, 43, 3577-3584.

(16) Edmonds, W. F.; Li, Z.B.; Hillmyer, M. A.; Lodge, T.P. *Macromolecules* **2006**, 39, 4526-4530.

(17) Yin, L.; Hillmyer, M.A. *Macromolecules* **2011**, 44, 3021-3028.

(18) Li, Z. B.; Chen, Z. Y.; Cui, H.; Hales, K.; Wooley, K. L.; Pochan, D. J. *Langmuir* **2007**, 23, 4689-4694.

(19) Pochan, D. J.; Chen, Z. Y.; Cui, H.; Hales, K.; Qi, K.; Wooley, K. L. *Science* **2004,** 306, 94-97.

(20) Du, J.; O'Reilly, R.K. *Chem. Soc. Rev*. **2011**, 40, 2402-2416.

(21) Du, J.; Chen, Y. *Angew. Chem., Int. Ed.* **2004**, 43, 5084–5087.

(22) Christian, D. A.; Tian, A.; Ellenbroek, W. G.; Levental, I.; Rajagopal, K.; Janmey, P.A.; Liu, A.J.; Baumgart, T.; Discher, D.E. *Nat. Mater.* **2009**, 8, 843–849.

(23) Kubowicz, S.; Baussard, J.F.; Lutz, J.F.; Thünemann, A.F.; von Berlepsch, H.; Laschewsky, A. *Angew. Chem. Int. Ed.* **2005**, 44, 5262–5265.

(24)Dupont, J.; Liu, G. *Soft Matter* **2010**, 6, 3654–3661.

(25)Pochan, D. J.; Zhu, J.; Zhang, K.; Wooley, K. L., Miesch, C.; Emrick, T. *Soft Matter* **2011**, 7, 2500–2506.

(26)Walther, A.; and Müller, A. H. E. *Soft Matter* **2008**, 4, 663-668.

(27)Lodge, T. P.; Rasdal, A.; Li, Z. B.; Hillmyer. M. A. *J. Am. Chem. Soc.* **2005**, 127, 17608–17609

(28)Schacher, F.; Betthausen, E.; Walther, A.; Schmalz, H.; Pergushov, D.V.; Müller, A.H.E. *ACS Nano* **2009**, 3, 2095–2102.

(29)Zhang, S.; Li, Z.; Samarajeewa, S.; Sun, G.; Yang, C.; Wooley, K.L. *J. Am. Chem. Soc.* **2011**, 133, 11046–11049.

(30)Zhang, Z.; Glotzer, S. C. *Nano Lett.* **2004**, 4, 1407–1413.

(31)Williamson, A.J.; Wilber, A.W.; Doye, J. P. K.; Louis, A. A. *Soft Matter* **2011**, 7, 3423-3431.

(32)Glotzer, S.C.; Solomon, M. J. *Nat. Mater.* **2007**, 6, 557–562.

(33)Motornov, M.; Malynych, S.Z.; Pippalla, D.S.; Zdyrko, B.; Royter, H.; Roiter, Y.; Kahabka, M.; Tokarev, A.; Tokarev, I.; Zhulina, E.; Kornev, K.G.; Luzinov, I.; Minko, S. *Nano Lett.*, **2012**, 12, 3814-3820.

(34)Meng, G.; Arkus, N.; Brenner, M. P.; Manoharan, V. N. *Science* **2010**, 327, 560-563.

(35)Saito, N.; Liu, C.; Lodge, T.P.; Hillmyer, M.A. *ACS Nano* **2010**, 4, 1907–1912.

(36)Fang, B.; Walther, A.; Wolf, A.; Xu, Y.; Yuan, J.; Müller, A.H.E. *Angew. Chem. Int. Ed.* **2009**, 48, 2877 –2880.

(37)Kuo, S.W.; Tung, P.H.; Lai, C.L.; Jeong, K.U.; Chang, F.C. *Macromol. Rapid. Commun.* **2008**, 29, 229-233.

(38)Li, G.; Shi, L.; Ma, R.; An, Y.; Huang, N. *Angew. Chem. Int. Ed.* **2006**, 45, 4959-4962.

(39)Dykes, G.M.; Smith, D.K.; Seeley, G.J. *Angew. Chem. Int. Ed. Engl.* **2002**, 41, 3254-3257.

(40)Chen, Z.; Cui, H.; Hales, K.; Li, Z.; Qi, K.; Pochan, D.J.; Wooley, K.L. *J. Am. Chem. Soc.* **2005**, 127, 8592-8593.

(41)Li, Z.; Chen, Z.; Cui, H.; Hales, K.; Qi, K.; Wooley, K.L.; Pochan, D.J. *Langmuir* **2005**, 21, 7533-7539.

(42)Cui, H.; Chen, Z.; Wooley, K.L.; Pochan, D.J. *Macromolecules* **2006**, 127, 8592-8593.

(43)Zhong, S.; Cui, H.; Chen, Z.; Wooley, K.L.; and Pochan, D.J. *Soft Matter* **2008**, 4, 90-93.

(44)Zhang, L.; Yu, K.; Eisenberg, A. *Science* **1996**, 272, 1777-1779.

(45)Yang, S.; Yu, X.; Wang, L.; Tu, Y.; Zheng, J.X.; Xu, J.; Van Horn, R. M.; Cheng, S. Z. D. *Macromolecules* **2010**, 43, 3018-3026.

(46)Choi, S.-H.; Lodge, T.P.; Bates, F.S. *Phys. Rev. Lett.* **2010**, 104, 047802.

(47) Dykes, G. M.; Smith, D. K. *Tetrahedron* **2003**, 59 3999–4009.

(48) Geng, Y.; Dalhaimer, P.; Cai, S.; Tsai, R.; Tewari, M.; Minko, T.; Discher, D.E. *Nat. Nano.* **2007**, 2, 249-255.

(49) Erhardt, R.; Bocker, A.; Zettl, H.; Kayz, H.; Pyckhout-Hintzen, W.; Krausch, G.; Abetz, V.; Müller, A. H. E. *Macromolecules* **2001**, 34, 1069-1075.

(50) Dayananda, K.; Dhamodharanm R. *J. of Polym. Sci.: Part A: Polym. Chem.* **2004**, 42, 902-915

(51) Wishart, D. S.; Bigam, C. G.; Yao, J.; Abildgaard, F.; Dyson, H. J.; Oldfield, E.; Markley, J. L.; Sykes, B. D. *J. of Biomolecular NMR* **1995**, *6*, 135-14

Chapter 4

Facile synthesis of clickable, water-soluble and degradable polyphosphoesters

[Portions of this work have been published previously as Shiyi Zhang, Ang Li, Jiong Zou, Lily Yun Lin, and Karen L. Wooley, *ACS Macro Lett.,* **2012**, *1*, 328-333.]

Abstract

"Click" chemistry is a library of efficient and reliable reactions, which have been used to functionalize various classes of bio- and synthetic macromolecular systems for the incorporation of designed properties and functions. In this report, azide-alkyne Huisgen cycloaddition and thiol-yne reactions, two classical "click" chemistries, were employed to functionalize biodegradable, clickable polyphosphoester homopolymers and their water-soluble copolymers. A stable alkyne-functionalized phospholane monomer was synthesized, its organocatalyzed polymerization kinetics were evaluated, and the resulting (co)polymers were utilized to develop this facile method that provides the synthesis of clickable, water-soluble and degradable polyphosphoesters, which can be adapted for various applications.

Introduction

Biodegradable synthetic polymers have been attracting considerable attention due to their potential for environmental and biological clearance, which allows for many applications, including in medical devices, for instance in tissue engineering, regenerative medicine, gene therapy, and controlled drug delivery.(1, 2) High molecular weight degradable polymers, including polyesters, polycarbonates and polyphosphoesters, are often prepared by ring-opening polymerization (ROP) of cyclic monomers, which mechanistically offers control over the polymer molecular weights, molecular weight distributions, compositions and structures. Furthermore, chemical functionalizations of these polymers expands their specific properties to tune their physical, chemical, biological, and mechanical behaviors.(3) Chemical modification of polymers *via* "click" chemistry has advantages including quantitative conversion, rapid reaction, and high

functional group tolerance, with an absence of byproducts and side reactions. A library of chemical reactions has been advanced for the preparation and functionalization of new polymeric materials.(4, 5) Recently, several classes of biodegradable polyesters(6-10) and polycarbonates(11-14) bearing “click” functionalities have been synthesized and post-functionalized. With the increasing breadth of the types of “click” chemistry reactions, several can be identified for combinations with ROP to afford functional degradable polymers, while avoiding incompatibilities with ROP conditions. Although initial systems have involved multistep monomer syntheses, tedious isolations, and/or limited water solubility,(6-14) a key goal is to increase the efficiency of monomer production and broaden the chemical and physical properties.

Besides polyesters and polycarbonates, polyphosphoesters are attractive for bio-related fields due to their biocompatibility, biodegradability (through hydrolysis that is either spontaneous or catalyzed by certain enzymes), and their structural similarity to nucleic and teichoic acids.(15) The ROP of cyclic phospholane monomers, which are prepared from the condensation of an alcohol and 2-chloro-2-oxo-1,3,2-dioxaphospholane (COP, **1**), is the most common process to obtain well-defined high molecular weight polyphosphoesters. Tailoring of the polyphospho-ester structure by manipulation of pendant groups on the pentavalent phosphorus atom enables precise control over the chemical functionalities and topological structures of the polymers.(16) Iwasaki *et al.* reported the first organocatalyzed ROP of cyclic phospholanes, by using 1,8-diazabicyclo[5.4.0]undec-7-ene (DBU) or 1,5,7-triazabicyclo[4.4.0]dec-5-ene (TBD), which eliminated the usage of environmentally-sensitive metal compounds, to fulfill the requirements of biomedical applications.(17) In this report, we synthesized a new type of reactive polyphosphoester bearing alkynyl groups, **2**, by using organocatalysis for the ROP of an alkynyl-functionalized phospholane monomer, **3**, and investigated the chemical availability of the alkyne groups by employing “click” type azide-alkyne Huisgen cycloaddition(4) and thiol-yne(18, 19) reactions, as shown in **Scheme 4-1**. In addition, a series of clickable, water-soluble and degradable polyphospho-ester copolymers with tunable solubilities, is also reported.

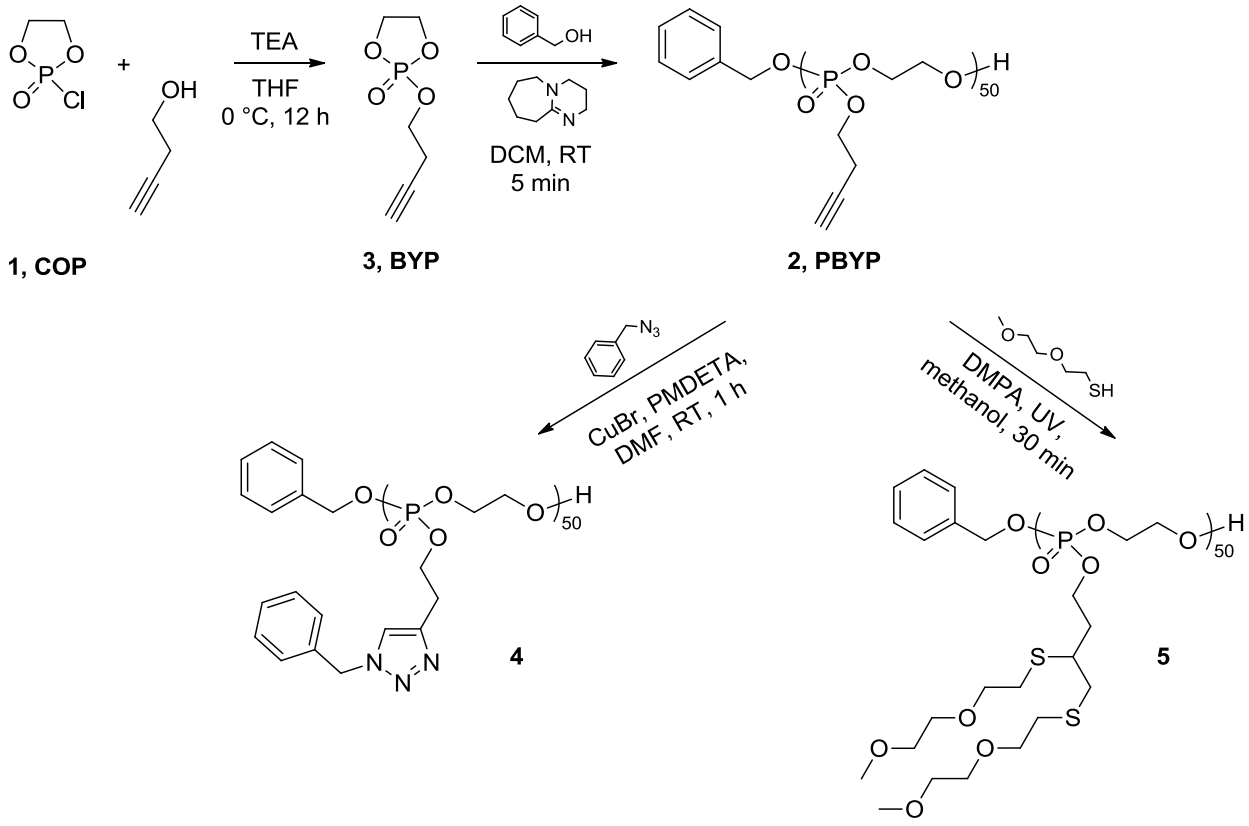

Scheme 4-1. Synthetic routes from monomer, 2-(but-3-yn-1-yloxy)-2-oxo-1,3,2-dioxaphospholane (BYP, 3), synthesis, to poly(2-(but-3-yn-1-yloxy)-2-oxo-1,3,2-dioxaphospholane) (PBYP, 2), and two "click" type reactions.

Results and Discussion

The monomer, butynyl phosphate (BYP, **3**) was synthesized by coupling COP to 3-butyn-1-ol, according to the approach that has been reported for a variety of cyclic phospholane monomers towards the preparation of functional degradable polymers.(20-24) In contrast, initial attempts at the preparation and isolation of the propargyl analog (PAP) was not successful. As monitored by ^{31}P NMR spectroscopy, two major products, among others, were generated during the reaction of propargyl alcohol with COP in the presence of triethylamine (**Figure 4-1**). Pure PAP could be obtained by vacuum distillation in only a low yield (<20%). Although the preparation and ROP of PAP, followed by the azide-alkyne Huisgen cycloaddition on the resulting polymers has been reported,(25) in our hands, we suspect that reactions

via the S_N2' mechanism might be responsible for the decomposition of the monomer. In fact, in the published work,(25) the expected signal of the terminal acetylene proton is absent or of too low intensity in the ^1H NMR spectra provided for PAP-based polyphosphoesters, suggesting loss or partial loss of the alkynyl functionality. For S_N2', unlike ordinary S_N2, the nucleophile attacks indirectly at the electrophilic site but in a conjugate addition over the double or triple bond (as depicted in **Scheme 4-2**).(26, 27) Since the phosphate group is a good leaving group,(28) it can be expelled even in the absence of a strong nucleophile. To eliminate the potential for S_N2' reaction, a methylene spacer between the phosphate and the propargyl group was incorporated. The resulting product, BYP (**3**), with high yield and purity, as shown in **Figure 4-2**, was obtained through a one-step esterification reaction between two commercially-available compounds, 3-butyn-1-ol and COP followed by simple filtration and vacuum distillation. In contrast, most clickable monomers for ROP involve multistep syntheses and tedious isolations.

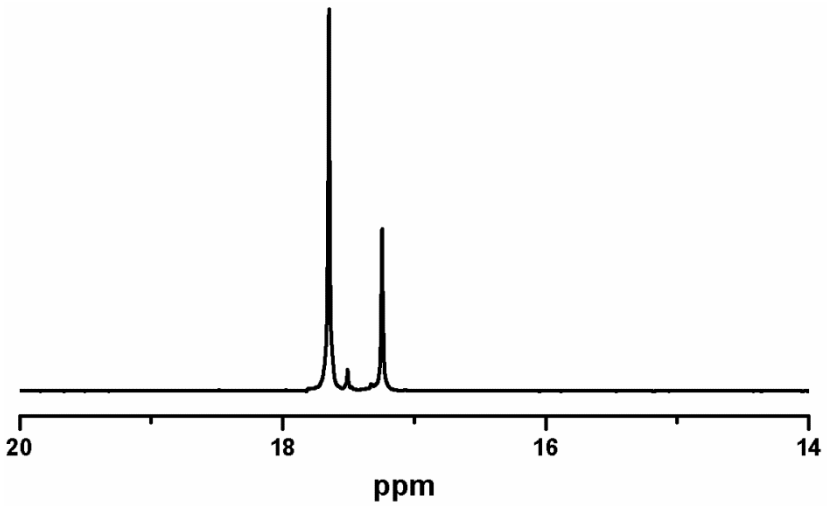

Figure 4-1. ^{31}P NMR spectrum (121 MHz, $CDCl_3$) of the crude reaction mixture of propargyl alcohol and 2-chloro-2-oxo-1,3,2-dioxaphospholane. Only the region of the spectrum that shows resonances for product signals is included; the starting material resonance is observed at 22.8 ppm and was fully consumed by the excess propargyl alcohol.

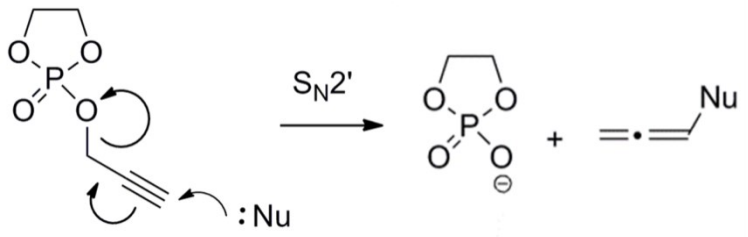

Scheme 4-2. Schematic representation of the decomposition of propargyl phosphate through S_N2 prime mechanism.

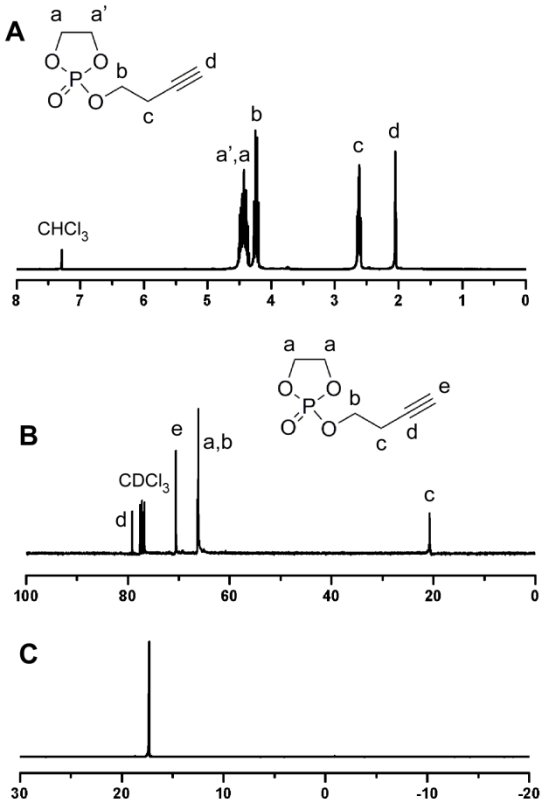

Figure 4-2. NMR spectra of BYP in $CDCl_3$ (ppm): (A) ^{1}H NMR (300 MHz), (B) ^{13}C NMR (75 MHz), (C) ^{31}P NMR (121 MHz).

The ROP of **3** was conducted by using DBU as the catalyst and benzyl alcohol as the initiator. After Iwasaki *et al.* reported organocatalytic ROP of cyclic phospholane monomer in sol-vent-free conditions,(17) Yan *et al.* also reported the ROP from a macroinitiator by using DBU as the catalyst under

solvent-free conditions.(29) When employing DBU as the catalyst, the reported monomer conversion reached *ca.* 60% after more than one hour, and the reactions were halted once the magnetic stirrer stopped moving due to high viscosity of the polymerization mixture. In order to achieve higher monomer conversion, we applied dichloromethane (DCM) as the solvent with monomer concentration of 1 g/mL. Interestingly, the polymerization under this low viscosity condition proceeded rapidly to high monomer conversion. The conversion of **3** quickly reached over 95 % after only 6 min with good control of the polymerization being retained. The reaction also proceeded faster than reported typically for $Sn(Oct)_2$ catalyzed polymerizations.(15, 24, 25, 30) However, when monomer concentration was lowered to 0.1 g/mL, high molecular weight polymer was not observed, even after more than 24 h.

We studied the kinetics of this ROP by conducting parallel experiments, which allowed for monitoring of this extremely fast reaction. First, **3** and benzyl alcohol (molar ratio of 100 : 1) were premixed in anhydrous DCM and the solution was divided equally into ten portions, to each of which was added solutions of DBU (molar ratio to initiator of 1.5 : 1) in anhydrous DCM. After being stirred for preset periods of time, the reactions were quenched by addition of acetic acid. The conversion of each individual polymerization was obtained from ^{31}P NMR, while the molecular weight and its distribution were determined by gel permeation chromatography (GPC), calibrated against linear polystyrene standards with DMF as the mobile phase. The linearity of M_n *vs* monomer conversion suggested that the number of macromolecules in the reaction system was constant during polymerization, up to 95% conversion (**Figure 4-3 A**). The polydispersity indices (PDI) were all less than 1.20, and when the conversion was controlled at lower than 80%, even lower PDI values were obtained (<1.10). The increased polydispersity could be attributed to adverse transesterification of the polymer backbone at high monomer conversions.(31) Kinetic plots of $\ln([M]_0/[M])$ *vs* time, showed first order kinetics, characteristic of ring-opening polymerization of **3** (**Figure 4-3 B**), and suggesting that the rate constant of initiation was more than or equal to the rate constant of propagation.(32)

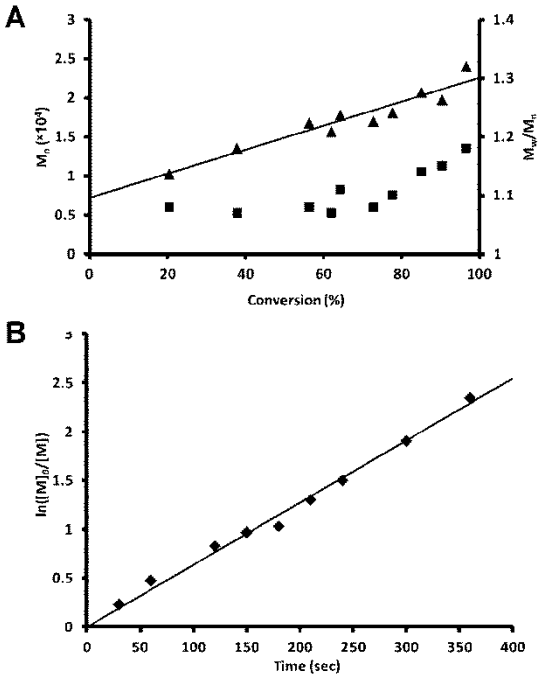

Figure 4-3. (A) Plot of M_n and M_w/M_n *vs* monomer conversion for the polymerization of **3** by using DBU as the catalyst and benzyl alcohol as the initiator, obtained from GPC analyses. Monomer : initiator : DBU ratio was 100 : 1 : 1.5. (B) Kinetic plots of $\ln([M]_0/[M])$ *vs* time, obtained from ^{31}P NMR spectroscopy data.

A series of **2** with different molecular weights was synthesized by controlling monomer to initiator ratios, as summarized in **Table 4-1**. The degrees of polymerization calculated from ^{31}P NMR-determined monomer conversion values agreed with those calculated from ^{1}H NMR chain end analyses, based upon comparison of the integration values of the benzyl group chain terminus protons and resonances for protons of the side groups of **2**. In each case, the terminal acetylene proton (2.18-2.04 ppm) was present within each repeat unit, as confirmed by being observed with the correct integration compared to the methylene protons (**Figure 4-4 A**). The glass transition temperature (T_g) for all samples of **2** was measured to be -35 ± 1 °C, which is attributed to their highly viscous liquid form at room temperature, and was independent of chain length over the range of DP_n 25 to 100. The high monomer conversion (>98 %) and stability of the clickable functionality enabled easy and fast synthesis of **2** with different chain lengths.

Table 4-1. Synthetic results of PBYP with different molecular weight.

Code	M : I [a] : DBU	Time (min)	Conversion (^{31}P NMR)	M_n (GPC)[b]	M_w/M_n (GPC)	M_n (Theo)[c]	M_n (^{1}H NMR)[d]	T_g
$PBYP_{25}$	25 : 1 : 1.5	5	99%	11240	1.14	4464	4684	– 35.5 °C
$PBYP_{50}$	50 : 1 : 1.5	7	100%	15860	1.15	8820	8732	– 36.5 °C
$PBYP_{100}$	100 : 1 : 1.5	10	99%	24050	1.19	17532	17884	– 34.3 °C

[a] Concentrations were all 1 g monomer per 1 mL dichloromethane. Reactions were all carried out at room temperature.

[b] Measured by GPC in DMF and calibrated using polystyrene standards.

[c] Calculated from the monomer to initiator ratio and corrected for conversion.

[d] Calculated from the monomer to initiator ratio based on ^{1}H NMR of final polymer product.

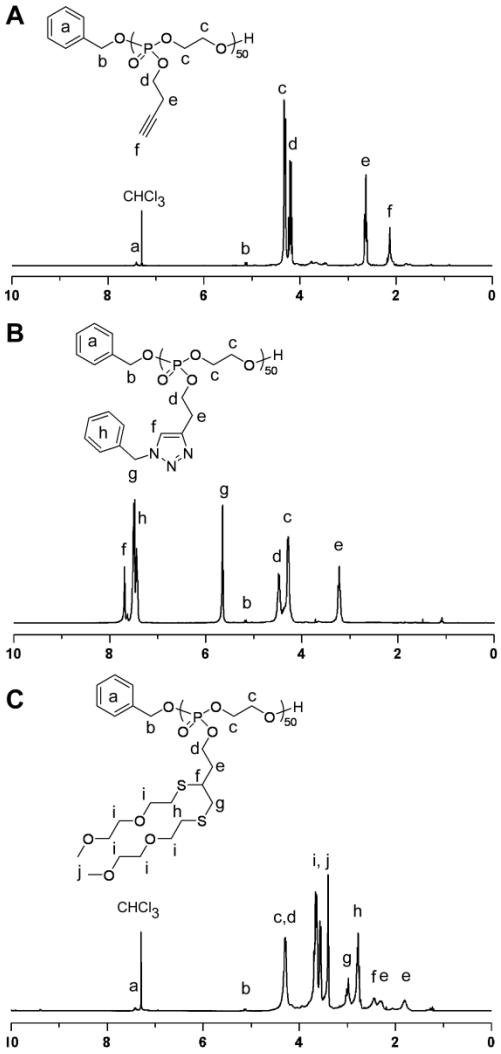

Figure 4-4. ^{1}H NMR spectra (300 MHz, $CDCl_3$, ppm) of **2** (A) and product polymers after azide-alkyne Huisgen cycloaddition, **4** (B), and thiol-yne reaction, **5** (C).

To demonstrate the presence and chemical availability of alkyne groups on **2**, we conducted azide-alkyne Huisgen cycloaddition to couple benzyl azide onto this degradable backbone, as shown in **Scheme 4-3**. Benzyl azide was chosen because this compound is commercially available, the resulting polymer was able to be analyzed by GPC and has no proton signals that overlap with resonance frequencies of the reactant polymer. ^{1}H NMR spectroscopy showed 100% conversion from alkyne group to triazole five-membered rings after 1 h reaction time, as observed by loss of the terminal acetylene proton signal at 2.06 ppm and appearance of the triazole proton resonating at 7.80 ppm. The GPC curve was shifted to higher molecular weight and retained a narrow distribution with a PDI of 1.15 (**Figure 4-5**). These results indicated that azide-alkyne Huisgen cycloaddition is compatible with the polyphosphoester backbone. TGA analysis under N_2 atmosphere also showed that benzyl groups and triazoles were attached onto the polymer backbone to make the polymer more thermally stable (**Figure 4-6**).

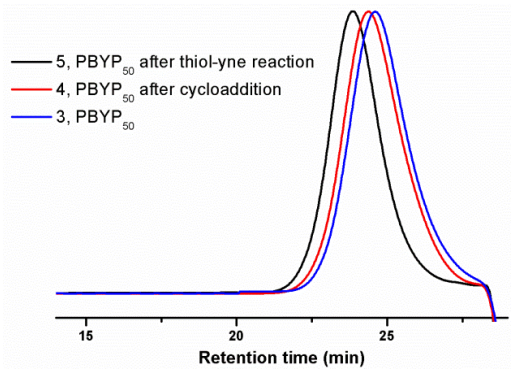

Figure 4-5. GPC traces of PBYP50 and PBYP50 after two "click" type reaction.

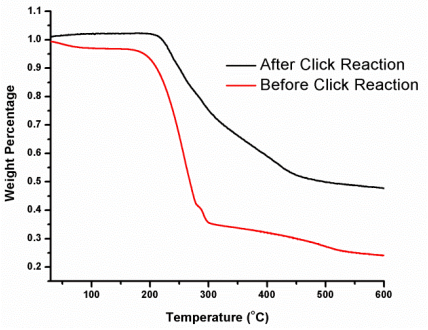

Figure 4-6. TGA traces of **2** (red trace) and **4** (black trace) PBYP before and after azide-alkyne cycloaddition with benzyl azide, respectively.

Radical-mediated thiol-yne chemistry, another “click” type reaction, is a robust and versatile method that tolerates a variety of functional groups to achieve high degrees of functionalization on alkyne groups.(33) Here, we utilized this reaction to densely functionalize PBYP, in the manner that two equivalents of thiol are coupled onto one alkyne to form a double addition product with 1,2-regioselectivity by using a chemical radical source. Twenty equivalents of thiols were used in the radical reaction to avoid chain-chain coupling and ensure high efficiency.(34) A comparison of ^{1}H NMR spectra of PBYP and PBYP after two types of click reactions is shown in **Figure 4-4**. The terminal acetylene protons were completely consumed and converted into the corresponding functional groups. The observed diastereotopic splitting of the methylene group agreed with 1,2-regioselectivity of thiol-yne chemistry. The success of the thiol-yne reaction was also demonstrated by GPC analyses (**Figure 4-5**), which indicated that radical-mediated thiol-yne didn't cause coupling or crosslinking of the backbone.

The polyphosphoester is regarded as a new candidate for thermoresponsive polymer, because its lower critical solution temperature (LCST) can be tuned with changing alkyl side chains of the monomer.(30, 35) Incorporation of a hydrophobic monomer, 2-isopropoxy-2-oxo-1,3,2-dioxaphospholane, produced lower LCST, while copolymerization with a more hydrophilic monomer, 2-methyl-2-oxo-1,3,2-dioxaphospholane (MP), resulted in higher LCST. Copolymerizations of BYP with MP at various molar fractions to tune the copolymer water solubilities were performed, to overcome the poor water solubility of PBYP, which is barely soluble over the temperature range from 5 to 85 °C. However, DBU was found to be an ineffective catalyst for the copolymerization of BYP and MP. TBD, a stronger base, was, therefore, chosen to catalyze the reaction (**Scheme 4-3**). To avoid increasing polydispersity resulting from adverse transesterification (**Figure 4-7** showing GPC traces of reactions quenched after longer copolymerization times), the polymerizations were conducted at 0 °C in DCM at 1 g/mL, and quenched by acetic acid solution only 20 seconds after TBD was added into the monomer and initiator mixture. Even under these conditions, over 98 % monomer conversion was achieved.

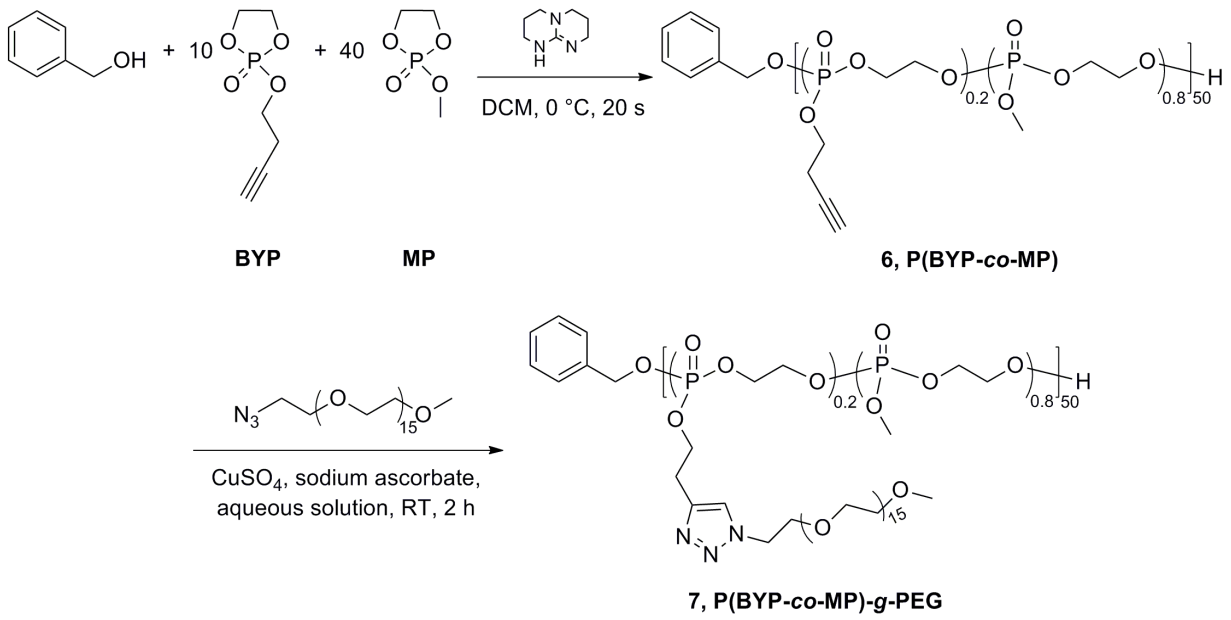

Scheme 4-3. Schematic representation of the copolymerization of BYP and MP and aqueous azide-alkyne Huisgen cycloaddition.

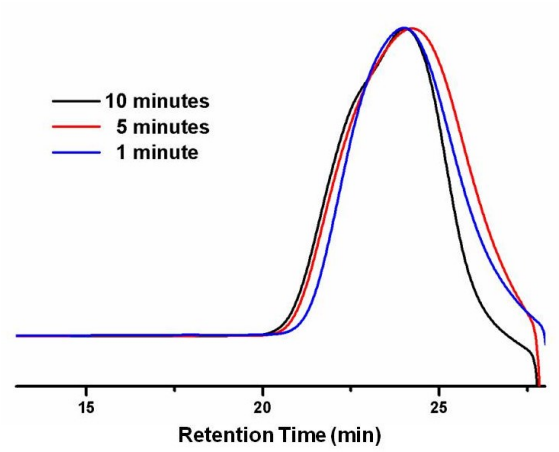

Figure 4-7. GPC traces of copolymerization of 50 % BYP and 50% MP quenched at different time points.

By employing this ultra fast ROP, a series of copolymers from 10 % to 50 % BYP incorporation with ten percent increment was synthesized (**Table 4-2**). MP and BYP had almost identical conversion in 20

seconds with TBD as the more active catalyst. We assume, therefore, that all copolymers were statistical copolymers. PBYP10%, PBYP20% and PBYP30% contained the least amounts of hydrophobic units and were all water soluble in the temperature range from 5 °C to 85 °C with no thermoresponsive behaviors observable by UV-vis spectroscopy studies. The copolymers having more than 50% of hydrophobic units were not water soluble over the same temperature range. Interestingly, PBYP40% exhibited increased solubility with increased temperatures, suggesting an upper critical solution temperature (UCST) type phase separation behavior, however, the transition as observed by temperature-ramped UV-vis spectroscopic measurements was quite broad and ill-defined. The aqueous solution-state behavior is unusual, in comparison to the reported LCST-type phase behavior of alkyl-functionalized phosphoester copolymers.(30, 35)

Table 4-2. Synthetic results of poly(BYP-co-MP)

Code	I/M	Feed ratio (BYP: MP)	Conversion of BYP	Conversion of MP	M_n	M_w/M_n	Water Soluble temperature range
PBYP10%	1:50	10:90	96%	97%	17460	1.13	5 °C – 85 °C
PBYP20%	1:50	20:80	96%	98%	16470	1.14	5 °C – 85 °C
PBYP30%	1:50	30:70	97%	96%	16770	1.17	5 °C – 85 °C
PBYP40%	1:50	40:60	98%	97%	15600	1.16	Soluble > 55°C
PBYP50%	1:50	50:50	98%	98%	16270	1.14	Insoluble

One of the water soluble copolymers, incorporated with 20% BYP, was chosen to couple with CH_3O-PEG-azide in aqueous solution by using copper sulfate and sodium ascorbate catalyst system (**Scheme 4-3**).(36) GPC traces of the PEGylated copolymer **7** and its precursor **6** (**Figure 4-8**) demonstrated that the grafting of PEG in water was successful. In ^{1}H NMR analysis, integration of the proton of the triazole ring (7.69 ppm) to the benzylic protons on the chain end (5.07-5.15 ppm) was 10 to 2, confirming the quantitative conversion from alkyne to triazole groups.

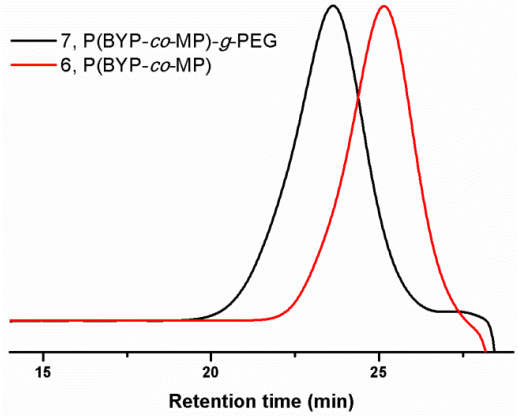

Figure 4-8. GPC traces of P(BYP-co-MP)$_{50}$, **6** and PEGylated P(BYP-co-MP)$_{50}$, **7** after aqueous azide alkyne Huisgen cycloaddition.

Conclusion

In summary, a stable alkyne-functionalized phospholane monomer was synthesized and its organocatalyzed polymerization kinetics and subsequent azide-alkyne and thiol-yne coupling reactions within the functional polymer materials were explored. By copolymerization of a water-soluble monomer with this monomer, a series of clickable and water-soluble polyphosphoesters was achieved. Although only two types of "click" reactions were demonstrated, others are available to derivatize this alkyne-functionalized polyphosphoester and its water-soluble copolymer with different moieties. Furthermore, with the control offered during the ROP and the ability to conjugate small molecules or polymers onto the backbone, the chemistry developed here has the potential to lead to highly complex and multi-functional polymer structures that can lead then also to complex, functional and degradable nanostructured materials. Efforts in this direction are being actively pursued.

Experimental

Materials. N,N-dimethylformamide (DMF), copper(I) bromide, acetone, diethyl ether, 1,8-diazabicyclo[5.4.0]undec-7-ene (DBU), 1,5,7-triazabicyclo[4.4.0]dec-5-ene (TBD), acetic acid, propargyl

alcohol, 3-butyn-1-ol, copper sulfate pentahydrate, sodium ascorbate, 2-(2-methoxyethoxy)ethanethiol, 2,2-dimethoxy-2-phenylacetophenone (DMPA), N,N,N',N",N"-pentamethyldiethylenetriamine and methanol were used as received from Sigma-Aldrich Company. 2-chloro-2-oxo-1,3,2-dioxaphospholane (95%) was used as received from Thermo Fisher Scientific Inc. Benzyl azide (94%) was used as received from Alfa Aesar. CH_3O-PEG_{750}-azide was used as received from RAPP Polymere. Triethylamine (TEA) was heated at reflux under N_2 atmosphere with calcium hydride and distilled. Tetrahydrofuran (THF) and dichloromethane were dried through columns (J. C. Meyer Solvent Systems, Inc.). Benzyl alcohol was purchased from Sigma-Aldrich and distilled from calcium hydride prior to use.

Instrumentation. ^{1}H NMR, ^{31}P NMR and ^{13}C NMR spectra were recorded on an Inova 300 MHz or Mercury 300 MHz spectrometer interfaced to a UNIX computer using VnmrJ software. Chemical shifts were referenced to the solvent resonance signals.

The DMF gel permeation chromatography (GPC) was conducted on a Waters Chromatography, Inc. (Milford, MA) system equipped with an isocratic pump model 1515, a differential refractometer model 2414, and a four-column set of 5 μm Guard (50 × 7.5 mm), Styragel HR 4 5 μm DMF (300 × 7.5 mm), Styragel HR 4E 5 μm DMF (300 × 7.5 mm), and Styragel HR 2 5 μm DMF (300 × 7.5 mm). The system was equilibrated at 70 °C in pre-filtered DMF containing 0.05 M LiBr, which served as polymer solvent and eluent (flow rate set to 1.00 mL/min). Polymer solutions were prepared at a concentration of *ca*. 3 mg/mL and an injection volume of 200 μL was used. Data collection and analysis were performed with Empower 2 v. 6.10.01.00 software (Waters, Inc.). The system was calibrated with polystyrene standards (Polymer Laboratories, Amherst, MA) ranging from 615 to 442,800 Da.

IR spectra were recorded on an IR Prestige 21 system (Shimadzu Corp.) and analyzed using IRsolution v. 1.40 software.

Glass transition temperatures (T_g) were measured by differential scanning calorimetry on a Mettler-Toledo DSC822® (Mettler-Toledo, Inc., Columbus, OH), with a heating rate of 10 °C /min. Measurements were analyzed using Mettler-Toledo STARe v. 7.01 software. The T_g was taken as the midpoint of the

inflection tangent, upon the third heating scan. Thermogravimetric analysis was performed under N_2 atmosphere using a Mettler-Toledo model TGA/SDTA851[e], with a heating rate of 5 °C /min. Measurements were analyzed by using Mettler-Toledo STARe v. 7.01 software.

Ultraviolet-visible spectroscopy (UV-vis) absorption measurements were made using a UV-2550 system (Shimadzu Corp.) equipped with a TMSPC-8 thermoelectric temperature controlling system using quartz cuvettes. Spectra were analyzed by using Tm analysis software module 1,2,1,0 and UV-Probe v. 2.33 software.

Attempts for Synthesis of Propargyl Phospholane (PAP) Monomer

To a stirred solution of propargyl alcohol (2.16 g, 38.6 mmol) and triethylamine (3.90 g, 38.6 mmol) in 200 mL of anhydrous THF at - 20 °C (or 0 °C) were dropwise added a solution of 2-chloro-2-oxo-1,3,2-dioxaphospholane (COP, 5.00 g, 35.1 mmol) in 50 mL of anhydrous THF, and the reaction mixture was allowed to stir for 12 h. After complete conversion of COP, as confirmed by TLC, the reaction mixture was filtered and the filtrate was concentrated *in vacuo*. The crude product readily decomposed during flash column chromatography purification (66% ethyl acetate /hexane, v/v) and no yield was isolated. Vacuum distillation was also applied to obtain purified product, but the yield was extremely low (<20%). Furthermore, the ^{31}P NMR spectrum (**Figure 4-1**) showed the presence of multiple products in the crude reaction mixture.

Synthesis of Butynyl Phospholane (BYP, 3) Monomer,

To a stirred solution of 3-butyn-1-ol (7.40 g, 106 mmol) and triethylamine (11.7 g, 116 mmol) in 200 mL of anhydrous THF at 0 °C were dropwise added a solution of COP (15.06 g, 106 mmol) in 50 mL of anhydrous THF, and the reaction mixture was allowed to stir for 12 h. After complete conversion of COP, as confirmed by TLC, the reaction mixture was filtered and the filtrate was concentrated. The concentrated filtrate was distilled under reduced pressure to obtain a faint yellow and viscous liquid (121 -

124 °C, 0.4 mmHg) with a yield of 65%. ^{1}H NMR ($CDCl_3$, ppm): δ 4.49 - 4.37 (m, 4H, POCH_2CH_2OP), 4.27 - 4.20 (m, 2H, POCH_2CH_2C), 2.62 (t, J = 6.0 Hz, 2H, POCH_2CH_2C), 2.05 (s, 2H, POCH_2CH_2C≡CH). ^{13}C NMR ($CDCl_3$, ppm): δ 79.14, 70.55, 66.23, 66.12, 20.70. ^{31}P NMR ($CDCl_3$, ppm): δ 17.32. +ESI MS: calculated $[M+H]^+$ for $C_6H_{10}O_4P$: 177.0317, found: 177.0308. IR: 3350 - 3175, 3050-2850, 1474, 1280, 1011, 926, 841, 748 cm^{-1}.

General Procedure for Polymerization of BYP

A solution of BYP (0.50 g, 2.8 mmol) and a given amount of benzyl alcohol (0.028 mmol to 0.112 mmol) in anhydrous dichloromethane (0.40 mL) was transferred into a flame-dried 5-mL shell vial equipped with a rubber septum and a stir bar. At 25 °C, a solution of a given amount of DBU (0.042 mmol to 0.168 mmol) in anhydrous dichloromethane (0.1 mL) was injected into the vial *via* syringe, while being maintained under a nitrogen gas atmosphere. After being stirred for a certain period of time (3 min to 6 min), the reaction vial was unstoppered and a solution of acetic acid (excess) in dichloromethane was added *via* pipet into the reaction mixture to quench the reaction. The poly(BYP) (PBYP, **2**) was purified by precipitation from dichloromethane into diethyl ether (3x), and was then dried under vacuum, to give an average yield of 80%. ^{1}H NMR ($CDCl_3$, ppm): δ 7.40 (m, 5H, Ar-H), 5.13 (d, J = 6.0 Hz, 2H, OCH_2Ar), 4.43 - 3.97 (b, 6nH, POCH_2CH_2OP, POCH_2CH_2C), 2.65 - 2.56 (b, 2nH, POCH_2CH_2C≡CH), 2.18 - 2.04 (b, 1nH, POCH_2CH_2C≡CH). ^{13}C NMR ($CDCl_3$, ppm): δ 79.53, 70.81, 66.45, 65.77, 20.61. ^{31}P NMR ($CDCl_3$, ppm): δ -1.88. DSC: (T_g) = -35 °C. TGA in N_2: 210–300 °C, 60% mass loss; 300–600 °C, 10% mass loss, 20 % mass remaining above 600 °C. IR: 3700 - 3100, 3100 - 2800, 1736, 1643, 1458, 1373, 1258, 964, 802, 733 cm^{-1}.

Synthesis of Methyl Phospholane (MP) Monomer

To a stirred solution of methanol (1.26 g, 39.4 mmol) and triethylamine (3.94 g, 39.0 mmol) in anhydrous THF (200 mL) at 0 °C were dropwise added a solution of COP (5.00 g, 35.1 mmol) in anhydrous THF (50 mL), and the reaction mixture was allowed to stir for 12 h. After complete conversion of COP, as

confirmed by TLC, the reaction mixture was filtered and the filtrate was concentrated. The concentrated filtrate was distilled under reduced pressure to obtain the monomer, MP, as colorless oil (74 - 78 °C, 0.4 mmHg) with a yield of 60%. ^{1}H NMR ($CDCl_3$, ppm): δ 4.47-4.33 (m, 4H, POCH_2CH_2OP), 3.84 (d, J = 12.0 Hz, 3H, POCH_3). ^{13}C NMR ($CDCl_3$, ppm): δ 66.18, 55.03. ^{31}P NMR ($CDCl_3$, ppm): δ 18.63. IR: 3100 - 2800, 1466, 1281, 1018, 926, 833, 764 cm^{-1}.

Procedure for Copolymerization of BYP and MP

A solution of BYP (0.300 g, 1.7 mmol), MP (0.235 g, 1.7 mmol) and benzyl alcohol (7.5 mg, 0.068 mmol) in anhydrous dichloromethane (0.60 mL) was transferred into a flame-dried 5-mL shell vial equipped with a rubber septum and a stir bar. The reaction mixture was cooled to 0 °C, and then a solution of TBD (19.0 mg, 0.14 mmol) in anhydrous dichloromethane (0.1 mL) was injected into the vial *via* syringe under a nitrogen gas atmosphere. After being stirred for 20 s, a solution of acetic acid (27.0 mg, 0.45 mmol) in dichloromethane (0.2 mL) was added into the reaction mixture *via* syringe to quench the reaction. The P(BYP-*co*-MP) was purified by precipitation from dichloromethane into diethyl ether (3x) and was then dried under vacuum to the copolymer, P(BYP-*co*-MP) (**6**), as a light yellow highly viscous liquid in 75 % yield. ^{1}H NMR ($CDCl_3$, ppm): δ 7.40 (m, 5H, Ar-*H*), 5.13 (m, 2H, OCH_2Ar), 4.43-3.97 (b, POCH_2CH_2OP, POCH_3, POC$H_2$$CH_2$), 2.65-2.56 (b, POC$H_2CH_2$C≡CH), 2.18-2.04 (b, POC$H_2CH_2$C≡C*H*). ^{13}C NMR ($CDCl_3$, ppm): δ 79.53, 70.75, 66.34, 65.72, 55.69, 20.61. ^{31}P NMR ($CDCl_3$, ppm): δ -0.40, -1.88. DSC: (T_g) = -31 - -35 °C. TGA in N_2: 210–300 °C, 60 % mass loss; 300–600 °C, 10% mass loss, 20% mass remaining above 600 °C. IR: 3700 – 3100, 3050 – 2850, 1643, 1458, 1258, 964, 810, 741 cm^{-1}. This same procedure was followed with various amounts of reagents to obtain a series of copolymers with an average yield of 75% (see data in Table S2 below).

Azide-Alkyne Huisgen Cycloaddition of PBYP with Benzyl Azide

A solution of PBYP (0.170 g, M_n = 12000, PDI = 1.16, 1.0 mmol alkynes), and benzyl azide (0.257 g, 2.0 mmol) in 5.0 mL of anhydrous DMF was placed in a flame-dried 5 mL shell vial and bubbled with nitrogen for 1 h. At room temperature, CuBr (13.4 mg, 0.1 mmol) and N,N,N',N',N''-pentamethyldiethylenetriamine (17.2 mg) were added. After being stirred for 1 h, the reaction mixture was passed through neutral alumina to remove most of the copper catalyst, and the product was precipitated from DMF or acetone into ethyl ether (3x) to remove excess benzyl azide. The product polymer **4** was obtained as a light green highly viscous liquid at 99% yield. ^{1}H NMR ($CDCl_3$, ppm): δ 7.51 (s, 50H, C=C*H*N), 7.32-7.26 (b, 5H, Ar-*H*), 5.56 (b, 100H, ArCH_2N), 5.13 (d, *J* = 6.0 Hz, 2H, OCH_2Ar), 4.37-3.93 (b, 300H, POCH_2CH_2OP, POCH_2CH$_2$C), 3.04 (b, 100H, POCH$_2$CH_2C). ^{13}C NMR ($CDCl_3$, ppm): δ 143.51, 135.07, 129.03, 128.59, 128.06, 122.47, 66.92, 66.38, 53.94, 26.97. ^{31}P NMR ($CDCl_3$, ppm): δ -1.36. GPC: M_n = 13400, PDI = 1.15. DSC: T_g = 15.7 °C. TGA in N_2: 210–450 °C, 50 % mass loss; 450–600 °C, 5 % mass loss, 45 % mass remaining above 600 °C. IR: 3700 – 3200, 3150 – 2850, 1575, 1458, 1265, 1011, 972, 802, 725 cm^{-1}.

Thiol-yne reaction of PBYP with 2-(2-Methoxyethoxy)ethanethiol

A solution of PBYP (0.030 g, M_n = 12000, PDI = 1.16, 0.4 mmol alkynes), 2-(2-methoxyethoxy)ethanethiol (0.460 g, 8.0 mmol), and 2,2-dimethoxy-2-phenylacetophenone (1.3 mg, 0.12 mmol) in 1.0 mL of methanol was bubbled with nitrogen for 15 min and then irradiated under UV irradiation (365 nm) for 1 h. The reaction mixture was precipitated from methanol or acetone into ethyl ether (3x) to remove excess 2-(2-methoxyethoxy)ethanethiol and 2,2-dimethoxy-2-phenylacetophenone and photoinitiator by-products to give the product polymer **5** in the form of a colorless highly viscous liquid in 78% yield. ^{1}H NMR ($CDCl_3$, ppm): δ 7.32-7.26 (b, 5H, Ar-*H*), 5.46 (d, *J* = 6.0 Hz, 2H, OCH_2Ar), 4.39-4.21 (b, 300H, POCH_2CH_2OP, POCH_2CH$_2$CH), 3.72-3.29 (b, 600H, OCH_2CH_2OCH_2), 3.07-2.91 (b, 300H, CH_3OCH$_2$CH$_2$), 2.85-2.71 (b, 100H, SCH_2CHS), 2.57-2.45 (b, 200H, OCH$_2$CH_2S), 2.39-2.20 (b, 50H, SCH$_2$C*H*S), 1.90-1.71 (b, 100H, POCH$_2$CH_2CH). ^{13}C NMR ($CDCl_3$, ppm): δ 71.89, 71.14, 70.25, 66.36, 59.08, 42.44, 39.00, 34.00, 32.24, 30.23. ^{31}P NMR ($CDCl_3$, ppm): δ -1.22. GPC: M_n = 16800 Da, PDI = 1.12. DSC: T_g = - 52 °C. TGA in N_2:

110–280 °C, 64 % mass loss; 280–600 °C, 11 % mass loss, 25 % mass remaining above 600 °C. IR: 3700 – 3200, 3100 – 2850, 1455, 1256, 964, 812, 743 cm^{-1}.

Aqueous Azide-Alkyne Huisgen Cycloaddition of P(BYP-*co*-MP) with CH_3O-PEG-azide

A solution of P(BYP-*co*-MP) (0.100 g, M_n = 11700, PDI = 1.14, 20% BYP units, 0.137 mmol alkynes), and CH_3O-PEG-azide (0.150 g, 0.206 mmol) in 5.0 mL water was placed in a flask equipped with stir bar and bubbled with nitrogen for 1 h. A solution of sodium ascorbate (2.8 mg in 0.5 mL water, 0.014 mmol) and a solution of $CuSO_4 \bullet 5H_2O$ (1.8 mg in 0.5 mL water, 0.007 mmol) were added into the previous mixture. After stirred at room temperature for 2 h, the crude mixture was purified by centrifugal filtration using Millipore Amicon Ultra-15 tubes (MW cutoff 3K, at 11K rpm, 7 min, 5 times), followed by lyophilization to yield PEGylated-P(BYP-*co*-MP) **7** in the form of colorless highly viscous liquid at 67% yield. ^{1}H NMR ($CDCl_3$, ppm): δ 7.69 (s 10H, C=C*H*N), 7.32-7.26 (b, 5H, Ar-*H*), 5.12 (m, 2H, OCH_2Ar), 4.67-4.17 (b, 340H, POCH_2CH_2OP, POCH_2, POCH_3), 4.00-3.49 (b, 650H, CH_2OCH_2CH_2OCH_2), 3.43-3.34 (b, 30H, $CH_2CH_2OCH_3$), 3.25-3.05 (b, 20H, $POCH_2CH_2C$). ^{13}C NMR ($CDCl_3$, ppm): δ 142.93, 71.93, 7056, 69.55, 66.31, 59.00, 54.77, 50.14, 26.97. ^{31}P NMR ($CDCl_3$, ppm): δ -0.40, -1.82. GPC: M_n = 20600, PDI = 1.20. DSC: T_g = - 39 °C, T_c = - 5 °C, T_m = 27 °C. TGA in N_2: 110–320 °C, 74 % mass loss; 320–600 °C, 6 % mass loss, 20 % mass remaining above 600 °C. IR: 3700 – 3200, 3150 – 2850, 1642, 1454, 1255, 959, 810, 748 cm^{-1}.

Acknowledgements

We gratefully acknowledge financial support from the National Heart Lung and Blood Institute of the National Institutes of Health as a Program of Excellence in Nanotechnology (HHSN268201000046C) and the National Science Foundation under grant numbers DMR-0906815 and DMR-1105304. The Welch Foundation is gratefully acknowledged for support through the W. T. Doherty-Welch Chair in Chemistry, Grant No. A-0001.

Reference

(1) Nair, L. S.; Laurencin, C. T. *Prog. Polym. Sci.* **2007**, *32*, 762.

(2) Ulery, B. D.; Nair, L. S.; Laurencin, C. T. *J. Polym. Sci., Part B: Polym. Phys.* **2011**, *49*, 832.

(3).Tang, Z.; Zhuang, X.; Chen, X.; Jing, X.; Tian, H. *Prog. Polym. Sci*. in press

(4) BKolb, H. C.; Finn, M. G.; Sharpless, K. *Angew. Chem. Int. Edit.* **2001**, *40*, 2004.

(5) Iha, R. K.; Wooley, K. L.; Nystrom, A. M.; Burke, D. J.; Kade, M. J.; Hawker, C. J.. *Chem. Rev.* **2009**, *109*, 5620.

(6) Jiang, X.; Vogel, E. B.; Smith, M. R.; Baker, G. L. *Macromolecules* **2008**, *41*, 1937.

(7) Riva, R.; Schmeits, S.; Jerome, C.; Jerome, R.; Lecomte, P. *Macromolecules* **2007**, *40*, 796.

(8) Xu, N.; Wang, R.; Du, F. S.*;* Li, Z. C*. J. Polym. Sci., Part A: Polym. Chem.* **2009**, *47*, 3583.

(9) Yu, Y.; Zou, J.; Yu, L.; Jo, W.; Li, Y. K.; Law, W. C.; Cheng, C. *Macromolecules* **2011**, *44*, 4793.

(10) Darcos, V.; El Habnouni, S.; Nottelet, B.; El Ghzaoui, A.; Coudane, J. *Polym. Chem.* **2010**, *1*, 280.

(11) Tempelaar, S.; Mespouille, L.; Dubois, P.; Dove, A. P. *Macromolecules* **2011**, *44*, 2084.

(12) Xu, J. W.; Prifti, F.; Song, J. *Macromolecules* **2011**, *44*, 2660.

(13) Chen, W.; Yang, H. C.; Wang, R.; Cheng, R.; Wei, W. X.; Zhong, Z. Y.; Meng, F. H. *Macromolecules* **2010**, *43*, 201.

(14) Zhang, X.; Zhong, Z.; Zhuo, R. *Macromolecules* **2011**, *44*, 1755.

(15) Wang, Y. C.; Yuan, Y. Y.; Du, J. Z.; Yang, X. Z.; Wang, J. *Macromol. Biosci.* **2009**, *9*, 1154.

(16) Liu, J. Y.; Pang, Y.; Huang, W.; Zhai, X. A.; Zhu, X. Y.; Zhou, Y. F.; Yan, D. Y. *Macromolecules* **2010**, *43*, 8416.

(17) Iwasaki, Y.; Yamaguchi, E. *Macromolecules* **2010**, *43*, 2664.

(18) Hoyle, C. E.; Lowe, A. B.; Bowman, C. N. *Chem. Soc. Rev.* **2010**, *39*, 1355.

(19) Kade, M. J.; Burke, D. J.; Hawker, C. J. *J. Polym. Sci., Part A: Polym. Chem.* **2010**, *48*, 743.

(20) Iwasaki, Y.; Akiyoshi, K. *Macromolecules* **2004**, *37*, 7637.

(21) Sun, T. M.; Du, J. Z.; Yan, L. F.; Mao, H. Q.; Wang, J. *Biomaterials* **2008**, *29*, 4348.

(22) Xiong, M. H.; Wu, J.; Wang, Y. C.; Li, L. S.; Liu, X. B.; Zhang, G. Z.; Yan, L. F.; Wang, J. *Macromolecules* **2009**, *42*, 893.

(23) Wang, Y. C.; Li, Y.; Sun, T. M.; Xiong, M. H.; Wu, J. A.; Yang, Y. Y.; Wang, J. *Macromol Rapid Comm* **2010**, *31*, 1201.

(24) Iwasaki, Y.; Komatsu, S.; Narita, T.; Akiyoshi, K.; Ishihara, K. *Macromol Biosci* **2003**, *3*, 238.

(25) Wang, Y. C.; Yuan, Y. Y.; Wang, F.*;* Wang, J. *J. Polym. Sci., Part A: Polym. Chem.* **2011**, *49*, 487.

(26) Molander, G. A.; Sommers, E. M.; Baker, S. R. *J. Org. Chem.* **2006**, *71*, 1563.

(27) Mikami, K.; Yoshida, A.; Matsumoto, Y. *Tetrahedron. Lett.* **1996**, *37*, 8515.

(28) Baeza, A.; Najera, C.; Sansano, J. M. *Eur. J. Org. Chem.* **2007**, 1101.

(29) Zhai, X.; Huang, W.; Liu, J.; Pang, Y.; Zhu, X.; Zhou, Y.; Yan, D. *Macromol. Biosci.* **2011**, *11*, 1603.

(30) Iwasaki, Y.; Wachiralarpphaithoon, C.; Akiyoshi, K. *Macromolecules* **2007**, *40*, 8136.

(31) Lohmeijer, B. G. G.; Pratt, R. C.; Leibfarth, F.; Logan, J. W.; Long, D. A.; Dove, A. P.; Nederberg, F.; Choi, J.; Wade, C.; Waymouth, R. M.; Hedrick, J. L. *Macromolecules* **2006**, *39*, 8574.

(32) Kamber, N. E.; Jeong, W.; Waymouth, R. M.; Pratt, R. C.; Lohmeijer, B. G. G.; Hedrick, J. L. *Chem. Rev.* **2007**, *107*, 5813.

(33) Hoogenboom, R. *Angew. Chem. Int. Edit.* **2010**, *49*, 3415.

(34) Albertazzi, L.; Amir, R. J.; Willis, J.; Khan, A.; Kang, T.; Hawker, C. J. *Angew. Chem. Int. Edit.* **2011**, *50*, 3425.

(35) Wang, Y. C.; Li, Y.; Yang, X. Z.; Yuan, Y. Y.; Yan, L. F.; Wang, J. *Macromolecules* **2009**, *42*, 3026.

(36) Zhang, S.; Li, Z.; Samarajeewa, S.; Sun, G.; Yang, C.; Wooley, K. L. *J. Am. Chem. Soc.* **2011**, *133*, 11046.

Chapter 5

Rapid and versatile construction of diverse and functional nanostructures derived from a polyphosphoester-based biomimetic block copolymer system

[Portions of this work have been published previously as Shiyi Zhang, Zou Jiong, Fuwu Zhang, Mahmoud Elsabahy, Simcha Felder, Jiahua Zhu, Darrin J. Pochan, and Karen L. Wooley, *J. Am. Chem. Soc.,* **2012**, *134*, 18467-18474]

Abstract

A rapid and efficient approach for the preparation and modification of a versatile class of functional polymer nanoparticles has been developed, for which the entire engineering process from small molecules to polymers to nanoparticles bypasses typical slow and inefficient procedures, and rather employs a series of steps that capture fully the "click" chemistry concepts that have greatly facilitated the preparation of complex polymer materials over the past decade. The construction of various nanoparticles with functional complexity from a versatile platform is a challenging aim to provide materials for fundamental studies and also optimization toward a diverse range of applications. In this paper, we demonstrate the rapid and facile preparation of a family of nanoparticles with different surface charges and functionalities based on a biodegradable polyphosphoester block copolymer system. From a retrosynthetic point of view, the non-ionic, anionic, cationic and zwitterionic micelles with hydrodynamic diameters between 13 nm to 21 nm and great size uniformity were quickly formed by suspending, independently, four amphiphilic diblock polyphosphoesters into water, which were functionalized from the same parental hydrophobic-functional AB diblock polyphosphoester by "click" type thiol-yne reactions. The well-defined (PDI < 1.2) hydrophobic-functional AB diblock polyphosphoester was synthesized by an ultrafast (< 5 min) organocatalyzed ring-opening polymerization in a two-step, one-pot manner with the quantitative conversions of two kinds of cyclic phospholane monomers. The whole programmable process starting from small molecules to nanoparticles could be completed within 6 h, as the most rapid approach for the anionic and non-ionic nanoparticles, although the cationic and zwitterionic nanoparticles

required *ca*. 2 days due to purification by dialysis. The micelles showed high biocompatibility, with even the cationic micelles exhibiting a 6-fold lower cytotoxicity toward RAW 264.7 mouse macrophage cells, as compared to the Lipofectamine® commercial transfection agent.

Introduction

Engineered nanoparticles with unique physical and chemical properties at the nanoscale, emulating natural nanosystems (*e.g.*, viruses, lipoproteins, and proteins) in both structural and functional features, have been bringing about a revolutionary impact on the pharmaceutical industry, due to their applications as diagnostic, therapeutic and theranostic agents for a wide variety of human diseases.(1-5) Polymeric micelles exhibit similarities with natural nanobiosystems in their overall structural features and the way of programmed construction from small compounds (monomers) to macromolecules to functional nanoscopic self-assemblies. Micellar nanostructures have attracted great attention for their distinctive core-shell morphology and their tunable sizes and chemistries in both the core and shell regions by using different functionalized block copolymers.(6) Recent advances in polymerization methodologies and the application of reactive, efficient and orthogonal functionalization reactions, such as "click" chemistries, have enabled the engineering of functional block polymers to direct their self assembly into nanoparticles with various sizes, surface charges and functionalities.(7-12) However, it is still challenging to rapidly construct a biodegradable system that serves as a versatile platform, beginning from the point of small molecules and engineering them stagewise towards multifunctional nanoparticles with tunable properties.

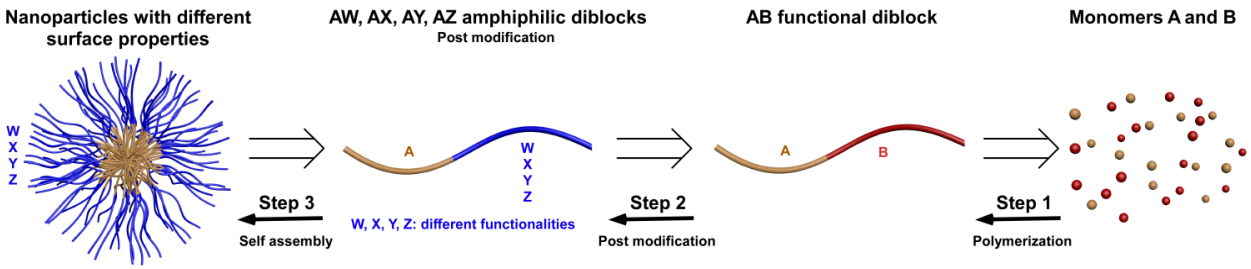

Scheme 5-1. Retrosynthetic analysis of polymeric micelles with different surface properties.

The standard retrosynthetic analysis of **Scheme 5-1** allows for the preparation of a series of polymeric nanoassemblies having different coronal compositions and properties, by the assembly of a family of diblock copolymers, with different functionalities along one of the block segments defined from post-polymerization modifications of a single diblock copolymer type, which is prepared from the polymerization of functional monomers. The key challenge with this approach is to achieve rapid and efficient chemical and physical transformations at each of the three steps. By taking advantage of modern polymerization methodologies, a variety of non-degradable and degradable amphiphilic block copolymers have been synthesized, with the incorporation of orthogonal chemistries and possessing capability for supramolecular assembly in water (step 1). "Click" chemistry has provided a library of chemical reactions for the chemical transformations of the specific functionalities installed in the initial polymerization step, and have greatly expedited step 2.(13) However, the advantageous features of "click" chemistry in step 2, such as quantitative conversion, rapid reaction, under mild conditions, high functional group tolerance, with an absence of byproducts and side reactions, have not been fully realized by the overall series of steps, due to the polymerizations in step 1 and the self-assembly processes in step 3 usually being time consuming, or involving incomplete conversion of monomers, or harsh reaction conditions.(9) Herein, we demonstrate a novel strategy to program a series of diverse, functional nanostructures from reactive monomers, in which all three steps are rapid, quantitative and conducted under mild conditions.

Our programmable platform towards various nanoparticles is based on polyphosphoesters. Like polyesters, polypeptides and polycarbonates, polyphosphoesters are attractive for biomedical applications, such as gene delivery, imaging, drug delivery and tissue engineering, due to their biocompatibility, biodegradability and their structural similarity to nucleic and teichoic acids.(14-16) As a result of the intrinsic degradability, the functionalization of polyesters, polypeptides and polycarbonates has additional challenges over non-degradable systems. Beyond those typical degradable polymers, however, the functionalities and properties of polyphosphoesters are conveniently controlled by manipulation of pendant groups on the pentavalent phosphorus atom of cyclic phospholane monomer

precursors. Since the retrosynthetic analysis reverts ultimately to the monomers, we designed and synthesized two kinds of cyclic phospholane monomers: one that carried an alkyne functionality for polymerization into segment B, followed by conversion into functional hydrophilic block segments (W, X, Y, Z), the other is a hydrophobic monomer to lead to the common segment A. As polyphosphesters are a relatively new type of synthetic polymer, the hydrophobic cyclic phospholane monomer, 2-ethylbutyl phospholane, was developed to overcome the hydrophilic nature of the polyphosphoester backbone. The polymerization activity of this novel monomer upon two organocatalysts was studied and compared with that of our recently reported functional monomer, butynyl phospholane.(17) In step 1, organocatalyzed ring opening polymerizations (ROP) were employed to fully convert the two monomers sequentially into the well-defined (PDI < 1.2) hydrophobic-functional AB diblock polyphosphoester in an ultrafast (< 5 min) one-pot manner by utilizing the reactivity difference between the two monomers. "Click" type thiol-yne reactions, in step 2, were applied to functionalize this parental hydrophobic-functional diblock precursor into four amphiphilic diblock copolymers with different charge types, such as non-ionic, anionic, cationic and zwitterionic. In the final step, a series of uniform polymeric micelles with different surface charges and functionalities was quickly achieved by directly dissolving each polymer material into water. Detailed physicochemical and biological studies of the polymeric micelles with different surface properties were conducted to understand the effect of surface functionalities on their behaviors. This programmable process greatly facilitates the preparation of degradable functional nanoparticles, when all advantageous features of "click"-type chemical concepts were realized in each step of this strategy.

Results and Discussion

Rapid and facile construction of diverse nanostructures is demonstrated starting from the simple syntheses of functional cyclic phospholane monomers and continuing at each stage through polymerization, chemical modification and supramolecular assembly steps. Ultrafast (< 5 min) one-pot sequential polymerization of two different cyclic phospholane monomers produced a single hydrophobic-functional AB diblock polyphosphoester, having reactive alkynyl side-chain chemical functionalities within only the B block segment. After its rapid (< 1 h) purification by precipitation and centrifugation, a series of

thiol-yne chemical transformations produced four different functionalized diblock copolymers, which were then assembled by direct dissolution into water to afford four different polymeric micelles with tunable surface properties.

Monomer design and synthesis. Polyphosphoesters can be prepared by ring-opening polymerization (ROP),(18) polycondensation,(19) transesterification,(20) and enzymatic polymerization.(21) Among all of these methods, the ROP of cyclic phospholane monomers by using metal compounds as initiators or polymerization catalysts, is a well-established process to provide linear or hyperbranched polyphosphoesters(22) with predictable molecular weight, narrow molecular weight distribution, and well-defined chain ends.(23) Recently, Iwasaki *et al.* first reported using 1,8-diazabicyclo[5.4.0]undec-7-ene (DBU) or 1,5,7-triazabicyclo[4.4.0]dec-5-ene (TBD) as organocatalysts to promote ROP of cyclic phospholanes.(24) To eliminate using environmentally-sensitive metal compounds, and better fulfill the requirements of biomedical applications, many groups have adopted the organocatalyzed ROP of phospholanes to prepare polyphosphoesters for biomaterials.(17, 22, 25-28)

Two phospholane monomers were required for our design: one having a reactive chemical functionality that would be stable during polymerization and then readily available for chemical modification, and the second providing hydrophobicity, ultimately to lead to amphiphilic block copolymers for assembly of nanostructures. Cyclic phospholane monomers are usually prepared from the condensation of 2-chloro-2-oxo-1,3,2-dioxaphospholane (COP) and an alcohol. A variety of functional cyclic phospholane monomers have been reported, including methyl,(29) ethyl,(30) isopropyl,(31) PEGylated,(32, 33) hydroxyl-functionalized,(34, 35) protected hydroxyl-functionalized,(36) protected amino-functionalized,(37, 38) protected thiol-functionalized,(39) acrylate-functionalized,(40) methacrylate-functionalized,(41) alkyne-functionalized(17) and alkene-functionalized.(27, 28) The ring opening polymerization (ROP) of those functional monomers produced corresponding high molecular weight functional polyphosphoesters. Our group recently developed a stable alkyne-functionalized cyclic phospholane monomer and studied its

polymerization kinetics under an organocatalyst, in addition to the chemical functionalization of this alkyne-functionalized polyphosphoester by “click” type azide-alkyne Huisgen cycloaddition and thiol-yne reaction.(17) This butynyl phospholane (BYP, **1**) monomer was, therefore, used to incorporate side-chain chemical functionality along the backbone of one segment of the AB block copolymer of this study, to allow for the versatile platform development.

A challenge associated with identification of the second phospholane monomer, for production of a hydrophobic polyphosphoester chain segment that could be utilized to drive supramolecular assembly into nanostructures in water, is related to the high water solubility of the polyphosphoester backbone. The hydrophobicity of the polyphosphoester system can be tuned by changing the alkyl side chains of the monomer or by copolymerizing monomers with different alkyl side chains, but the water solubility of alkyl-substituted polyphosphoesters has been typically observed to be temperature dependent.(29, 30) For instance, a hydrophobic monomer, 2-isopropoxy-2-oxo-1,3,2-dioxaphospholane, produced an isopropyl-functionalized polyphosphoester that exhibited a lower critical solution temperature (LCST), and when incorporated into a diblock copolymer, poly(ethylene glycol)-*block*-poly(2-isopropoxy-2-oxo-1,3,2-dioxaphospholane), served as a hydrophobic domain of an amphiphilic core-shell morphological nanoparticle only at temperatures above its LCST.(25, 42) To achieve a polyphosphoester with high hydrophobicity over a wide temperature range, we attempted to couple COP with several alcohols with long or bulky alkyl groups. A tertiary alcohol, *tert*-butanol, was employed to react with COP, but the product monomer decomposed in the reaction mixture. The cyclic phospholane monomer from the coupling of a secondary alcohol, 3-pentanol, and COP also decomposed upon heating during vacuum distillation. The boiling point of 1-decanol and that of the resulting monomer were too similar to allow for good purification. To avoid the poor purification abilities, 2-ethyl-1-butanol was chosen to functionalize COP because of its relatively bulky hydrophobic alkyl group. Finally, the monomer, 2-ethylbutyl phospholane (EBP, **2**), was obtained through the one-step esterification of two commercially-available compounds, 2-ethyl-1-butanol and COP followed by simple filtration and vacuum distillation (**Scheme 5-2**).

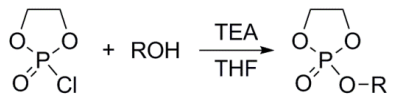

1, BYP, R = 3-butynyl
2, EBP, R = 2-ethylbutyl

Scheme 5-2. Synthesis of cyclic phospholane monomers from COP and primary alcohols

Table 5-1. Polymerization results of 2 with DBU and TBD under different conditions.

entry	Catalyst	M : I : Catalyst (molar ratios)	Temp	Time (min)	Conversion (^{31}P NMR)	M_n, Da (GPC)	M_w/M_n (GPC)	M_n, Da (Theor)	M_n, Da (^{1}H NMR)
1	DBU	25 : 1 : 1.5	RT	15	51%	5600	1.31	2700	3000
2	DBU	50 : 1 : 1.5	RT	30	43%	6700	1.34	5600	5200
3	DBU	100 : 1 : 1.5	RT	60	32%	8300	1.42	6800	7100
4	TBD	25 : 1 : 1.5	0 °C	1	99%	7100	1.14	5300	5600
5	TBD	50 : 1 : 1.5	0 °C	2	100%	10300	1.14	10400	11000
6	TBD	100 : 1 : 1.5	0 °C	4	99%	17200	1.16	21000	20500

Concentrations for all entries were 1 g monomer (M) per 1 mL dichloromethane. Initiator (I) was benzyl alcohol for all entries.

M_n (GPC) and M_w/M_n (GPC) were measured by DMF GPC calibrated using polystyrene standards.

M_n (Theor) was calculated from the monomer to initiator ratio and corrected for conversion.

M_n (^{1}H NMR) was calculated from the monomer to initiator ratio based on ^{1}H NMR of final polymer product.

Homopolymerization of EBP by organocatalysts. The polymerization behavior of **2** with organocatalysts DBU or TBD was studied (Table 1). The polymerizations of **2** upon addition of DBU (entries 1-3 in Table 1) were conducted at room temperature to allow the direct comparison to our published polymerization results of BYP.(17) In our previous report, the conversion of **1** reached 99% in 10 min with different ratios of monomer-to-initiator. In contrast, the conversion of **2** did not reach 60% even over a period of 1 h under the same conditions, which suggested that the reactivity of **2** is much lower than that of **1**, potentially because of the sterically-bulky side chain. Also, DBU gave poor control over the molecular weight distribution (PDI > 1.30) for the polymerization of **2**. When TBD was used as a catalyst instead of DBU, the polymerization of **2** proceeded to 99% conversion in less than 5 min at 0 °C (entries 4-6 in **Table 5-1**). The dual activation of TBD, simultaneously serving as a hydrogen-bond donor to the monomer *via* the N−H site and also as a hydrogen-bond acceptor to the hydroxyl proton of the propagating alcohol, explains the significant increase in the polymerization rate.(27) When the

polymerization of **2** with TBD was quenched by acetic acid upon the completion of the reaction, good control over the molecular weight distribution (PDI < 1.20) could be achieved. Therefore, well-defined poly(2-ethylbutyl phospholane) (PEBP, **3**) with predictable molecular weight could be synthesized by using TBD as a catalyst.

One-pot sequential ROP. To prepare diblock polyphospohoester, we first attempted to polymerize **1** and then **2** by using TBD or DBU as a catalyst and benzyl alcohol as an initiator (**Scheme 5-3**). After the complete conversion of the first monomer **1**, the second monomer **2** was added into the reaction mixture. However, there was no conversion of **2** (monitored by ^{31}P NMR) and no chain extension (characterized by DMF GPC). We speculated that TBD or DBU associated with poly(butynyl phospholane) (PBYP) or residual **1**, predominately, over **2**, due to the bulky side chain of **2**. Therefore, when **1**, PBYB, and catalyst (TBD or DBU) were all present in the reaction mixture neither catalyst was able to successfully promote the ROP of **2** to achieve chain extension.

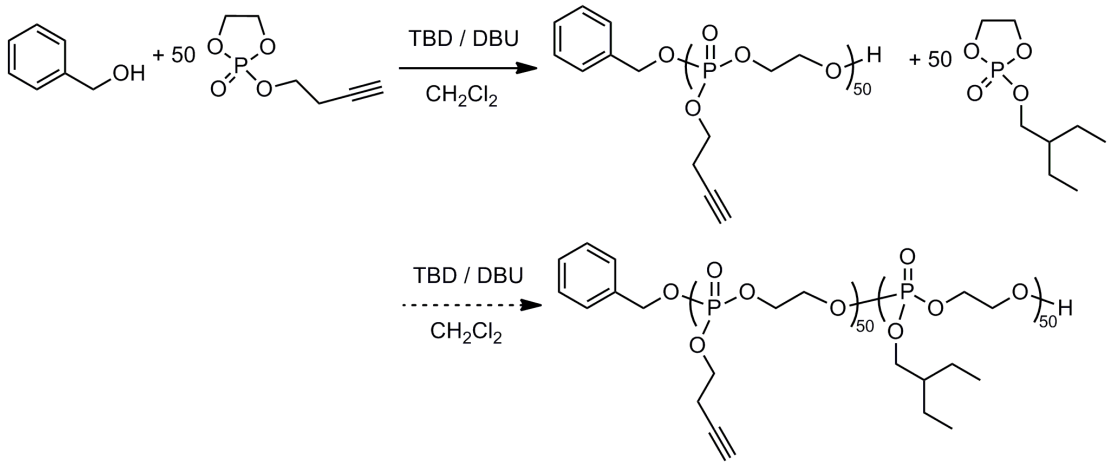

Scheme 5-3. The failed synthetic route towards diblock polyphosphoester by polymerizing BYP first and then EBP, which led to no chain extension of the second block.

Successful chain extension was achieved and poly(2-ethylbutyl phospholane)$_{50}$-*b*-poly(butynyl phospholane)$_{50}$ (PEBP$_{50}$-*b*-PBYP$_{50}$, **4**) was synthesized after the addition order of the two monomers in the sequential polymerization was reversed (**Scheme 5-4**). The less reactive monomer, **2**, was first polymerized at relatively high concentration in dichloromethane with TBD as a catalyst and benzyl alcohol as an initiator at 0 °C. After complete conversion of **2** (monitored by ^{31}P NMR) in 2 min, the more reactive monomer, **1**, was transferred into the reaction mixture for the chain extension. Over 99% conversion of **1** was reached quickly (in 1 min), however GPC analysis of the diblock polymer showed poor control over the molecular weight distribution and the possibility of transesterification (**Figure 5-1**). To decrease the polymerization rate as well as the possibility of transesterification, the second step of sequential polymerizations was conducted at lower monomer concentration and -20 °C by diluting and cooling the reaction mixture before the second monomer was added. A two minute polymerization of **2** at 0 °C and 3 mol/L monomer concentration and the sequential one minute polymerization of **1** at -20 °C and 1 mol/L monomer concentration provided over 99% conversion of each monomer in the individual steps and retained a narrow molecular weight distribution with a PDI of 1.17 for the diblock polyphospohoester (**Figure 5-2**). The diblock copolymer **4** was easily purified by precipitation from dichloromethane or acetone into a pentane and diethyl ether mixture (3 : 1 vol ratio) followed by centrifugation.

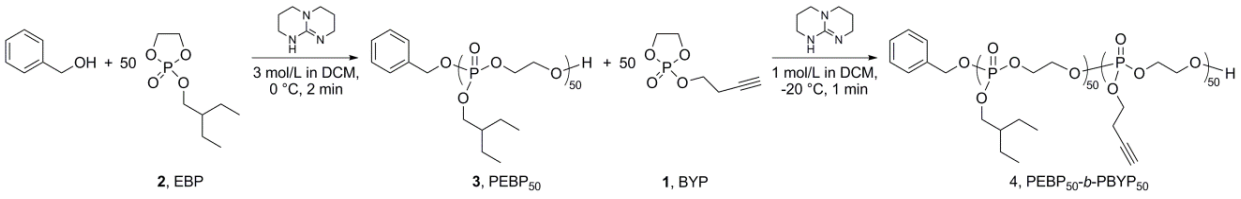

Scheme 5-4. Synthesis of PEBP$_{50}$-*b*-PBYP$_{50}$, **4**, diblock polyphosphoester bearing a hydrophobic block (PEBP) and a functional block (PBYP) *via* a one-pot sequential ROP.

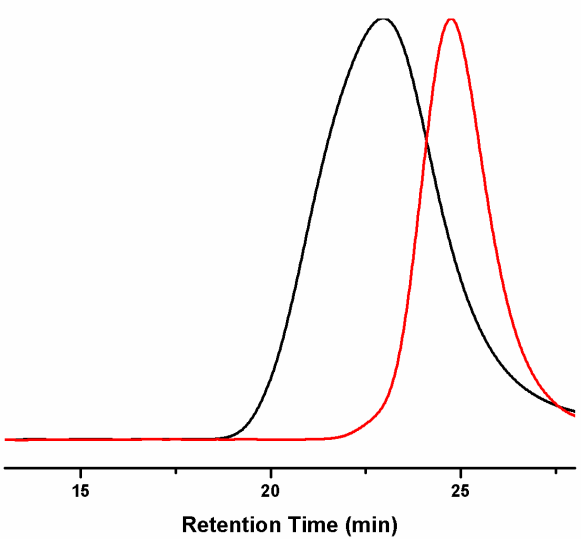

Figure 5-1. GPC traces of $PEBP_{50}$ at M_n = 10000 g/mol and PDI = 1.13. (red line) and $PEBP_{50}$-*b*-$PBYP_{50}$ block copolymer at M_n = 18700 g/mol and PDI = 1.54 (black line) after one-pot sequential ROP under conditions, 0 °C without cooling and diluting the reaction mixture upon the addition of the second monomer, which led to inadequate control over the polymerization.

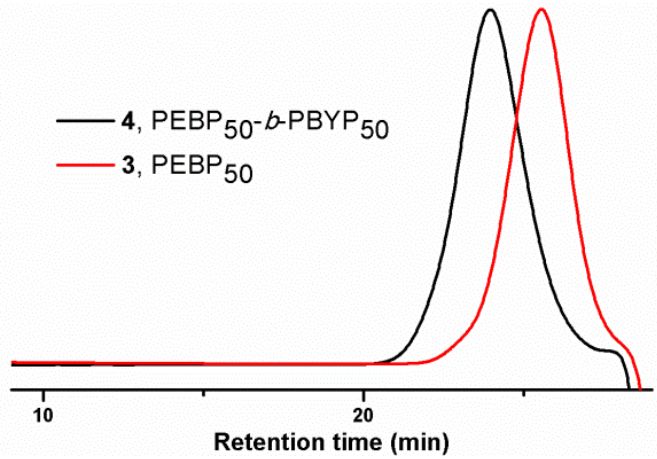

Figure 5-2. GPC traces of $PEBP_{50}$ at M_n = 9800 g/mol and PDI = 1.14 (red line) and $PEBP_{50}$-*b*-$PBYP_{50}$ diblock copolymer at M_n = 16700 g/mol and PDI = 1.17 (black line) produced by the one-pot sequential ROP.

This facile polymerization provided a strategy to prepare diblock polyphosphoester with precise structural control in an atom-efficient synthesis manner.(43) Confirmation of the diblock composition was made by ^{31}P NMR spectroscopy of the purified polymer, which displayed two signals at −1.19 and −1.83 ppm that were assigned to the two ^{31}P environments in the PEBP and PBYP blocks, respectively (**Figure 5-3**). ^{1}H NMR also showed full retention of the alkyne group of the functional PBYP block and alkyl group in hydrophobic PEBP block. The sequential polymerization of two monomers in a one-pot method at multigram scale was completed in less than 5 min, and the 3 precipitations and centrifugations could be accomplished in less than 1 hour. The ultrafast one-pot sequential synthesis of a well-defined diblock polyphosphoester, is more advantageous than the chain extension from purified macro-initiator, which requires the complete removal of acetic acid used for quenching the first polymerization step.(27)

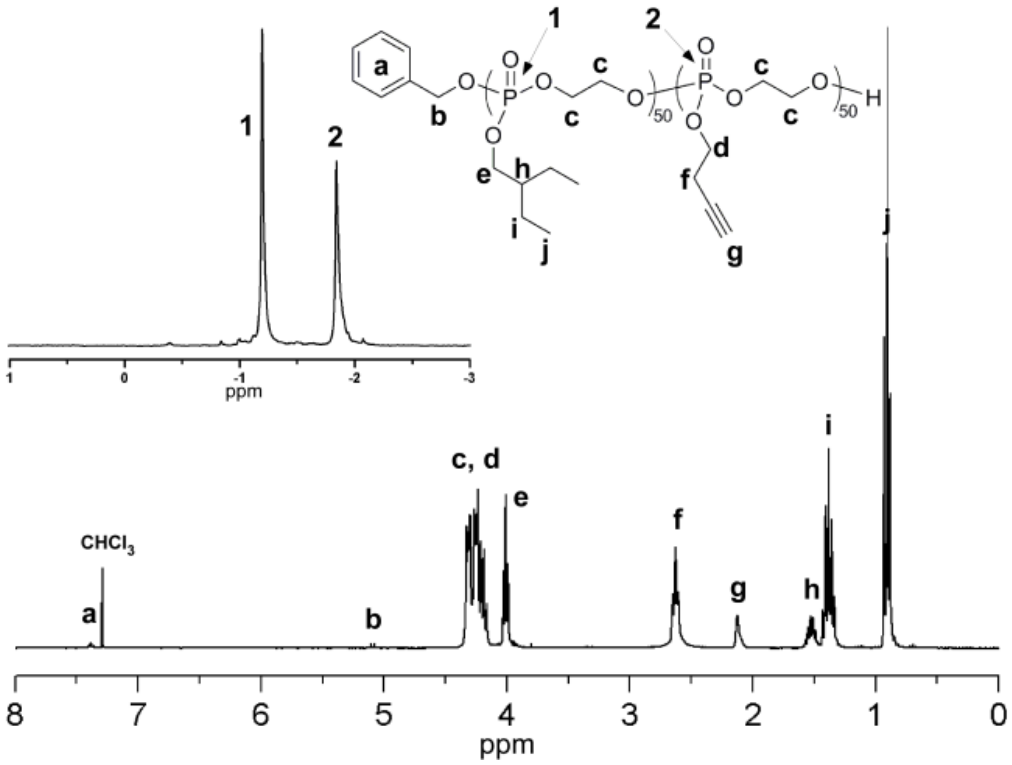

Figure 5-3. ^{1}H NMR and ^{31}P NMR (upper left inset) spectra ($CDCl_3$) of purified $PEBP_{50}$-*b*-$PBYP_{50}$ diblock copolymer.

Functionalization by thiol-yne reactions. The hydrophobic-functional AB diblock polyphosphoester, **4**, was then functionalized into four amphiphilic diblock polyphosphoesters by "click" type thiol-yne reaction with thiol-containing molecules including 2-(2'-methoxyethoxy)ethanethiol, 3-mercaptopropionoic acid, cysteamine hydrochloride and l-cysteine hydrochloride monohydrate (**Scheme 5-5**). Radical-mediated thiol-yne chemistry, a "click" type reaction, is a robust and versatile method that tolerates a variety of functional groups, such as carboxylic acids and amines, to densely functionalize alkynyl groups.(44) In our previous report, we demonstrated that the radical-mediated thiol-yne reaction was compatible with the polyphosphoester backbone without causing any coupling or crosslinking.(17) Ten equivalents of thiols to alkyne groups were used in the radical reaction to avoid chain-chain coupling, while two hours exposure to UV irradiation with DMPA as the photo-initiator ensured complete conversion.

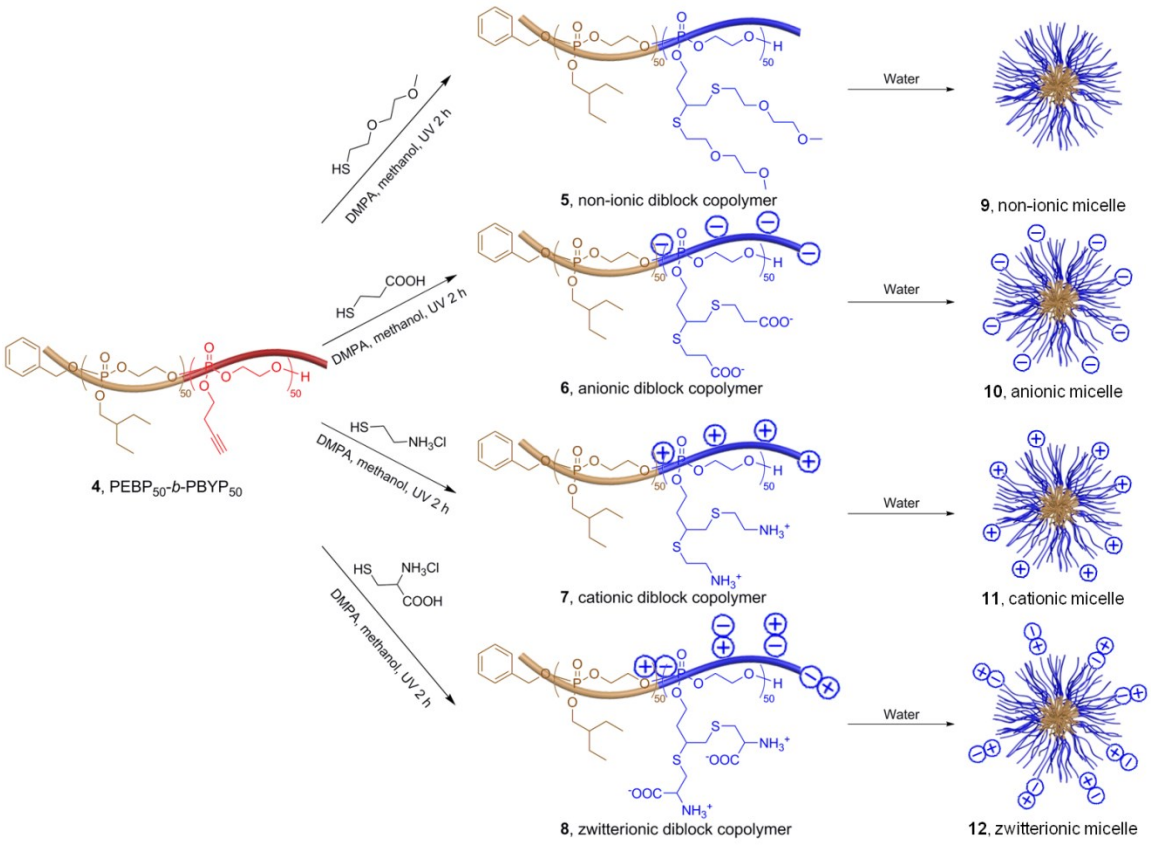

Scheme 5-5. Schematic representation of the functionalizations of $PEBP_{50}$-*b*-$PBYP_{50}$ with four different charged or non-charged thiols and the self assembly of four resulting amphiphilic diblock copolymers:

non-ionic block copolymer (**5**), anionic block copolymer (**6**), cationic block copolymer (**7**) and zwitterionic block copolymer (**8**) into four micelles, **9**-**12**, respectively, with different surface charges.

Each functionalized diblock copolymer was readily purified and its structure was confirmed. Given the use of ten-fold excess amounts of the thiols, the conditions employed for purification were defined by and their physical characteristics. The non-ionic diblock, **5**, and anionic diblock, **6**, could be purified by direct precipitation from methanol or acetone into a pentane and diethyl ether (3 : 1 vol ratio) three times and dried under vacuum. However, the salt-based thiols required that the cationic diblock, **7**, and zwitterionic diblock, **8**, were purified by dialysis against a pH 3.0 HCl solution, an acidic condition to ensure the amine group was protonated, in the cold room (4-8 °C) for 2 days and then lyophilized. The disappearance of terminal acetylene protons (2.18-2.04 ppm) in the ^{1}H NMR spectra of the four product polymers confirmed the full consumption of the alkyne groups. The diastereotopic splitting of the methylene protons (1.76-1.92, 2.31-2.47 ppm), corresponding to the 1,2-regioselectivity of thiol-yne chemistry, and the presence of other functional groups also verified the successful installation of the four different thiols onto **4**. The thiol-yne reaction was demonstrated to efficiently transform the hydrophobic-functional AB diblock polyphosphoester into four different kinds of amphiphilic polyphosphoesters. Besides thiol-yne reaction, another "click" type reaction, azide-alkyne Huisgen cycloaddition could also be employed to efficiently functionalize hydrophobic-functional AB diblock polyphosphoester with polyethylene glycol (PEG). The preparation and application of PEGylated polyphosphoester-based nanoparticles are currently underway in our group.

Self-assembly of amphiphilic polyphosphoesters. All four amphiphilic polyphosphoesters were dissolved in nanopure water by sonication for 5 min at room temperature and spontaneously formed spherical nanoparticles, **9**, **10**, **11** and **12**, with narrow size distributions (**Figure 5-4**). The glass transition temperatures (T_g) were far below room temperature (- 50 °C) so that all polymer chain segments, whether hydrophilic or hydrophobic, had sufficient mobility and were able to undergo rapid relaxation or extension

in response to the varied electrostatic interactions to self-organize into micellar structures with core-shell morphology easily. In the nanoparticle assemblies, it is expected that the hydrophobic PEBP block aggregated in the particle core, and was shielded from the aqueous medium by the shell region consisting of functionalized PBYP blocks, due to the highly hydrophilic nature of the oligo(ethylene glycol), carboxyl, and amino group.

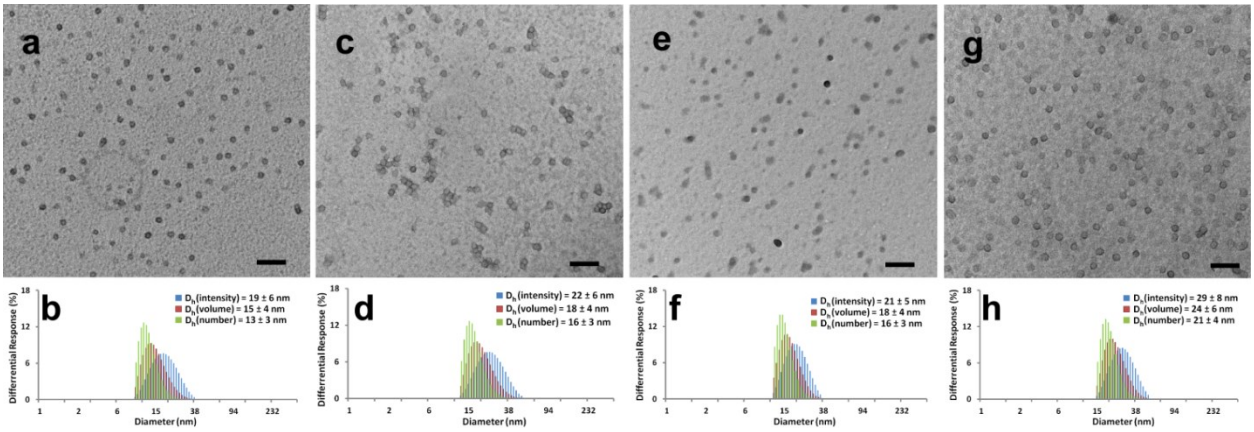

Figure 5-4. Self-assembly results of non-ionic micelle **9** (a, e), anionic micelle **10** (b, f), cationic micelle **11** (c, g), zwitterionic micelle **12**(d, h) in nanopure water. a, TEM image of **9**, average diameter is 15 ± 3 nm, after counting more than 100 particles. b, DLS results of **9**: D_h(intensity) = 19 ± 6 nm, D_h(volume) = 15 ± 4 nm, D_h(number) = 13 ± 3 nm. c, TEM image of **10**, average diameter is 18 ± 4 nm, after counting more than 100 particles. d, DLS results of **10**: D_h(intensity) = 22 ± 6 nm, D_h(volume) = 18 ± 4 nm, D_h(number) = 16 ± 3 nm. e, TEM image of **11**, average diameter is 18 ± 5 nm, after counting more than 100 particles. f, DLS results of **11**: D_h(intensity) = 21 ± 5 nm, D_h(volume) = 18 ± 4 nm, D_h(number) = 16 ± 3 nm. g, TEM image of **12**, average diameter is 23 ± 3 nm, after counting more than 100 particles. h, DLS results of **12**: D_h(intensity) = 29 ± 8 nm, D_h(volume) = 24 ± 6 nm, D_h(number) = 21 ± 4 nm. All scale bars in TEM images are 100 nm.

The morphological influence of varying PBYP block functionalities on the aqueous self-assembled nanoparticles was characterized by both transmission electron microscopy (TEM) and dynamic light

scattering (DLS). Bright-field TEM images of **9**, **10**, **11** and **12** prepared in nanopure water showed uniform particles with average sizes of approximately 15, 18, 18 and 23 nm, respectively (Fig. 3a, 3b, 3c, 3d). Due to the collapsing of swelled hydrophilic block chains during dry TEM sample preparation, the core-shell architecture was not directly observed. DLS results showed mono-modal size distribution of particles in all four aqueous assembly samples. The number-average hydrodynamic diameter values (D_h(number)) of **9**, **10**, **11** and **12** were 13 ± 3 nm, 16 ± 3 nm, 16 ± 3 nm and 21 ± 4 nm, respectively (Fig. 3e, 3f, 3g, 3h). Due to differences in the hydrophilic-hydrophobic balance and potential repulsive effects within and between hydrophilic chains with the same micellar assemblies, those constructed from the anionic- (**6**) or cationic- (**7**) functionalized PBYP chains were of slightly increased particle sizes than the non-ionic (**5**) functionalized PBYP chains, as measured by both TEM and DLS results. Zwitterionic functionalized polymer **8** assembled into particles with the largest particle size, however, all of the particle sizes were similar. It is remarkable that such uniform particle size distributions were produced by a simple, rapid, direct dissolution of the bulk block copolymer samples into nanopure water or buffer solutions.

Surface charges of the micelle systems. The surface charge densities, measured as zeta potential values, were characterized for the resulting micelles in pH 5.0 and pH 7.4 buffer solutions by Delsa Nano C particle analyzer (**Figure 5-5**). Non-ionic micelles, **9**, were slightly negatively-charged with zeta potentials of -12.2 mV at pH 7.4 and -18.0 at pH 5.0, which is common for neutral polymer nanoparticles, including those based on polyphosphoesters.(15),(36) The anionic and cationic characteristics of micelles formed from **10** and **11** were confirmed through zeta potential measurements. The anionic micelles were more negatively charged at pH 7.4 than at pH 5.0 due to the higher degree of deprotonation of carboxylic groups at pH 7.4 than at pH 5.0. Similarly, because of a higher extent of protonation of amino groups at pH 5.0 than at pH 7.4, the cationic micelles were more positively charged at pH 5.0 than at pH 7.4. In the case of the zwitterionic micelles, the positive charge of amino groups and the negative charge of carboxylic groups counteracted each other, which resulted in almost neutral micelles at both pH 5.0 and 7.4, with zeta potentials of -5.2 and -8.1 mV, respectively.

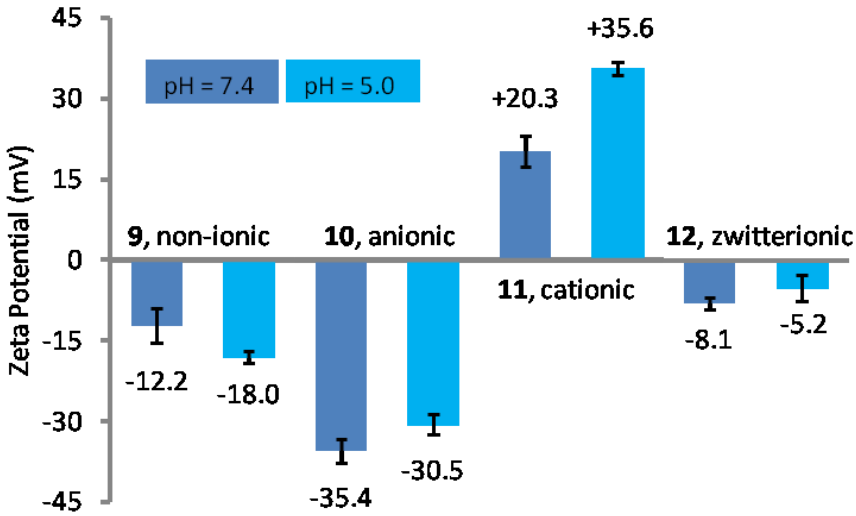

Figure 5-5. Zeta potential values of **9**, **10**, **11** and **12** in PBS buffer solutions at pH 7.4 and pH 5.0. The average values and their standard deviations, from six measurements, are shown.

Cytotoxicity of micellar systems. To understand the surface charge-dependent cytotoxicity of the polymeric micelles, we tested four micelles against RAW 264.7 mouse macrophages. The surface chemistries of nanoparticles play a dominant role in determining their fate both *in vitro* and *in vivo.*(45, 46) Although it is easier to control the surface charge of inorganic nanoparticles,(47-49) there is a limited understanding of the correlation between the cytotoxicity and the surface properties of polymeric micelles, due to the difficulty of preparing polymeric micelles with different surface charges and functionalities, while maintaining similar particle sizes. The micellar systems developed in this study had the same polymer backbone, similar sizes and size distribution characteristics (**Figure 5-4**), with various side chain functionalities that resulted in micellar nanoparticles with various surface charges, which allowed for direct comparison of their biological properties.

Four micelles, **9**, **10**, **11** and **12** were tested for their cytotoxicity in RAW 264.7 mouse macrophages at different concentrations (**Figure 5-6**). No cytotoxicity was observed for the non-ionic, zwitterionic and anionic micelles at the range of the tested concentrations (5-to-3000 μg/mL after 24 h-incubation), except

for the highest tested concentration of the anionic micelles. On the contrary, the cationic micelles showed a dose-dependent toxicity, which is in accordance with the known cytotoxicity of cationic nanoparticles, due to the interactions with the negatively-charged cell membranes. As the cationic micelles may have potential applications as transfection reagents and nucleic acids-delivery carriers, their cytotoxicity was compared with that of Lipofectamine®, a commercially-available cationic transfection agent. The IC_{50} value of the cationic micelles was 180 ± 48 µg/mL, while that of Lipofectamine® was 31 ± 6 µg/mL. The approximately 6-fold lower cytotoxicity for the polyphosphoester-based cationic nanoparticles may result from the degradability or the surface characteristics of the system, and may provide an alternative cationic carrier with better biocompatibility.(50) Due to their low toxicity, investigations of the transfection properties and their use in other biological applications are currently underway.

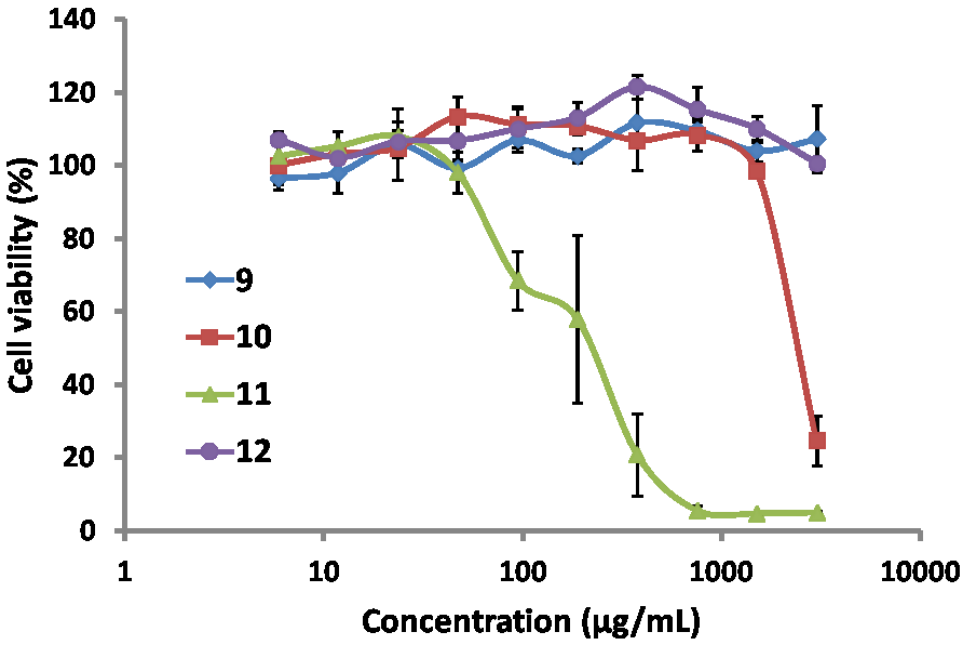

Figure 5-6. Cytotoxicity of the non-ionic micelle **9**; anionic micelle **10**; cationic micelle **11** and zwitterionic micelle **12** in RAW 264.7 mouse macrophages after treatment at a concentration range of 5-to-3000 µg/mL for 24 h.

Conclusion

In this study, a retrosynthetic methodology has been used to develop a versatile platform for the construction of a family of polymeric micelles with varying surface charges and functionalities based on biodegradable polyphosphoesters. In this strategy, all steps of the entire engineering process, from small molecule chemistry to nanoparticle assembly, were equipped with "click" type advantageous features, such as quantitative conversion, rapid reaction, mild conditions, high functional group tolerance, with an absence of byproducts and side reactions. The construction of the polymeric micelle system began from the preparation of hydrophobic and alkyne-functionalized monomers, continued through their polymerization, followed by chemical modification and finally involved supramolecular assembly by direct addition of water. To overcome the hydrophilic nature of the polyphosphoester backbone, a hydrophobic monomer (2-ethylbutyl phospholane), was synthesized and its polymerization activity under two organocatalysts was evaluated through the comparison with that of an alkyne-functionalized monomer butynyl phospholane. By taking advantage of the reactivity difference of the two monomers, the well-defined AB diblock polyphosphoester containing a hydrophobic block and a functional block was synthesized by an ultrafast ring-opening polymerization in a one-pot sequential manner. The clickable alkynyl groups on the functional portion of the hydrophobic-functional AB diblock polyphosphoester were transformed with four different thiols by photo-initiated, radical-mediated thiol-yne chemistry, forming four amphiphilic diblock polyphosphoesters with different charge types. Those non-ionic, anionic, cationic and zwitterionic amphiphilic diblock polyphosphoesters underwent self assembly in water by direct dissolution and sonication to afford uniform spherical micelles with average sizes of *ca*. 15, 18, 18 and 23 nm (by TEM), respectively. The surface charges of those four micelles were found to coincide with the presence of their respective chemical functional groups. The micelles have also shown high biocompatibility, and even the cationic micelles had a 6-fold lower cytotoxicity when compared to Lipofectamine®, a commercial transfection agent. Currently, this degradable nanoparticle family is being applied to various bio-applications.

Experimental

Materials. N,N-dimethylformamide (DMF), ethyl acetate, acetone, diethyl ether, methanol, acetone, diethyl ether, 1,8-diazabicyclo[5.4.0]undec-7-ene (DBU), 1,5,7-triazabicyclo[4.4.0]dec-5-ene (TBD), acetic acid, 3-butyn-1-ol, cysteamine hydrochloride, 2-ethyl-1-butanol, 2-(2-methoxyethoxy)ethanethiol, 3-mercaptopropanoic acid, L-cysteine hydrochloride monohydrate, benzyl alcohol, acetic acid, triethylamine (TEA), and 2,2-dimethoxy-2-phenylacetophenone (DMPA) were used as received from Sigma-Aldrich Company (St. Louis, MO). 2-chloro-2-oxo-1,3,2-dioxaphospholane (COP, 95%) was used as received from Thermo Fisher Scientific Inc (Pittsburgh, PA). Tetrahydrofuran (THF) and dichloromethane (DCM) were dried through columns (J. C. Meyer Solvent Systems, Inc., Laguna Beach, CA). Nanopure water (18 MΩ·cm) was acquired by means of a Milli-Q water filtration system, Millipore Corp. (St. Charles, MO).

Characterization Techniques. ^{1}H NMR, ^{31}P NMR and ^{13}C NMR spectra were recorded on an Inova 300 or Mercury 300 spectrometer interfaced to a UNIX computer using VnmrJ software. Chemical shifts were referenced to the solvent resonance signals. The DMF gel permeation chromatography (GPC) was conducted on a Waters Chromatography, Inc. (Milford, MA) system equipped with an isocratic pump model 1515, a differential refractometer model 2414, and a four-column set of 5 μm Guard (50 × 7.5 mm), Styragel HR 4 5 μm DMF (300 × 7.5 mm), Styragel HR 4E 5 μm DMF (300 × 7.5 mm), and Styragel HR 2 5 μm DMF (300 × 7.5 mm). The system was equilibrated at 70 °C in pre-filtered DMF containing 0.05 M LiBr, which served as polymer solvent and eluent (flow rate set to 1.00 mL/min). Polymer solutions were prepared at a concentration of *ca*. 3 mg/mL and an injection volume of 200 μL was used. Data collection and analysis were performed with Empower 2 v. 6.10.01.00 software (Waters, Inc.). The system was calibrated with polystyrene standards (Polymer Laboratories, Amherst, MA) ranging from 615 to 442,800 Da. IR spectra were recorded on an IR Prestige 21 system (Shimadzu Corp.) and analyzed using IRsolution v. 1.40 software. Glass transition temperatures (T_g) were measured by differential scanning calorimetry on a Mettler-Toledo DSC822® (Mettler-Toledo, Inc., Columbus, OH), with a heating rate of 10 °C /min. Measurements were analyzed using Mettler-Toledo STARe v. 7.01 software. The T_g was taken as the midpoint of the inflection tangent, upon the third heating scan. Thermogravimetric analysis was performed under N_2 atmosphere using a Mettler-Toledo model TGA/SDTA851^e, with a heating rate of

5 °C /min. Measurements were analyzed by using Mettler-Toledo STARe v. 7.01 software. Transmission electron microscopy (TEM) was conducted on a Hitachi H-7500 microscope, operating at 100 kV. Samples for TEM measurements were prepared as follows: 4 μL of the dilute solution (with a polymer concentration of 0.1 mg/mL) was deposited onto a carbon-coated copper grid, and after 2 min, the excess of the solution was quickly wicked away with a piece of filter paper. The samples were then negatively stained with 1 *wt*% phosphotungstic acid (PTA) aqueous solution. After 1 min, the excess staining solution was quickly wicked away with a piece of filter paper and the samples were left to dry under ambient conditions overnight. The average diameter of nanoparticles on the TEM grid was obtained by measuring the core domain of 200 sphere particles at different areas of the TEM specimen and the standard deviation was presented as error. Dynamic light scattering (DLS) measurements were conducted using a Delsa Nano C from Beckman Coulter, Inc. (Fullerton, CA) equipped with a laser diode operating at 658 nm. Scattered light was detected at 165° angle and analyzed using a log correlator over 70 accumulations for a 0.5 mL of sample in a glass size cell (0.9 mL capacity). The photomultiplier aperture and the attenuator were automatically adjusted to obtain a photon counting rate of *ca.* 10 kcps. The calculation of the particle size distribution and distribution averages was performed using CONTIN particle size distribution analysis routines using Delsa Nano 2.31 software. The peak averages of histograms from intensity, volume and number distributions out of 70 accumulations were reported as the average diameter of the particles. All determinations were repeated 10 times. The zeta potential values of the nanoparticles were determined by Delsa Nano C particle analyzer (Beckman Coulter. Fullerton, CA) equipped with a 30 mW dual laser diode (658 nm). The zeta potential of the particles in suspension was obtained by measuring the electrophoretic movement of charged particles under an applied electric field. Scattered light was detected at a 30° angle at 25 °C. The zeta potential was measured at five regions in the flow cell and a weighted mean was calculated. These five measurements were used to correct for electroosmotic flow that was induced in the cell due to the surface charge of the cell wall. All determinations were repeated 6 times.

Synthesis of hydrophobic monomer, 2-ethylbutyl phospholane (EBP). To a stirred solution of 2-ethyl-1-butanol (7.87 g, 78 mmol) and triethylamine (7.80 g, 78 mmol) in 250 mL of anhydrous THF at 0 °C was added a solution of COP (10.0 g, 70 mmol) in 50 mL of anhydrous THF dropwise, and the reaction mixture was allowed to stir for 12 h in an ice bath. After complete conversion of COP, as confirmed by TLC, the reaction mixture was filtered and the filtrate was concentrated. The concentrated filtrate was distilled under reduced pressure to obtain a colorless viscous liquid (118-121 °C, 0.4 mmHg, 10.6 g, Yield: 73 %). ^{1}H NMR ($CDCl_3$, ppm): δ 0.86 (t, *J* = 7.5 Hz, 6H, $POCH_2CH(CH_2\mathit{CH_3})_2$), 1.34 (m, 4H, $POCH_2CH(C\mathit{H_2}CH_3)_2$), 1.46 (m, 1H, $POCH_2C\mathit{H}$), 4.03 (m, 2H, $POC\mathit{H_2}CH$), 4.36 (m, 4H, $POC\mathit{H_2}C\mathit{H_2}OP$). ^{13}C NMR ($CDCl_3$, ppm): δ 10.85, 22.64, 41.55, 66.01, 70.75. ^{31}P NMR ($CDCl_3$, ppm): δ 17.70. HRMS: calculated $[M+H]^+$ for $C_8H_{18}O_4P$: 209.0943, found: 209.1013. IR (cm^{-1}): 3010-2850, 1462, 1286, 1016, 927, 836, 772 cm^{-1}.

General Procedure for Polymerization of EBP

A solution of EBP (0.50 g, 2.4 mmol) and a given amount of benzyl alcohol (0.023 mmol to 0.093 mmol) in anhydrous dichloromethane (0.40 mL) was transferred into a flame-dried 5-mL shell vial equipped with a rubber septum and a stir bar. In the cases of using DBU as the catalyst, at 25 °C, a solution of a given amount of DBU (0.035 mmol to 0.140 mmol) in anhydrous dichloromethane (0.1 mL) was injected into the vial *via* syringe, while being maintained under a nitrogen gas atmosphere. In the cases of using TBD as the catalyst, at 0 °C, a solution of a given amount of TBD (0.035 mmol to 0.140 mmol) in anhydrous dichloromethane (0.1 mL) was injected into the vial *via* syringe, while being maintained under a nitrogen gas atmosphere. After being stirred for a certain period of time, the reaction vial was unstoppered and a solution of acetic acid (excess) in dichloromethane was added *via* pipet into the reaction mixture to quench the reaction. The poly(EBP) (PEBP) was purified by precipitation from dichloromethane into pentane (3x), and was then dried under vacuum. A series of polymers was prepared (Table 1), with the characterization data for a particular sample reported here: ^{1}H NMR ($CDCl_3$, ppm): δ 0.93 (t, *J* = 7.4 Hz, $POCH_2CH(CH_2\mathit{CH_3})_2$), 1.40 (m, $POCH_2CH(C\mathit{H_2}CH_3)_2$), 1.55 (m, 1H, $POCH_2C\mathit{H}$), 4.07 (m, $POC\mathit{H_2}CH$), 4.23-4.31 (br m, $POC\mathit{H_2}C\mathit{H_2}OP$). ^{13}C NMR ($CDCl_3$, ppm): δ 10.90, 22.67, 41.49, 66.04-66.21, 70.07. ^{31}P

NMR ($CDCl_3$, ppm): δ -1.19. DSC: T_g = - 55.4 °C. TGA in N_2: 180–260 °C, 60% mass loss, 260–600 °C, 17% mass loss, 23 % mass remaining above 600 °C. IR (cm^{-1}): 3010-2850, 1644, 1459, 1381, 1273, 1016, 964, 869, 808 cm^{-1}.

Synthesis of $PEBP_{50}$-*b*-$PBYP_{50}$ diblock copolymer. A solution of EBP (1.500 g, 7.2 mmol) and benzyl alcohol (15.6 mg, 0.14 mmol) in anhydrous dichloromethane (2.0 mL) was transferred into a flame-dried 25-mL round flask equipped with a rubber septum and a stir bar in an ice bath. At 0 °C, a solution of TBD (40.2 mg, 0.28 mmol) in anhydrous dichloromethane (0.4 mL) was injected quickly into the flask *via* syringe, while being maintained under a nitrogen gas atmosphere. After being stirred for 2 min, another 2.4 mL of anhydrous dichloromethane was injected into the flask to dilute the reaction mixture and sodium chloride was mixed with the surrounding ice bath (at a wt ratio of 1 : 3) to provide a cooling system for -20 °C. Less than 0.1 mL of the reaction mixture was withdrawn to determine the conversion of EBP by ^{31}P NMR and the molecular weight and polydispersity by DMF GPC. After the reaction mixture had been stirred at -20 °C and the lower concentration for 3 min, a solution of BYP (1.27 g, 7.2 mmol) in anhydrous dichloromethane (2.4 mL) was injected quickly into the flask *via* syringe. After being stirred for 1 min at -20 °C, the reaction vial was unstoppered and a solution of acetic acid (excess) in dichloromethane was added *via* pipet into the reaction mixture to quench the reaction. After the reaction was quenched, the conversion of BYP was determined by ^{31}P NMR. The conversions of EBP and BYP were each above 99%. The PEBP-*b*-PBYP, **3** was purified by precipitation from 20 mL of dichloromethane into 240 mL pentane and diethyl ether mixture (3 : 1 vol ratio) three times, and was then dried under vacuum, to give the product polymer as a colorless viscous liquid in a yield of 84%. ^1H NMR ($CDCl_3$, ppm): δ 0.93 (t, J = 7.4 Hz, $POCH_2CH(CH_2CH_3)_2$), 1.40 (m, $POCH_2CH(CH_2CH_3)_2$), 1.55 (m, 1H, $POCH_2CH$), 2.18-2.04 (br s, $POCH_2CH_2C{\equiv}CH$), 2.65-2.57 (br m, $POCH_2CH_2C{\equiv}CH$), 4.19-3.99 (br m, $POCH_2CH$, $POCH_2CH_2$), 4.31-4.21 (br, $POCH_2CH_2OP$,), 5.13 (d, J = 6.0 Hz, OCH_2Ar), 7.40 (m, Ar-*H*). ^{13}C NMR ($CDCl_3$, ppm): δ 10.79, 20.48, 22.56, 41.37, 66.46-65.66, 69.92, 70.76, 79.47, 127.84, 128.51. ^{31}P NMR ($CDCl_3$, ppm): δ -1.19, -1.83. GPC: M_n = 16700 g/mol, PDI = 1.17. DSC: T_g = - 37.2 °C. TGA in N_2: 185–260 °C, 52% mass loss;

260–300 °C, 10% mass loss, 300–600 °C, 11% mass loss, 27 % mass remaining above 600 °C. IR (cm^{-1}): 3700-3100, 3020-2840, 1644, 1459, 1383, 1270, 1012, 972, 869, 805 cm^{-1}.

General procedure of thiol-yne reactions of $PEBP_{50}$-*b*-$PBYP_{50}$ with functional thiols. A solution of $PEBP_{50}$-*b*-$PBYP_{50}$ (0.30 g, M_n = 19000, 0.79 mmol alkynes), functional thiol (7.8 mmol), and DMPA (31.0 mg, 0.12 mmol) in 10.0 mL of methanol was bubbled with nitrogen for 5 min and then irradiated under UV irradiation (365 nm) for 2 h. For non-ionic thiol (2-(2-methoxyethoxy)ethanethiol) functionalized and anionic thiol (3-mercaptopropionoic acid) functionalized diblock copolymers, the reaction mixtures were precipitated from methanol or acetone into pentane and diethyl ether mixture (3 : 1 ratio) three times to remove excess functional thiols and photoinitiator by-products to give the product polymers. For cationic thiol (cysteamine hydrochloride) functionalized and zwitterionic thiol (L-cysteine hydrochloride monohydrate) functionalized diblock copolymers, the methanol solutions were transferred to dialysis tubing (MWCO: 6-8 kDa) and dialyzed against nanopure water with hydrochloride (pH = 3.0) in the cold room (4-8 °C) for 36 h, to remove excess functional thiols and DMPA and photoinitiator by-products. The micelle solution was lyophilized to give the product polymers.

The non-ionic diblock product was obtained in the form of a colorless viscous liquid in a yield of 50%. ^{1}H NMR (CD_3OD, ppm): δ 0.97 (t, *J* = 7.4 Hz, $POCH_2CH(CH_2CH_3)_2$), 1.43 (m, $POCH_2CH(CH_2CH_3)_2$), 1.58 (m, 1H, $POCH_2CH$), 1.76-1.92, 2.31-2.47 (br, $POCH_2CH_2$), 2.77-3.14 (br, $CH_2SCH_2CHSCH_2$), 3.40 (br, $CH_2OCH_2CH_2OCH_3$), 3.54-3.75 (br, $CH_2OCH_2CH_2OCH_3$), 3.96-4.47 (br, $POCH_2CH$, $POCH_2CH_2$, $POCH_2CH_2OP$,), 5.13 (d, *J* = 6.0 Hz, OCH_2Ar), 7.40 (m, Ar-*H*). ^{13}C NMR (CD_3OD, ppm): δ 10.80, 22.58, 30.23, 32.24, 34.00, 41.39, 42.43, 59.10, 66.48-65.68, 70.07, 71.89, 127.86, 128.54. ^{31}P NMR (CD_3OD, ppm): δ -1.19, -1.27. DSC: T_g = - 49.6 °C. TGA in N_2: 185–260 °C, 57% mass loss; 260–600 °C, 14% mass loss, 29 % mass remaining above 600 °C. IR: 3020-2800, 1646, 1457, 1356, 1273, 1091, 1020, 972, 808 cm^{-1}.

The anionic diblock product was obtained in the form of a colorless solid in a yield of 96%. ^{1}H NMR (CD_3OD, ppm): δ 0.97 (t, *J* = 7.4 Hz, $POCH_2CH(CH_2CH_3)_2$), 1.45 (m, $POCH_2CH(CH_2CH_3)_2$), 1.58 (m, 1H,

$POCH_2CH$), 1.76-1.93, 2.31-2.46 (b, $POCH_2CH_2$), 2.63-2.73 (b, CH_2COOH), 2.75-3.09 (br, $CH_2SCH_2CHSCH_2$), 3.89-4.42 (br, $POCH_2CH$, $POCH_2CH_2$, $POCH_2CH_2OP$,), 5.13 (d, J = 6.0 Hz, OCH_2Ar), 7.40 (m, Ar-H). ^{13}C NMR (CD_3OD, ppm): δ 10.90, 22.67, 30.23, 32.24, 34.01, 38.96, 41.49, 42.44, 59.06, 66.04-66.23, 70.15, 71.13, 71.89, 164.99. ^{31}P NMR (CD_3OD, ppm): δ -1.19, -1.43. DSC: T_g = - 57.1 °C. TGA in N_2: 100–200 °C, 14% mass loss; 200–260 °C, 39% mass loss, 260–600 °C, 15% mass loss, 32 % mass remaining above 600 °C. IR: 3200-2800, 2800-2190, 1997-1823, 1791, 1459, 1409, 1020, 920, 805 cm^{-1}.

The cationic diblock polymer was obtained as a faint yellow product with a yield of 63%. Due to the hygroscopic nature, the product polymer was kept under vacuum in the desiccators. ^1H NMR (d_6-DMSO, ppm): δ 0.86 (t, J = 7.4 Hz, $POCH_2CH(CH_2CH_3)_2$), 1.32 (m, $POCH_2CH(CH_2CH_3)_2$), 1.48 (m, 1H, $POCH_2CH$), 1.65-1.84, 2.17-2.36 (b, $POCH_2CH_2$), 2.76-3.14 (br, $CH_2SCH_2CHSCH_2$, CH_2NH_3), 3.90-4.39 (br, $POCH_2CH$, $POCH_2CH_2$, $POCH_2CH_2OP$,), 5.05 (d, OCH_2Ar), 7.40 (m, Ar-H). ^{13}C NMR (d_6-DMSO, ppm): δ 11.07, 22.61, 27.72, 29.00, 33.76, 37.45, 41.29, 41.75, 43.89, 66.31-67.01, 69.25, 69.33, 128.19, 128.88. ^{31}P NMR (d_6-DMSO, ppm): δ -1.19, -1.47. DSC: T_g = - 51.4 °C. TGA in N_2: 170–330 °C, 55 % mass loss; 330–600 °C, 17 % mass loss, 28 % mass remaining above 600 °C. IR: 3600–3300, 3300–2400, 1608, 1462, 1255, 1017, 964, 801 cm^{-1}.

The zwitterionic diblock polymer was obtained as a faint yellow powder with a yield of 68%. Due to the hygroscopic nature, the product polymer was kept under vacuum in a desiccator. ^1H NMR (d_6-DMSO, ppm): δ 0.83 (m, $POCH_2CH(CH_2CH_3)_2$), 1.30 (m, $POCH_2CH(CH_2CH_3)_2$), 1.43 (m, 1H, $POCH_2CH$), 1.72-1.87, 2.07-2.23 (b, $POCH_2CH_2$), 2.80-3.18 (br, $CH_2SCH_2CHSCH_2$, $CH_2CH(NH_3)COOH$), 3.92-4.35 (br, $POCH_2CH$, $POCH_2CH_2$, $POCH_2CH_2OP$,), 5.02 (d, J = 8.2 Hz, OCH_2Ar), 7.40 (m, Ar-H). ^{13}C NMR (d_6-DMSO, ppm): δ 11.06, 22.62, 27.72, 29.02, 33.76, 37.45, 41.29, 41.75, 59.48, 66.31-67.00, 69.26, 69.34, 168.04. ^{31}P NMR (d_6-DMSO, ppm): δ -1.19, -1.43. DSC: T_g = - 54.7 °C. TGA in N_2: 115–180 °C, 11 % mass loss; 180–270 °C, 38 % mass loss, 270–600 °C, 21 % mass loss, 30 % mass remaining above 600 °C. IR: 3300-2480, 2390-2280, 1739, 1629, 1462, 1381, 1253, 1017, 967, 801 cm^{-1}.

Self-assembly of functional diblock copolymers. The functional diblock copolymers (5.0 mg) were suspended into nanopure water (1.0 mL) and sonicated for 10 min.

Cytotoxicity assays. RAW 264.7 mouse macrophages (2 x 10^4 cells/well) were plated in a 96-well plate in Dulbecco's Modified Eagle Medium (DMEM) (10% fetal bovine serum and 1% penicillin/streptomycin). Cells were incubated at 37 °C in a humidified atmosphere containing 5% CO_2 for 24 h to adhere. Then, the medium was replaced with a fresh medium 1-h prior to the addition of 20 μL of the various micellar formulations to 100 μL of the medium (final concentrations ranged from 5-to-3000 μg/mL). The cytotoxicity of Lipofectamine® 2000 (Invitrogen, Grand Island, NY) was also tested at final concentrations ranging from 1-to-160 μg/mL using the same procedures. The cells were incubated with the formulations for 24 h and washed once with phosphate-buffered saline (PBS) and 100 μL of the complete media was added to the cells. The MTS combined reagent (20 μL) was added to each well (Cell Titer 96® Aqueous Non-Radioactive Cell Proliferation Assay, Promega Co., Madison, WI). The cells were incubated with the reagent for 2 h at 37 °C in a humidified atmosphere containing 5% CO_2 protected from light. Absorbance was measured at 490 nm using SpectraMax M5 (Molecular Devices Co., Sunnyvale, CA). The cell viability was calculated based on the relative absorbance to the control-untreated cells. The 0% and 100% cell viabilities were considered as the control medium (no cells) and cells with no treatment, respectively. The calculations of the IC_{50} values were performed using GraphPad Prism four-parameter fit (GraphPad Software, Inc., La Jolla, CA).

Acknowledgements

We gratefully acknowledge financial support from the National Heart Lung and Blood Institute of the National Institutes of Health as a Program of Excellence in Nanotechnology (HHSN268201000046C) and the National Science Foundation under grant number DMR-1105304. The Welch Foundation is gratefully acknowledged for support through the W. T. Doherty-Welch Chair in Chemistry, Grant No. A-0001. The transmission electron microscopy facilities at Washington University in St. Louis, Department of

Otolaryngology, Research Center for Auditory and Visual Studies funded by NIH P30 DC004665 are gratefully acknowledged. The authors thank Adriana Pavia for her kind assistance with illustrations.

Reference

(1) Riehemann, K.; Schneider, S. W.; Luger, T. A.; Godin, B.; Ferrari, M.; Fuchs, H. *Angew. Chem. Int. Edit.* **2009**, *48*, 872.

(2) Yan, Y.; Such, G. K.; Johnston, A. P. R.; Best, J. P.; Caruso, F. *ACS Nano* **2012**, *6*, 3663.

(3) Singh, R.; Lillard, J. W. *Exp. Mol. Pathol.* **2009**, *86*, 215.

(4) Torchilin, V. P. *Adv. Drug. Deliver. Rev.* **2006**, *58*, 1532.

(5) Ma, X.; Zhao, Y.; Liang, X. *Accounts Chem. Res.* **2011**, *44*, 1114.

(6) Elsabahy, M.; Wooley, K. L. *J. Polym. Sci., Part A: Polym. Chem.* **2012**, *50*, 1869.

(7) Kiesewetter, M. K.; Shin, E. J.; Hedrick, J. L.; Waymouth, R. M. *Macromolecules* **2010**, *43*, 2093.

(8) Hawker, C. J.; Wooley, K. L. *Science* **2005**, *309*, 1200.

(9) Iha, R. K.; Wooley, K. L.; Nystrom, A. M.; Burke, D. J.; Kade, M. J.; Hawker, C. J. *Chem. Rev.* **2009**, *109*, 5620.

(10) Choi, H. S.; Ashitate, Y.; Lee, J. H.; Kim, S. H.; Matsui, A.; Insin, N.; Bawendi, M. G.; Semmler-Behnke, M.; Frangioni, J. V.; Tsuda, A. *Nat. Biotechnol.* **2010**, *28*, 1300.

(11) Lee, S. M.; Chen, H.; O'Halloran, T. V.; Nguyen, S. T. *J. Am. Chem. Soc.* **2009**, *131*, 9311.

(12) Zhang, S.; Li, Z.; Samarajeewa, S.; Sun, G.; Yang, C.; Wooley, K. L. *J. Am. Chem. Soc.* **2011**, *133*, 11046.

(13) Ladmiral, V.; Mantovani, G.; Clarkson, G. J.; Cauet, S.; Irwin, J. L.; Haddleton, D. M. *J. Am. Chem. Soc.* **2006**, *128*, 4823.

(14) Liu, J.; Huang, W.; Pang, Y.; Huang, P.; Zhu, X.; Zhou, Y.; Yan, D. *Angew. Chem. Int. Edit.* **2011**, *50*, 9162.

(15) Xiong, M.; Bao, Y.; Yang, X.; Wang, Y.; Sun, B.; Wang, J. *J. Am. Chem. Soc.* **2012**, *134*, 4355.

(16) Wang, Y.; Yuan, Y.; Du, J.; Yang, X.; Wang, J. *Macromol. Biosci.* **2009**, *9*, 1154.

(17) Zhang, S.; Li, A.; Zou, J.; Lin, L. Y.; Wooley, K. L. *ACS. Macro. Lett.* **2012**, *1*, 328.

(18) Libiszowski, J.; Kaluzynski, K.; Penczek, S. *J. Polym. Sci., Part A: Polym. Chem.* **1978**, *16*, 1275.

(19) Richards, M.; Dahiyat, B. I.; Arm, D. M.; Lin, S.; Leong, K. W. *J. Polym. Sci., Part A: Polym. Chem.* **1991**, *29*, 1157.

(20) Pretula, J.; Kaluzynski, K.; Szymanski, R.; Penczek, S. *J. Polym. Sci., Part A: Polym. Chem.* **1999**, *37*, 1365.

(21) Wen, J.; Zhuo, R. X. *Macromol. Rapid. Comm.* **1998**, *19*, 641.

(22) Liu, J.; Pang, Y.; Huang, W.; Zhai, X.; Zhu, X.; Zhou, Y.; Yan, D. *Macromolecules* **2010**, *43*, 8416.

(23) Xiao, C.; Wang, Y.; Du, J.; Chen, X.; Wang, J. *Macromolecules* **2006**, *39*, 6825.

(24) Iwasaki, Y.; Yamaguchi, E. *Macromolecules* **2010**, *43*, 2664.

(25) Zhai, X.; Huang, W.; Liu, J.; Pang, Y.; Zhu, X.; Zhou, Y.; Yan, D. *Macromol. Biosci.* **2011**, *11*, 1603.

(26) Yuan, Y.; Du, J.; Wang, J. *Chem. Commun.* **2012**, *48*, 570.

(27) Clément, B.; Grignard, B.; Koole, L.; Jérôme, C.; Lecomte, P. *Macromolecules* **2012**, *45*, 4476.

(28) Du, J.; Du, X.; Mao, C.; Wang, J. *J. Am. Chem. Soc.* **2011**, *133*, 17560.

(29) Wang, Y.; Li, Y.; Yang, X.; Yuan, Y.; Yan, L.; Wang, J. *Macromolecules* **2009**, *42*, 3026.

(30) Iwasaki, Y.; Wachiralarpphaithoon, C.; Akiyoshi, K. *Macromolecules* **2007**, *40*, 8136.

(31) Iwasaki, Y.; Nakagawa, C.; Ohtomi, M.; Ishihara, K.; Akiyoshi, K. *Biomacromolecules* **2004**, *5*, 1110.

(32) Du, J.; Chen, D.; Wang, Y.; Xiao, C.; Lu, Y.; Wang, J.; Zhang, G. *Biomacromolecules* **2006**, *7*, 1898.

(33) Zhu, W.; Sun, S.; Xu, N.; Gou, P.; Shen, Z. *J. Appl. Polym. Sci.* **2012**, *123*, 365.

(34) Liu, J.; Huang, W.; Pang, Y.; Zhu, X.; Zhou, Y.; Yan, D. *Biomaterials* **2010**, *31*, 5643.

(35) Liu, J. Y.; Pang, Y.; Huang, W.; Zhu, Z.; Zhu, X.; Zhou, Y.; Yan, D. *Biomacromolecules* **2011**, *12*, 2407.

(36) Song, W.; Du, J.; Liu, N.; Dou, S.; Cheng, J.; Wang, J. *Macromolecules* **2008**, *41*, 6935.

(37) Sun, T.; Du, J.; Yan, L.; Mao, H.; Wang, J. *Biomaterials* **2008**, *29*, 4348.

(38) Sun, T.; Du, J.; Yao, Y.; Mao, C.; Dou, S.; Huang, S.; Zhang, P.; Leong, K. W.; Song, E. W.; Wang, J. *ACS Nano* **2011**, *5*, 1483.

(39) Wang, Y.; Li, Y.; Sun, T.; Xiong, M.; Wu, J.; Yang, Y.; Wang, J. *Macromol. Rapid. Comm.* **2010**, *31*, 1201.

(40) Shao, H.; Zhang, M.; He, J.; Ni, P. *Polymer* **2012**, *53*, 2854.

(41) Wachiralarpphaithoon, C.; Iwasaki, Y.; Akiyoshi, K. *Biomaterials* **2007**, *28*, 984.

(42) Wang, Y.; Tang, L.; Li, Y.; Wang, J. *Biomacromolecules* **2009**, *10*, 66.

(43) Ober, C. K.; Cheng, S. Z. D.; Hammond, P. T.; Muthukumar, M.; Reichmanis, E.; Wooley, K. L.; Lodge, T. P. *Macromolecules* **2009**, *42*, 465.

(44) Hoyle, C. E.; Lowe, A. B.; Bowman, C. N. *Chem. Soc. Rev.* **2010**, *39*, 1355.

(45) Elsabahy, M.; Wooley, K. L. *Chem. Soc. Rev.* **2012**, *41*, 2545.

(46) Albanese, A.; Tang, P. S.; Chan, W. C. W. *Annu Rev Biomed Eng.* **2012**, *14*, 1.

(47) Goodman, C. M.; McCusker, C. D.; Yilmaz, T.; Rotello, V. M. *Bioconjugate Chem.* **2004**, *15*, 897.

(48) Arvizo, R. R.; Miranda, O. R.; Thompson, M. A.; Pabelick, C. M.; Bhattacharya, R.; Robertson, J. D.; Rotello, V. M.; Prakash, Y. S.; Mukherjee, P. *Nano. Lett.* **2010**, *10*, 2543.

(49) Walkey, C. D.; Olsen, J. B.; Guo, H. B.; Emili, A.; Chan, W. C. W. *J. Am. Chem. Soc.* **2012**, *134*, 2139.

(50) Wang, J.; Mao, H.; Leong, K. W. *J Am Chem Soc* **2001**, *123*, 9480.

Chapter 6

Poly(ethylene oxide)-*block*-polyphosphester-based Paclitaxel conjugates as a platform for ultra-high Paclitaxel-loaded multifunctional nanoparticles

[Portions of this work have been published previously as Shiyi Zhang,[†] Jiong Zou,[†] Mahmoud Elsabahy, Amolkumar Karwa, Ang Li, Dennis A. Moore, Richard B. Dorshow, and Karen L. Wooley, *Chem. Sci.* **2013** DOI: 10.1039/C3SC50252J]

[†] These two authors contributed equally.

Abstract

A new type of degradable, nanoscopic polymer assembly containing ultra-high levels of drug loading *via* covalent attachment within amphiphilic core-shell nanoparticle morphology has been generated as a potentially effective and safe anti-cancer agent. Poly(ethylene oxide)-*block*-polyphosphoester-based paclitaxel drug conjugates (PEO-*b*-PPE-*g*-PTX) were synthesized by rapid, scalable and versatile approach that involves only two steps: organocatalyst-promoted ring-opening-polymerization followed by click reaction-based conjugation of a PTX prodrug. Variations in the polymer-to-PTX stoichiometries allowed for optimization of the conjugation efficiency, the PTX drug loading and the resulting water solubilities of the entire polymer and the PTX content. The PEO-*b*-PPE-*g*-PTX formed well-defined micelles in aqueous solution, with a PTX loading capacity as high as 65 *wt*%, and a maximum PTX concentration of 6.2 mg/mL in water, which is 25000-fold higher than the aqueous solubility of free PTX. The positive cell-killing activity of PEO-*b*-PPE-*g*-PTX against several cancer cell lines is demonstrated, and the presence of pendant reactive functionality provides a powerful platform for future work to involve conjugation of multiple drugs and imaging agents to achieve chemotherapy and bioimaging.

Introduction

Paclitaxel (PTX), a microtubule-interfering agent, has demonstrated a broad spectrum of antitumor activity against various cancers including breast, lung and advanced ovarian cancers,(1, 2) however, there are several challenges with its formulation that remain unmet. The low solubility of PTX and the difficulty of achieving sufficiently high concentration in solution that is suitable for *in vivo* administration and clinical applications have led to the development of various strategies to increase its bioavailability, which utilize low molecular weight surfactants (Taxol®),(3) coat the drug with albumin (Abraxane®),(4) or conjugate it to water-soluble polymers (PTX poliglumex, functionalized gold nanoparticles,(12) polylactide(PLA)-PTX conjugated nanoparticles(13) and PTX cross-linked PLA based nanocomposites.(14) It still remains challenging to obtain high PTX loadings for polymer drug conjugates (PDCs) and also maintain high water solubility to be suitable for *in vivo* administration and clinical applications. Therefore, we have taken advantage of current state-of-the-art synthetic polymer chemistry and orthogonal conjugation chemistries(15, 16) to produce, through a rapid, versatile and scalable two-step approach, unique degradable diblock copolymers of poly(ethylene oxide) and functional polyphosphoesters that allow for click conjugation of PTX onto a selective region of the amphiphilic diblock copolymer, thereby, allowing ultra-high PTX loading within nanoscopic carriers in water.

Based upon an interest to incorporate a non-reactive, water-soluble polymer chain segment, to mediate the supramolecular assembly process in water and provide a shell layer that imparts serum stability, together with a highly- and selectively-reactive chain segment for high-loading conjugation of PTX, a new type of poly(ethylene oxide)-*b*-polyphosphoester (PEO-*b*-PPE)-based polymer drug conjugate for PTX delivery was designed. Surface modification of nanoparticles with PEO moieties have the benefits of prolonged blood circulation and enhanced accumulation in the tumor tissues *via* the enhanced permeability and retention (EPR) effect.(17) The PPE portion of the system was constructed based upon our recent development of a new type of degradable and water-soluble polyphosphoester bearing alkynyl

functionalities by using organocatalyst-promoted ring opening polymerization (ROP).(18, 19) The alkynyl groups on the side chain have been shown to undergo high-efficiency reactions in "click"-type azide-alkyne Huisgen cycloaddition. Therefore, an azide-functionalized PTX was synthesized by esterification, in which the most reactive 2'-hydroxyl group of PTX reacted with 6-azidohexanoic acid to form an ester linkage, and then this azide-functionalized PTX was further conjugated onto the PPE backbone through click reaction, resulting in PEO-*b*-PPE-*g*-PTX drug conjugates that assembled in water into nanoscopic micelles with up to 65 *wt*% PTX loading. To our best knowledge, this drug loading capacity is the highest, compared to the reported polymer-PTX conjugates. The high content of PTX in the drug conjugates is important to decrease of the total amount of polymers required to deliver a particular amount of the drug, to reduce any potential toxicities that might be associated with the delivery vehicle, and furthermore to reduce the cost of production of the nanoparticles. Taking advantage of the high solubility of the PPE backbone and the PEO shielding, the solubility of PTX could reach 6.2 mg/mL. The potency of the resulting PEO-*b*-PPE-*g*-PTX drug conjugates was also tested against multiple cancer cell lines. Though PEO-*b*-PPE-*g*-PTX micelles were one-to-two orders of magnitude less potent than free PTX, their cell killing ability was better than or equal to the performance of PGA-PTX. Residual alkynyl groups were decorated with fluorescent dyes to track the cellular uptake of the PEO-*b*-PPE-*g*-PTX conjugates *in vitro*.

Results and Discussion

The PEO-*b*-(PPE-*g*-PTX) conjugates were synthesized as illustrated in **Figure 6-1**. PEO (average M_n ~2,000 Da) (**1**) was used to initiate the ROP of butynyl phospholane (BYP), **2**, which yielded the well-defined diblock copolymer, PEO_{44}-*b*-$PBYP_{30}$, **3**. This controlled organocatalyzed ROP of the cyclic phospholane monomer gave quantitative conversion in only 4 min, and was highly reproducible. With a 1:30 stoichiometry of PEO:BYP, **3** was produced having M_n = 7200 Da, in agreement with the theoretical degrees of polymerization, as determined by ^{1}H NMR spectroscopy, and narrow molecular weight distribution, M_w/M_n = 1.17, as determined by gel permeation chromatography (GPC) (for full characterization data, see supporting information).

To equip PTX with a functionality for coupling to PEO-*b*-PPE, the C-2'-OH position of PTX was functionalized with an azido group through an ester linkage, by reaction with 6-azidohexanoic acid and employing a slight excess of PTX (1.2 eq), in the presence of *N,N'*-dicyclohexylcarbodiimide and 4-(dimethylamino)pyridine in CH_2Cl_2 heated at reflux for 3 d to afford PTX C2'-ester **4** as the predominant product. Automated high performance flash chromatography with prepacked fine spherical silica gel (20-40 μm) was used to isolate **4** in 78% yield. The selective condensation between 2'-OH and 6-azidohexanoic acid was confirmed by ^{1}H NMR. The chemical shift of 2'(CH)-OH on PTX in $CDCl_3$ is 4.78 ppm. In the ^{1}H NMR of azido-PTX, no peak was observed between 4.6-4.9 ppm (see supporting information). No significant chemical shift change was observed on (C-7)-CH-OH (4.40 ppm) before and after esterification. By using DCC/DMAP promoted condensation, only 2'-OH of PTX is active.(20)

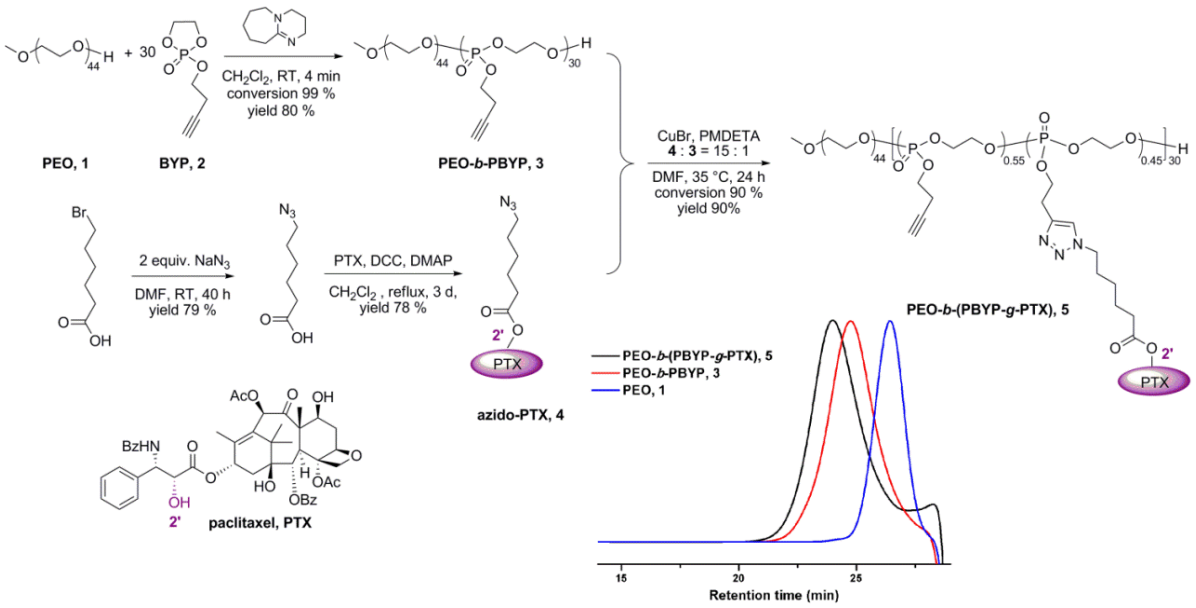

Figure 6-1. Schematic representation of the synthesis of PEO-*b*-(PTX-*g*-PBYP). GPC traces of PEO, PEO-*b*-PBYP and PEO-*b*-(PTX-*g*-PBYP) are inserted.

Azide-alkyne Huisgen cycloaddition (CuAAC) was employed to attach **4** onto the backbone of **3** and afford PEO-*b*-(PPE-*g*-PTX), **5**. PEO-*b*-(PPE-*g*-PTX) conjugates were synthesized with a range of feed ratios of azido-PTX to PEO-*b*-PPE alkyne (20%, 50% and 100%). As shown in **Figure 6-2**, even though the conjugation efficiency decreased as the feed ratio increased, the click reaction showed higher conjugation efficiency than that observed for esterification-based conjugation of sterically-bulky PTX onto polymers.(14, 21, 22) The highest PTX loading capacity, 65 wt%, was reached when the feed ratio was 100%, however, this polymer had a poor solubility in water (lower than 0.5 mg/mL). The optimal polymer had conjugation efficiency as high as 90%, PTX loading capacity of 55 wt%, and high water solubility (11.3 mg/mL) when the feeding ratio of **4** to **3** was 15 to 1 (feed ratio of azido-PTX to alkyne was 50%). Unreacted **4** was removed by repeated precipitation from acetone into diethyl ether 3 times, because PTX and azido-PTX were well soluble in diethyl ether. Complete removal of the unreacted **4** was confirmed by ^{1}H NMR, GPC and HPLC (**Figure 6-3** shows the comparison of **5** and PTX) analysis of the product.

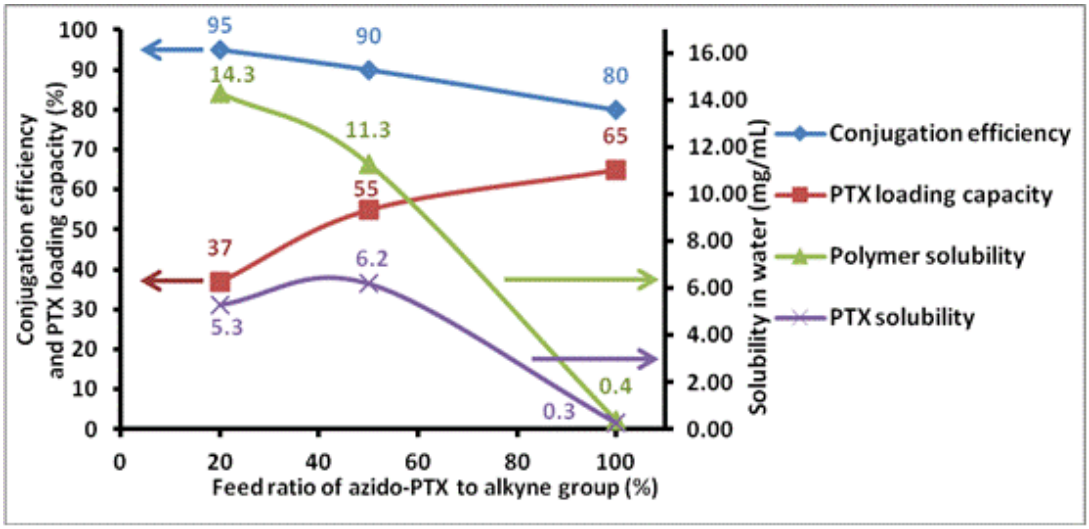

Figure 6-2. Optimization of click reaction with three different feed ratios of azido-PTX to alkyne group on PEO-b-PBYP. Three resulting polymers with feed ratios (20%, 50% and 100% respectively) were plotted in the figure as a function of conjugation efficiency (left), PTX loading capacity (left), polymer solubility in water (right) and PTX solubility in water (right).

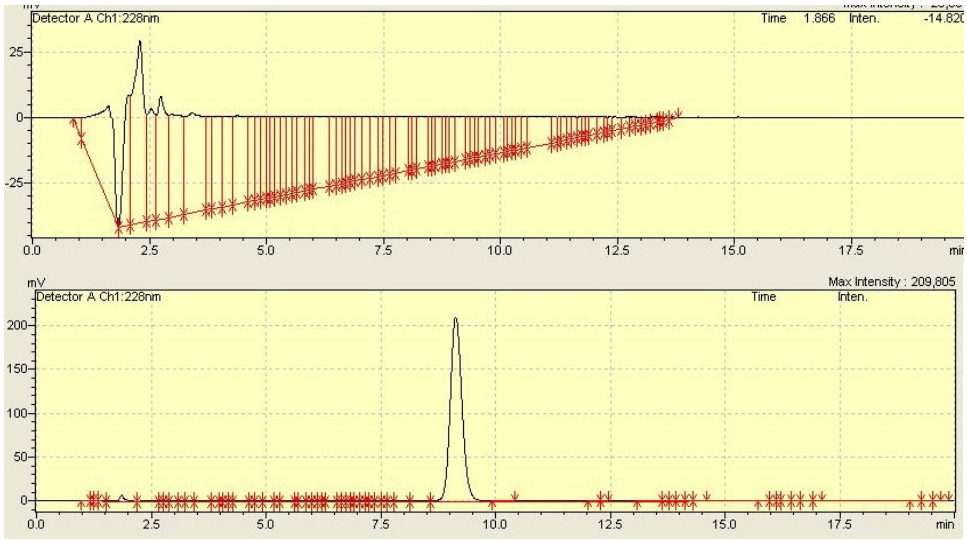

Figure 6-3. Comparison of the HPLC spectra of **5** (top) and free PTX (bottom) confirmed the complete removal of free PTX by precipitation after the click reaction.

The PEO-*b*-(PPE-*g*-PTX) drug conjugates, **5**, were further purified and supramolecularly assembled in water by being dissolved in acetone and dialyzed against nanopure water containing Chelex 100 resin (100-200 mesh) for 2 d, to remove copper and other potential ion contaminants, and also to trigger self assembly. The resulting micelle solution was obtained and then passed through a 450 nm polypropylene filter to remove dust and large aggregates. The micelle solution was lyophilized to give a faint yellow powder with an overall yield above 90%. The lyophilized PEO-*b*-(PPE-*g*-PTX) conjugates could be easily dissolved into water at a concentration as high as 11.3 mg/mL (equivalent PTX concentration of 6.2 mg/mL) by applying sonication for 3 min (see supporting information for the solubility test). Dynamic light scattering (DLS) analysis indicated the number-average hydrodynamic diameter of the micelles was 26 ± 7 nm, and transmission electron microscopy (TEM) images confirmed that the PEO-*b*-(PPE-*g*-PTX) nanoassemblies were well-dispersed in water in the form of micellar nanoparticles with a narrow size distribution D_{av} = 24 ± 6 nm (**Figure 6-4**).

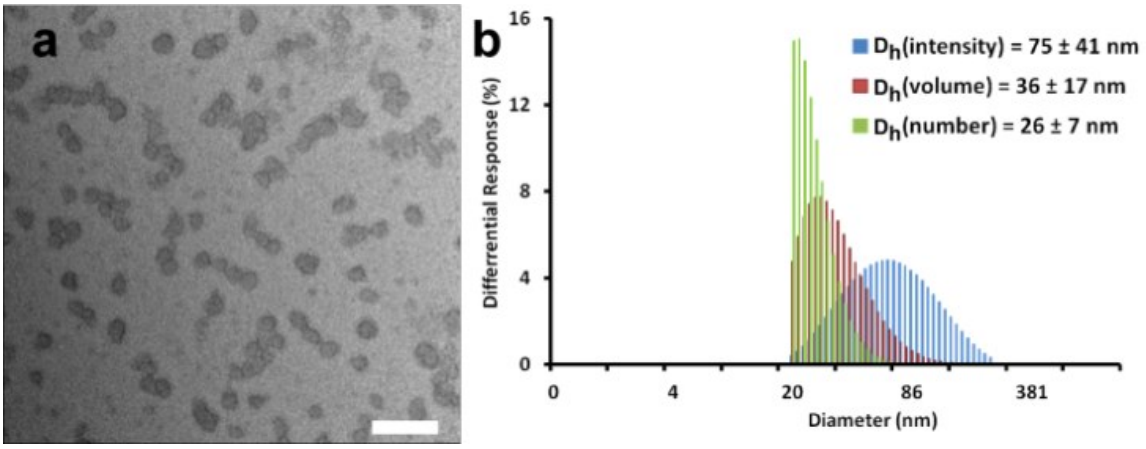

Figure 6-4. Micelles of **5** w/55 wt% PTX: a, TEM image, D_{av} = 24 ± 6 nm (scale bar: 100 nm); b, DLS in water.

Click reactions have been shown to be highly efficient when coupling large-sized anticancer drugs.(20, 23, 24) Here, click chemistry provided a highly-efficient strategy to load PTX onto reactive polymer backbones in high coupling conversion and PTX loading capacity. PEO-*b*-(PPE-*g*-PTX) drug conjugates, **5**, were dissolved in water at the equivalent PTX concentration of 6.2 mg/mL, exhibiting significantly enhanced solubility, *ca*. 25,000-fold, as compared to the free drug, and 2.4-fold higher than that reported for the PTX conjugates with PGA.(9)

The lyophilized, powder-like PEO-*b*-(PPE-*g*-PTX) conjugates showed no evidence of degradation of structure or properties over 3 months when stored under nitrogen at -20°C. The GPC profile and DLS analysis confirmed that the chemical compositions of the polymer-drug conjugates and the particle sizes of the micelles did not change after 3 months of storage (data shown in **Figure 6-5**). Hence, the powder form of the conjugates might provide a promising platform for clinical applications, due to the ease by which it can be stored, transported and re-suspended prior to use.

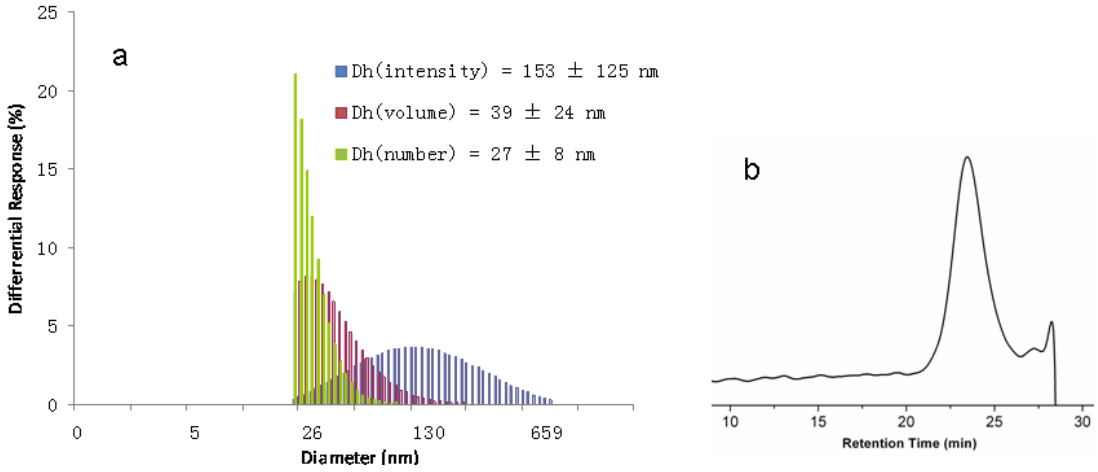

Figure 6-5. DLS a) and GPC b) profiles of PEO-*b*-(PBYP-*g*-PTX) after kept 3 month in -20 °C.

An important aspect of the PEO-*b*-(PPE-*g*-PTX) nanoparticle system is an ability to undergo hydrolytic degradation to release the PTX and allow it to perform its chemotherapeutic activity, while also eliminating the polymer nanoparticle structure. Aqueous solution-state hydrolysis studies were, therefore, conducted by observing breakdown of the polyphosphoester backbone by ^{31}P NMR spectroscopy as a function of time and pH, using the PEO-*b*-PPE block copolymer **3** as a model system, dissolved in D_2O at different pH values (see **Figure 6-6**). At neutral pH, the polyphosphoester was fully stable over the entire period of measurement, >150 h. The rate and extent of hydrolysis increased with increasing pH. As the pH was reduced to acidic values, complications occurred with aggregation and precipitation events preventing accurate determination of the extent of hydrolysis, however, there was a general trend of increased hydrolysis, relative to neutral pH. A full study of the hydrolytic characteristics of these highly interesting polyphosphoester block copolymer nanoassemblies, as a function of composition and structure, is receiving further attention as a full, separate study. The hydrolytic release of PTX from PPE-PTX conjugates were measured by HPLC. However, only 5 % of PTX was released from PPE-PTX micelles after 4 days incubation in 20 mM acetate buffer at pH = 6.0. The lower released PTX may due to the inaccessibility of 2' PTX-ester in the hydrophobic core. To improve the release rate of PTX from PPE-PTX conjugates, next generations of PPE-PTX drug conjugates with acid-liable and redox-liable linkages are currently under development.

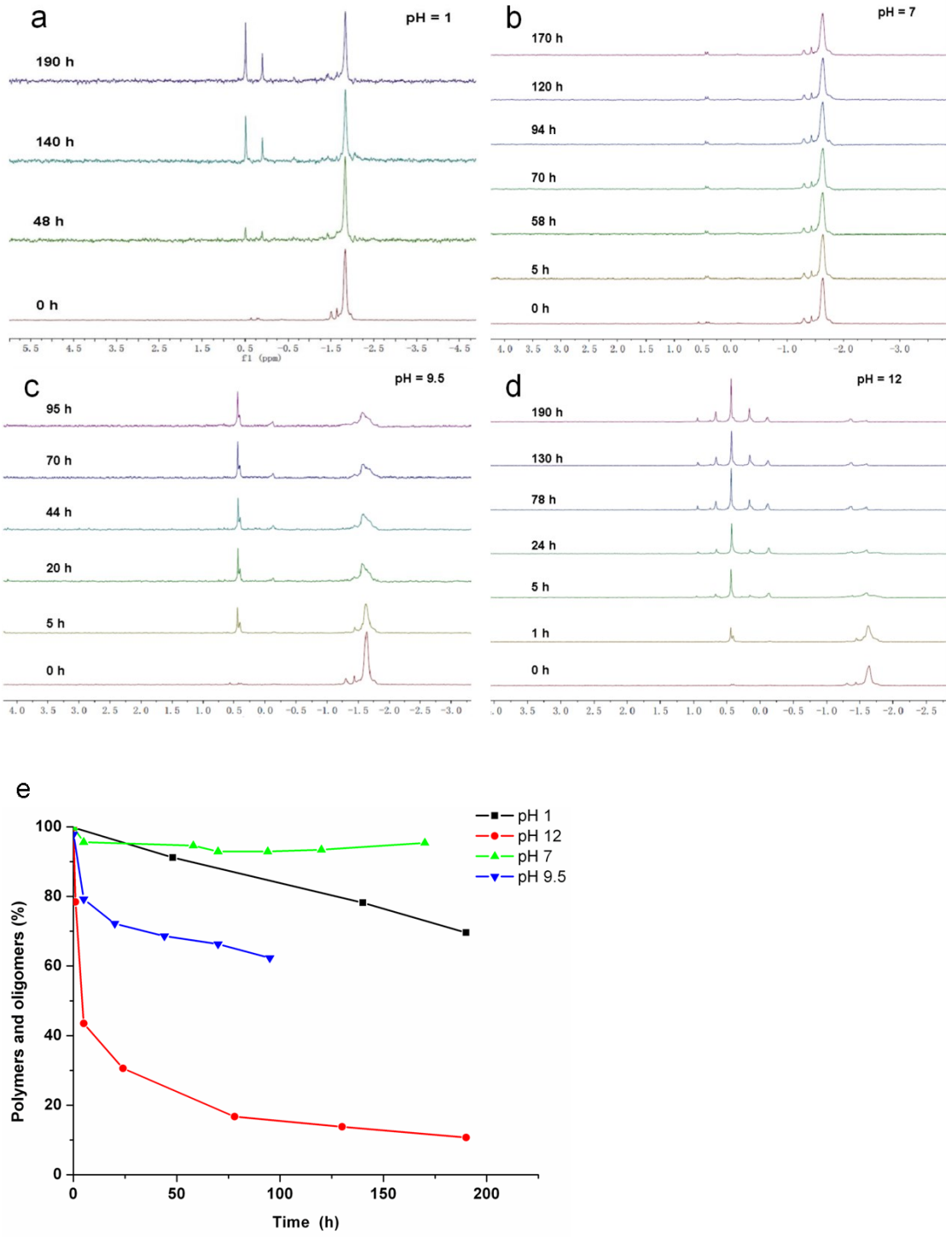

Figure 6-6. ^{31}P NMR spectra of PEG-*b*-PBYP **3** as a function of time at different pH. (a). pH = 1; (b). pH = 7; (c). pH = 9.5; (d). pH = 12. (e). Polyphosphoester and oligo-phosphoester (-1.5 to -3.0 ppm) percentage in degradation mixture during the hydrolytic degradation.

The PEO-*b*-(PPE-*g*-PTX) nanoparticle system (55 wt% PTX loading) was studied for its cytotoxic effect against several cancer cell lines. Both the Cremophor-EL/ethanol (1:1 *v*/*v*) and PEO-*b*-PPE polymers (control polymer **8**, see **Figure 6-7** for the chemical structure) were not cytotoxic to the cells at the concentrations that were tested for the delivery of PTX (data not shown). The PTX conjugated onto the nanoparticles showed 8-to-63-fold lower cytotoxicity than the commercial PTX, depending on the sensitivity of the tested cell line to the drug (**Table 6-1**). The reduced cytotoxicity is explained by the time required for dissociation of the conjugated drug from the PEO-*b*-PPE backbone, followed by the physical release from the nanoparticles, in contrast to the drug that is physically loaded into the low molecular weight surfactant, Cremophor-EL. Lower cytotoxicities of PTX-polymeric drug conjugates, due to the slow *in vitro* release kinetics, have been previously reported in the literature. For instance, PGA-PTX conjugates exhibited 6-to-180-fold lower cytotoxicity than PTX, depending on the cell line utilized.(25) A contributing explanation could be the low cellular entry of the nanoparticles *versus* the possibility of the instantaneous release of PTX from the Cremophor-EL low molecular weight surfactant in the cell culture media, which can then passively diffuse into the cells and induce cytotoxicity.

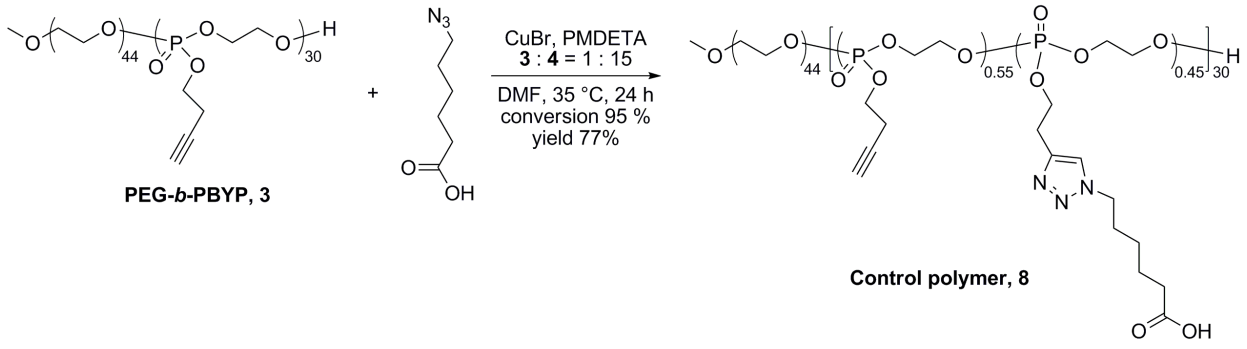

Figure 6-7. The synthetic route of the control polymer, **8**.

Table 6-1. Comparison of the IC_{50} values of PTX (as a Taxol®-mimicking formulation; Cremophor-EL and ethanol, 1:1 *v*/*v* with OVCAR-3 and RAW 264.7 cells, and free PTX with KB and A549 cell lines) and PTX conjugate, **5**, having 55 wt% PTX loading, incubated for 72 h.

Formulation	IC50 (μM)			
	OVCAR-3	RAW 264.7	KB cells	A549 cells
PTX	0.007	0.044	0.004	0.287
5	0.119	2.829	0.039	1.471

To investigate the cell internalization of the PEO-*b*-(PPE-*g*-PTX) conjugates, a portion of the residual alkynyl groups were labeled with azido-functionalized fluorescein (**Figures 6-8** and **6-9**). The cellular uptake of the fluorescein-labeled PEO-*b*-(PPE-*g*-PTX) nanoparticles into OVCAR-3 cells and RAW 264.7 mouse macrophages was tested at different concentrations. After 5-h incubation (low cell viability was observed after longer incubation time.) and at PTX concentration of 15 μM, the nanoparticles could be visualized (green) in the cytoplasm of the RAW 264.7 cells surrounding the nucleus (blue) (**Figure 6-10**). In addition, morphological changes in the nucleus are observed, which may be due to apoptosis, induced by the released PTX (red arrows on **Figure 6-10**).(26) Lower concentrations on the same cell line (3 μM) or on OVCAR-3 (lower concentration (0.5 μM) is used due to the high sensitivity of this cell line to PTX, **Table 1**) could not observe the cellular uptake of the nanoparticles (**Figure 6-11**). Even in the absence of visible nanoparticle uptake, nuclear fragmentation due to the released PTX was observed, however, to a lesser extent (indicated also by the red arrows in **Figure 6-11**). Control-untreated cells or cells treated with PEO-*b*-PPE lacking PTX did not show any morphological changes in the nuclei.

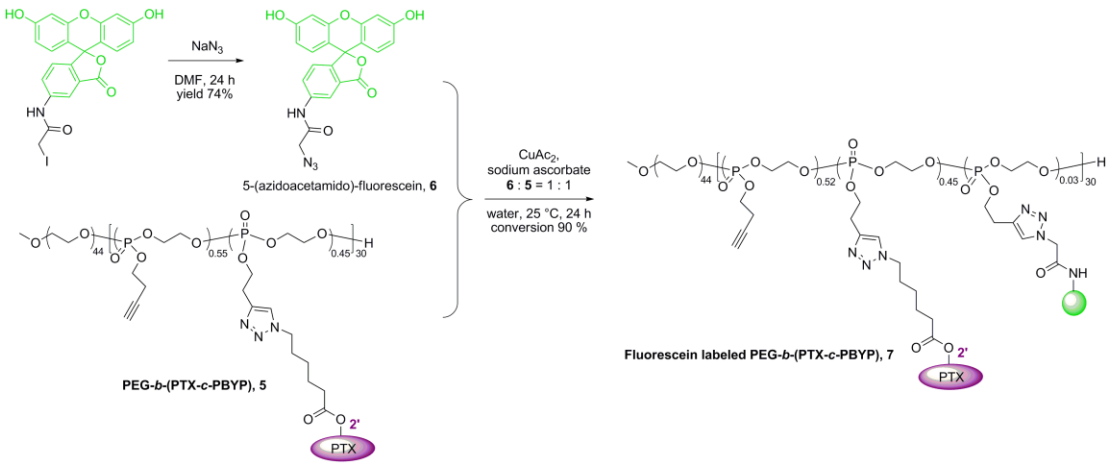

Figure 6-8. The synthetic route of fluorescein labeled PEO-*b*-(PBYP-*g*-PTX), **7**.

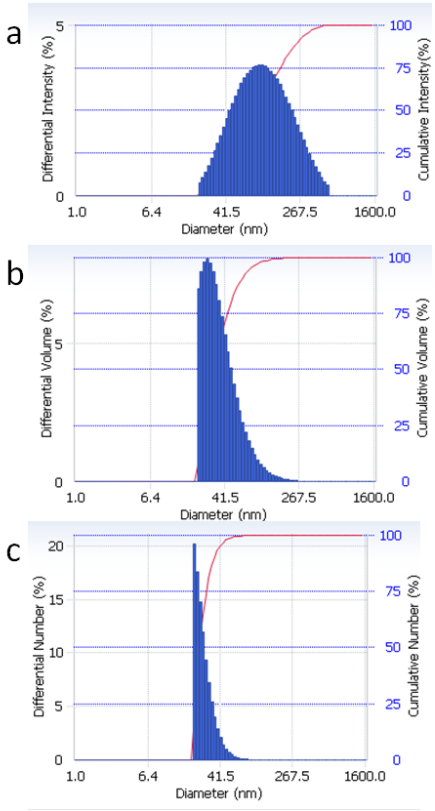

Figure 6-9. DLS results of **7**, D_h (intensity) = 128 ± 93 nm; D_h (volume) = 40 ± 23 nm; D_h (number) = 28 ± 8 nm.

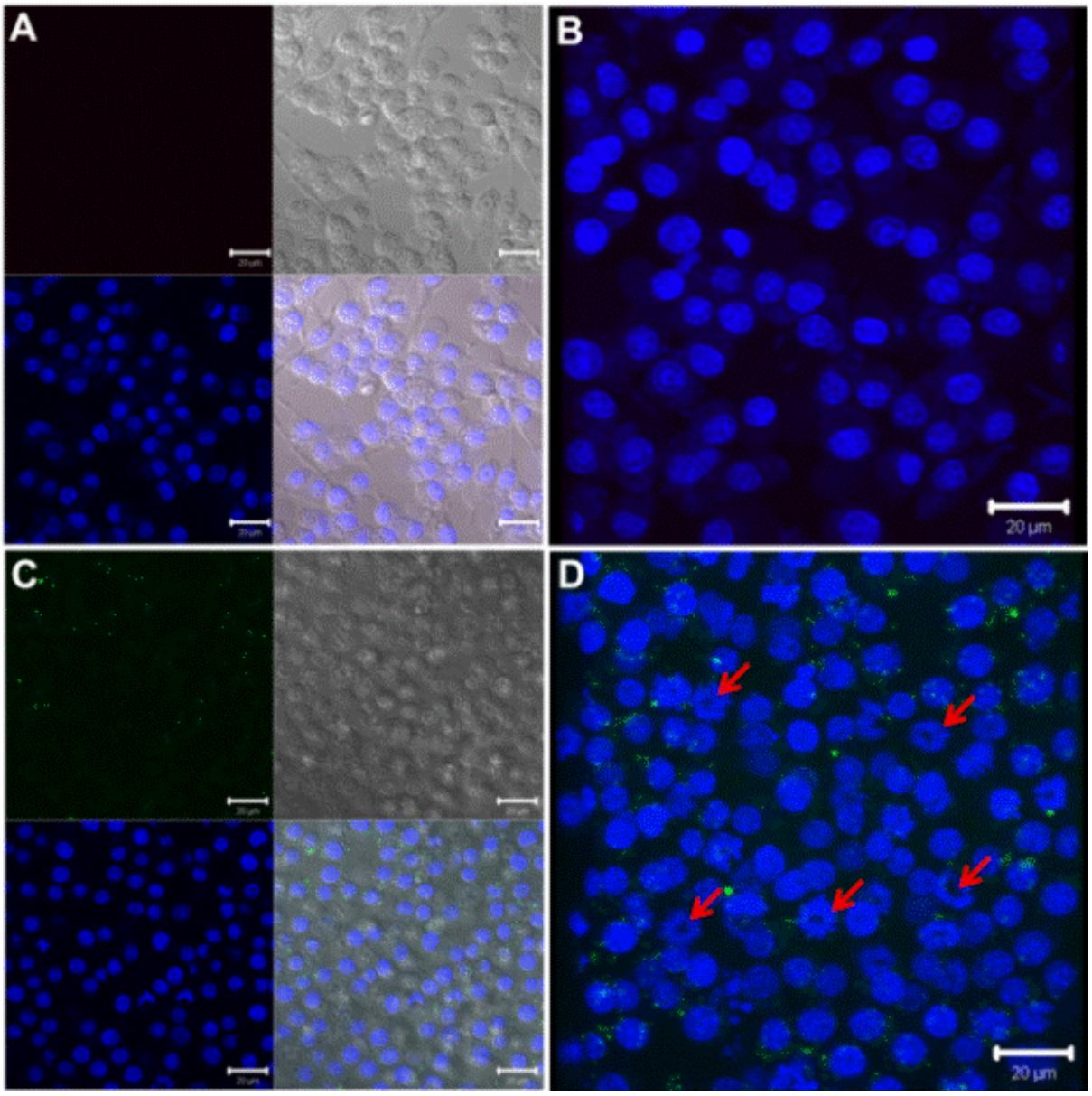

Figure 6-10. Laser scanning confocal microscopy analysis of the cellular uptake of fluorescein-labeled PPE-PTX nanoparticles (green panel) into RAW 264.7 mouse macrophages. Two- and three-dimensional images were collected for both the control-untreated cells (A and B) and the cell-treated with the PTX-loaded nanoparticles (15 μM, C and D). The nuclei were stained with DRAQ5 nuclear stain (blue panel), where whereas the fluorescein appears in green. The transmitted light-images and merged images are also indicated. The changes in the nuclear morphology due to the treatment with the nanoparticles are demonstrated by the red arrows.

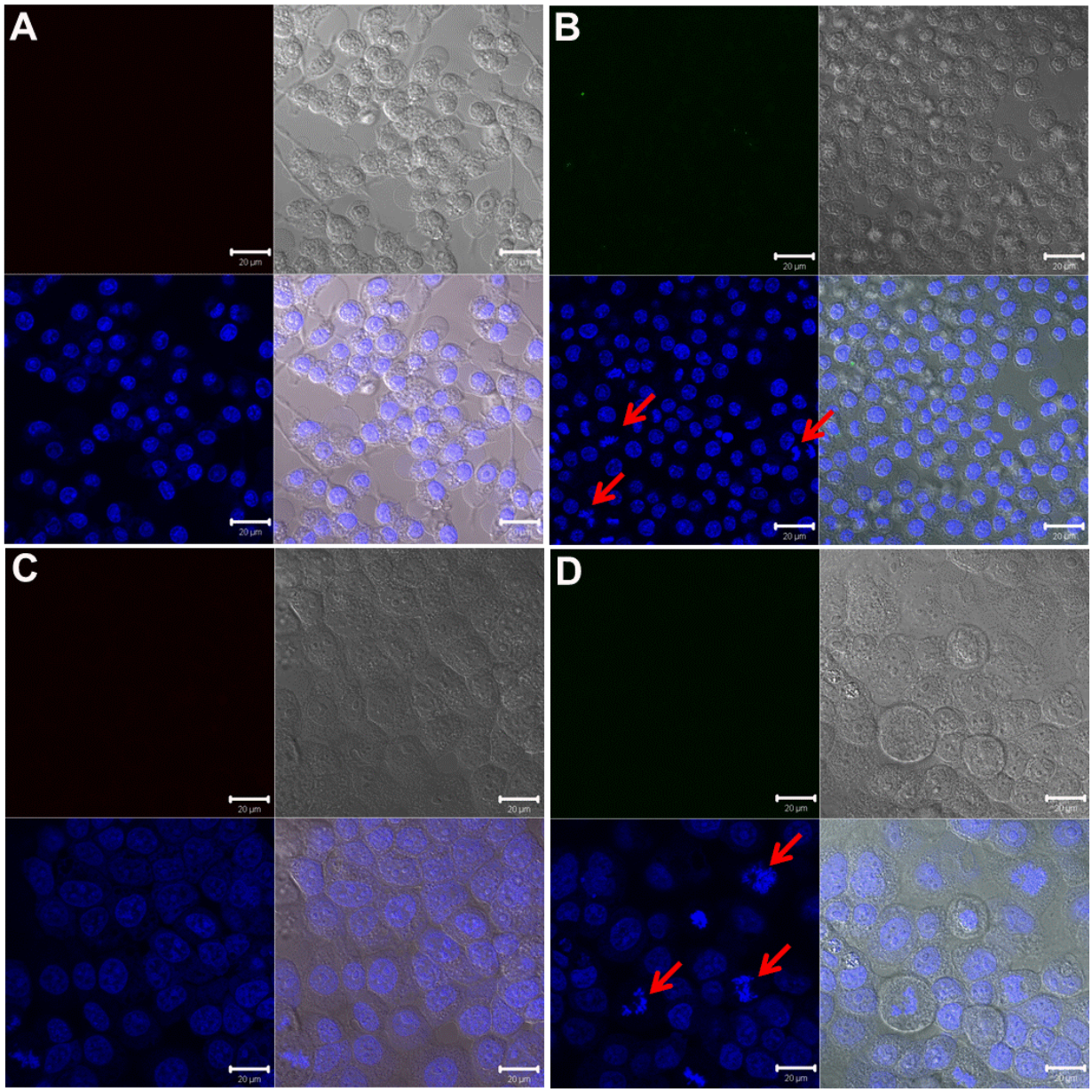

Figure 6-11. Laser scanning confocal microscopy analysis of the mouse macrophages (A and B) and OVCAR-3 (C and D) that either untreated (A and C) or treated with fluorescein-labeled nanoparticles (0.5 μM and 3 μM for B and D, respectively). The nucleus were stained with DRAQ5 nuclear stain (blue panel), whereas the fluorescein appears in green (no uptake was observed at the tested concentrations). The transmitted light-images and merged images are also indicated. The changes in the nuclear morphology due to the treatment with the nanoparticles are demonstrated by the red arrows.

Conclusion

In conclusion, we have developed a novel PEO-*b*-(PPE-*g*-PTX) drug conjugate system. Click chemistry was employed to attach bulky PTX molecules covalently and densely onto a select portion of the amphiphilic block copolymer backbone, and to label the resulting PEO-*b*-PPE-*g*-PTX system with fluorescein. In addition, residual alkynes provide possibilities of further post-chemical modifications (*e.g.* crosslinking, radio-labeling, decoration with targeting ligands), as opposed to the limited functionalizability of Taxol or Abraxane. Also in contrast to other promising PTX-based nanoparticle systems, the partitioning of separate PEO and PTX-functionalized PPE constituents within different regions along the block copolymer structure allows for placement of the components and their functions within different regions of the resulting nanoparticulate block copolymer micelle framework. The PEO-*b*-(PPE-*g*-PTX) achieved a PTX loading capacity as high as 65 wt% and, by balancing PTX loading capacity and polymer solubility, a water solubility at equivalent PTX concentration of 6.2 mg/mL was obtained (at 55 wt% PTX loading). Visualization of fluorescein-labeled PEO-*b*-(PPE-*g*-PTX) in cells by confocal fluorescence microscopy demonstrated the successful cellular internalization. Although the cell-killing activity of the covalently-conjugated PTX of PEO-*b*-(PPE-*g*-PTX) was reduced, relative to the physically-associated PTX of the Cremophor-EL and ethanol formulation, against several cancer cell lines, the lower cytotoxicity of the conjugates might be advantageous by providing increased safety for *in vivo* applications. For instance, the PEO-*b*-(PPE-*g*-PTX) nanoparticle micelle system could provide stability during blood circulation and allow release primarily after high accumulation in tumor tissues *via* the enhanced permeability and retention effect. The observation that accelerated hydrolytic degradation occurred for the polyphosphoester backbone at acidic pH is further promising for selective release in tumor cell environments, with a potential also for enzymatic catalysis. This PEO-*b*-(PPE-*g*-PTX) system provides a powerful platform for combinational therapy and bioimaging. Plans are underway for *in vivo* studies.

Experimental

Materials. N,N-dimethylformamide (DMF), ethyl acetate, acetone, diethyl ether, copper(I) bromide, acetone, diethyl ether, 1,8-diazabicyclo[5.4.0]undec-7-ene (DBU), acetic acid, 3-butyn-1-ol, triethylamine (TEA), *N,N'*dicyclohexylcarbodiimide (DCC), 6-bromohexanoic acid, 4-(dimethylamino)pyridine (DMAP), sodium azide, copper(II) acetate monohydrate, sodium ascorbate, *N,N,N',N'',N''*-pentamethyldiethylenetriamine (PMDETA), poly(ethylene glycol) methyl ether (average M_n ~2,000 Da, PEO), methanol and 5-(iodoacetamido)fluorescein were used as received from Sigma-Aldrich Company (St. Louis, MO). 2-chloro-2-oxo-1,3,2-dioxaphospholane (95%) was used as received from Thermo Fisher Scientific Inc (Pittsburgh, PA). Paclitaxel (PTX) was used as received from Cedarburg Hauser Pharmaceuticals (Denver, CO). Chelex 100 Resin was used as received from Bio-Rad Laboratories (Hercules, CA). Tetrahydrofuran (THF) and dichloromethane (DCM) were dried through columns (J. C. Meyer Solvent Systems, Inc., Laguna Beach, CA). Nanopure water (18 MΩ·cm) was acquired by means of a Milli-Q water filtration system, Millipore Corp. (St. Charles, MO).

Instrumentation. ^{1}H NMR, ^{31}P NMR and ^{13}C NMR spectra were recorded on an Inova 300 MHz or Mercury 300 MHz spectrometer interfaced to a UNIX computer using VnmrJ software. Chemical shifts were referenced to the solvent resonance signals.

The DMF gel permeation chromatography (GPC) was conducted on a Waters Chromatography, Inc. (Milford, MA) system equipped with an isocratic pump model 1515, a differential refractometer model 2414, and a four-column set of 5 μm Guard (50 × 7.5 mm), Styragel HR 4 5 μm DMF (300 × 7.5 mm), Styragel HR 4E 5 μm DMF (300 × 7.5 mm), and Styragel HR 2 5 μm DMF (300 × 7.5 mm). The system was equilibrated at 70°C in pre-filtered DMF containing 0.05 M LiBr, which served as polymer solvent and eluent (flow rate set to 1.00 mL/min). Polymer solutions were prepared at a concentration of *ca*. 3 mg/mL and an injection volume of 200 μL was used. Data collection and analysis were performed with Empower 2 v. 6.10.01.00 software (Waters, Inc.). The system was calibrated with polystyrene standards (Polymer Laboratories, Amherst, MA) ranging from 615 to 442,800 Da.

IR spectra were recorded on an IR Prestige 21 system (Shimadzu Corp.) and analyzed using IRsolution v. 1.40 software.

Ultraviolet-visible spectroscopy (UV-vis) absorption measurements were made using a UV-2550 system (Shimadzu Corp.) equipped with a TMSPC-8 thermoelectric temperature controlling system using quartz cuvettes. Spectra were analyzed by using Tm analysis software module 1,2,1,0 and UV-Probe v. 2.33 software.

Glass transition temperatures (T_g) were measured by differential scanning calorimetry on a Mettler-Toledo DSC822® (Mettler-Toledo, Inc., Columbus, OH), with a heating rate of 10 °C /min. Measurements were analyzed using Mettler-Toledo STARe v. 7.01 software. The T_g was taken as the midpoint of the inflection tangent, upon the third heating scan. Thermogravimetric analysis was performed under N_2 atmosphere using a Mettler-Toledo model TGA/SDTA851^e, with a heating rate of 5 °C /min. Measurements were analyzed by using Mettler-Toledo STARe v. 7.01 software.

Transmission electron microscopy (TEM) was conducted on a Hitachi H-7500 microscope, operating at 100 kV. Samples for TEM measurements were prepared as follows: 4 μL of the dilute solution (with a polymer concentration of 0.1 mg/mL) was deposited onto a carbon-coated copper grid, and after 2 min, the excess of the solution was quickly wicked away by a piece of filter paper. The samples were then negatively stained with 1 *wt*% phosphotungstic acid (PTA) aqueous solution. After 1 min, the excess staining solution was quickly wicked away by a piece of filter paper and the samples were left to dry under ambient conditions overnight. The average diameter of nanoparticles on TEM grid was obtained by measuring the core domain of 200 sphere particles at different area of TEM specimen and the standard deviation was presented as error.

DLS measurements were conducted using a Delsa Nano C from Beckman Coulter, Inc. (Fullerton, CA) equipped with a laser diode operating at 658 nm. Scattered light was detected at 165° angle and analyzed using a log correlator over 70 accumulations for a 0.5 mL of sample in a glass size cell (0.9 mL capacity). The photomultiplier aperture and the attenuator were automatically adjusted to obtain a photon counting rate of ca. 10 kcps. The calculation of the particle size distribution and distribution averages was

performed using CONTIN particle size distribution analysis routines using Delsa Nano 2.31 software. The peak averages of histograms from intensity, volume and number distributions out of 70 accumulations were reported as the average diameter of the particles. All determinations were repeated 10 times.

The zeta potential values of the nanoparticles were determined by Delsa Nano C particle analyzer (Beckman Coulter. Fullerton, CA) equipped with a 30 mW dual laser diode (658 nm). The zeta potential of the particles in suspension was obtained by measuring the electrophoretic movement of charged particles under an applied electric field. Scattered light was detected at a 30° angle at 25 °C. In each measurement, NaCl solution was added to adjust the sample to 10 mM. The zeta potential was measured at five regions in the flow cell and a weighted mean was calculated. These five measurements were used to correct for electroosmotic flow that was induced in the cell due to the surface charge of the cell wall. All determinations were repeated 5 times.

Synthesis of 6-azidohexanoic acid

In a 100 mL round-bottom flask equipped with a magnetic stirring bar, 6-bromohexanoic acid (3.88 g, 20 mmol) and sodium azide (2.6 g, 40 mmol) were added and dissolved in DMF (20 mL). After being stirred under room temperature for 36 h, the reaction mixture was added 30 mL DCM and then extracted with water (30 mL), brine (30 mL) and saturated $NaHCO_3$ aqueous solution (30 mL) respectively. The combined organic layers were dried over $MgSO_4$ and filtered. The filtrate was concentrated in *vacuo*, and the resulting mixture was purified by column chromatography on silica gel using hexane/EtOAc gradient as eluent and gave 6-azidohexanoic acid as a pale yellow liquid (2.48 g, yield: 79%) ^{1}H NMR ($CDCl_3$, ppm): δ 1.42 (m, 2H, $N_3CH_2CH_2CH_2CH_2CH_2$), 1.64 (m, 4H, $N_3CH_2CH_2CH_2CH_2CH_2$), 2.36 (t, 2H, J = 7 Hz, CH_2CH_2COOH), 3.27 (t, 2H, J = 7 Hz, $N_3CH_2CH_2CH_2CH_2$), 9.70 (br, 1H, COO*H*). ^{13}C NMR ($CDCl_3$, ppm): δ 24.2, 26.1, 28.5, 33.8, 51.2, 178.9. FT-IR (cm^{-1}): 3600-3100, 2931, 2092, 1700, 1242, 941. HRMS: calculated $[M-H]^-$ for $C_6H_{10}N_3O_2$: 156.0773, found: 156.0777.

Synthesis of azido-PTX, 4

In a 25-mL round flask equipped with a magnetic stirring bar, 6-azidohexanoic acid (204 mg; 1.3 mmol) and PTX (920 mg; 1.08 mmol) were added and dissolved in dichloromethane (10 mL). After stirring at r.t. for 1 h, DCC (268 mg; 1.30 mmol) and DMAP (27 mg; 0.23 mmol) were added. The mixture was heated to reflux for 3 days, filtrated, concentrated, and then separated by flash chromatography using silica gel with hexane and ethyl acetate as eluent in gradient (until hexane/ethyl acetate = 50/50, v/v) and gave the targeted compound as a pale yellow solid (840 mg, Yield: 78.3 %). ^{1}H NMR ($CDCl_3$, ppm): δ 1.13 (s, 3H, (C-16)-CH_3), 1.25-1.40 (m, 5H, (C-17)-CH_3 and $N_3CH_2CH_2CH_2CH_2CH_2$), 1.50-1.70 (m, 7H, (C-19)-CH_3 and $N_3CH_2CH_2CH_2CH_2CH_2$), 1.82-1.95 (m, 5H, (C-6)-CH, 1-OH and (C-18)-CH_3), 2.15 (m, 1H, (C-14)-CH), 2.23 (s, 3H, 10-OAc), 2.34-2.62 (m, 8H, 4-OAc, (C-6)-CH, (C-14)-CH, 7-OH and CH_2CH_2COO(PTX)), 3.21 (t, 2H, J = 7 Hz, $N_3CH_2CH_2CH_2$), 3.81 (d, 1H, J = 7 Hz, (C-3)-CH), 4.20 (d, 1H, J = 8 Hz, (C-20)-CH), 4.31 (d, 1H, J = 8 Hz, (C-20)-CH), 4.46 (m, 1H, (C-7)-CH), 4.94 (dd, 1H, J = 9 Hz, J = 2 Hz, (C-5)-CH), 5.51 (d, 1H, J = 3 Hz, (C-2')-CH), 5.68 (d, 1H, J = 7 Hz, (C-2)-CH), 5.95 (dd, 1H, J = 9 Hz, J = 3 Hz, (C-3')-CH), 6.23-6.29 (m, 2H, (C-10)-CH and (C-13)-CH), 6.85 (d, 1H, J = 9 Hz, 3'-NH), 7.34-7.64 (m, 11H, PhH), 7.73 (d, 2H, J = 8 Hz, PhH), 8.14 (d, 2H, J = 8 Hz, PhH). ^{13}C NMR ($CDCl_3$, ppm): δ 9.6, 14.9, 20.9, 22.2, 22.7, 24.2, 26.0, 28.4, 33.5, 35.6, 43.2, 45.6, 51.1, 52.8, 58.5, 71.8, 72.2, 73.9, 75.1, 75.6, 76.5, 79.2, 81.1, 84.5, 126.5, 127.1, 128.5, 128.8, 129.1, 129.2, 130.3, 132.1, 132.8, 133.7, 137.0, 142.8, 167.1, 168.1, 169.8, 171.3, 172.5, 203.9. FT-IR (cm^{-1}): 2939, 2098, 1782, 1659, 1528, 1450, 1365, 1234, 1065, 980, 902, 794. HRMS: calculated $[M+Li]^+$ for $C_{53}H_{60}N_4O_{15}Li$: 999.4215, found: 999.4187.

Synthesis of butynyl phospholane (BYP, 2) Monomer

To a stirred solution of 3-butyn-1-ol (7.40 g, 106 mmol) and triethylamine (11.7 g, 116 mmol) in 200 mL of anhydrous THF at 0 °C were dropwisely added a solution of COP (15.1 g, 106 mmol) in 50 mL of anhydrous THF, and the reaction mixture was allowed to stir for 12 h. After complete conversion of COP, as confirmed by TLC, the reaction mixture was filtered and the filtrate was concentrated. The concentrated filtrate was distilled under reduced pressure to obtain a faint yellow and viscous liquid (121-124 °C, 0.4 mmHg, 12.1 g, Yield: 65 %). ^{1}H NMR ($CDCl_3$, ppm): δ 2.05 (s, 2H, $POCH_2CH_2C{\equiv}CH$), 2.62 (t, J = 6.0 Hz, 2H, $POCH_2CH_2C$), 4.27-4.20 (m, 2H, $POCH_2CH_2C$), 4.49-4.37 (m, 4H, $POCH_2CH_2OP$). ^{13}C

NMR ($CDCl_3$, ppm): δ 20.7, 66.12, 66.23, 70.6, 79.1. ^{31}P NMR ($CDCl_3$, ppm): δ 17.32. HRMS: calculated $[M+H]^+$ for $C_6H_{10}O_4P$: 177.0317, found: 177.0308. IR (cm^{-1}): 3350 - 3175, 3050-2850, 1474, 1280, 1011, 926, 841, 748.

Synthesis of PEO-*b*-PBYP, 3

A solution of BYP (0.528 g, 3.0 mmol) and PEO (0.200 g, 0.1 mmol) in anhydrous dichloromethane (0.7 mL) was transferred into a flame-dried 5-mL shell vial equipped with a rubber septum and a stir bar. At 25 °C, a solution of DBU (0.023 g, 0.15 mmol) in anhydrous dichloromethane (0.1 mL) was injected into the vial *via* syringe, while being maintained under a nitrogen gas atmosphere. After being stirred for 4 min, the reaction vial was unstoppered and a solution of acetic acid (excess) in dichloromethane was added *via* pipet into the reaction mixture to quench the reaction. After the reaction was quenched, the conversion was monitored by ^{31}P NMR and reached 99%. The PEO-*b*-PBYP, **3** was purified by precipitation from dichloromethane into diethyl ether (3x), and was then dried under vacuum, to give an average yield of 80%. ^{1}H NMR ($CDCl_3$, ppm): δ 2.18-2.02 (br, $POCH_2CH_2C{\equiv}C\mathit{H}$), 2.66-2.54 (br, $POCH_2\mathit{CH_2}C{\equiv}CH$), 3.36 (s, $CH_2CH_2OC\mathit{H_3}$), 3.87-3.49 (br, $C\mathit{H_2}OC\mathit{H_2}C\mathit{H_2}OC\mathit{H_2}$), 4.43-3.87 (br, $POC\mathit{H_2}C\mathit{H_2}OP$, $POC\mathit{H_2}CH_2C$). ^{13}C NMR ($CDCl_3$, ppm): δ 20.5, 65.8-66.3, 69.9, 70.8, 79.5. ^{31}P NMR ($CDCl_3$, ppm): δ -1.73. GPC: M_n = 12200 g/mol, PDI = 1.17. DSC: T_g = - 34.2 °C, T_m = - 37.1 °C. TGA in N_2: 50–270 °C, 37% mass loss; 270–340 °C, 33% mass loss, 30 % mass remaining above 600 °C. IR (cm^{-1}): 3700-3100, 3100-2750, 1643, 1428, 1353, 966, 810.

Synthesis of PEO-*b*-(PBPY-*g*-PTX), 5

In a 10-mL Schlenk flask equipped with a magnetic stirring bar, PEO_{2k}-*b*-$PBYP_{30}$, **3** (73 mg; 0.01 mmol), azido PTX, **4** (150 mg; 0.15 mmol), CuBr (21.6 mg; 0.15 mmol) and PMDETA (26.7 mg; 0.15 mmol) were added and dissolved in DMF (1 mL). The reaction mixture was deoxygenated by freeze-pump-thaw (4×) and then placed in a preheated reaction bath at 40 °C. After 24 h, the resulting mixture was precipitated from acetone into ethyl ether (3x) to remove unreacted azide-functionalized PTX. The crude product was

collected and dissolved in 10 mL acetone formed clear solution. The acetone solution was transferred to dialysis tubing (MWCO: 8 kDa) and dialyzed against nanopure water with the existence of Chelex 100 resin (100-200 mesh) for 2 days, to remove copper ion and trigger self-assembly. A bluish-colored micelle solution was obtained and then passed through a 450 nm polypropylene filter to get rid of dust and large aggregates. The micelle solution was lyophilized to give a faint yellow powder with a yield of 90%. ^{1}H NMR ($CDCl_3$, ppm): δ 1.14-2.80 (broad multiple peaks, protons from PTX and CH_2C≡CH), 2.91 (br, CH_2C≡CH), 3.05 (br, $N_3CH_2CH_2CH_2$), 3.37 (s, 3H, PEO-OCH_3), 3.64 (br, CH_2 from PEO), 3.75 (br, CH from PTX(C-3)-CH), 3.82-4.60 (br, POCH_2CH_2 from PPE backbone and POCH_2CH_2CCH from side chain), 4.90 (br, CH from PTX(C-5)-CH), 5.50 (br, CH from PTX(C-2')-CH), 5.62 (br, CH from PTX(C-2)-CH), 5.92 (br, CH from PTX(C-3')-CH), 6.19 (br, CH from PTX(C-13)-CH), 6.32 (br, CH from PTX(C-10)-CH), 7.28-7.68 (br, PhH from PTX), 7.77 (br, PhH from PTX), 8.13 (br, PhH from PTX). ^{31}P NMR ($CDCl_3$, ppm): δ -1.72. ^{13}C NMR (75 MHz, $CDCl_3$, 25 °C, ppm): δ 9.7, 14.8, 20.9, 22.8, 23.9, 25.7, 26.7, 29.8 , 33.3, 35.3-35.9 (multiple overlapping br), 43.2, 45.8, 49.9, 53.4, 58.4, 66.3-67.1 (multiple overlapping br), 70.5, 71.9, 74.0, 75.0, 78.9, 81.0, 84.4, 126.5-129.3 (multiple overlapping br), 130.2, 132.3, 132.8, 133.7, 137.0, 142.3, 166.9, 167.3, 170.0, 171.0, 172.4, 203.7. GPC: M_n = 18900 g/mol, PDI = 1.12. FT-IR (cm^{-1}): 3550-3100, 2940, 1728, 1643, 1450, 1366, 1242, 1072, 1026, 980, 802. TGA in N_2: 200–420 °C, 60% mass loss; 40 % mass remaining above 420 °C.

Solubility test of PEO-*b*-(PBPY-*g*-PTX), 5

Certain amount of powder like product PEO-b-(PBPY-g-PTX) was resuspended in certain amount of nanopure water and sonicated for 3min to obtain micelles. The insoluble drug conjugates were collected by ultracentrifuge at 7000 rpm for 5 min, and weighted after dried by the vacuum to calculate the highest concentration of the formulation.

Synthesis of 5-(azidoacetamido)-fluorescein, 6

In a 10 mL round-bottom flask equipped with a magnetic stirring bar, 5-(iodoacetamido)fluorescein (100 mg, 0.19 mmol) and sodium azide (35.0 mg, 0.53 mmol) were added and suspended in DMF (5 mL). After being stirred under room temperature for 24 h, the DMF was removed by vacuum pump. The mixture was suspended into 30 mL 0.1 M HCl solution. The aqueous phase was extracted with 30 mL ethyl acetate for 4 times. The combined organic layers were dried over $MgSO_4$ and filtered. The filtrate was concentrated in *vacuo* and gave a yellow solid as the crude product (84 mg, yield: 98%). The product was dissolved in 8 mL DMF and stored at -20 °C. ^{1}H NMR (DMSO-d6, ppm): δ 4.28 (s, 2H, C*H*$_2$N$_3$), 6.70 (m, 4H, Ar-*H*), 6.82 (d, m, 2H, Ar-*H*), 7.33 (m, 2H, Ar-H), 8.05 (m, 1H, Ar-H), 8.52 (s, 1H, CON*H*), 10.67 (br, 1H, Ar-O*H*), 11.22 (s, 1H, COO*H*). HRMS: calculated $[M+H]^+$ for $C_{22}H_{15}N_4O_6$: 431.0991, found: 431.0620. UV-vis: (H_2O) λ_{max} = 491.0 nm. Fluorescence: (H_2O, pH=8.4) λ_{em} = 522.0 nm.

Synthesis of Fluorescein labeled PEO-*b*-(PBPY-*g*-PTX), 7

To an aqueous solution of the PEO-*b*-(PBPY-*g*-PTX) (1.1 mL, 4 mL) was added a solution of 5-(azidoacetamido)-fluorescein (10 mg/mL, 9 µL, 1 dye per polymer) in DMF, a solution of copper(II) acetate monohydrate (21 mM, 10 µL) and solution of sodium ascorbat (41 mM, 10 µL). The reaction mixture was allowed to stir for 1 days and was then transferred to presoaked dialysis tubing (MWCO *ca*. 6000-8000 Da) and extensively dialyzed against nanopure water with the existence of Chelex 100 resin (100-200 mesh) for 3 days to remove excess dye and copper catalyst. D_h (DLS, intensity) = 128 ± 93 nm; D_h (DLS, volume) = 40 ± 23 nm; D_h (DLS, number) = 28 ± 8 nm. UV-vis: (H_2O) λ_{max} = 489.0 nm. Fluorescence: (H_2O, pH=8.4) λ_{em} = 523.0 nm.

Synthesis of the Control Polymer, 8

In a 10-mL Schlenk flask equipped with a magnetic stirring bar, PEO_{2k}-*b*-$PBYP_{30}$, **3** (100 mg; 0.013 mmol), 6-azidohexanoic acid (32.4 mg; 0.20 mmol), CuBr (28.4 mg; 0.20 mmol) and PMDETA (35.2 mg; 0.20 mmol) were added and dissolved in DMF (4 mL). The reaction mixture was deoxygenated by freeze-

pump-thaw (4×) and then placed in a preheated reaction bath at 35 °C. After 24 h, the resulting mixture was transferred to dialysis tubing (MWCO: 3500 Da) and dialyzed against nanopure water with the existence of Chelex 100 resin (100-200 mesh) for 3 days, to remove copper ion and unreacted 6-azidohexanoic acid. The solution was lyophilized to give a faint yellow solid (102 mg, yield: 77%). ^{1}H NMR ($CDCl_3$, ppm): δ 1.24-1.89 (br, $CH_2CH_2CH_2CH_2$CH2COOH), 2.24-2.02 (br, $POCH_2CH_2C{\equiv}CH$), 2.40-2.52 (br, CH_2CH_2COOH), 2.69-2.54 (br, $POCH_2CH_2C{\equiv}CH$), 3.09 (br, $N_3CH_2CH_2CH_2$), 3.38 (s, $CH_2CH_2OCH_3$), 3.85-3.52 (br, $CH_2OCH_2CH_2OCH_2$), 4.82-3.85 (br, $POCH_2CH_2OP$, $POCH_2CH_2C$), 7.76 (s, $HC(=C)N$). ^{31}P NMR ($CDCl_3$, ppm): δ -1.71. ^{13}C NMR ($CDCl_3$, ppm): δ 20.6, 24.3, 26.4, 28.9, 34.1, 59.1, 66.5-65.8, 70.6, 79.5, 165.0. FT-IR (cm^{-1}): 3600-3200, 3150 – 2850, 1700, 1454, 1255, 842. DSC: T_g = -37.5 °C, T_m = - 43.7 °C. TGA in N_2: 100–250 °C, 9% mass loss; 250–420 °C, 46% mass loss, 45 % mass remaining above 420 °C.

Cytotoxicity assays:

Human ovarian adenocarcinoma cells (OVCAR-3) ($5x10^3$ cells/well) and RAW 264.7 mouse macrophages ($2x10^4$ cells/well) were plated in 96-well plate in RPMI-1640 medium and Dulbecco's Modified Eagle's Medium (DMEM) (20% and 10% fetal bovine serum, for the OVCAR-3 and RAW 264.7, respectively and 1% penicillin/streptomycin). Cells were incubated at 37°C in a humidified atmosphere containing 5% CO_2 for 24h to adhere. Then, the medium was replaced with a fresh medium 1-h prior to the addition of the various formulations at concentrations ranged from $1x10^{-4}$ to 60 μM of paclitaxel. The paclitaxel conjugate was prepared as described previously, and the Taxol®-mimicking formulation was prepared in similar composition to Taxol® (*i.e.* Cremophor-EL and ethanol, 1:1 *v*/*v*). For each well, 20 μL of every formulation was added to 100 μL of the medium. The cells were incubated with the formulations for 72h and washed once with phosphate-buffered saline (PBS) and 100 μL of the complete medium was added to the cells. 20 μL of the MTS combined reagent was added to each well (Cell Titer 96® Aqueous Non-Radioactive Cell Proliferation Assay, Promega Co., Madison, WI). The cells were incubated with the reagent for 3 h at 37°C in a humidified atmosphere containing 5% CO_2 protected from light. Absorbance was measured at 490 nm using SpectraMax M5 (Molecular Devices Co., Sunnyvale, CA). The cell

viability was calculated based on the relative absorbance to the control untreated cells. The IC_{50} values were calculated using GraphPad Prism four-parameter fit, considering the 0% and 100% viabilities correspond to the medium control (no cells) and cells-treated with PBS, respectively.

Laser Scanning Confocal Microscopy (LSCM):

RAW 264.7 and OVCAR-3 ($1x10^5$ cells/well) cells were plated in six-well glass-bottom plates (MatTek Co., Ashland, MA) in DMEM and RPMI-1640 medium, respectively. Cells were incubated at 37°C in a humidified atmosphere containing 5% CO_2 for 24h to adhere. Then, the medium was replaced with a fresh medium 1-h prior to the addition of the fluorescein-labeled nanoparticles (final paclitaxel concentrations of 0.5 μM for OVCAR-3 and 3 or 15 μM for RAW 264.7). The cells were incubated with the formulation for 5h and washed extensively with PBS. Then, DRAQ-5 (Biostatus Ltd., Shepshed, Leicestershire, UK) was utilized to stain the nucleus (30-min incubation, followed by extensive washing with PBS). The cells were then fixed with 1% formaldehyde for 20 minutes, washed once with PBS. The cells were then stored in 1 mL PBS in the refrigerator. The cellular uptake of the nanoparticles was investigated by LSCM (LSM 510, Zeiss, Jena, Germany). The images were collected under the same conditions (*e.g.* laser power and detector gain) for consistency, and $\lambda_{excitation}$ and $\lambda_{emission}$ of 488 and 633 nm were utilized for the fluorescein and DRAQ-5, respectively.

Acknowledgements

We gratefully acknowledge financial support from Covidien, Inc., the National Heart Lung and Blood Institute of the National Institutes of Health as a Program of Excellence in Nanotechnology (HHSN268201000046C) and the National Science Foundation under grant numbers DMR-0906815 and DMR-1105304. The Welch Foundation is gratefully acknowledged for support through the W. T. Doherty-Welch Chair in Chemistry, Grant No. A-0001. The transmission electron microscopy facilities at

Washington University in St. Louis, Department of Otolaryngology, Research Center for Auditory and Visual Studies funded by NIH P30 DC004665 are gratefully acknowledged.

Reference

(1) Rowinsky, E. K.; Donehower, R. C. *New Engl. J. Med.* **1995**, *332*, 1004.

(2) Spencer, C. M.; Faulds, D. *Drugs* **1994**, *48*, 794.

(3) Gelderblom, H.; Verweij, J.; Nooter, K.; Sparreboom, A. *Eur. J. Cancer* **2001**, *37*, 1590.

(4) Gradishar, W. J. *Expert Opin. Pharmaco.* **2006**, *7*, 1041.

(5) Singer, J. W. *J. Control Release* **2005**, *109*, 120.

(6) Davis, M. E.; Chen, Z.; Shin, D. M. *Nat. Rev. Drug Discov.* **2008**, *7*, 771.

(7) Brannon-Peppas, L.; Blanchette, J. O. *Adv. Drug Deliver. Rev.* **2004**, *56*, 1649.

(8) Li, C.; Yu, D. F.; Newman, R. A.; Cabral, F.; Stephens, L. C.; Hunter, N.; Milas, L.; Wallace, S. *Cancer Res.* **1998**, *58*, 2404.

(9) Van, S.; Das, S. K.; Wang, X. H.; Feng, Z. L.; Jin, Y.; Hou, Z.; Chen, F.; Pham, A.; Jiang, N.; Howell, S. B.; Yu, L. *Int. J. Nanomed.* **2010**, *5*, 825.

(10) Bonomi, P. *Expert. Rev. Anticanc.* **2007**, *7*, 415.

(11) Li, C.; Wallace, S. *Adv. Drug Deliver. Rev.* **2008**, *60*, 886.

(12) Zhang, X. Q.; Xu, X. Y.; Lam, R.; Giljohann, D.; Ho, D.; Mirkin, C. A. *ACS Nano* **2011**, *5*, 6962.

(13) Tong, R.; Cheng, J. J. *Angew. Chem. Int. Edit.* **2008**, *47*, 4830.

(14) Zou, J.; Yu, Y.; Yu, L.; Li, Y. K.; Chen, C. K.; Cheng, C. *J. Polym. Sci., Part A: Polym. Chem.* **2012**, *50*, 142.

(15) Iwasaki, Y.; Yamaguchi, E. *Macromolecules* **2010**, *43*, 2664.

(16) Du, J. Z.; Du, X. J.; Mao, C. Q.; Wang, J. *J. Am. Chem. Soc.* **2011**, *133*, 17560.

(17) Elsabahy, M.; Wooley, K. L. *Chem. Soc. Rev.* **2012**, *41*, 2545.

(18) Zhang, S.; Li, A.; Zou, J.; Lin, L. Y.; Wooley, K. L. *ACS Macro Lett.* **2012**, *1*, 328.

(19) Zhang, S.; Zou, J.; Zhang, F.; Elsabahy M.; Felder, S.; Zhu, J.; Pochan, D. J.; Wooley, K. L. *J. Am. Chem. Soc.*, **2012** *134*, 18467.

(20) Ernsting, M. J.; Tang, W. L.; MacCallum, N.; Li, S. D. *Bioconjugate Chem.* **2011**, *22*, 2474.

(21) Nakamura, J.; Nakajima, N.; Matsumura, K.; Hyon, S. H. *Anticancer Res.* **2010**, *30*, 903.

(22) Johnson, J. A.; Lu, Y. Y.; Burts, A. O.; Lim, Y. H.; Finn, M. G.; Koberstein, J. T.; Turro, N. J.; Tirrell, D. A.; Grubbs, R. H. *J. Am. Chem. Soc.* **2011**, *133*, 559.

(23) Yu, Y.; Zou, J.; Yu, L.; Jo, W.; Li, Y. K.; Law, W. C.; Cheng, C. *Macromolecules* **2011**, *44*, 4793.

(24) Iha, R. K.; Wooley, K. L.; Nystrom, A. M.; Burke, D. J.; Kade, M. J.; Hawker, C. J. *Chem. Rev.* **2009**, *109*, 5620.

(25) Yang, D.; Van, S.; Liu, J.; Wang, J.; Jiang, X. G.; Wang, Y. T.; Yu, L. *Int. J. Nanomed.* **2011**, *6*, 2557.

(26) Ang, E. S. M.; Pavlos, N. J.; Chim, S. M.; Feng, H. T.; Scaife, R. M.; Steer, J. H.; Zheng, M. H.; Xu, J. *J. of Cell. Biochem.* **2012**, *113*, 946.

Chapter 7

A simple and efficient synthesis of an acid-labile polyphosphoramidate by organobase-catalyzed ring-opening polymerization and transformation to polyphosphoester ionomers by acid treatment

[Portions of this work have been considered for publication as Shiyi Zhang, Hai Wang, Yuefei Shen, Fuwu Zhang, Kellie Seetho, Jiong Zou, John-Stephen A. Taylor, Andrew P. Dove, and Karen L. Wooley]

Abstract

The direct synthesis of an acid-labile polyphosphoramidate by organobase-catalyzed ring-opening polymerization and an overall two-step preparation of polyphosphodiester ionomers (PPEI) by acid-assisted cleavage of the phosphoramidate bonds along the backbone of the polyphosphoramidate were developed in this study. The ultrafast organobase-catalyzed ring-opening polymerization of a cyclic phospholane methoxyethyl amidate monomer initiated by benzyl alcohol allowed for the preparation of well-defined polyphosphoramidates (PPA) with predictable molecular weights, narrow molecular weight distributions (PDI<1.10), and well-defined chain ends. Cleavage of the acid-labile phosphoramidate bonds on the polyphosphoramidate repeat units was evaluated under acidic conditions over a pH range of 1-5, and the complete hydrolysis produced polyphosphodiesters. The thermal properties of the resulting polyphosphoester ionomer acid and polyphosphoester ionomer sodium salt exhibited significant thermal stability. The parent PPA and both forms of the PPEIs showed low cytotoxicities toward HeLa cells and RAW 264.7 mouse macrophage cells. The synthetic methodology developed here has enriched the family of water-soluble polymers prepared by rapid and convenient organobase-catalyzed ring-opening polymerizations and straightforward chemical medication reactions, which are designed to be hydrolytically degradable and have promise for numerous biomedical and other applications.

Introduction

There has been considerable interest recently in the synthesis of synthetic functional bio-polymers that have compositions and architectures similar to those of polymers found in Nature and, thereby, possess ability for natural clearance mechanisms, and are explored for their biological and environmental applications, for instance tissue engineering, regenerative medicine, gene therapy, controlled drug delivery, oil recovery (viscosity control), paper manufacturing, agriculture (stimulation of plant growth) and packaging materials.(1, 2) Synthetic functional bio-polymers with various specific chemical structures and physical/biological properties are needed for biological and environmental applications because of the diversity and complexity of *in vivo* and natural environments. Inspired by our initial interest in polyphosphoesters,(3, 4) which were based upon phosphotriester repeat units that allowed for the introduction of various side chain functionalities, we expanded the synthetic methodology to the direct synthesis of acid-labile polyphosphoramidates (PPA) and their direct conversion to phosphodiester ionomeric repeat units. PPA and PPEI share the same polyphosphodiester backbone, PPA has side groups connecting to the backbone through an acid-labile phosphoramidate bond, while PPEI has a phosphate group on each repeat unit which is also represented on the natural nucleic and teichoic acids. This improved two-step preparation of polyphosphoester ionomers (PPEI) by organobase-catalyzed ring-opening polymerization (ROP) and acid-catalyzed side chain hydrolysis (**Scheme 7-1**) is a powerful alternative to the traditional metal catalyst-promoted ROP.(5-10)

Scheme 7-1. (a) Synthesis of cyclic phospholane amidate monomer from 2-chloro-2-oxo-1,3,2-dioxaphospholane (COP) and primary amine, methoxyethylamine (MOEA). (b) Polymerization of cyclic phospholane amidate monomer by using TBD as the catalyst and benzyl alcohol as the initiator and side chain hydrolytic cleavage of the PPA, PMOEPA, with the formation of PPEI (acid form and sodium salt form).

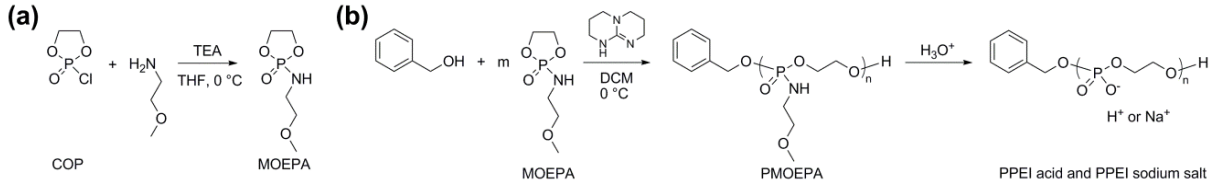

In this manuscript, we describe a direct synthesis of acid-labile PPA *via* organobase-catalyzed ROP of cyclic phospholane amidate monomer (**Scheme 7-1**). As reported previously, PPAs are conventionally prepared by the polymerization of 4-methyl-2-oxo-2-hydro-1,3,2-dioxaphospholane in the presence of metal catalyst triisobutylaluminum, followed by the modification of the resulting poly(1,2-propylene H-phosphonate) using amines *via* an Atherton–Todd reaction (**Scheme 7-2**).(11) After the development of this method towards PPAs, a family of PPAs with different pendant amino groups was synthesized and applied for the delivery of nucleic acids.(12, 13) Due to the limited reactivity of the Atherton–Todd reaction, at least 25% of the P–H groups were converted into phosphates rather than phosphoramidate bonds,(14) which resulted in a random copolymer of PPA and PPEI being isolated. The lack of a simple and reliable synthetic route to functional PPA constitutes a significant barrier to the widespread practical application of this degradable polymer platform. Recently, organobase-catalyzed ROP of cyclic phospholanes has greatly facilitated the preparation of polyphosphoesters, which share the similar polymer backbone with PPA but have side groups through the phosphoester linkage instead of the phosphoramidate linkage, with predictable molecular weight, narrow molecular weight distribution, well-defined chain ends and different polymer architectures.(3, 4, 15-18) Herein, we took advantage of this state-of-the-art polymerization technique to synthesize PPA from a cyclic monomer in the presence of organocatalysts. The ultrafast organobase-catalyzed ROP offered control over the molecular weights,

molecular weight distributions, compositions and structures, and also eliminates the usage of metal compounds, to fulfill the requirements of biomedical and environmental applications.

Scheme 7-2. Reported synthetic approach for PPAs.(11)

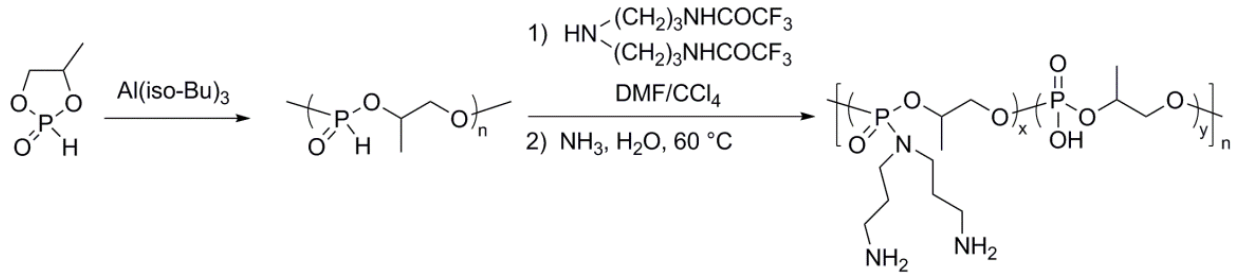

After the complete side chain cleavage of the acid-labile phosphoramidate bond, the PPEI, a new type of degradable polymer, was prepared (**Scheme 7-1**). The PPEI has phosphodiester linkages along the backbone and a phosphate group on each repeat unit, and shares the same phosphate group with the nucleic and teichoic acids. Phosphate group-containing polymers, mostly based on non-degradable polymers, have served as dental materials and bone tissue engineering scaffolds, because of the formation of complexes of phosphonic acid or acidic phosphate groups with calcium in hydroxyapatite and improved adhesion on the tooth surface.(19) Recently, increasing efforts have been devoted to degradable polymers with phosphate groups. Poly(propylene phosphate) was first synthesized by Penczek and colleagues in 1982 by the metal-catalyzed ROP of a cyclic phosphite monomer followed by oxidation (**Scheme 7-3a**).(20) Later, the polymer was demonstrated as a thermo-sensitive injectable biomaterial whose gelation was induced by calcium ions.(21) Another synthetic approach for PPEI-type materials was based on the demethylation of a methoxy side chain containing polyphosphoester, with an uncertain selectivity and a high risk of backbone degradation, by treating the polymer with sodium hydroxide (**Scheme 7-3b**). The free phosphate group on the PPEI provided the opportunity for the functionalization of the polymer backbone and ionical cross-linking by calcium ions.(22) Poly(hydroxyoxyethylene phosphate) could be converted *via* Atherton-Todd reaction (**Scheme 7-3c**) from

the poly(oxyethylene H-phosphonate), which was synthesized by condensation polymerization and had very broad molecular weight distribution and uncontrollable molecular weight.(23) More recently, a PPEI-type copolymer was synthesized from the removal of benzyl protecting groups on a polyphosphoester precursor,(24) which was synthesized by ROP from an unstable that was difficult to purify, 2-benzyl-2-oxo-1,3,2-dioxaphospholane (**Scheme 7-3d**).(25) Even with some synthetic drawbacks, those advances on synthetic PPEI-type materials confirmed its capacity for aqueous solubility and for functionalization of the side chain phosphate group,(22) and including by the simple complexation with calcium ions, for instance for use in tooth repair or as bone-specific drug delivery vehicles for the treatment of osteoporosis and osseous metastases.(26, 27) Here, the side chain cleavage of PPA provided a reliable strategy to synthesize PPEI homopolymer with controlled molecular weight, narrow molecular weight distribution and well-defined chain ends, which is expected to further advance the capabilities and development of these kinds of bio-mimicking, ionic, degradable polymer materials. The synthetic advances of PPA and PPEI, as well as their interesting chemical, physical and biological properties are discussed in this manuscript.

Scheme 7-3. Reported synthetic approaches for PPEI-type materials.(20, 22-24)

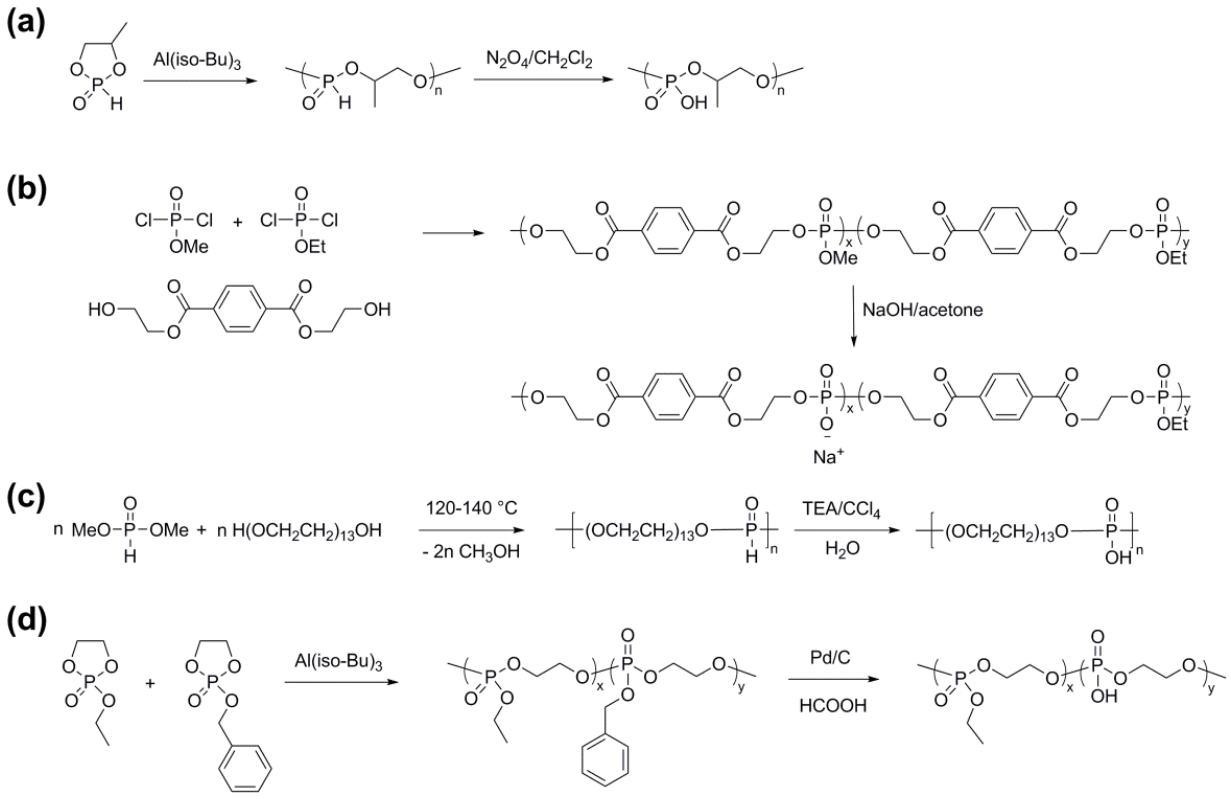

Experimental

Materials. *N,N*-Dimethylformamide (DMF), triethylamine (NEt_3), acetone, diethyl ether, ethyl acetate, hexanes, glycine, hydrochloric acid, sodium acetate, acetic acid, trifluoroacetic acid (TFA), deuterium oxide (D_2O), 1,8-diazabicyclo[5.4.0]undec-7-ene (DBU), 1,5,7-triazabicyclo[4.4.0]dec-5-ene (TBD), 2-methoxyethylamine and methanol were used as received from Sigma-Aldrich Company (St. Louis, MO). Amberlite™ IR120, H form, ion-exchange resin, Amberlite™ IR120, Na form, ion-exchange resin and 2-chloro-2-oxo-1,3,2-dioxaphospholane (95%) were used as received from Thermo Fisher Scientific Inc. (Pittsburgh, PA). Tetrahydrofuran (THF) and dichloromethane (DCM) were dried through columns (J. C. Meyer Solvent Systems, Inc. Laguna Beach, CA). Benzyl alcohol was purchased from Sigma-Aldrich and distilled from calcium hydride prior to use.

Instrumentation. ^{1}H NMR, ^{31}P NMR and ^{13}C NMR spectra were recorded on an Inova 300 or Mercury 300 spectrometer interfaced to a UNIX computer using VnmrJ software. Chemical shifts were referenced to the solvent resonance signals. The DMF gel permeation chromatography (GPC) was conducted on a Waters Chromatography, Inc. (Milford, MA) system equipped with an isocratic pump model 1515, a differential refractometer model 2414, and a four-column set of 5 μm Guard (50 × 7.5 mm), Styragel HR 4 5 μm DMF (300 × 7.5 mm), Styragel HR 4E 5 μm DMF (300 × 7.5 mm), and Styragel HR 2 5 μm DMF (300 × 7.5 mm). The system was equilibrated at 70 °C in pre-filtered DMF containing 0.05 M LiBr, which served as polymer solvent and eluent (flow rate set to 1.00 mL/min). Polymer solutions were prepared at a concentration of *ca*. 3 mg/mL and an injection volume of 200 μL was used. Data collection and analysis were performed with Empower 2 v. 6.10.01.00 software (Waters, Inc.). The system was calibrated with polystyrene standards (Polymer Laboratories, Amherst, MA) ranging from 615 to 442,800 Da. IR spectra were recorded on an IR Prestige 21 system (Shimadzu Corp.) and analyzed using IRsolution v. 1.40 software. Glass transition temperatures (T_g) were measured by differential scanning calorimetry on a Mettler-Toledo DSC822® (Mettler-Toledo, Inc., Columbus, OH), with a heating rate of 10 °C /min. Measurements were analyzed using Mettler-Toledo STAR^{e} v. 7.01 software. The T_g was taken as the midpoint of the transition recorded during the second heating scan. Thermogravimetric analysis was performed under N_2 atmosphere using a Mettler-Toledo model TGA/SDTA851^{e}, with a heating rate of 5 °C /min. Measurements were analyzed by using Mettler-Toledo STAR^{e} v. 7.01 software.

Synthesis of 2-((2-methoxyethyl)amino)-1,3,2-dioxaphospholane 2-oxide, *N*-methoxyethyl phospholane amidate (MOEPA). To a stirred solution of 2-methoxyethylamine (5.8 g, 77 mmol) and triethylamine (7.8 g, 77 mmol) in 200 mL of anhydrous THF in a cold room (4 - 6 °C) was added dropwise a solution of COP (10.0 g, 70 mmol) in 50 mL of anhydrous THF, and the reaction mixture was allowed to stir for 12 h. After complete conversion of COP, as confirmed by TLC, the reaction mixture was filtered and the filtrate was concentrated. The concentrated filtrate was purified by column chromatography on silica gel using ethyl acetate as eluent and gave a pale yellow liquid. The pale yellow liquid was further purified by recrystallization from ether/DCM 1:1 mixture and gave *N*-methoxyethyl phospholane amidate

(MOEPA) as a white crystalline solid (8.0 g, yield: 63%). ^{1}H NMR ($CDCl_3$, ppm): δ 4.45-4.24 (m, 4H, POCH_2CH_2OP), 3.69–3.55 (b, 1H, PNHCH_2), 3.42 (t, $^{3}J_{H\text{-}H}$ = 5.1 Hz, 2H, NHCH_2CH_2OCH_3), 3.33 (s, 3H, NHCH_2CH_2OCH_3), 3.07 (dt, $^{3}J_{H\text{-}H}$ = 5.1 Hz, $^{3}J_{H\text{-}H}$ = 6.2 Hz, 2H, NHCH_2CH_2OCH_3). ^{13}C NMR ($CDCl_3$, ppm): δ 72.44, 65.72, 58.91, 41.28. ^{31}P NMR ($CDCl_3$, ppm): δ 25.82. +ESI MS: calculated $[M+H]^+$ for $C_5H_{13}NO_4P$: 182.0582, found: 182.0534. IR: 3300-3100, 3000-2800, 1446, 1241, 1108, 1087, 1033 cm^{-1}.

General Procedure for Polymerization of MOEPA to afford PMOEPA. MOEPA was weighed inside a glove box and distributed into flame-dried 5 mL shell vials equipped with a rubber septum and a stir bar (about 0.200 g, 1.1 mmol for each) and stored in a vacuum desiccator under vacuum before being used for polymerizations. A solution of a given amount of benzyl alcohol (0.044 mmol to 0.011 mmol) in anhydrous dichloromethane (0.20 mL) was transferred via syringe into the shell vial. At 0 °C, a solution of a given amount of TBD (0.088 mmol to 0.011 mmol) in anhydrous dichloromethane (0.1 mL) was injected into the vial *via* syringe, while being maintained under a nitrogen gas atmosphere. After being stirred for a certain period of time (10 sec to 5 min), the reaction vial was unstoppered and 2 mL of dichloromethane was added *via* pipet into the reaction mixture to dilute the solution and quench the reaction. The poly(MOEPA) (PMOEPA, **2**) was purified by precipitation from dichloromethane into diethyl ether (3×), and was then dried under vacuum, to give an average yield of 80%. ^{1}H NMR ($CDCl_3$, ppm): δ 7.40-7.28 (m, 5H, Ar-H), 5.00 (d, J = 7.5 Hz, 2H, OCH_2Ar), 4.30-4.04 (b, 4nH, POCH_2CH_2OP), 4.02-3.83 (b, nH, PNHCH_2), 3.40 (t, $^{3}J_{H\text{-}H}$ = 5.1 Hz, 2nH, NHCH_2CH_2OCH_3), 3.31 (s, 3nH, NHCH_2CH_2OCH_3), 3.07 (dt, $^{3}J_{H\text{-}H}$ = 5.1 Hz, $^{3}J_{H\text{-}H}$ = 6.2 Hz, 2nH, NHCH_2CH_2OCH_3). ^{13}C NMR ($CDCl_3$, ppm): δ 128.63, 127.87, 72.77, 65.32, 58.70, 41.03. ^{31}P NMR ($CDCl_3$, ppm): δ 10.09. DSC: (T_g) = -23 °C. TGA in N_2: 180–270 °C, 12% mass loss; 270–310 °C, 15% mass loss, 310–600 °C, 33% mass loss, 40 % mass remaining above 600 °C. IR: 3300-3100, 3000-2800, 1450, 1230, 1113, 1083, 1020, 953 cm^{-1}.

Kinetic study of the side chain cleavage of MOEPA. In a typical side chain cleavage experiment, PMOEPA (0.10 g) was dissolved into 1 mL of buffer solutions (100 mM hydrogen chloride solution as a

pH 1.0 buffer, 100 mM glycine-HCl solution as a pH 3.0 buffer and 100 mM sodium acetate-acetic acid solution as a pH 5.0 buffer). 10 vol % of D_2O (0.1 mL) was added to the buffer solutions. The mixture solution was stirred at room temperature allowing for the degradation. The ^{31}P chemical shifts were measured by Inova 300 spectrometer during the degradation.

Preparation of polyphosphoester ionomer (PPEI). PMOEPA (0.50 g) was dissolved into 10 mL of 100 mM HCl solution and stirred at room temperature for 11 h. The mixture solution was transferred to dialysis tubing (MWCO: 3.5 kDa) and dialyzed against nanopure water with the existence of Amberlite™ IR120, H form, ion-exchange resin or Amberlite™ IR120, Na form, ion-exchange resin in the cold room (4 - 6 °C) for 2 days, to remove small compounds. The clear solution was lyophilized to give white solids (for the H form PPI, 0.31 g, yield: 90 %; for the Na form PPI, 0.34 g, yield: 85 %). ^1H NMR (D_2O, ppm): δ 7.50-7.38 (m, 5H, Ar-*H*), 4.94 (d, *J* = 7.2 Hz, 2H, OC*H*$_2$Ar), 4.01-3.92 (b, 4nH, POC*H*$_2$C*H*$_2$OP). ^{13}C NMR (D_2O, ppm): δ 128.54, 127.82, 67.58, 65.59, 60.67. ^{31}P NMR (D_2O, ppm): δ 1.01. Polyphosphoester ionomer sodium salt: DSC: (T_g) = 43 °C. TGA in N_2: 260–320 °C, 30% mass loss, 70 % mass remaining above 600 °C. IR: 3650-3000, 3000-2800, 1650, 1455, 1224, 1077, 1033, 941 cm^{-1}. Polyphosphoester ionomer acid: DSC: (T_g) = -14 °C. TGA in N_2: 220–290 °C, 19% mass loss, 290–540 °C, 14% mass loss, 540–600 °C, 12% mass loss, 55 % mass remaining above 600 °C. IR: 3600-2400, 1650, 1450, 1214, 1077, 960 cm^{-1}.

Cytotoxicity assays. HeLa cells and RAW 264.7 cells were seeded in a 96-well plate at a density of 1 × 10^4 cells/well and cultured in 100 µL Dulbecco's Modified Eagle Medium (DMEM) containing 10% Fetal bovine serum (FBS) for 24 h. Then the medium was replaced with fresh medium, to which polyphosphoramidates and polyphosphoester ionomers (the PMOEA, PPEI acid and PPEI sodium salt) were added to make a final volume of 100 µL (final concentrations of polymers ranged from 5-to-2500 µg/mL). After 24 h, cytotoxicity was quantified by the CellTiter-Glo® Luminescent Cell Viability Assay (Promega) using 100 µL of CellTiter-Glo reagent. The contents were mixed and the plate was shaken for

5 min at 600 rpm, and then allowed to incubate at room temperature for 10 min to stabilize the luminescence signal. Luminescence intensities were recorded on a Luminoskan Ascent® luminometer (Thermo Scientific) with an integration time of 1 second/well. The relative cell viability was calculated by the following equation: Cell viability (%) = $\text{luminescence}_{(\text{sample})}$ / $\text{luminescence}_{(\text{negative control})}$) × 100.

Results and Discussion

The synthetic efforts began from the one-step preparation and easy purification of cyclic phospholane amidate monomer, 2-((2-methoxyethyl)amino)-1,3,2-dioxaphospholane 2-oxide, N-methoxyethyl phospholane amidate (MOEPA). The polymerization behavior and kinetics of MOEPA by 1,5,7-triazabicyclo[4.4.0]dec-5-ene (TBD) were then carefully evaluated. The pH-dependent phosphoramidate bond cleavage and thermal properties of resulting PPEI acid and PPEI sodium salt were studied. All degradable polymers showed high biocompatibility toward HeLa cells and RAW 264.7 mouse macrophages.

Monomer design and synthesis. MOEPA was synthesized by coupling 2-chloro-2-oxo-1,3,2-dioxaphospholane (COP) to 2-methoxyethylamine in the presence of triethylamine (NEt_3), according to the approach that has been widely used for the synthesis of cyclic phospholane ester monomers. As shown in **Scheme 7-1a**, the coupling reaction of COP to 2-methoxyethylamine was conducted at 4 °C in anhydrous THF with NEt_3. MOEPA was purified by column chromatography on silica gel using ethyl acetate as eluent and followed by recrystallization from diethyl ether/DCM 1:1 mixture to give pure MOEPA as a white crystalline solid. Unlike most cyclic phospholane ester monomers, MOEPA was highly hygroscopic. To prevent absorption of moisture from the air, MOEPA was weighed and distributed into aliquots inside a glove box and stored in a vacuum desiccator under vacuum before being used for polymerizations or characterization. The ^{1}H NMR spectrum of the monomer showed five groups of resonances at 4.45-4.24, 3.69–3.55, 3.42, 3.33 and 3.07 ppm, which were assigned to protons as shown in **Figure 7-1 A-C**. Resonances at 72.44, 65.72, 58.91 and 41.28 ppm in its ^{13}C NMR spectrum also

confirmed the chemical structure. In addition, the ^{31}P NMR spectrum of the monomer exhibited a resonance at 25.82 ppm, consistent with the ^{31}P chemical shift values of other reported cyclic phospholane amidate structures.(28)

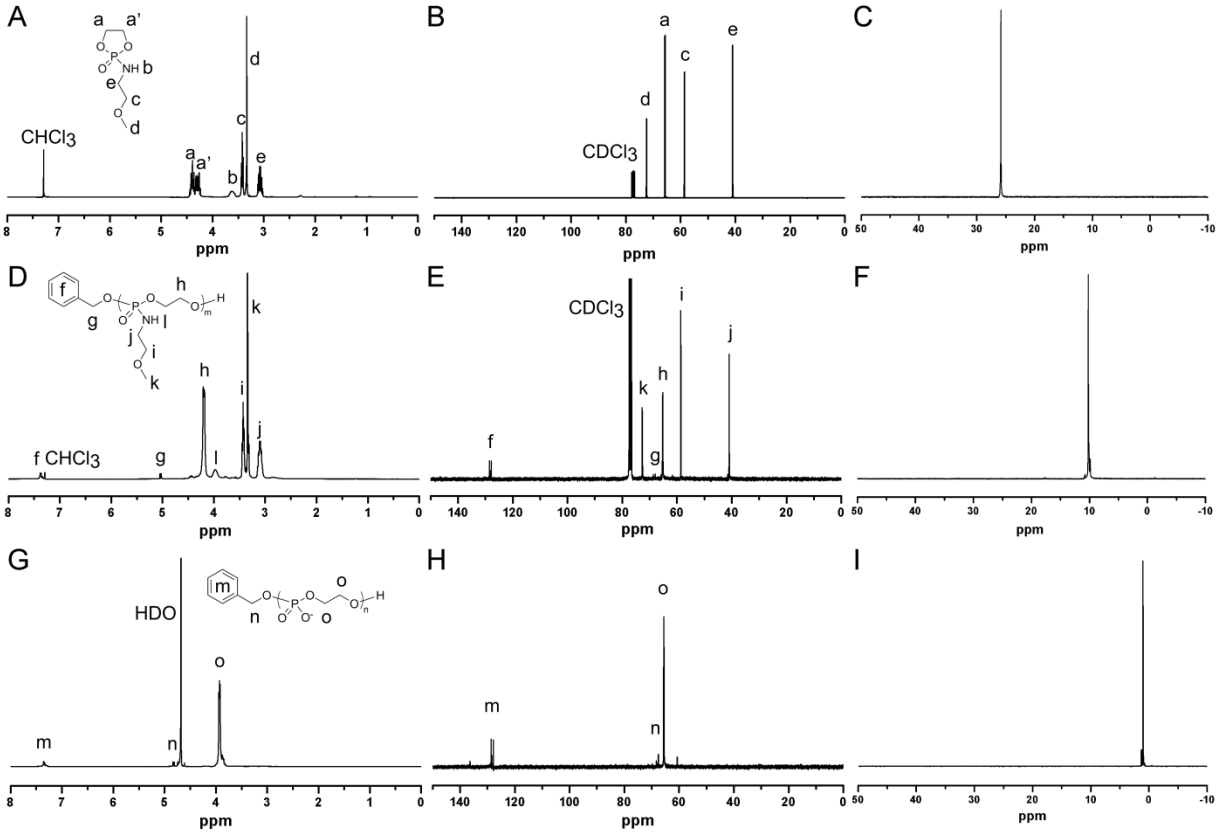

Figure 7-1. NMR spectra of MOEPA in $CDCl_3$ (ppm): (A) ^{1}H NMR (300 MHz), (B) ^{13}C NMR (75 MHz), (C) ^{31}P NMR (121 MHz). NMR spectra of PMOEPA in $CDCl_3$ (ppm): (D) ^{1}H NMR (300 MHz), (E) ^{13}C NMR (75 MHz), (F) ^{31}P NMR (121 MHz). NMR spectra of PPEI in D_2O (ppm): (G) ^{1}H NMR (300 MHz), (H) ^{13}C NMR (75 MHz), (I) ^{31}P NMR (121 MHz).

Polymerization of MOEPA by organobase catalysis. Two organocatalysts, 1,8-diazabicyclo[5.4.0]undec-7-ene (DBU) and 1,5,7-triazabicyclo[4.4.0]dec-5-ene (TBD), were used to test the ROP of MOEPA (**Table 7-1**). Initially, DBU was employed to catalyze the polymerization of

MOEPA initiated by benzyl alcohol at room temperature (entries 1-3 in **Table 7-1**). Although DBU has been reported to be efficient in promoting the polymerization of several cyclic phosphoester monomers at low catalyst-to-monomer molar ratios (in the range of 0.5 % to 5 % depending on the conditions),(3, 4, 15-17) it was unable catalyze the ROP of MOEPA, even at a relatively high catalyst-to-monomer molar ratio of 10 mol%. Switching to the more basic catalyst TBD (**Scheme 7-1b**), which has dual activation effects: simultaneously serving as a hydrogen-bond donor to the monomer *via* the N−H site and also as a hydrogen-bond acceptor to the hydroxyl proton of the propagating alcohol,(5, 15, 17) MOEPA polymerization proceeded rapidly at 0 °C (entries 4-12 in **Table 7-1**). For these polymerizations, the monomer, MOEPA, and initiator, benzyl alcohol, were dissolved in a certain amount of anhydrous dichloromethane (DCM) and allowed to stir at 0 °C. The conversion of MOEPA quickly reached over 55% within only 1 min with good control of the polymerization being retained (entry 5 in **Table 7-1**). After 1-5 min, the reaction was quenched by diluting the reaction mixture with ten times volume of DCM, instead of the typical method of quenching the polymerization by the addition of acid. Our control experiment showed by ^{31}P NMR spectroscopy that the monomer conversion remained constant for several hours after the reaction mixture was diluted (data not shown). Although DBU was not effective, TBD was an efficient catalyst to promote the ROP of the cyclic phospholane amidate monomer, MOEPA.

The catalytic behavior of TBD in the polymerization of MOEPA was studied further by tuning the polymerization conditions, including the catalyst-to-monomer molar ratio, the monomer concentration, the initiator-to-monomer molar ratio and the reaction time (**Table 7-1**). Polymerization with different catalyst-to-monomer molar ratios 1% (entries 9-10), 2% (entries 5-6) and 3% (entry 4) suggested that the amount of TBD didn't alter the molecular weight of the PMOEPA polymer products when the conversions were similar, but only affected the rates of the polymerizations. The monomer concentration played a major role in the polymerization rate; the polymerization slowed significantly after diluting to twice the volume (entries 5-6 *vs* entries 7-8). The polydispersity indices (PDI) were all less than 1.10 and the gel permeation chromatography (GPC) traces were symmetrically mono-modal when the monomer conversion was limited to < 70% by quenching the reaction mixture at early stages (GPC traces see

Figure 7-2). After the conversion gradually reached over 70%, the GPC traces became increasingly asymmetrical, due to a growing high molecular weight shoulder, and eventually became bimodal (**Figure 7-3**). The increased breadths of the molecular weight distributions clearly indicated that adverse transesterification reactions of the polymer backbone were occurring and becoming dominant after the monomer conversion reached 70%. Therefore, quenching the polymerization reaction at conversions lower than 70% was found to be critical to obtain well-defined PMOEPA with low PDIs.

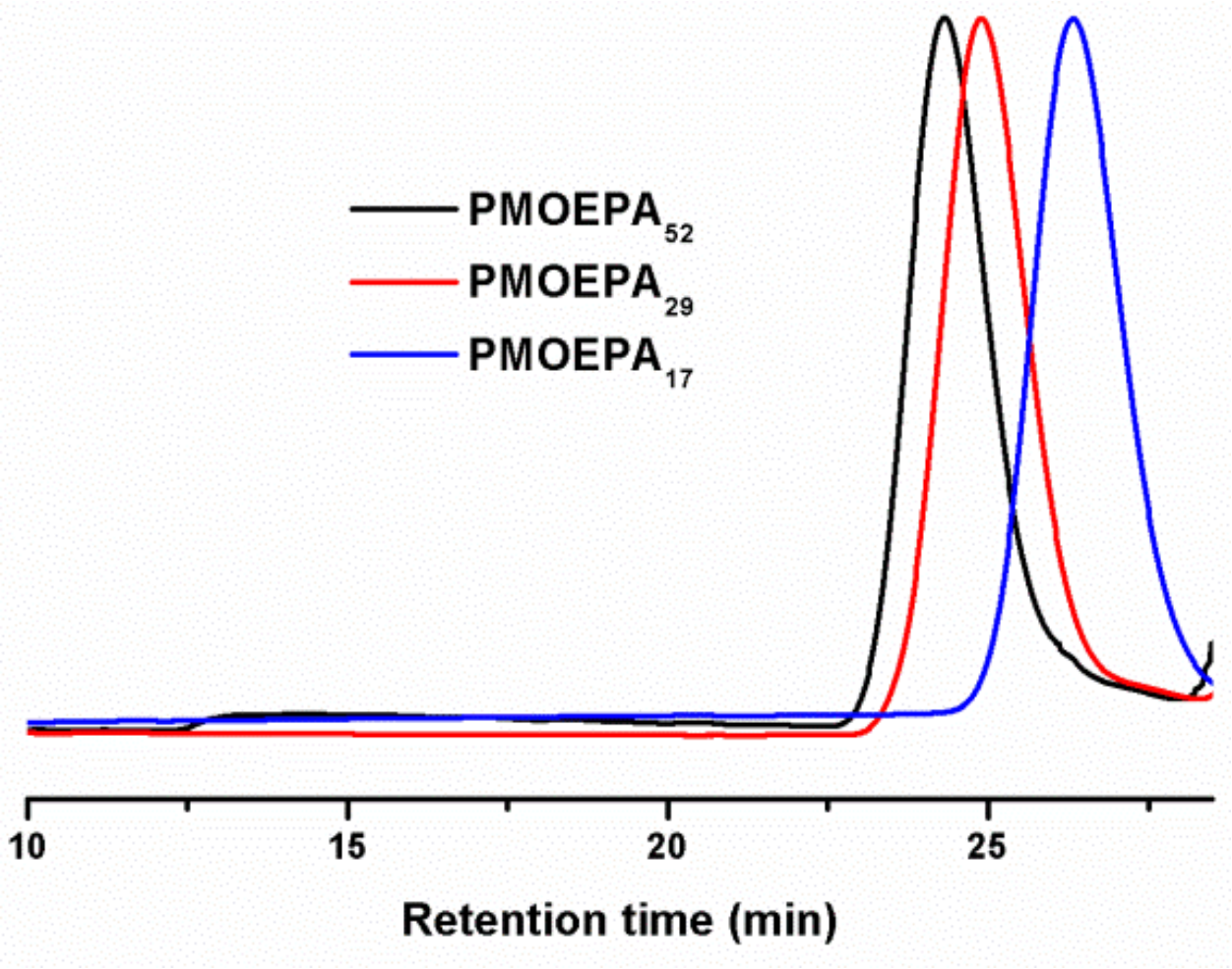

Figure 7-2. GPC traces of $PMOEPA_{52}$, $PMOEPA_{29}$ and $PMOEPA_{17}$.

Table 7-1. Polymerization results of MOEPA with DBU and TBD under different conditions.

entry	Catalyst	M : I : Catalyst (molar ratios)	Conc. (g/mL)	Time (min)	Conversion (^{31}P NMR)	M_n, Da (GPC)[a]	M_w/M_n (GPC)[b]	M_n, Da (Theor)[c]	M_n, Da (^{1}H NMR)[d]
1	DBU	50 : 1 : 1.5	0.5	15	1 %	N.A.	N.A.	N.A.	N.A.
2	DBU	50 : 1 : 2.5	0.5	30	2 %	N.A.	N.A.	N.A.	N.A.
3	DBU	50 : 1 : 5.0	0.5	30	2 %	N.A.	N.A.	N.A.	N.A.
4	TBD	50 : 1 : 1.5	0.5	1	77 %	15000	1.34	7100	7300
5	TBD	50 : 1 : 1.0	0.5	1	58 %	10000	1.08	5400	5500
6	TBD	50 : 1 : 1.0	0.5	2	75 %	13000	1.17	6900	6800
7	TBD	50 : 1 : 1.0	0.25	1	41 %	7200	1.07	3800	3900
8	TBD	50 : 1 : 1.0	0.25	3	66 %	12000	1.07	6100	6300
9	TBD	50 : 1 : 0.5	0.5	1	34 %	6200	1.08	3200	3300
10	TBD	50 : 1 : 0.5	0.5	4	62 %	10000	1.07	5700	5400
11	TBD	100 : 1 : 1.0	0.5	5	51 %	14000	1.05	9300	9000
12	TBD	25 : 1 : 0.25	0.5	1	68 %	6200	1.08	3200	3400

Entries 1-3 were under room temperature; entries 4-12 were at 0 °C. Initiator (I) was benzyl alcohol for all entries. Solvent was anhydrous dichloromethane for all entries.

[a,b] M_n (GPC) and M_w/M_n (GPC) were measured by DMF GPC calibrated using polystyrene standards.

[c] M_n (Theor) was calculated from the monomer to initiator ratio and corrected for the conversion.

[d] M_n (^{1}H NMR) was calculated from the monomer to initiator ratio based on ^{1}H NMR of final polymer product.

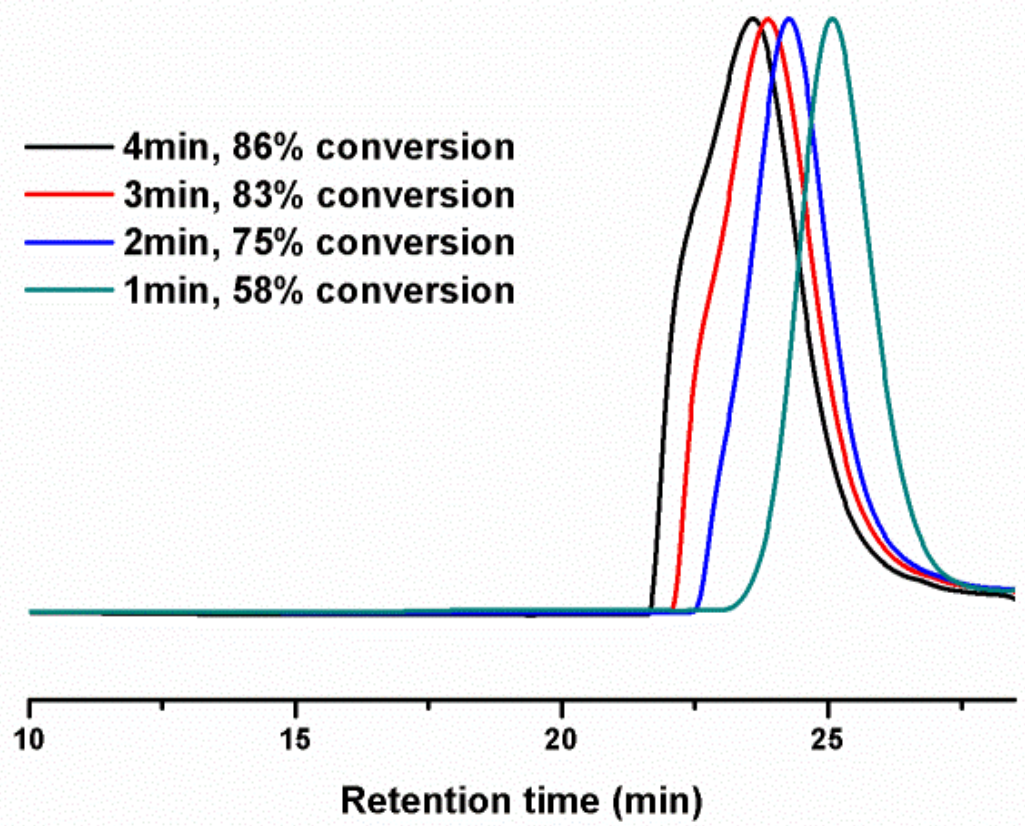

Figure 7-3. GPC traces of the polymerizations of MOEPA under conditions corresponding to those of entry 5 of Table 1: 0°C, I:M:catalyst = 1:50:1, concentration: 0.5 g/mL, however, allowed to proceed to longer time points and higher monomer conversions prior to quenching aliquots *via* dilution.

We further studied the kinetics of the ROP of the cyclic phospholane amidate by conducting parallel experiments, which allowed for monitoring of the extremely fast reaction. MOEPA and benzyl alcohol (at monomer-to-initiator molar ratios of 100 : 1 and 50 : 1) were premixed in anhydrous DCM and the solutions were divided equally into several portions, to each of which was added solutions of TBD (catalyst-to-monomer molar ratio 1%) in anhydrous DCM. After being stirred at 0 °C for preset periods of time, the reactions were quenched by diluting with DCM. The conversions were obtained from ^{31}P NMR spectra, while the molecular weights and molecular weight distributions were determined by GPC. The linearity of M_n *vs* monomer conversion suggested that the numbers of macromolecules in the reactions were constant during polymerization (**Figure 7-4 (A)**). PDIs were all less than 1.10 when the monomer

conversions were held to lower than 70%. Kinetic plots of $\ln[([M]_0-[M]_{equil})/([M]-[M]_{equil})]$ *vs* time showed first order kinetics, characteristic of ROP of MOEPA (**Figure 7-4 (B)**), and suggesting that the rate constant of initiation was more than or equal to the rate constant of propagation and that the concentration of growing chains in the reaction was approximately constant during the polymerization. Those data, similar with that from ROP of cyclic phospholane monomers, confirmed the characteristics of a controlled/living polymerization of the ROP of cyclic phospholane amidate monomers into PMOEPA.

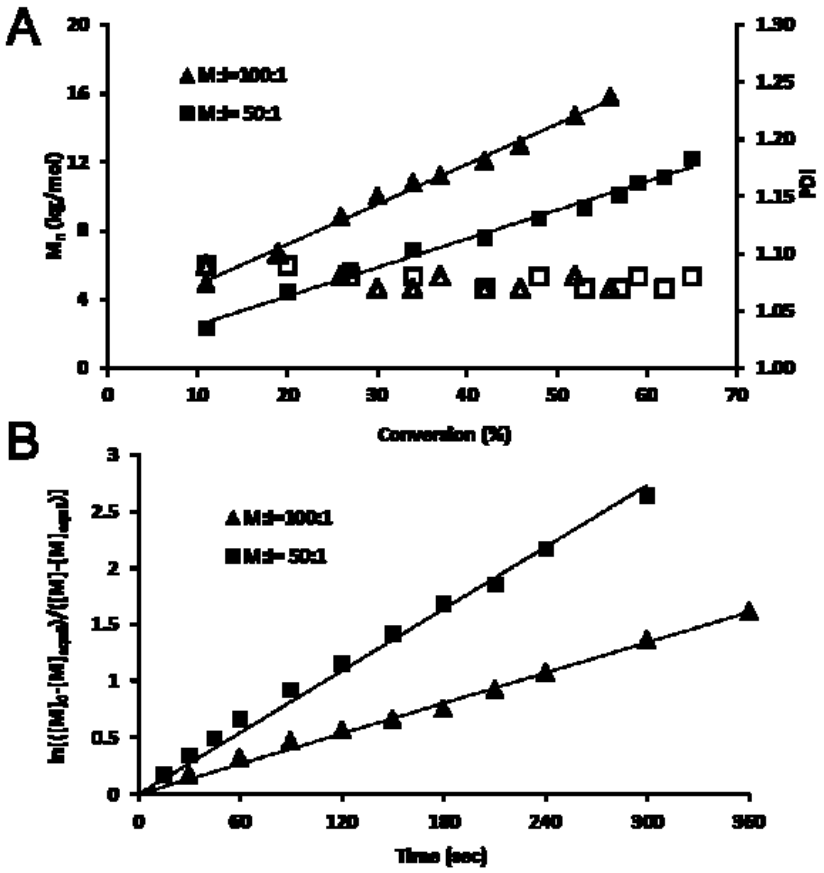

Figure 7-4. (A) Plot of M_n and M_w/M_n (PDI) *vs* monomer conversion for the polymerizations of MOEPA by using TBD as the catalyst and benzyl alcohol as the initiator, obtained from a combination of GPC and ^{31}P NMR analyses. Monomer : initiator ratios were 100 : 1 and 50 : 1. (B) Kinetic plots of $\ln[([M]_0-[M]_{eq})/([M]-[M]_{eq})]$ *vs* time, obtained from ^{31}P NMR spectroscopy data.

By controlling the monomer-to-initiator ratios as well as the reaction times, a series of poly(*N*-methoxyethyl phospholane amidates) (PMOEPAs) with different molecular weights were synthesized, and purified by precipitation from acetone into diethyl ether thrice. ^{31}P NMR cleared showed only one phosphorus environment at a chemical shift of 10.09 ppm, which corresponds to the phosphorus on the PMOEPA (**Figure 7-1 E**).(11, 29) ^{1}H NMR and ^{13}C NMR spectroscopic analyses also confirmed the structure of PMOEPA. Their highly viscous liquid form at room temperature was attributed to the low glass transition temperatures (T_g) for all samples of PMOEPA, which were measured to be -23 ± 4 °C, independent of chain length over the range of degrees of polymerization measured, from 17 to 52. This ROP method allows the simple and efficient synthesis of well-defined PPAs from the cyclic phospholane amidate monomers. A variety of cyclic phospholane amidate monomers with different pendant functionalities, such as methyl, ethyl, isopropyl, alkenyl and alkynyl, for the syntheses of different functional PPAs are currently under further development.

Cleavage of acid-labile phosphoramidate bond. PPAs have side groups connecting to a phosphoester backbone through a phosphoramidate bond, which was reported to be labile in acidic environments, but relatively stable at neutral pH.(30-32) Recently, acid-cleavable phosphoramidate linkages have been applied in biological nanomaterials to trigger release of conjugated drugs, macromolecules, coatings or other moieties.(33-36) However, the acid cleavability of this phosphoramidate bond on the PPAs had not yet been studied. Therefore, we demonstrated the acid cleavability of the phosphoramidate bonds of PMOEPA and studied the side chain cleavage kinetics; furthermore, a novel PPEI homopolymer was synthesized by taking advantage of the acid-cleavable phosphoramidate linkage.

The side chain cleavage kinetics of the phosphoramidate bonds on the well-defined PMOEPAs were studied in three aqueous acidic buffer solutions, hydrogen chloride solution, glycine-HCl solution and sodium acetate-acetic acid solution having pH values of 1.0, 3.0 and 5.0, respectively (**Figure 7-5**).

Cleavage of the phosphoramidate groups generated the PPEI, as shown in Scheme 7-1b. The distinct ^{31}P chemical shift (1.01 ppm) of PPEI allowed for monitoring of the percentage conversion of side chain cleavage by ^{31}P NMR spectroscopy. At pH 5.0, *ca*. 7% of the phosphoramidate bonds were converted into phosphate in 130 h. At the higher pHs, such as 7.4 and 9.0, the PMOEPA was found to be stable for more than 10 days with negligible changes (data not shown). In the more acidic environment, pH 3.0, greater than 23% of the phosphoramidate bonds were cleaved slowly in a controlled manner over 130 h. This slow side chain cleavage kinetics at pH 3.0 may enable PPAs to be responsive biomaterials for oral drug delivery, which requires sustained release in the acidic environment of the gastrointestinal tract. At pH 1.0, the side chain cleavage was greatly accelerated and complete hydrolysis was reached within about 10 h. These results indicate an interesting pH-dependent and gradual, tunable side cleavage rate for PMOEPA, which may be a general characteristic of PPA systems.

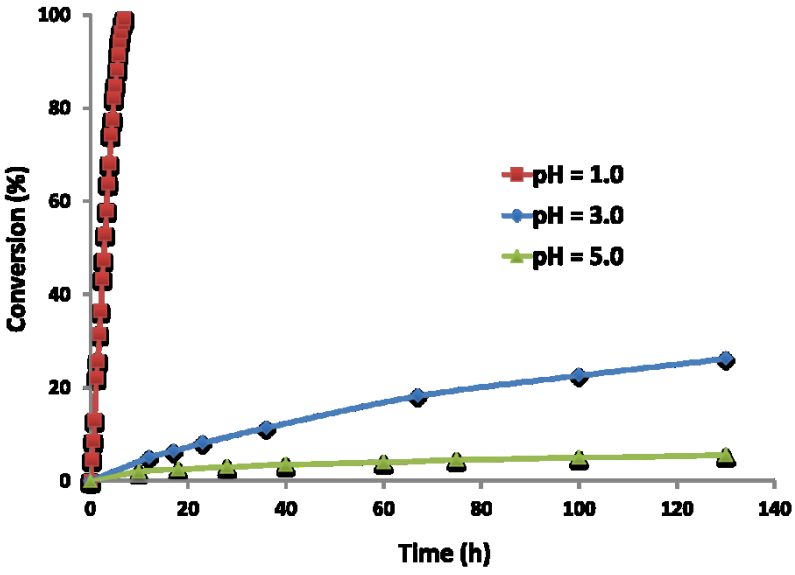

Figure 7-5. Selective hydrolytic side chain cleavage kinetics of phosphoramidate bonds along the backbone of PMOEPA, monitored by ^{31}P NMR spectroscopy.

Chemical and physical properties of PPEIs. After the complete side chain cleavage, the product PPEI was purified and ion exchanged by dialysis against nanopure water in the presence of Amberlite^{TM} IR120, H form, ion-exchange resin or Amberlite^{TM} IR120, Na form, ion-exchange resin to generate PPEI acid and PPEI sodium salt (**Scheme 7-1b**), respectively, and then confirmed by ^{1}H, ^{13}C and ^{31}P NMR spectroscopies (**Figure 7-1 (G)-(I)**). The resulting PPEI acid and PPEI sodium salt had the identical ^{1}H, ^{13}C and ^{31}P NMR spectra. Beyond the chain end group, there was only one peak in each of the three spectra, which confirmed the chemical structure of PPEI with only one chemical environment of the protons, carbons and phosphorus for the polymer repeat units, and no signals characteristic of the MOEA amine by-product. The PPEI acid and PPEI sodium salt had the same number of repeat units, calculated from the main chain units to chain end ratio based on ^{1}H NMR, as the that of PMOEPA before the side chain cleavage. The fact that the phosphodiester backbone remained from the conditions employed for the side chain hydrolysis at pH 1.0 for 10 h, proved this method as a reliable synthetic methodology for the preparation of PPEI containing high contents of acidic phosphate groups, and points to relatively high hydrolytic stability for this polymer material. It is expected that DNAse and/or RNAse enzymes may be active against this polymer, and such studies are underway.

The PPEI acid and PPEI sodium salt had distinct thermal properties differences. The glass transition temperature (T_g) of the PPEI acid was -14 °C, while that of the PPEI sodium salt was 43 °C, measured by differential scanning calorimetry (DSC). Thermogravimetric analysis (TGA) of the PPEI acid exhibiteda multiple-stage mass loss profile: it was stable until 225 °C (**Figure 7-6 (A)**); from 225 °C to 273 °C (**Figure 7-6 (B)**), 21 % of mass was rapidly lost and the remaining mass agreed with the calculated value for H_3PO_4 on each repeat unit; from 273 °C to 520 °C (**Figure 7-6 (C)**), another 15 % of mass was gradually lost and the remaining mass was calculated as HPO_3 for each repeat unit; to 600 °C (**Figure 7-6 (D)**), final 7 % of mass was lost and the remaining mass was calculated as $PO_{2.5}$ for each repeat unit. In contrast, the PPEI sodium salt had only one mass loss temperature window: from 265 °C (**Figure 7-6 (E)**) to 310 °C (**Figure 7-6 (F)**), 30 % of mass was lost and the remaining mass corresponded to that calculated for $NaPO_3$ from each repeat unit; and after 310 °C, no additional mass was lost. The higher

decomposing temperature of PPEI sodium salt showed the higher stability when compared with PPEI acid. The ultra-high 70 wt% phosphorus and oxygen content, as much as that of ammonium polyphosphate, along with the high decomposition temperatures and decomposition products may enable PPEI sodium salt to perform as a promising fire-retardant material.(37)

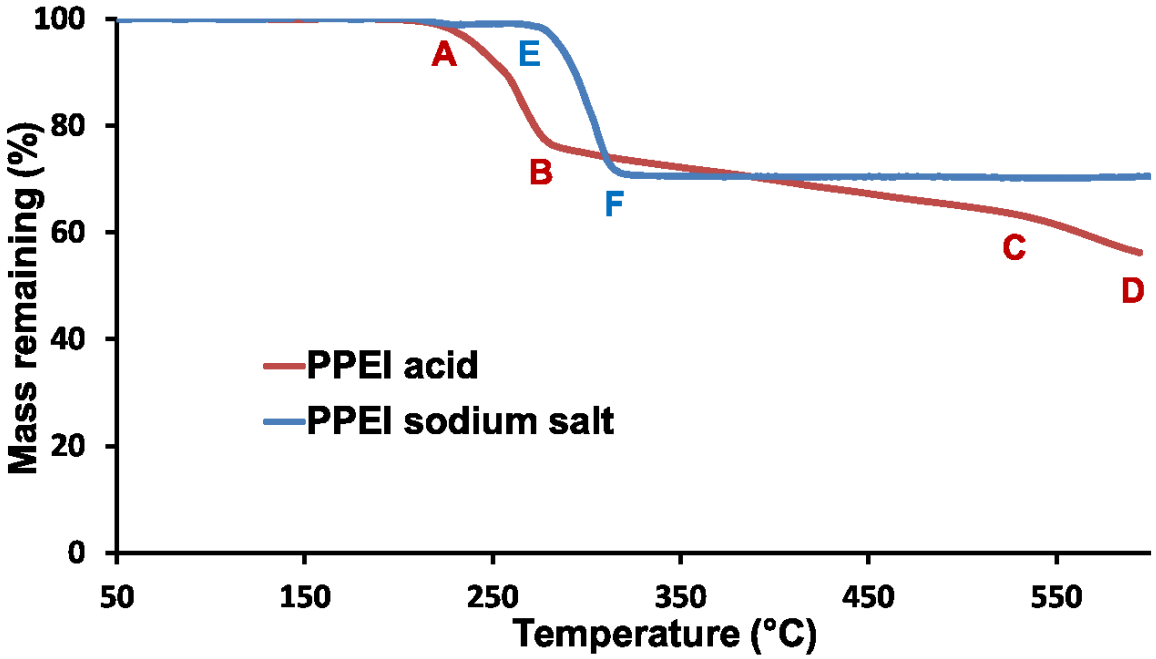

Figure 7-6. Thermogravimetric analyses of PPEI acid and PPEI sodium salt.

Cytotoxicity of degradable polymers. To demonstrate the biocompatibilities of PPAs and PPEIs, the PMOEPA, PPEI acid and PPEI sodium salt were tested for their cytotoxicity in both HeLa cells and RAW 264.7 mouse macrophage cells at different concentrations (**Figure 7-7**). No cytotoxicity was observed for all three polymers over the range of concentrations from 5-to-1250 μg/mL in both cell lines after 24 h-incubation. Only at the highest tested concentration (2500 μg/mL), the polymers exhibited dose-dependent toxicities against both cell lines. Therefore, PPAs and PPEIs could be used at a broad range of concentrations without causing cytotoxicity for biological applications.

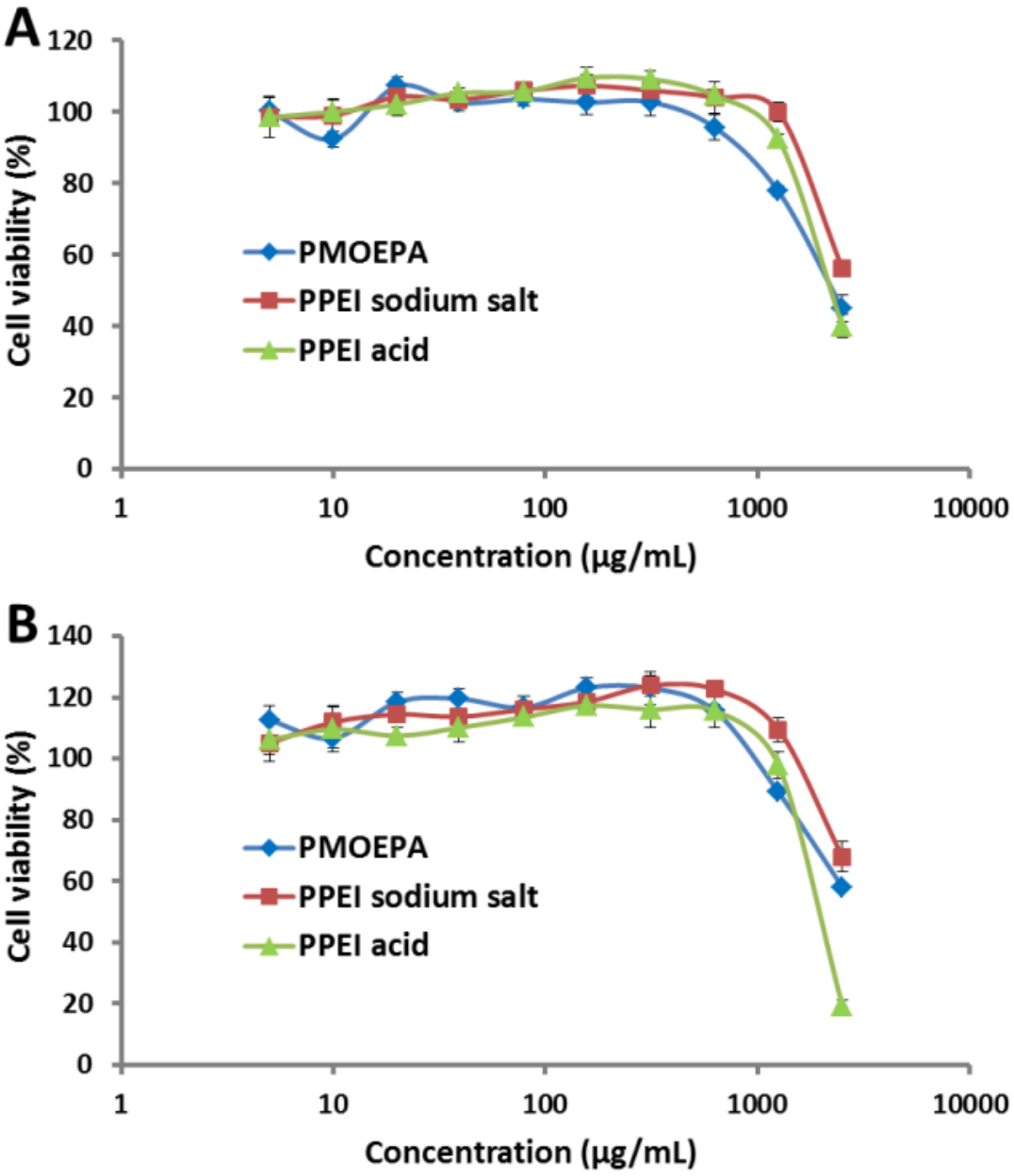

Figure 7-7. Cytotoxicity of PMOEPA, PPEI sodium salt and PPEI acid in HeLa cells (A) and RAW 264.7 mouse macrophage cells (B) after treatment over a concentration range of 5-to-2500 µg/mL for 24 h.

Conclusions

In this study, we have demonstrated the direct polymerization of a cyclic phospholane amidate monomer by organobase catalysis in the presence of an alcohol initiator, and transformation of the resulting polyphosphoramidate to polyphosphoester ionomer acid and sodium salts by hydrolytically cleaving the acid-labile phosphoramidate bonds in acidic solutions. The prolonged chain cleavage profiles of the polyphosphoramidates even at pH 1.0 might be useful for polyphosphoramidates serving as responsive biomaterials for localized drug release in the gastrointestinal tract. The high thermal stability and ultrahigh 70 wt% phosphorus and oxygen content of the polyphosphoester ionomer sodium salt promises applicability as an alternative fire-retardant material. In addition, polyphosphoramidate, polyphosphoester ionomer acid and polyphosphoester ionomer sodium salt showed high biocompatibility toward HeLa cells and RAW 264.7 mouse macrophages. The phosphoramidate and phosphoester ionomer functionalities may also provide for bonding to inorganic substrates in vivo, for instance to achieve targeting to bone in the treatment of osteosarcomas, leukemia, etc. and bone and tooth repair. Therefore, overall, this work represents novel and reliable synthetic methodology to obtain two degradable polymer systems with diverse potential.

Acknowledgements

We gratefully acknowledge financial support from the National Heart Lung and Blood Institute of the National Institutes of Health as a Program of Excellence in Nanotechnology (HHSN268201000046C) and the National Science Foundation under grant numbers DMR-0906815 and DMR-1105304. The Welch Foundation is gratefully acknowledged for support through the W. T. Doherty-Welch Chair in Chemistry, Grant No. A-0001.

Reference

(1) Nair, L. S.; Laurencin, C. T. *Prog. Polym. Sci.* **2007**, *32*, 762.

(2) Gross, R. A.; Kalra, B. *Science* **2002**, *297*, 803.

(3) Zhang, S. Y.; Zou, J.; Zhang, F. W.; Elsabahy, M.; Felder, S. E.; Zhu, J. H.; Pochan, D. J.; Wooley, K. L. *J. Am. Chem. Soc.* **2012**, *134*, 18467.

(4) Zhang, S. Y.; Li, A.; Zou, J.; Lin, L. Y.; Wooley, K. L. *ACS Macro Lett.* **2012**, *1*, 328.

(5) Dove, A. P. *ACS Macro Lett.* **2012**, *1*, 1409.

(6) Sanders, D. P.; Fukushima, K.; Coady, D. J.; Nelson, A.; Fujiwara, M.; Yasumoto, M.; Hedrick, J. L. *J. Am. Chem. Soc.* **2010**, *132*, 14724.

(7) Jeong, W.; Hedrick, J. L.; Waymouth, R. M. *J. Am. Chem. Soc.* **2007**, *129*, 8414.

(8) Dove, A. P.; Pratt, R. C.; Lohmeijer, B. G. G.; Waymouth, R. M.; Hedrick, J. L. *J. Am. Chem. Soc.* **2005**, *127*, 13798.

(9) Coulembier, O.; Mespouille, L.; Hedrick, J. L.; Waymouth, R. M.; Dubois, P. *Macromolecules* **2006**, *39*, 4001.

(10) Coulembier, O.; Moins, S.; Dubois, P. *Macromolecules* **2011**, *44*, 7493.

(11) Wang, J.; Zhang, P. C.; Lu, H. F.; Ma, N.; Wang, S.; Mao, H. Q.; Leong, K. W. *J. Control. Release* **2002**, *83*, 157.

(12) Zhang, X. Q.; Wang, X. L.; Huang, S. W.; Zhuo, R. X.; Liu, Z. L.; Mao, H. Q.; Leong, K. W. *Biomacromolecules* **2005**, *6*, 341.

(13) Jiang, X.; Qu, W.; Pan, D.; Ren, Y.; Williford, J.-M.; Cui, H.; Luijten, E.; Mao, H.-Q. *Adv. Mater.* **2013**, *25*, 227.

(14) Ren, Y.; Jiang, X. A.; Pan, D.; Mao, H. Q. *Biomacromolecules* **2010**, *11*, 3432.

(15) Iwasaki, Y.; Yamaguchi, E. *Macromolecules* **2010**, *43*, 2664.

(16) Liu, J. Y.; Pang, Y.; Huang, W.; Zhai, X. A.; Zhu, X. Y.; Zhou, Y. F.; Yan, D. Y. *Macromolecules* **2010**, *43*, 8416.

(17) Clement, B.; Grignard, B.; Koole, L.; Jerome, C.; Lecomte, P. *Macromolecules* **2012**, *45*, 4476.

(18) Du, J. Z.; Du, X. J.; Mao, C. Q.; Wang, J. *J. Am. Chem. Soc.* **2011**, *133*, 17560.

(19) Monge, S.; Canniccioni, B.; Graillot, A.; Robin, J. J. *Biomacromolecules* **2011**, *12*, 1973.

(20) Biela, T.; Penczek, S.; Slomkowski, S.; Vogl, O. *Makromol. Chem-Rapid* **1982**, *3*, 667.

(21) Shin, E. J.; Brown, H. A.; Gonzalez, S.; Jeong, W.; Hedrick, J. L.; Waymouth, R. M. *Angew. Chem. Int. Edit.* **2011**, *50*, 6388.

(22) Wan, A. C. A.; Mao, H. Q.; Wang, S.; Phua, S. H.; Lee, G. P.; Pan, J. S.; Lu, S.; Wang, J.; Leong, K. W. *J. Biomed. Mater. Res. B* **2004**, *70B*, 91.

(23) Troev, K.; Tsatcheva, I.; Koseva, N.; Georgieva, R.; Gitsov, I. *J. Polym. Sci., Part A: Polym. Chem.* **2007**, *45*, 1349.

(24) Iwasaki, Y.; Kawakita, T.; Yusa, S. *Chem. Lett.* **2009**, *38*, 1054.

(25) Amigues, E. J.; Migaud, M. E. *Tetrahedron Lett.* **2004**, *45*, 1001.

(26) Wang, J.; Sun, D. D. N.; Shin-ya, Y.; Leong, K. W. *Macromolecules* **2004**, *37*, 670.

(27) Ikeuchi, R.; Iwasaki, Y. *Journal of Biomed. Mater. Res. Part A* **2013**, *101A*, 318.

(28) Modro, A. M.; Modro, T. A.; Bernatowicz, P.; Schilf, W.; Stefaniak, L. *Magn. Reson. Chem.* **1997**, *35*, 774.

(29) N'Guyen, T. T. T.; Oussadi, K.; Montembault, V.; Fontaine, L. *J. Polym. Sci., Part A: Polym. Chem.* **2013**, *51*, 415.

(30) Rahil, J.; Haake, P. *J. Am. Chem. Soc.* **1981**, *103*, 1723.

(31) Benkovic, S. J.; Sampson, E. J. *J. Am. Chem. Soc.* **1971**, *93*, 4009.

(32) Garrison, A. W.; Boozer, C. E. *J. Am. Chem. Soc.* **1968**, *90*, 3486.

(33) Leriche, G.; Chisholm, L.; Wagner, A. *Bioorgan. Med. Chem.* **2012**, *20*, 571.

(34) Jeong, J. H.; Kim, S. W.; Park, T. G. *Bioconjugate. Chem.* **2003**, *14*, 473.

(35) Romberg, B.; Hennink, W. E.; Storm, G. *Pharm. Res.* **2008**, *25*, 55.

(36) Yoon, S.; Kim, W. J.; Yoo, H. S. *Small* **2013**, *9*, 284.

(37) Li, Y. C.; Mannen, S.; Morgan, A. B.; Chang, S. C.; Yang, Y. H.; Condon, B.; Grunlan, J. C. *Adv. Mater.* **2011**, *23*, 3926.

Chapter 8

Conclusions

This research dissertation includes two parts. Chapters 2 and 3, the first part, focuses on the development of asymmetrically-functionalized nanoparticles with anisotropic distributions of chemical functionalities. Chapters 4-6, the second part, discusses the synthesis of functional degradable polyphosphoesters, the preparation of two derivative degradable nanoparticle systems and potential biological applications of those nanoparticle systems. Chapter 7 describes the synthesis of novel polyphosphoramidates and their transformation into polyphosphoester ionomers.

In Chapters 2 and 3, two methods are developed for the preparation of nanoparticles with anisotropic distributions of chemical functionalities. Chapter 2 demonstrates a novel, efficient and recyclable approach to construct orthogonal dual-clickable Janus nanoparticles, through a desymmetrization cycle based on complementarily reactive nanoscopic templates and covalent pattern transfer. The robustness of nanostructures is critical in this approach. This strategy can be further expanded as a general route to desymmetrize and dual-functionalize a large family of soft matter nanoparticles for anisotropic modification toward complex devices. Chapter 3, reported a hierarchical assembly strategy of utilizing pre-formed block copolymer nanoparticles as building units to assemble into higher-ordered, multicompartment superstructures including 1-D chains, 2-D rings and 3-D aggregates. Crown ether moieties, in the PAA block of the PAA-*b*-PMMA copolymer, provided tunable inter-particle interactions for the hierarchical assembly processes. And then, internal nanoparticle core morphological phase segregation of the PB and PMMA was affected by associations between the shells of different nanoparticles. The hierarchical assemblies could then be disassembled by addition of potassium ion into multicompartment nanoparticles, including sandwich-like and concentric triangle-shaped structures. The approach in Chapter 2 relied on chemical reactions between nanoparticles, while the approach in Chapter 3 was based on the physical interactions within and between nanoparticles.

The approach in Chapter 2 may apply to a wide range of soft nanoparticle, including degradable nanoparticles, but has the limitation for the large-scale production, even by this recyclable process. In contrast, the approach in Chapter 3 holds the possibility for the gram-scale production, but has the limitation of polymer compositions, since the known phase separation only applied to several kinds of polymer combinations. A better solution needs, with the combination of merits of two approaches, to be developed for the large-scale production of a broad range of polymeric nanoparticles, which will facilitate the direct applications of Janus nanoparticles. The biological applications of bioactive moieties-functionalized Janus nanoparticles would attract a great attention and play an important role in nanomedicine.

The alkyne-functionalized polyphosphoester developed in Chapter 4 provided a great degradable polymer platform for the nanoparticle productions in Chapter 5 and Chapter 6. In Chapter 4, a stable alkyne-functionalized phospholane monomer was synthesized and its organocatalyzed polymerization kinetics were explored. The “click” type azide-alkyne Huisgen cycloaddition and radical-mediated thiol-yne reactions were demonstrated to be compatible with the degradable polyphosphoester backbone, and allowed the facile functionalization of the alkyne-functionalized polyphosphoester.

In Chapter 5, a retrosynthetic methodology has been used to develop a versatile platform for the construction of a family of polymeric micelles with varying surface charges and functionalities based on the alkyne-functionalized polyphosphoester and its thiol-yne reactions demonstrated in Chapter 4. The construction of the polymeric micelle system began from the preparation of hydrophobic and alkyne-functionalized monomers, to the synthesis of well-defined hydrophobic-functional AB diblock polyphosphoester. The clickable alkynyl groups on the functional portion of the hydrophobic-functional AB diblock polyphosphoester were transformed with four different thiols by photo-initiated, radical-mediated thiol-yne chemistry, forming four amphiphilic diblock polyphosphoesters with different charge

types. The non-ionic, anionic, cationic and zwitterionic amphiphilic diblock polyphosphoesters underwent self-assembly in water by direct dissolution and sonication to afford uniform spherical micelles with similar average sizes (between 15-21 nm). The micelles have also shown high biocompatibility, and even the cationic micelles had a 6-fold lower cytotoxicity when compared to Lipofectamine®.

The whole programmable process allowed us to prepare well defined degradable nanoparticles with desired properties very quickly. For example, the preparation of anionic NPs starting from small molecules could be completed within 6 h. For cationic NPs, it only took two days due to the purification by dialysis. Nanoparticles created here were novel, simple, and we wanted them to be applicable. So we were actively exploring a variety of biological applications of those nanoparticles. For instance, the anionic and zwitterionic nanoparticles were used for the loading of silver ions by sulfur-sliver interaction in the application of treating lung infections. And *in vivo* studies of those systems, performed in Prof. Carolyn Cannon's lab, showed superior bacterial-resistance than small compounds, silver ion itself and silver carbene. To better understand the mechanism of the excellent pharmaceutical effects of nanoparticles loaded with silver, the radioactive ^{111}Ag was loaded into anionic and zwitterionic nanoparticles to track of the bio-distribution of silver in mice lung. And we, together with Prof. Suzanne Lapi's lab found out that the silver delivered by nanopaticles had better retention in lung than small compounds, which explained the better efficiency. In the exploration of applications of the cationic nanoparticles, at the beginning, we We were trying to develop biodegradable cationic nanoparticles to delivery nucleic acids for the treatment of acute lung injury (ALI) by regulating the inducible Nitric oxide synthase (iNOS) expression. After we started to work with Prof. John Taylor's lab, we found something different yet interesting. The cationic nanoparticles, as a novel degradable drug complex, demonstrated efficient inhibition of inducible nitric oxide synthase (iNOS) without further loading any other therapeutic drugs, as one of their degradation products might be a new inhibitor to iNOS pathway. Cationic nanoparticles showed much more effective iNOS inhibition than the small molecule, due to higher cellular uptake as a condensed cationic nanoparticle and fast degradation. This degradable PPE-based cationic nanoparticle indicated the potential to serve as a promising anti-iNOS and/or anti-inflammatory agent

toward the treatment of acute lung injury. The intermediate, hydrophobic-functional AB diblock polyphosphoester, was grafted with PEG by azide-alkyne Huisgen cycloaddition and resulting PEG-grafted diblock was served as the vehicle to load PTX in a very high water solubility and studies both *in vitro* and *in vivo*. In the meantime, we studied the degradation profiles by monitoring the changes in particle size and charge and the immunotoxicities of those nanoparticles and their degradation products. Beyond the biological application of nanoparticles produced from this programmable process, the strategy also provided a general platform, on which a variety of degradable nanoparticles with different polymer compositions, like polylactic acid and poly sugars, and nanoparticule morphologies, like cylinders, were able to be created in the same rapid and versatile manner.

In Chapter 6, we have developed a novel PEO-*b*-(PPE-*g*-PTX) drug conjugate system. Azide-alkyne Huisgen cycloaddition was employed to attach bulky PTX molecules covalently and densely onto a block copolymer backbone. In addition, residual alkynes provide possibilities of further post-chemical modifications (*e.g.* crosslinking, radio-labeling, decoration with targeting ligands), as opposed to the limited functionalizability of Taxol or Abraxane. The PEO-*b*-(PPE-*g*-PTX) achieved a PTX loading capacity as high as 65 wt% and, by balancing PTX loading capacity and polymer solubility, a water solubility at equivalent PTX concentration of 6.2 mg/mL was obtained (at 55 wt% PTX loading). Although the cell-killing activity of the covalently-conjugated PTX of PEO-*b*-(PPE-*g*-PTX) was reduced, relative to the physically-associated PTX of the Cremophor-EL and ethanol formulation, against several cancer cell lines, the lower cytotoxicity of the conjugates might be advantageous by providing increased safety for *in vivo* applications. This PEO-*b*-(PPE-*g*-PTX) system provides a powerful platform for combinational therapy and bioimaging. The decreased cytotoxicity of this PTX drug conjugate might be due to the hard release of PTX from the polymer backbone. To solve this problem and to achieve better cytotoxicity, the second generation of the PTX drug conjugate was designed to have a β-thiopropionate bond, an acid-sensitive linkage, between PTX and the polymer for the easy release of PTX in acidic intracellular environment. And the third generation was being developed to have both acid-labile β-thiopropionate

linkage and redox-sensitive disulfide linkage between PTX and the polymer. All three generations of PTX drug conjugates are being planned for *in vitro* and *in vivo* studies.

In Chapter 7, we demonstrated the direct polymerization of cyclic phospholane amidate monomer by organo-base and the preparation of polyphosphoester ionomer acid and sodium salts by cleaving the acid-labile phosphoramidate bond on the resulting polyphosphoramidate with acidic solutions. The slow side chain cleavage profile of polyphosphoramidate at lower pHs might be useful for polyphosphoramidate serving as responsive biomaterials for localized drug releasing in stomach. The high thermal stability and ultrahigh 70 wt% P_2O_5 content of polyphosphoester ionomer sodium salt promised polyphosphoester ionomer sodium salt to be an alternative fire-retardant material. In addition, polyphosphoramidate, polyphosphoester ionomer acid and polyphosphoester ionomer sodium salt showed high biocompatibility toward Hela cells and RAW 264.7 momjuse macrophages. And polyphosphoester ionomer would serve as the macromolecular targeting ligand for the bond related diseases. The novel nanostructure based on polyphosphoramidate or polyphosphoester ionomers and their applications are under investigation in Wooley group.

In Chapters 4-7, the two beneficial features, easy functionalization and water soluble, of polyphosphoesters over other major synthetic degradable polymers, such as polyesters, polypeptides and polycarbonates, had shown great advantages in the rapid and large-scale production of well-defined nanoparticles and polymers with easily-tunable properties and high water solubility to carry a significant amount of hydrophobic payloads. The polyphosphoester-based degradable nanoparticles with designed properties are highly promising for various biological applications, even they still needs more careful evaluations in the *in vitro* and *in vivo* studies. And, the novel polymers, polyphosphoramidates and phosphoester ionomers, are still under very early stage of investigations for different applications.

To summarize this dissertation, the research activities covered the polymer synthesis (Chapter 4 and 7), the self-assembly and Janus nanoparticles (Chapter 2 and 3) and degradable nanoparticles for biomedical application (Chapter 4 and 5). The direct applications of those researches have not yet realized, as many properties still need to be further studied, but this dissertation provides several platforms striving towards the next generations of polymerization techniques, self-assembly strategies and advanced biomedical materials.

VITA

Shiyi Zhang obtained his Bachelor of Science degree in Chemistry from Peking University at Beijing in 2008. He then entered the Ph.D program in the Chemistry Department at Washington University in St. Louis in August 2008 under the guidance of Professor Karen L. Wooley. In November 2009, He moved to Texas A&M University with Dr. Wooley while maintained the student status in Washington University in St. Louis. He obtained his Doctor of Philosophy degree in Chemistry awarded by Washington University in St. Louis in May, 2013.

Shiyi Zhang may be reached *via* email at zhangshiyi5@gmail.com. Thank you for reading my dissertation to the very end.